

A Free Volume Theory of Polymer Dynamics

by

Chi Pui Jeremy Wong

A thesis submitted in partial fulfillment of the requirements for the degree of

Doctor of Philosophy

in

Chemical Engineering

Department of Chemical and Materials Engineering

University of Alberta

© Chi Pui Jeremy Wong, 2020

Abstract

It is not trivial to understand the underlying principle of polymer dynamics due to its wide range of applications in our daily lives. This thesis mainly focuses on the theory and simulation of polyethylene melts, which are not only restricted to the classic linear structure, but also extended to ring and four-arm symmetrical star structures. The size dependence of the dynamic properties of these polyethylene molecules, such as diffusivity and viscosity, demonstrates a crossover from unentangled to entangled regimes. In the literature, there are two classic models, known as the Rouse model and reptation model, only for polyethylene with linear structure, which accounts for the crossover in the dynamics of linear polyethylene as a function of chain length (N) at a particular temperature.

The Rouse model is a simplified version of Brownian dynamics (BD) model for unentangled polymers, in which the inertia term is neglected. If such inertia term is included, it is then possible to compute the velocity time correlation function using the eigenvalue and eigenfunction method. The eigenfunctions can then be used to construct different time correlation functions. Such analysis can also be applied to ring and star polymers, by modifying the resultant matrix equation in such model. It was also found that by incorporating a finite equilibrium length in the harmonic bond stretching term in Rouse model, it becomes a nonlinear BD model, which makes the equation of motion nonlinear and the analytical derivation of eigenfunctions impossible. This is also true in MD simulation, which explicitly includes all the highly nonlinear atomic force as a result of the bonded and non-bonded potentials in the equation of motion. Proper orthogonal decomposition (POD), which is a method that can generate a reduced ordered model, was applied to the numerical data so as to obtain ‘eigenfunctions’, which are later regarded as eigenmodes, for calculating relaxation times and

viscosities. With the aid of POD analysis, it was observed that the viscosities calculated from nonlinear BD model and MD simulations concur with one another.

Another notable fact is that the diffusivity of linear polyethylene melt as a function of chain length as predicted by Rouse model is $D_{cm} \sim N^{-\nu}$ and $\eta \sim N^{\nu}$, with the exponent $\nu = 1$, whereas in reality, ν is larger than 1 and it becomes larger when temperature decreases with $\nu = 2.6$ at 343.5 K for diffusivity. The same trend was also observed for viscosity with $\nu = 1.8$.

In the same way as the Rouse model, the classic reptation model for linear polyethylene predicts that $D_{cm} \sim N^{-2}$ at $T = 448$ K, whereas a stronger exponent was experimentally observed having a value of -2.2 . Similarly, based upon such model, it can be calculated that $\eta \sim N^3$, whereas in reality, $\eta \sim N^{3.4}$ for linear polyethylene. The reptation model is based on the assumption that a polymer chain is reptating through a tube as defined by a number of fixed obstacles, known as entanglements. However, a foundation, i.e., how does the repulsive force among the chains give rise to the entanglements, leading to a reptative motion?, for the entanglement concept in such model is still lacking. In addition, to our knowledge, the quantification of the entanglements for identifying the primitive path is only possible in linear polymer, but not ring polymer.

With regard to this, an alternative free volume theory was proposed, for which many parameters can be theoretically obtained using the generic van der Waals' equation of state and the distribution function theory of polymer melts. Different radial distribution functions in this case can be obtained either by either MD simulation or more elegantly the Polymer Reference Interaction Site Model (PRISM). The free volume theory proposed in this work, which only considers the amount of free volume distributed within the macromolecules, can account for the crossover in the dynamics of both linear, ring and star polymers.

In summary, this work shed light on the theoretical approach of evaluating the dynamic properties of polymers with linear, ring as well as star structures. The proposed free volume theory also offers an alternative way of understanding the diffusivity and viscosity of both unentangled and entangled polymer melts within a particular range of molecular weight.

Preface

All of the data reported in this thesis were collected by Chi Pui Jeremy WONG, and the writings were refined by Prof. Phillip CHOI. The derivation of the free volume theory, interpretation as well as discussion of the results were the very original work of Chi Pui Jeremy WONG under the supervision of Prof. Phillip CHOI.

Versions of Chapters 3, 4, 5, 6, 7 and 8 have been published in [*Comput. Mater. Sci.*, 2018, 155, 320-324], [*Macromol. Theory Simul.*, 2019, 28, 1800072], [*Soft Matter*, 2019, 15, 9300-9309], [*Soft Matter*, 2020, 16, 2350-2362], [*Soft Matter*, 2020, 16, 4283-4289] and [*Soft Matter*, 2020, 16, 7458-7469] respectively. A version of Appendix A has been published in [*Mol Simul*, 2020, 1-12] as a review paper.

To those who truly love science.

Acknowledgements

I would like to thank my supervisor, Prof. Phillip CHOI, for offering me this invaluable opportunity of performing research in polymer physics. The high degree of academic freedom given by him allowed me to conduct scientific research gleefully. He introduced this interesting problem of entangled polymer dynamics and free volume to me, which eventually invigorated me to derive a free volume theory of polymer dynamics that will be discussed in the forthcoming sections of this PhD thesis.

I would also like to acknowledge the supervisory committee (Prof. Hao ZHANG and Prof. João SOARES from Department of Chemical and Materials Engineering), the examiner (Prof. Tian TANG from Department of Mechanical Engineering), the external examiner (Prof. Alejandro REY from McGill University) as well as the chair of my PhD thesis examination (Prof. Anastasia ELIAS from Department of Chemical and Materials Engineering). The steadfast love of my family as well as the financial support from Natural Sciences and Engineering Research Council of Canada are also greatly appreciated.

Table of Contents

1	Introduction	1
1.1	Overview of the thesis	1
1.2	BD and Langevin dynamics of a classical particle	4
1.2.1	Case 1: $\frac{k}{m} > \frac{\zeta^2}{4m^2}$	5
1.2.2	Case 2: $\frac{\zeta^2}{4m^2} > \frac{k}{m}$	6
1.2.3	Brownian Dynamics	7
1.3	Statistical mechanics and distribution function theory of simple liquid	8
1.3.1	Canonical Ensemble and Classical Statistical Thermodynamics	8
1.3.2	Radial Distribution Function	10
1.3.3	Pressure Equation	11
1.3.4	Percus-Yevick Equation	12
1.3.5	Fourier Transform Method	13
1.4	Maxwell-Boltzmann Distribution and Transport Coefficients of Dilute Gas	15
1.4.1	Derivation of Boltzmann Distribution and Mean-Free Path	15
1.4.2	Viscosity	21
1.4.3	Diffusion Coefficient	22
1.4.4	A More Rigorous Approximation of Transport Coefficient	23
1.5	Static properties of polymers	27
1.5.1	Partition Function and Probability	28
1.5.2	Exact Calculation of End-to-End Vector	31
1.5.3	Exact Calculation of Mean-Square End-to-End Distance and Characteristic Ratio	35
1.6	Summary	37
2	Molecular Dynamics, Numerical Simulations and Numerical Analysis	38
2.1	MD Simulation	38
2.1.1	Temperature and Pressure Coupling: Nonholonomic Constraints of the Equation of Motion	39
2.1.2	Integration of the Equation of Motion	40
2.2	Implicit Euler Method	43
2.3	Numerical Analysis of the Trajectory	45
2.3.1	Proper Orthogonal Decomposition	45
2.3.2	Time Correlation Function and Mean Square Displacement	46
2.3.3	Voronoi Tessellation	47
3	Velocity Time Correlation Function of a Rouse Chain	50
3.1	Introduction	50
3.2	Numerical Simulation Details	51
3.3	Preliminaries	52
3.3.1	Langevin Dynamics of a Single Particle: without Inertia Term	52
3.3.2	Langevin Dynamics of a Single Particle: with Inertia Term	53
3.3.3	Rouse Dynamics: without Inertia Term	54

3.4	Velocity Time Correlation Function of a Rouse Chain	56
3.4.1	Rouse Dynamics: with Inertia Term	56
3.5	Conclusion	61
4	Analysis of Brownian Dynamics and Molecular Dynamics Data of Unentangled Polymer Melts Using Proper Orthogonal Decomposition	63
4.1	Introduction	63
4.2	BD Simulation Details	66
4.3	MD Simulation Details	68
4.4	Proper Orthogonal Decomposition	71
4.5	Non-Linear BD of Polyethylene with $b = \sqrt{C_\infty} b_0$	72
4.6	MD Simulation	79
4.7	Zero-Shear Viscosity from BD and MD Simulations	85
4.8	Conclusions	87
5	A Free Volume Theory on the Chain Length Dependence of the Diffusivity of Linear Polymers	88
5.1	Introduction	88
5.2	The Free Volume Theory of Polymers	90
5.3	Molecular Dynamics (MD) Simulation	95
5.4	Results and Discussion	97
5.4.1	Free Volume Analysis	97
5.4.2	Center-of-mass Diffusion Coefficient of Polyethylene	106
5.5	Conclusion	108
6	On the Diffusivity of Ring Polymers	109
6.1	Introduction	109
6.2	Preliminary: Free Volume Theory Revisited	112
6.3	Calculation Details	113
6.3.1	Integral Equation Theory of Ideal Ring Polymers	113
6.3.2	Molecular Dynamics Simulation	115
6.4	Results and Discussion	117
6.4.1	PRISM Theory	117
6.4.2	Molecular Dynamics Simulation	121
6.4.3	Center-of-Mass Diffusion Coefficient	128
6.5	Conclusion	134
7	A Theory for the Temperature Effect on the Chain Length Dependence of the Diffusivity of Oligomers	136
7.1	Introduction	136
7.2	Integral Equation Theory of Polymers	139
7.2.1	Validity of Neglecting Chain Ends	141
7.3	A Brief Introduction of Free Volume Theory	141
7.4	Calculation of Parameters and Comparison with Experimental Data	142
7.5	Conclusion	148
8	Prediction of Crossover in the Molecular Weight Dependence of Polyethylene Viscosity Using a Polymer Free Volume Theory	150
8.1	Introduction	150
8.2	Theoretical Background	155
8.2.1	Viscosity of a Dilute Polymer Medium	155
8.2.2	Free Volume Theory for Polyethylene with Different Structures	157
8.2.3	PRISM Theory	159
8.2.4	Pressure Equation, Intramolecular Term and GvdW Equation of State	161
8.3	Results and Discussion	164

8.3.1	Length Scales and GvdW Parameters	164
8.3.2	Molecular Weight Dependence of Zero-Shear Viscosity	169
8.3.3	Temperature Dependence of Zero-Shear Viscosity	171
8.4	Conclusion	174
9	Conclusion	175
9.1	Main Findings and Contributions	175
9.2	Future Work	176
9.2.1	Nonlinear BD model and POD method	176
9.2.2	Free Volume Theory	176
9.2.3	Relation among the Velocity Time Correlation Function, the POD Method and the Free Volume Theory	178
	References	180
	Appendix A A Review on the Relaxation Dynamics Analysis of Unentangled Polymers with Different Structures	186
A.1	Introduction	186
A.2	Preliminaries	188
A.2.1	Case 1: $\frac{k}{m} > \frac{\zeta^2}{4m^2}$	189
A.2.2	Case 2: $\frac{\zeta^2}{4m^2} > \frac{k}{m}$	190
A.3	Analytical Solution of Linear Dynamics: Time Correlation Functions and Velocity Correlation Functions of Linear, Ring, and Star Polymers	191
A.3.1	Linear Polymer	192
A.3.2	Ring Polymer	193
A.3.3	Four-Arm Symmetrical Star Polymer	196
A.4	Application of Rouse Mode, Extraction of Relaxation Times from Simulation Data using Rouse Modes as well as other Available Methods	197
A.4.1	Eigenmodes from POD	199
A.4.2	Zero-Shear Viscosity: Rouse model and POD method	201
A.5	Conclusion	205
	Appendix B Supporting Information for Chapter 3	207
B.1	C++ program for numerical simulation	207
B.2	Python 3.5 program for initial conformation construction using rotational isomeric state model	213
	Appendix C Supporting Information for Chapter 4	224
C.1	Harmonic Potential with $b = 0$	224
C.2	Preliminaries: Linear Brownian Dynamics of Polymer with $b = 0$	225
C.2.1	Linear Structure	225
C.2.2	Ring Structure	227
C.2.3	Star Structure	229
C.3	$\sqrt{\langle R_g^2 \rangle}$ of Polyethylene with Different Structures in BD and MD Simulations	231
C.4	D_{cm} of Polyethylene with Different Structures in BD and MD Simulations	232
C.5	$\sqrt{\langle R^2 \rangle}$ of Polyethylene with Different Structures in BD Simulation Compared with $\sqrt{NC_\infty b_0}$	234
C.6	C++ Program for Numerical Simulation of Star Polymer with $b = 0$	234
C.7	C++ Program for Numerical Simulation of Star Polymer with $b = 4.42 \text{ \AA}$	241
C.8	Proper Orthogonal Decomposition Analysis	259
	Appendix D Supporting Information for Chapter 6	265
D.1	PRISM Theory Calculation Program	265

Appendix E Supporting Information for Chapter 8	268
E.1 First Approximation	268
E.2 Evaluation of the Component p_{xy}	269
E.3 Integration in Evaluation of η_d	271
E.4 Normal Distribution Approximation of $\int_{\phi^+}^{\infty} P_d(\phi)d\phi$	272
E.5 $\hat{\omega}(k)$ of Polyethylene with Different Structures	274
E.6 Intramolecular Contribution to the Equation of State	276

List of Tables

1.1	Molecular weight dependence of D_{cm} and η below and above M_c for polyethylene at $T = 450$ K.	2
1.2	Formulae of $\langle r^2 \rangle$ for different model chains.	28
1.3	Z as a function of n for $\sigma = 0.543$ and $\omega = 0.088$	31
4.1	β_1 and τ_1 of the most dominant eigenmodes in BD simulation, and τ_1^R in the classic Rouse model as presented in the Supporting Information. ($N = 50$ for linear and ring structures, and $N = 49$ for star structure)	76
4.2	β_1 and τ_1 of the most dominant eigenmodes in MD simulation. ($N = 50$ for linear and ring structures, and $N = 49$ for star structure)	82
4.3	τ_v of time correlation functions of different vectors in Rouse model, BD simulation and MD simulation. ($N = 50$ for linear and ring structures, and $N = 49$ for star structure)	85
5.1	Number of chains, box dimension and root-mean-square radius of gyration in the MD simulation for systems with different N	96
5.2	Fitting results of the parameters a and b in the gamma distribution	105
6.1	Number of rings, dimension of the box and root-mean-square radius of gyration of ring PE melts.	117
6.2	Fitting results of the parameters a and b in the gamma distribution.	125
8.1	r_c , r^+ and α for polyethylene with different structures at $T = 450$ K. These quantities are not dependent significantly on M	164
8.2	T dependence of different r_c , r^+ and α of linear polyethylene chain with $M = 2128 \text{ g} \cdot \text{mole}^{-1}$	165
8.3	Parameter B of polyethylene with three different structures and M . These values are listed in this Table as the difference is not obvious as depicted in Figure 8.4b at $T = 450$ K. Yet, we found that a small difference in B can lead to a significant disparity in free volume calculation.	166
8.4	Parameter B as a function of temperature for linear polyethylene with $M = 1190 \text{ g} \cdot \text{mole}^{-1}$, $M = 2128 \text{ g} \cdot \text{mole}^{-1}$ and $M = 11306 \text{ g} \cdot \text{mole}^{-1}$. The change in these values of parameters B with temperature are listed in this Table as it is not obvious as shown in Figure 8.5b.	168
8.5	Slopes of the linear curves as shown in Figure 8.6 for polyethylene with different structures, as well as the corresponding values of $\phi^+ - F$	171
8.6	GvdW parameters obtained at different temperatures and the very same value of ϕ^+ evaluated from above results were input in Equation (8.20) to calculate $\eta(T)$ for polyethylene with different M and structures. The apparent activation energy E_a^{app} is derived from fitting of both the calculated and experimental data to an Arrhenius form.	172

List of Figures

1.1	A box containing multiple compartments with the same N , V and T	9
1.2	(a) Direct and (b) indirect interactions between particle 1 and particle 2 in a many-body system. Particle 3 can influence the motion of particle 1 by indirectly interacting with particle 2.	12
1.3	Radial distribution function of monatomic liquid at different number densities.	14
1.4	Calculated pressure as a function of number density.	15
1.5	A plate on the top of the fluid moving with a velocity of U , leading to a velocity gradient. It is argued that the momentum can transfer along the z direction, and most of the momentum transfer is from above as the velocity of the particle near the top is faster.	21
1.6	An illustration of one particle traveling at a velocity of v_r , colliding with another stationary particle. Collision is elastic in this case, that the magnitude of v_r does not change after the collision.	23
1.7	$p_{g+;i}$ of different bond i and different n . The $p_{g+;i}$ for $n > 2$ is shifted up for better presentation purpose.	32
1.8	x and y components of $\langle \vec{r} \rangle$ evaluated using Equation (1.188) at different n	34
1.9	x and y components of $\langle \vec{r} \rangle$ at different n for polyethylene in interdependent hindered rotation model.	35
1.10	C_n at different n for polyethylene for free rotation model, independent hindered rotation model as well as interdependent hindered rotation model.	36
2.1	Different bonded potentials, such as (a) harmonic bond stretching potential, (b) angle bending potential and (c) angle torsion potential, in MD simulation. (cf., Equation (2.17), Equation (2.18) and Equation (2.19))	41
2.2	Illustration of periodic boundary condition in MD simulation. (This figure was created by Germain Salvato-Vallverdu and the corresponding source file can be found on http://www.texample.net/tikz/examples/periodic-boundaries-conditions/ .)	43
2.3	Illustration of sampling for time averaging of time correlation function and mean-square-displacement for a MD trajectory with six snapshots from 0 ps to 5 ps (represented by the blue circle).	47
2.4	Voronoi tessellation of a 2D system with only four points.	48
2.5	A more complicated example of Voronoi tessellation in two dimensional space.	49
3.1	Normal mode time correlation functions for different cases.	60
3.2	Velocity time correlation functions for different cases.	60
3.3	Time correlation functions of \mathbf{R} and \mathbf{v}_n	61
4.1	Final configurations of polyethylene with different structures after the NVT MD simulation. ($N = 50$ for linear and ring structures, and $N = 49$ for star structure)	70
4.2	The first three most dominant eigenmodes in different directions obtained from the POD analysis in linear structure.	73

4.3	The first three most dominant eigenmodes in different directions obtained from the POD analysis in the ring structure.	74
4.4	The first three most dominant eigenmodes in different directions obtained from the POD analysis in the star structure.	75
4.5	Time correlation functions of different eigenmodes in BD simulation. ($N = 50$ for linear and ring structures, and $N = 49$ for star structure)	76
4.6	N/p dependence of τ_p for polyethylene with different structures. (BD)	77
4.7	Nomenclature of different bead in polyethylene with different structures. . .	78
4.8	Time correlation functions of different vectors of linear, ring and star structures ($b = 4.42 \text{ \AA}$) ($N = 50$ for linear and ring structures, and $N = 49$ for star structure).	79
4.9	First three most dominant eigenmodes of one of the many chains in x direction for different molecular structures of polyethylene.	80
4.10	Time correlation functions of different eigenmodes in many-chain systems of linear, ring and star polyethylene. ($N = 50$ for linear and ring structures, and $N = 49$ for star structure)	81
4.11	N/p dependence of τ_p for polyethylene with different structures. (MD simulation)	83
4.12	Time correlation functions of different vectors ($N = 50$ for linear and ring structures, and $N = 49$ for star structure) (MD simulation).	84
4.13	η_0 of polyethylene with linear, ring and star structures in BD and MD simulations, and comparison with the literature data.	86
5.1	Final configuration of $N = 105$ linear chains with imposed periodic boundary condition in MD simulation.	95
5.2	Number density of the bead in the system with different N fitted to an empirical function: $\rho_b = \rho_{b,\infty} - \frac{C_1}{N}$ with $\rho_{b,\infty} = 32.760 \text{ nm}^{-3}$ and $C_1 = 83.759 \text{ nm}^{-3}$	96
5.3	Mean-square displacements for different numbers of polymer chains used in the MD simulations with (a) $N = 30$ and (b) $N = 405$	97
5.4	$g(r)$, $\omega(r)$, $\omega_{bond}(r)$ and $I(r)$ as a function of r for polyethylene chain with $N = 405$ obtained in MD simulation.	101
5.5	N dependence of $\langle v_f \rangle$ and B as determined from the GvdW.	102
5.6	Determined value of E_a in this work, compared with that of von Meerwall <i>et al.</i> [1] at $T = 450 \text{ K}$ and $\phi^+ = 0.22$	103
5.7	(a) Distribution of Voronoi cell volume in linear chain with different N . (b) F derived from the Voronoi cell analysis and the solid line is Equation (5.34).	105
5.8	Dependence of the probability of finding the critical volume upon N . The solid line is the empirical function: $C_1 + C_2/N$ with $C_1 = 0.252$ and $C_2 = 1.10$ determined by Equation (5.3), as well as $C_1 = 0.172$ and $C_2 = 3.38$ determined by Equation (5.34).	105
5.9	P_d distribution extracted directly from VT of the MD data and compared with the approximation using Equation (5.11).	106
5.10	N dependence of (a) D_{cm} as well as (b) \mathcal{P} in linear polymer with MD simulation data and other literature data compared with our theory (cf., Equation (5.4)).	107
6.1	The methylene groups of a ring PE (left) are coarse-grained to beads (right) in all our calculations.	111
6.2	Final snapshot of MD simulation of ring PE with $N = 305$ at $T = 450 \text{ K}$. . .	115
6.3	Number density of beads at different N at $T = 450 \text{ K}$. The data are fitted to the empirical relation $C_1 - C_2/N$ with $C_1 = 32.7 \text{ nm}^{-3}$ and $C_2 = 23.8 \text{ nm}^{-3}$	117
6.4	$g(r)$ and $I(r)$ of ring PE with $N = 405$ from the PRISM theory.	118
6.5	Compressibility factor, B and $\langle v_f \rangle_{ideal}$ as a function of N . The solid lines depicted are guides only.	119

6.6	Temperature dependence of (a) $g(r)$, (b) f and (c) r^+ for ring PE with $N = 80$ obtained by the PRISM theory. The data reported in (b) were fitted to the relation $f = C_1 + C_2T$ with $C_1 = -0.0373$ and $C_2 = 0.00107 \text{ K}^{-1}$. The data in (c) were fitted to Equation (6.26) with $d_0 = 0.404 \text{ nm}$ and $d_1 = 0.0563 \text{ K}^{-0.5}$.	120
6.7	$g(r)$, $\omega(r)$, $\omega_{bond}(r)$ and $I(r)$ of ring polymer with $N = 405$ from MD simulation.	123
6.8	N dependence of B and $\langle v_f \rangle$. The solid lines depicted are guides only.	124
6.9	Probability distribution functions of the free volume in the ring PE melts as determined by the Voronoi tessellation for $N = 30$, $N = 105$, $N = 205$, $N = 305$ and $N = 405$, and the cumulative distribution functions for all ring PEs. The data in (a) and (b) were fitted to probability distribution function and cumulative distribution function of the gamma distribution, respectively, with the parameters as shown in Table 8.1.	125
6.10	Probability of finding v_i^* for ring PE with different N . The data were fitted to the relation: $F = C_1 + C_2/N$ and $F_{ct} = C_{1,ct} + C_{2,ct}/N$. The values of the parameters are $C_1 = 0.141$ and $C_2 = 0.886$, as well as $C_{1,ct} = 0.252$ and $C_{2,ct} = 0.107$.	126
6.11	$P_d(\phi)$ distribution extracted directly from VT of the MD data and compared with the approximation using Equation (6.3) for (a) $N = 105$ and (b) $N = 405$.	127
6.12	Temperature dependence of (a) $g(r)$ as well as (b) f of ring PE with $N = 80$ obtained from MD simulation. The data reported in (b) were fitted to the relation $f = C_1 + C_2T$ with $C_1 = -0.04$ and $C_2 = 8.74 \times 10^{-4} \text{ K}^{-1}$.	128
6.13	Log-log plots of $g_{cm}(t)$ of ring PEs with $N = 30$ and $N = 405$. The slopes and the y -intercepts of the black linear curves are 1.00 and $5.45 \times 10^{-3} \text{ nm}^2$, as well as 1.04 and $9.58 \times 10^{-5} \text{ nm}^2$, for $N = 30$ and $N = 405$, respectively, which were then used in the calculation of D_{cm} .	129
6.14	N dependence of (a) D_{cm} and (b) \mathcal{P}/N of ring PE melts. D_{cm} calculated from our MD simulation and theory are compared with Hur <i>et al.</i> [2, 3], Tsolou <i>et al.</i> [4], Brown <i>et al.</i> [5] and Halverson <i>et al.</i> [6].	130
6.15	Temperature dependence of D_{cm} of ring PE with $N = 80$. $\phi^+ = 0.17$ for MD simulation and $\phi^+ = 0.47$ for the PRISM theory. The solid line is the fitting curve to the MD data, which has the form of $D_{cm}(T) = D_{cm}(T') \exp \left[-E_a^{app} \left(\frac{1}{RT} - \frac{1}{RT'} \right) \right]$, with $E_a^{app} = 3.84 \text{ kcal} \cdot \text{mole}^{-1}$.	133
7.1	$g(r)$ derived from Equation (7.8) and Equation (7.13). The scalar approximation in Equation (7.13) is indeed accurate.	141
7.2	$g(r)$ at different temperatures for alkane with $N = 30$.	143
7.3	$I(r)$ at different temperatures for alkane with $N = 30$.	143
7.4	F_{ct} s at different chain lengths of alkane and temperatures, which were obtained from the free volume analysis. The markers are results from our calculations, and the solid lines are best fit to the data with the form: $C_1/N + C_2$. The values of C_1 and C_2 are: $C_1 = 0.52$, $C_2 = 0.2$ ($T = 343.5 \text{ K}$); $C_1 = 0.61$, $C_2 = 0.22$ ($T = 363.5 \text{ K}$); $C_1 = 0.72$, $C_2 = 0.25$ ($T = 383.5 \text{ K}$); $C_1 = 0.77$, $C_2 = 0.28$ ($T = 403.5 \text{ K}$); $C_1 = 0.86$, $C_2 = 0.31$ ($T = 423.5 \text{ K}$); $C_1 = 0.93$, $C_2 = 0.33$ ($T = 443.5 \text{ K}$).	144
7.5	Effect of temperature on $P_d(\phi)$ distribution of oligomer with $N = 30$.	145
7.6	Effect of chain length on $P_d(\phi)$ distribution of oligomers at $T = 443.5 \text{ K}$.	146
7.7	D_{cm} calculated using our free volume theory (markers) with that of the experimental data of von Meerwall <i>et al.</i> [1] (solid lines). The indicated slopes are the values calculated from our theory.	147

7.8	The magnitude of the integral $\frac{1}{N} \int_{\phi^+}^1 P_d(\phi) d\phi$ computed using our free volume theory at different temperatures (markers) fitted to the linear curves (solid lines).	147
8.1	A summary of a free volume approach for calculating η and D_{cm}	155
8.2	Compressibility factor with and without incorporation of intramolecular term in the pressure equation as a function of M for linear chain, ring as well as four-arm symmetrical star at $T = 450$ K.	162
8.3	A plot of $I(r)$ as a function of r for polyethylene with different structures. Four length scales r_c , r^+ , r_{pm} and r_{fm} are extracted from this plot at $T = 450$ K.	165
8.4	GvdW parameters A and B as a function of M for polyethylene with different structures at $T = 450$ K. A and B are calculated using Equation (8.41) and Equation (8.42). The solid lines are guides only.	166
8.5	GvdW parameters A and B as a function of T for linear polyethylene chain with different M . A and B are calculated using Equation (8.41) and Equation (8.42). The solid lines are guides only.	167
8.6	Zero-shear viscosity as a function of M for polyethylene with different structures at $T = 450$ K calculated using Equation (8.19) and the parameters obtained from the free volume analysis (filled markers). Our calculation results of linear polyethylene were compared with experimental data by Pearson <i>et al.</i> (\square) [7] as well as simulation data of Padding and Briels (\triangle) [8], as well as Halverson <i>et al.</i> (∇) [6]. Results for ring polyethylene were compared with simulation data by Halverson <i>et al.</i> (\diamond) [6] as well as Tsolou <i>et al.</i> (\triangleright) [4]. Results for four-arm symmetrical star polyethylene are compared with our MD simulation data (\triangleleft) [9]. It should be noted that the data from Halverson <i>et al.</i> [6] have been shifted accordingly to compare with our theory as in their work, the viscosity are in reduced unit. Note that the blue, red and green colours as depicted in the plots correspond to linear, ring and four-arm symmetrical polyethylene, respectively. Slopes of these linear curves below and above M_c are listed in Table 8.5.	169
8.7	Temperature dependence of η for linear polyethylene chain with $M = 1190$ g · mole ⁻¹ , $M = 2128$ g · mole ⁻¹ and $M = 11396$ g · mole ⁻¹ . The filled markers are data calculated using Equation (8.20) and the unfilled markers are experimental data of Pearson <i>et al.</i> [7]. The solid and dashed linear curves are fitting of the calculated and the experimental to the Arrhenius relation, which gives us the apparent activation energy in Table 8.6.	173
A.1	Indices of beads in four-arm star polyethylene $N = 9$. This figure is reproduced with permission from [9].	197
A.2	Flow chart showing the procedure of POD analysis.	200
A.3	Dependence of zero-shear viscosities on size of polymer in the unentangled regime of our nonlinear Brownian dynamic and MD simulation data compared with other simulation and experimental data from other research groups. These figures are reproduced with permission from [9].	205
B.1	Initial conformation of chain with $N = 50$ in the numerical simulation described in the letter, which is generated using the Python 3.5 program above.	223
C.1	Time correlation function of the end-to-end vector of a linear polyethylene compared with the exact solution.	226
C.2	Time correlation function of the m -to- n vector of the ring structure compared with the exact solution.	228
C.3	Eigenfunctions for the three most dominant normal modes of the star structure with $N = 49$	230

C.4	τ_p in star polymer with $N = 49$	230
C.5	Time correlation function of the arm vector compared with the exact solution.	231
C.6	$\sqrt{\langle R_g^2 \rangle}$ of polyethylene with linear, ring and star structures in BD and MD simulations as well as the literature data.	232
C.7	Comparison of D_{cm} derived from MD simulation with different references in the literature.	233
C.8	$\sqrt{\langle R^2 \rangle}$ of polyethylene with linear, ring and star structures in BD as well as that calculated by $\sqrt{NC_\infty}b_0$	234
S1	Comparison of $\int_{\phi^+}^{\infty} P_d(\phi)d\phi$ as a function of N evaluated using Equation (E.41) and Equation (18) with $F = 0.45$ and $x = 2$, as well as $\phi^+ = 0.49$ and $\phi^+ = 0.50$ in the former and latter cases, respectively.	273
S2	Nomenclature of different bead in polyethylene with different structure.	275

Lists of Symbols

List of Symbols for Section 1.1 to Section 1.4

a_i	Number of compartments at the i th energy level
a_i^*	Number of compartments at the i th energy level as $\mathcal{A}_{total} \rightarrow \infty$
\mathcal{A}_{total}	Total number of compartments in NVT ensemble
$c(r)$	Direct correlation function
$\hat{c}(k)$	Fourier transform of $c(r)$
$\delta(t)$	Dirac delta function
D	Diffusivity of particle
D_{cm}	Center-of-mass diffusion coefficient of polymer
η	Zero-shear viscosity
E_i	i th energy level in NVT ensemble
E_{total}	Total energy of the box in NVT ensemble
f	Phase space function
f_j	Phase space function of j th particle
\mathbf{F}	Force vector in 3D space
\mathbf{F}_j	Force vector acting upon the j th particle in 3D space
F_k	Component of the force vector in k direction that k can be either x , y or z
$g^{(2)}(r)$ or $g(r)$	Radial distribution function
$h(r)$	$g(r) - 1$
$\hat{h}(k)$	Fourier transform of $h(r)$
k	Spring constant
k_b	Boltzmann constant
l	Mean free path of the particle
m	Mass of particle
$m(\mathbf{p}, \mathbf{q})$	Microscopic property of the system
m_j	Mass of the j th particle
\mathcal{M}	Macroscopic property of the system
M_c	Critical molecular weight
μ_{ij} or μ	$m_i m_j / (m_i + m_j)$
N	Number of particles
N_c	Critical chain length
\mathbf{p}	Vector containing the momenta of all particles in 3D space

$P^{(N)}$	Probability density of finding atom 1 at $d\mathbf{r}_1$, atom 2 at $d\mathbf{r}_2$, ..., atom N at $d\mathbf{r}_N$
\mathbf{q}	Vector containing the positions of all particles in 3D space
r	Distance between two particles
\mathbf{r}_j	Position vector of the j th particle
r_{ij}	Distance between i th and j th particles
ρ	Number density of particle
ρ_j	Number density of the j th particle
σ	Diameter of the particle
σ_{kl}	The k th and l th component of the stress tensor that k and l can be either x , y or z
t	Time
T	Temperature
$u(r)$	Intermolecular potential
$u_{ij}(r)$	Intermolecular potential between i th and j th particles
U_N	Total potential energy
v	Magnitude of \mathbf{v}
\mathbf{v}	Velocity vector of particle in 3D space
\mathbf{v}_c	Center-of-mass velocity vector in 3D space
\mathbf{v}_j	Velocity vector of the j th particle in 3D space
v_k	Component of \mathbf{v} in k direction that k can be either x , y or z
\mathbf{v}_r	Relative velocity vector in 3D space
$v(t)$	Velocity of particle in 1D space
V	Volume
$V(s)$	Laplace transform of $v(t)$
$w(r)$	Effective intermolecular potential
$W(\mathbf{a})$	Number of ways arranging compartments with different energy levels
$x(t)$	Position of particle in 1D space
$X(s)$	Laplace transform of $x(t)$
ζ	Friction coefficient with unit of mass per unit time

List of Symbols for Section 1.5

\mathbf{B}	Matrix containing eigenvectors of matrix \mathbf{U}_i
C_n	Chain length dependent characteristic ratio of polymer
C_∞	Characteristic ratio of polymer as $n \rightarrow \infty$
ε	Energy in the second-order transition in either g^+g^- or g^-g^+ states
E_g	Energy of gauche state
E_t	Energy of trans state
l^2	Square of the bond length
\vec{l}_i	Bond vector of the i th bond
$\mathbf{\Lambda}$	Matrix containing eigenvalues of matrix \mathbf{U}_i

n	Chain length of the polymer
ω	Boltzmann statistical weight corresponding to g^+g^- or g^-g^+ states
ϕ	Torsion angle
ϕ_g	Torsion angle for the gauche state
ϕ_t	Torsion angle for the trans state
\vec{r}	End-to-end vector
$\langle r^2 \rangle$	Mean-square end-to-end distance
R	Ideal gas constant
\mathbf{R}_i	Transformation matrix
σ	Product of Boltzmann statistical weights of trans and gauche states
θ	Bond angle
\mathbf{T}_i	The i th rotation matrix
\mathbf{U}_i	The i th matrix containing Boltzmann statistical weights
Z	Partition function

List of Symbols for Chapter 2

b or l	Equilibrium spring length
β_p	Stretching factor in the time correlation function of the p th eigenmode
c_p	Constant in the torsion potential
\mathbf{C}	Correlation matrix in the POD method
$C(\ddot{\mathbf{r}})$	Curvature function as proposed by Gauss
C_{ij}	i th and j th component of the correlation matrix \mathbf{C} in the POD method
Δt	Finite time step
ε	Potential well of 12-6 Lennard-Jones potential
\mathbf{F}	Force vector acting upon all particles.
\mathbf{F}_i	Force vector acting upon the i th particle
$\dot{\mathbf{F}}_i$	First derivative of \mathbf{F}_i with respect to time
\mathbf{F}_{ij}	Force vector acting upon the i th particle by the j th particle
$\dot{\mathbf{F}}_{ij}$	First derivative of \mathbf{F}_{ij} with respect to time
F_{ik}	k direction component of the force vector acting upon the i th particle
$g(\dot{\mathbf{r}})$	Constraint function
\mathbf{J}	Jacobian matrix
k	Spring constant
k_θ	Angle bending force constant
λ	Lagrange multiplier, which is equivalent to the friction coefficient with a unit of per unit time
m_i	Mass of the i th particle
$\mu_p(t)$	Time correlation function of the p th eigenmode
N	Total number of particles in the system (Section 2.1.1) or number of atoms of a polymer chain (Section 2.3.1)
N_{snap}	Number of snapshots of the MD trajectory

p	Pressure
ϕ	Torsion angle
$\tilde{\psi}_{pq}$	Normalized p th eigenmode in q direction
q_i	Position of the i th particle in q direction that q can be either x , y or z
$q'_i(t)$	Fluctuation in the position of the i th bead from the centre-of-mass of the polymer in q direction at time t
r	Distance between the i th and j th particle
\mathbf{r}	Position vector of all particles.
$\dot{\mathbf{r}}_i$	First derivative of position vector of the i th particle with respect to time
$\ddot{\mathbf{r}}_i$	Second derivative of position vector of the i th particle with respect to time
\mathbf{r}_{ij}	Distance vector between i th and j th particles
$\dot{\mathbf{r}}_{ij}$	First derivative of \mathbf{r}_{ij} with respect to time
r_{ik}	k direction component of the position vector of the i th particle
\mathbf{R}	End-to-end vector of linear polymer
\mathcal{R}_{iq}	Residue for the i th particle in q direction in numerical integration by implicit Euler method
σ	Distance between two particles when $u_{LJ} = 0 \text{ kJ} \cdot \text{mole}^{-1}$
τ_p	Relaxation time corresponding to the p th eigenmode
θ	Bond angle
θ_0	Equilibrium bond angle
u	Total potential
$u_{bending}(\theta)$	Angle bending potential
u_{LJ}	12-6 Lennard-Jones potential
$u_{torsion}(\phi)$	Torsion potential
$u_b(r_{ij})$	Bond stretching potential
\mathbf{v}	Velocity vector of all particles
V	Volume
$X'_{pq}(t)$	p th normal coordinate in q direction from POD analysis at time t
ξ	Friction coefficient with unit of per unit time
ζ	Friction coefficient with unit of mass per unit time

List of Symbols for Chapter 3

$f(t)$	Stochastic force acting upon a single particle
$\mathbf{f}_n(t)$	Force vector acting upon the n th bead at time t
$g_{n,q}$	Stochastic force acting upon the n th bead in q direction
k	Spring constant
k_b	Boltzmann constant
$-\lambda_p^2$	The p th eigenvalue of the operator $\partial^2/\partial n^2$
m	Mass of a bead or a single particle
n	Index of the bead of polymer
N	Chain length of polymer

\mathbf{q}	Vector containing positions and velocities of all beads of polymer in the q direction
$\mathbf{R}(t)$	End-to-end vector at time t
\mathbf{R}_n	Position vector of n th bead of polymer
$R_{n,q}$	Position of n th bead of the polymer in q direction
T	Temperature
v	Velocity of a single particle in 1D space
\mathbf{v}	Velocity vector of a single particle in 3D space
v_0	Initial velocity of a single particle in 1D space
$\mathbf{v}_n(t)$	Velocity vector of the n th bead at time t
$V_{n,q}$	Velocity of n th bead of the polymer in q direction
$\mathbf{V}_p(t)$	p th normal coordinate for velocity at time t
x	Position of a single particle in 1D space
x_0	Initial position of a single particle in 1D space
$\mathbf{X}_p(t)$	p th normal coordinate for position at time t
ξ	Friction coefficient with a unit of per unit time
ζ	Friction coefficient with a unit of mass per unit time

List of Symbols for Chapter 4

b	Equilibrium spring length in bond stretching potential
β_p	Stretching factor in the time correlation function of the p th eigenmode
\mathbf{C}	Correlation matrix in the POD method
C_∞	Characteristic ratio of polyethylene when $N \rightarrow \infty$
C_{ij}	i th and j th component of the correlation matrix \mathbf{C} in the POD method
d_{nm}	Distance between n th and m th beads of the polyethylene
\mathbf{d}_{nm}	Distance vector between the n th and m th beads of the polymer
Δt	Finite time step
η_0	Zero-shear viscosity of polyethylene melt
$\mathbf{f}_n(t)$	Stochastic force vector acting upon the n th bead at time t
\mathbf{F}_n	Bond stretching force acting upon the n th bead of the polymer
$F_{n,q}$	Bond stretching force acting upon the n th bead of the polymer in q direction
\mathbf{g}_n	Stochastic force vector acting on the n th bead of the polymer
$g_{n,q}$	Stochastic force acting upon n th bead in q direction
$G(t)$	Shear relaxation modulus of polyethylene melt at time t
\mathbf{J}	Jacobian matrix of bond stretching force
\mathbf{J}_{qs}	Element of Jacobian matrix in q, s directions
k	Spring constant
k_b	Boltzmann constant
l	Bead size
M	Molecular weight of polyethylene

$\mu_p(t)$	Time correlation function of the p th eigenmode
n	Index of the bead of polyethylene
N	Chain length of polyethylene
N_{snap}	Number of snapshots of the MD trajectory
ψ_p^q	p th eigenmode in q direction
$\tilde{\psi}_p^q$	Normalized p th eigenmode in q direction
\mathbf{q}	Position vector of all beads of the polyethylene
$\bar{q}(t)$	Center-of-mass of the polyethylene at time t in q direction
$q_i(t)$	Position of the i th bead at time t in q direction
$q'_i(t)$	Fluctuation in the position of the i th bead from the centre-of-mass of the polymer in q direction at time t
\mathbf{q}_j	Position vector of all beads of the polyethylene at the j th time step
\mathbf{q}_n	Position vector of the n th bead of the polyethylene
\mathbf{r}	Vector containing residues for all the beads of the polyethylene in the numerical integration using implicit Euler method
$r_{n,q}$	Residue for the n th bead in q direction
R	Ideal gas constant
$\mathbf{R}(t)$	Specific vector of linear, ring and four-arm symmetrical star polyethylene at time t
\mathbf{R}_n	Position vector of n th bead of polyethylene
$\langle R_g^2 \rangle$	Mean-square radius of gyration
ρ	Mass density of polyethylene melt
s_n or q_n	Position of the n th bead of the polymer in s or q direction that q or s can be either x , y or z
τ_1	Longest relaxation time
τ_1^R	Longest relaxation time in Rouse model
τ_p	Effective relaxation time corresponding to the p th eigenmode
τ_p^*	Relaxation time corresponding to the p th eigenmode
τ_v	Relaxation time of specific vector of linear, ring and four-arm symmetrical star polyethylene
T	Temperature
$\mathbf{X}_p(t)$	p th normal coordinate for position at time t
$X'_{pq}(t)$	p th normal coordinate in q direction from POD analysis at time t
ζ	Friction coefficient with a unit of mass per unit time

List of Symbols for Chapter 5

a and b	Parameters in the gamma distribution of free volume within the polymer melt
A and B	GvdW parameters
α	Overlapping parameter of free volume
β	$\frac{1}{k_b T}$

c	Normalization constant of P_d distribution
D	Diffusivity of monoatomic liquids
D_0	Chapman-Enskog self-diffusion coefficient
D_{cm}	Center-of-mass diffusion coefficient of polymer
E_a	Activation energy
ε	Small number with magnitude in the order of 10^{-5} or magnitude of the potential well for 6-12 Lennard-Jones potential
f	Fractional free volume
F	Probability for one single bead to find free volume being equal to or more than αv_i^+ as derived from the gamma distribution
F_{ct}	Cohen-Turnbull probability for one single bead to find free volume being equal to or more than v_i^+
$g(r)$	Intermolecular radial distribution function
$g_{cm}(t)$	Mean-square-displacement of center-of-mass of polymer
l_b	r at the maximum value of $I_b(r)$
M	Molecular weight of polymer
M_c	Critical molecular weight of polymer
n_f	Number of beads of polymer having sufficient free volume for diffusive motion
N	Chain length of polymer
$\omega(r)$	Intramolecular radial distribution function due to 6-12 Lennard Jones potential interaction average over all sites
$\omega^{\alpha,\gamma}(r)$	Intramolecular radial distribution function due to 6-12 Lennard Jones potential interaction between sites α and γ
$\omega_{bond}(r)$	Intramolecular radial distribution function due to bond stretching potential interaction average over all sites
$\omega_{bond}^{\varepsilon,\varepsilon+1}(r)$	Intramolecular radial distribution function due to bond stretching potential interaction between sites ε and $\varepsilon + 1$
ϕ	Fraction of beads of polymer having sufficient free volume for diffusive motion
ϕ^+	Critical fraction of beads of polymer having sufficient free volume for diffusive motion
p	Pressure
p_{eff}	Effective pressure
P	Probability distribution of free volume
\mathcal{P}	$\int_{\phi^+}^1 P_d d\phi$
P_d	Distribution of fraction of beads of polymer having sufficient free volume for diffusive motion
r	Distance between two beads
r^+	Effective diameter of the bead
r_c	Leviation diameter of the bead
r_{fm}	Distance corresponding to the force minimum due to $u(r)$
$\mathbf{r}_i(t)$	Position vector of the i th bead of polymer at time t
r_{pm}	Distance corresponding to the potential minimum of $u(r)$

$\mathbf{r}_{\text{cm}}(t)$	Center-of-mass position vector of polymer at time t
$\langle r_b^2(t) \rangle$	Mean-square-displacement of one bead of the polymer
$\langle r_{\text{cm}}^2(t) \rangle$	Mean-square-displacement of the center-of-mass of polymer at time t
$\langle r_i^2(t) \rangle$	Mean-square-displacement of the i th bead of the polymer
ρ	Number density of polymer
ρ_b	Number density of beads
$\rho_{b,\infty}$	Number density of beads as $N \rightarrow \infty$
R	Ideal gas constant
$\langle R_g^2 \rangle$	Mean-square radius of gyration
σ	Distance between beads at the minimum of 6-12 Lennard-Jones potential
T	Temperature
$u(r)$	6-12 Lennard-Jones potential
$u_{\text{bond}}(r)$	Bond stretching potential
v_c	Leviation volume of the bead
v_i^+	Effective diameter of particle or the i th bead
v_i^*	Activation volume of the i th bead used in the calculation of F derived from the Voronoi distribution of free volume
V	Volume of the system
$\langle v_f \rangle$	Mean free volume in monoatomic liquid or per polymer chain
$\langle v_{f,i} \rangle$	Mean free volume for the i th bead

List of Symbols for Chapter 6

a and b	Parameters in the gamma distribution of free volume within the polymer melt
A and B	GvdW parameters
α	Overlapping parameter of free volume
β	$\frac{1}{k_b T}$
c	Normalization constant of P_d distribution
$c(r)$	Direct correlation function
$\hat{c}(k)$	Fourier transform of direct correlation function
$\mathbf{C}(r)$	Matrix containing the direct correlation function between different beads of the ideal ring polymer
$\mathbf{\Omega}(r)$	Matrix containing the intramolecular distribution functions between different sites of the ideal ring polymer
D	Diffusivity of monoatomic liquids
D_0	Chapman-Enskog self-diffusion coefficient
D_{cm}	Center-of-mass diffusion coefficient of polymer
E_a	Activation energy
E_a^{app}	Apparent activation energy
ε	Small number with magnitude in the order of 10^{-5} or magnitude of the potential well for 6-12 Lennard-Jones potential

f	Fractional free volume
F	Probability for one single bead to find free volume being equal to or more than αv_i^+ as derived from the gamma distribution
F_{ct}	Cohen-Turnbull probability for one single bead to find free volume being equal to or more than v_i^+
$g(r)$	Intermolecular radial distribution function average over all sites
$g_{cm}(t)$	Mean-square-displacement of center-of-mass of polymer
$h(r)$	$g(r) - 1$
$\hat{h}(k)$	Fourier transform of $h(r)$
k_{bond}	Spring constant in bond stretching potential
l_b	r at the maximum value of $I_b(r)$
M	Molecular weight of polymer
M_c	Critical molecular weight of polymer
n_f	Number of beads of polymer having sufficient free volume for diffusive motion
N	Chain length of polymer
N_c	Critical chain length of polymer
$\omega(r)$	Intramolecular radial distribution function of an ideal ring polymer average over all sites (in PRISM) or that due to 6-12 Lennard Jones potential interaction average over all sites (in MD simulation)
$\omega^{\alpha,\gamma}(r)$	Intramolecular radial distribution function due to 6-12 Lennard Jones potential interaction between sites α and γ
$\omega_{bond}(r)$	Intramolecular radial distribution function due to bond stretching potential interaction average over all sites
$\omega_{bond}^{\varepsilon,\varepsilon+1}(r)$	Intramolecular radial distribution function due to bond stretching potential interaction between sites ε and $\varepsilon + 1$
ϕ	Fraction of beads of polymer having sufficient free volume for diffusive motion
ϕ^+	Critical fraction of beads of polymer having sufficient free volume for diffusive motion
p	Pressure
p_{eff}	Effective pressure
\mathcal{P}	$\int_{\phi^+}^1 P_d d\phi$
P_d	Distribution of fraction of beads of polymer having sufficient free volume for diffusive motion
r	Distance between two beads
r^+	Effective diameter of the bead
r_c	Leviation diameter of the bead
r_{fm}	Distance corresponding to the force minimum due to $u(r)$
$\mathbf{r}_i(t)$	Position vector of the i th bead of polymer at time t
r_{pm}	Distance corresponding to the potential minimum of $u(r)$
$\mathbf{r}_{cm}(t)$	Center-of-mass position vector of polymer at time t
ρ	Number density of polymer
ρ_b	Number density of beads

$\rho_{b,\infty}$	Number density of beads as $N \rightarrow \infty$
R	Ideal gas constant
$\langle R_g^2 \rangle$	Mean-square radius of gyration
T	Temperature
$u(r)$	6-12 Lennard-Jones potential
$u_{bond}(r)$	Bond stretching potential
v_c	Leviation volume of the bead
v_i^+	Effective diameter of particle or the i th bead
v_i^*	Activation volume of the i th bead used in the calculation of F derived from the Voronoi distribution of free volume
V	Volume of the system
$\langle v_f \rangle$	Mean free volume in monoatomic liquid or per polymer chain
$\langle v_f \rangle_{ideal}$	Mean free volume per ideal ring polymer
$\langle v_{f,i} \rangle$	Mean free volume for the i th bead

List of Symbols for Chapter 7

A and B	GvdW parameters
α	Overlapping parameter of free volume
β	$\frac{1}{k_b T}$
c	Normalization constant of P_d distribution
$c(r)$	Direct correlation function average over all sites
$c_{\alpha,\gamma}(r)$	Direct correlation function between sites α and γ
$\hat{c}(k)$	Fourier transform of direct correlation function
$\mathbf{C}(r)$	Matrix containing the direct correlation function between different beads of the oligomer
$\hat{\mathbf{C}}(k)$	Fourier transform of $\mathbf{C}(r)$
D	Diffusivity of monoatomic liquids
D_0	Chapman-Enskog self-diffusion coefficient
D_{cm}	Center-of-mass diffusion coefficient of oligomer
E_a	Activation energy
E_a^{app}	Apparent activation energy
ε	Small number with magnitude in the order of 10^{-5}
$\varepsilon_{\alpha\gamma}$	Potential well for 6-12 Lennard-Jones potential between sites α and γ
F_{ct}	Cohen-Turnbull probability for one single bead to find free volume being equal to or more than αv_i^+
$g(r)$	Intermolecular radial distribution function average over all sites
$g_{\alpha\gamma}(r)$	Intermolecular radial distribution function between sites α and γ
$h(r)$	$g(r) - 1$
$\hat{h}(k)$	Fourier transform of $h(r)$ average over all sites
$\hat{h}_{\alpha\gamma}(k)$	Fourier transform of $h(r)$ between sites α and γ
k_b	Boltzmann constant

m	Mass of a bead
M	Molecular weight of oligomer
n_f	Number of beads of oligomer having sufficient free volume for diffusive motion
N	Chain length of oligomer
$\omega(r)$	Intramolecular radial distribution function of oligomer average over all sites
$\omega^{\alpha,\gamma}(r)$	Intramolecular radial distribution function between sites α and γ
$\hat{\omega}(k)$	Fourier transform of $\omega(r)$
$\mathbf{\Omega}(r)$	Matrix containing the intramolecular distribution functions between different sites of the oligomer
$\hat{\mathbf{\Omega}}(k)$	Fourier transform of $\mathbf{\Omega}(r)$
p	Pressure
p_{eff}	Effective pressure
P_d	Distribution of fraction of beads of oligomer having sufficient free volume for diffusive motion
ϕ	Fraction of beads of oligomer having sufficient free volume for diffusive motion
ϕ^+	Critical fraction of beads of oligomer having sufficient free volume for diffusive motion
r	Distance between two beads
r^+	Effective diameter of the bead
r_c	Leviation diameter of the bead
r_{fm}	Distance corresponding to the force minimum due to $u(r)$
r_{pm}	Distance corresponding to the potential minimum of $u(r)$
ρ	Number density of oligomers
ρ_1	Extrapolated number density of the particle
ρ_b	Number density of beads
R	Ideal gas constant
T	Temperature
$u(r)$	6-12 Lennard-Jones potential
$u_{\alpha\gamma}(r)$	6-12 Lennard-Jones potential between sites α and γ
v^+	Critical free volume for the activation of diffusive motion in monoatomic liquids
v_i^+	Critical free volume for the activation of diffusive motion of the i th bead
$\langle v_f \rangle$	Mean free volume per oligomer or in monoatomic liquids
$\langle v_{f,i} \rangle$	Mean free volume for the i th bead

List of Symbols for Chapter 8

A and B	GvdW parameters
α	Overlapping parameter of free volume

β	$\frac{1}{k_b T}$
\mathbf{c}	Velocity vector of a bead
\mathbf{c}_0	Flow velocity vector of beads
$c_{0,k}$	Flow velocity of beads in k direction
\mathbf{C}	Peculiar velocity vector of a bead
C_k	Peculiar velocity of a bead in the k direction
$\langle C \rangle$	Average peculiar velocity of a bead
D_{cm}	Center-of-mass diffusion coefficient of polymer
ε	Potential well of 6-12 Lennard-Jones potential
η_0	Viscosity of a bead in a dilute polymer medium
η_d	Viscosity of polymer in a dilute medium
E_a^{app}	Apparent activation energy
F	Cohen-Turnbull probability for one single bead to find free volume being equal to or more than αv_i^+
$g(r)$	Intermolecular radial distribution function average over all sites
$h(r)$	$g(r) - 1$
$\hat{h}(k)$	Fourier transform of $h(r)$
$\hat{h}_{\alpha,\gamma}(k)$	Fourier transform of $h(r)$ between sites α and γ
k_b	Boltzmann constant
k_{bond}	Force constant in bond stretching potential of polyethylene
m	Mass of a bead
M	Molecular weight of polyethylene
M_a	Molecular weight of the arm of four-arm symmetrical polyethylene
M_c	Critical molecular weight of polyethylene
M_e	Entanglement molecular weight of polyethylene
n_f	Number of beads of polymer having sufficient free volume for diffusive motion and momentum transfer
N	Chain length of polyethylene
$\omega(r)$	Intramolecular radial distribution function of polyethylene average over all sites
$\hat{\omega}(k)$	Fourier transform of $\omega(r)$
$\hat{\omega}_{\alpha,\gamma}(k)$	Fourier transform of $\omega(r)$ between sites α and γ
$\mathbf{\Omega}(r)$	Matrix containing the intramolecular distribution functions between different sites of polyethylene
$\hat{\mathbf{\Omega}}(k)$	Fourier transform of $\mathbf{\Omega}(r)$
ϕ	Fraction of beads of polymer having sufficient free volume for momentum transfer
ϕ^+	Critical fraction of beads of polymer having sufficient free volume for momentum transfer
p	Pressure
p_{eff}	Effective pressure
$P(r)$	Probability distribution function of the distance between two beads within the same Gaussian chain molecule

P_1	Pressure in Gaussian chain molecules without any intermolecular interaction
P_d	Distribution of fraction of beads of polymer having sufficient free volume for momentum transfer
$\Psi^{(0)}$	Normal solution to the Boltzmann equation
$\Psi^{(1)}$	First approximation of the solution to the Boltzmann equation
r	Distance between two beads
r^+	Effective diameter of the bead
r_c	Leviation diameter of the bead
r_{fm}	Distance corresponding to the force minimum due to $u(r)$
r_{pm}	Distance corresponding to the potential minimum of $u(r)$
$\langle r^2 \rangle$	Mean-square distance between two beads within the same chain
ρ	Number density of polyethylene chains
ρ_b	Number density of beads
R	Ideal gas constant
σ	Diameter of a hard-sphere bead or the distance at the 6-12 Lennard-Jones potential minimum
T	Temperature
$u(r)$	6-12 Lennard-Jones potential
v^+	Critical free volume for the activation of diffusive motion in monoatomic liquids
v_i^+	Critical free volume for the activation of diffusive motion of the i th bead
$\langle v_f \rangle$	Mean free volume per polyethylene or in monoatomic liquids
$\langle v_{f,i} \rangle$	Mean free volume for the i th bead
$\mathcal{W}(R)$	The required work done to move the beads in dense polymer melt for a particular distance R per a factor of $2\pi/3$
W	Number of ways to arrange n_f beads for a polymer with N
$y(r)$	Direct correlation function average over all sites
$\hat{y}(k)$	Fourier transform of direct correlation function
$\mathbf{Y}(r)$	Matrix containing the direct correlation function between different beads of polyethylene
$\hat{\mathbf{Y}}(k)$	Fourier transform of $\mathbf{Y}(r)$

List of Symbols for Appendix A

b	Statistical segmental length of the polymer
β_p	Stretching factor in the time correlation function of the p th eigenmode
C_∞	Characteristic ratio of polyethylene when $N \rightarrow \infty$
\mathbf{C}	Correlation matrix in the POD method
C_{ij}	i th and j th component of the correlation matrix \mathbf{C} in the POD method
D	Diffusivity of particle
D_{cm}	Center-of-mass diffusion coefficient of polymer

η	Viscosity
η_0	Zero-shear viscosity of polyethylene melt
$f(t)$	Stochastic force acting upon a single particle at time t
$f_{p,i}$	The p th relaxation mode of the i th atom in the relaxation mode analysis
$\mathbf{f}_n(t)$	Stochastic force vector acting upon the n th bead at time t
\mathbf{F}_j	Force vector acting upon the j th bead
\mathbf{F}_{ij}	Force vector acting upon the i th bead by j th bead
$G(t)$	Shear relaxation modulus of polyethylene melt at time t
k	Spring constant
k_b	Boltzmann constant
$-\lambda_p$	The p th eigenvalue in the relaxation mode analysis
$-\lambda_p^2$	The p th eigenvalue of the operator $\partial^2/\partial n^2$
m	Mass of a bead or a single particle
M	Molecular weight of polyethylene
$\mu_p(t)$	Time correlation function of the p th eigenmode
n	Index of the bead of polymer
N	Chain length of polymer
N_c	Critical chain length of polymer
N_{snap}	Number of snapshot of the MD trajectory
ψ_p^q	p th eigenmode in q direction
$\tilde{\psi}_p^q$	Normalized p th eigenmode in q direction
ψ_p	
$\bar{q}(t)$	Center-of-mass of the polymer at time t in q direction
$q_i(t)$	Position of the i th bead at time t in q direction
$q'_i(t)$	Fluctuation in the position of the i th bead from the centre-of-mass of the polymer in q direction at time t
$\mathbf{r}_n(t)$	Position vector of n th bead of polymer at time t
\mathbf{r}_{ij}	Distance vector between i th and j th beads
R	Ideal gas constant
$\mathbf{R}(t)$	0-to- $(N - 1)/2$ vector of ring polymer at time t
ρ	Mass density of polymer melt
$\sigma(t)$	Stress tensor at time t
σ_{kl}	kl components of the stress tensor $\sigma(t)$ that k and l can be either x , y or z
τ_p	Effective relaxation time corresponding to the p th eigenmode
τ_p^*	Relaxation time corresponding to the p th eigenmode
T	Temperature
v	Velocity of a single particle in 1D space
\mathbf{v}	Velocity vector of a single particle in 3D space
v_0	Initial velocity of a single particle in 1D space
$\mathbf{v}_n(t)$	Velocity vector of the n th bead at time t
$\mathbf{v}_{\mathbf{k},\mathbf{n}}(t)$	Vector containing velocities of all beads of polymer in k direction at time t (k can be either x , y or z)
$V_{n,q}$	Velocity of n th bead of the polymer in q direction
$\mathbf{V}_p(t)$	p th normal coordinate for velocity of ring polymer at time t
$\mathbf{W}_p(t)$	Another p th normal coordinate for velocity of ring polymer at time t

x	Position of a single particle in 1D space
x_0	Initial position of a single particle in 1D space
\mathbf{x}_n	Vector containing positions of all beads of polymer in x direction
$\mathbf{X}_p(t)$	p th normal coordinate for position of ring polymer at time t
$X'_{pq}(t)$	p th normal coordinate in q direction from POD analysis at time t
ξ	Friction coefficient with a unit of per unit time
\mathbf{y}_n	Vector containing positions of all beads of polymer in y direction
$\mathbf{Y}_p(t)$	Another p th normal coordinate for position of ring polymer at time t
\mathbf{z}_n	Vector containing positions of all beads of polymer in z direction
ζ	Friction coefficient with a unit of mass per unit time

Chapter 1

Introduction

1.1 Overview of the thesis

There are three transport phenomena in nature, namely mass, momentum as well as energy transport. These quantities are always conserved and the corresponding transport processes are governed by the laws of conservation. Transport coefficients, such as diffusivity, viscosity and conductivity can be inferred from the equations of mass, momentum and energy transport, and they give us an idea of transfer rate of these entities. These transport coefficients can be evaluated theoretically by understanding science from a molecular point of view as demonstrated by Boltzmann in his kinetic theory of gas. Such theoretical understanding of transport phenomena can be also applied in the analysis of dense liquid, such as polymer melt, even though the problem has become more complex due to the strong intramolecular and intermolecular interactions of the polymer chains.

Polymers are macromolecules, which are ubiquitous in nature. For instance, DNA molecules in our body is one of the many examples of polymers that exist in nature, and they can exhibit shapes such as cyclic ring. Common synthetic polymers, such as polyethylene, polystyrene, have a wide range of applications in our daily lives as they are inexpensive materials. Transport coefficients of polymer melts exhibit peculiar dependence relation with their molecular weight as well as their structures. The most classic structure of polymer is a linear structure with two chain ends. Diffusivity and viscosity of such linear polymers both demonstrate a change in the molecular weight dependence relation as a function of molecular weight, i.e.

a crossover in the molecular weight dependence. Such crossover occurs at certain critical molecular weight (M_c) or critical chain length (N_c). To be explicit, for linear polyethylene, the change at $T = 450$ K is tabulated in Table 1.1.

Table 1.1: Molecular weight dependence of D_{cm} and η below and above M_c for polyethylene at $T = 450$ K.

Transport Coefficients	Below M_c	Above M_c
D_{cm}	$D_{cm} \sim M^{-1.5}$	$D_{cm} \sim M^{-2.3}$
η	$\eta \sim M^{1.8}$	$\eta \sim M^{3.4}$

The region below M_c and above M_c are known as unentangled and entangled regimes, respectively, due to several theoretical considerations. Interestingly, it is worthwhile to note that such M dependence also changes with temperature that the M dependence becomes weaker as temperature increases (cf., Chapter 7).

In polymer science literature, two classic theoretical models for unentangled and entangled regimes, known as Rouse model and reptation model, respectively, were developed to account for the M dependence of D_{cm} as well as η . Rouse model predicts that $D_{cm} \sim M^{-1}$ and $\eta \sim M^1$, which are slightly weaker than that as listed in Table 1.1. Generally, Rouse model is an equation of motion of Brownian dynamics of a polymer chain. From such equation of motion, one can obtain time correlation function of the positions of the beads, relaxation times of different normal modes and both D_{cm} as well as η of the polymer chain. Based on the Rouse model, we found an interesting mathematical problem, i.e. is it possible to obtain the velocity time correlation function from such a Rouse chain, and to see if integration of such velocity time correlation function will give us $D_{cm} \sim M^{-1}$? In addition, the Rouse model can be easily changed for polymers with different structures, such as ring and star shapes. The harmonic potential associated in the Rouse model can also be modified such that finite equilibrium distance between two beads is always a non-zero positive value to yield reasonable values of relaxation times as well as zero-shear viscosities of polyethylene melt.

Reptation theory is simply an equation of motion for chain in curvilinear coordinate. It is assumed that such chain is immersed in a medium of fixed obstacles as if there exists a many-chain effect on the motion of the polymer chain. The chain diffuses along the primitive path with diffusion coefficient obtained from the Rouse model. With this, the reptation

theory predicts $D_{cm} \sim M^{-2}$ and $\eta \sim M^3$, which are also weaker than that as listed in Table 1.1. Such theory also leads to questions, such as ‘How can one define an entanglement from first principle? How are these entanglements related to the many-chain effect? Why does this “many-chain effect” suddenly becomes so prominent once M is above M_c ?’ Indeed, these may not be hard questions, as the so-called many-chain effect can be easily understood armed with knowledge in thermodynamics.

Intuitively, the many-chain effect can be alternatively understood as the amount of free volume or distribution of free volume in a polymer melts. The success of free volume concept in polymer science is manifested in the account for temperature dependence of viscosity as well as glass transition phenomenon. The only limitation of free volume concept, to our knowledge, seems to be empirical nature of the theory, such as parameters in Williams-Landel-Ferry equation, that many parameters in free volume theory are empirical and they could be only obtained by curve fitting to experimental data. Nonetheless, these associated empirical parameters have physical meanings, and some of them can even be theoretically calculated. With these, an interesting question to ask is ‘Can we apply the free volume concept to account for the M dependence as listed in Table 1.1?’ Furthermore, as mentioned above, the M dependence as listed in Table 1.1 can also change with temperature, and such temperature effect is not captured by both Rouse model and reptation theory. On the contrary, the free volume concept should enable us to capture such temperature effect, as it is well known that free volume varies significantly with temperature.

This thesis aims to attack the questions raised above. In particular, we would like to focus on the material, polyethylene due to its simple structure. The methylene group, methyl group of polyethylene can be modeled as beads with distinct interaction potential parameters, and any electrostatic interaction is negligible. And this significantly shortens the computation time in our studies of polyethylene. Experimental data of such materials are also reliable.

In this thesis, this chapter presents the basic concept of the equation of motion, such as the Brownian dynamics (BD) and Langevin dynamics. Fundamentals of statistical mechanics, such as the canonical ensemble, distribution function theory of simple liquids, Boltzmann equation and transport properties, are also reviewed. Additionally, the rotational isomeric state model for determining the static properties of a polyethylene chain, which is used in

the initial configuration preparation step in MD simulation, is discussed. Chapter 2 shows the details of the molecular dynamics simulation, such as the preparation of the initial configuration of polymers, equilibration, production runs and forcefield parameters, numerical integration of nonlinear equation of motion in BD dynamics as well as the POD method are included. Chapter 3 reports the evaluation of velocity time correlation function after the inclusion of an inertia term in the Rouse model, compared with the numerical results. Chapter 4 shows the analysis of the nonlinear BD as well as MD data of polymers with different structures using POD analysis. A free volume theory for chain length dependence of linear and ring polymers is proposed in Chapter 5 and Chapter 6, respectively. In Chapter 7, the effect of temperature on the chain length dependence of the diffusivity of linear oligomers studied by the proposed free volume theory is investigated. In Chapter 8, the free volume theory was extended to the calculation of viscosity of unentangled and entangled polyethylene melts of different structures within a particular range of M . Finally, conclusions and future work can be found in Chapter 9.

1.2 BD and Langevin dynamics of a classical particle¹

Consider the simplest case that a single classical particle is subjected to a harmonic potential. The Langevin dynamics equation of motion for a single particle under such potential can be written as follows:

$$m \frac{d^2x}{dt^2} + \zeta \frac{dx}{dt} = -kx + f(t) \quad (1.1)$$

ζ is the friction coefficient, m is the mass of that single classical particle, k is the spring constant and x is the position of the particle. Alternatively, Equation (1.1) can be rewritten in a system of two ordinary differential equations.

$$m \frac{dv}{dt} + \zeta v = -kx + f(t) \quad (1.2)$$

$$v = \frac{dx}{dt} \quad (1.3)$$

This system of differential equations can be easily solved by rewriting in the state-space representation.

$$\frac{d}{dt} \begin{bmatrix} x \\ v \end{bmatrix} = \begin{bmatrix} 0 & 1 \\ -\frac{k}{m} & -\frac{\zeta}{m} \end{bmatrix} \begin{bmatrix} x \\ v \end{bmatrix} + \begin{bmatrix} 0 \\ \frac{f(t)}{m} \end{bmatrix} \quad (1.4)$$

¹A version of this section has been published in *Mol Simul*, 2020, 1-12. (cf., Appendix A)

The solution is as follows:

$$\begin{bmatrix} x \\ v \end{bmatrix} = e^{\mathbf{A}t} \begin{bmatrix} x \\ v \end{bmatrix}_0 + e^{\mathbf{A}t} \int_0^t e^{-\mathbf{A}\tau} \begin{bmatrix} 0 \\ \frac{f(\tau)}{m} \end{bmatrix} d\tau \quad (1.5)$$

Laplace transformation of the above solution gives us:

$$\begin{bmatrix} X(s) \\ V(s) \end{bmatrix} = (s\mathbf{I} - \mathbf{A})^{-1} \begin{bmatrix} x \\ v \end{bmatrix}_0 + (s\mathbf{I} - \mathbf{A})^{-1} \begin{bmatrix} 0 \\ \frac{F(s)}{m} \end{bmatrix} \quad (1.6)$$

The task has become evaluating $(s\mathbf{I} - \mathbf{A})^{-1}$, which has the following form:

$$(s\mathbf{I} - \mathbf{A})^{-1} = \begin{bmatrix} \frac{s + \frac{\zeta}{m}}{s(s + \frac{\zeta}{m}) + \frac{k}{m}} & \frac{1}{s(s + \frac{\zeta}{m}) + \frac{k}{m}} \\ \frac{-\frac{k}{m}}{s(s + \frac{\zeta}{m}) + \frac{k}{m}} & \frac{s}{s(s + \frac{\zeta}{m}) + \frac{k}{m}} \end{bmatrix} \quad (1.7)$$

1.2.1 Case 1: $\frac{k}{m} > \frac{\zeta^2}{4m^2}$

This can be transformed back to the time domain. If $\frac{k}{m} \gg \frac{\zeta^2}{4m^2}$:

$$e^{\mathbf{A}t} = e^{-\frac{\zeta t}{2m}} \begin{bmatrix} \cos(\sqrt{\frac{k}{m} - \frac{\zeta^2}{4m^2}} t) + \frac{\zeta \sin(\sqrt{\frac{k}{m} - \frac{\zeta^2}{4m^2}} t)}{2m(\sqrt{\frac{k}{m} - \frac{\zeta^2}{4m^2}})} & \frac{\sin(\sqrt{\frac{k}{m} - \frac{\zeta^2}{4m^2}} t)}{\sqrt{\frac{k}{m} - \frac{\zeta^2}{4m^2}}} \\ -\frac{k \sin(\sqrt{\frac{k}{m} - \frac{\zeta^2}{4m^2}} t)}{m\sqrt{\frac{k}{m} - \frac{\zeta^2}{4m^2}}} & \cos(\sqrt{\frac{k}{m} - \frac{\zeta^2}{4m^2}} t) - \frac{\zeta \sin(\sqrt{\frac{k}{m} - \frac{\zeta^2}{4m^2}} t)}{2m\sqrt{\frac{k}{m} - \frac{\zeta^2}{4m^2}}} \end{bmatrix} \quad (1.8)$$

Leading to the following solutions:

$$x(t) = x(0)e^{-\frac{\zeta t}{2m}} \left[\cos(\sqrt{\frac{k}{m} - \frac{\zeta^2}{4m^2}} t) + \frac{\zeta \sin(\sqrt{\frac{k}{m} - \frac{\zeta^2}{4m^2}} t)}{2m(\sqrt{\frac{k}{m} - \frac{\zeta^2}{4m^2}})} \right] + v(0) \frac{e^{-\frac{\zeta t}{2m}} \sin(\sqrt{\frac{k}{m} - \frac{\zeta^2}{4m^2}} t)}{\sqrt{\frac{k}{m} - \frac{\zeta^2}{4m^2}}} + h(t) \quad (1.9)$$

$$v(t) = -x(0)e^{-\frac{\zeta t}{2m}} \frac{k \sin(\sqrt{\frac{k}{m} - \frac{\zeta^2}{4m^2}} t)}{m\sqrt{\frac{k}{m} - \frac{\zeta^2}{4m^2}}} + v(0)e^{-\frac{\zeta t}{2m}} \left[\cos(\sqrt{\frac{k}{m} - \frac{\zeta^2}{4m^2}} t) - \frac{\zeta \sin(\sqrt{\frac{k}{m} - \frac{\zeta^2}{4m^2}} t)}{2m\sqrt{\frac{k}{m} - \frac{\zeta^2}{4m^2}}} \right] + g(t) \quad (1.10)$$

where,

$$h(t) = e^{-\frac{\zeta t}{2m}} \int_0^t e^{\frac{\zeta \tau}{2m}} \frac{\sin(\sqrt{\frac{k}{m} - \frac{\zeta^2}{4m^2}}(t - \tau))}{\sqrt{\frac{k}{m} - \frac{\zeta^2}{4m^2}}} f(\tau) d\tau \quad (1.11)$$

$$g(t) = e^{-\frac{\zeta t}{2m}} \int_0^t e^{\frac{\zeta \tau}{2m}} \left[\cos(\sqrt{\frac{k}{m} - \frac{\zeta^2}{4m^2}}(t - \tau)) + \frac{\zeta \sin(\sqrt{\frac{k}{m} - \frac{\zeta^2}{4m^2}}(t - \tau))}{2m\sqrt{\frac{k}{m} - \frac{\zeta^2}{4m^2}}} \right] f(\tau) d\tau \quad (1.12)$$

We can then obtain different time correlation functions of the position and velocity:

$$\langle x(t)x(0) \rangle = \langle x^2 \rangle e^{-\frac{\zeta t}{2m}} \left[\cos\left(\sqrt{\frac{k}{m} - \frac{\zeta^2}{4m^2}} t\right) + \frac{\zeta \sin\left(\sqrt{\frac{k}{m} - \frac{\zeta^2}{4m^2}} t\right)}{2m\left(\sqrt{\frac{k}{m} - \frac{\zeta^2}{4m^2}}\right)} \right] \quad (1.13)$$

$$\langle v(t)v(0) \rangle = \langle v^2 \rangle e^{-\frac{\zeta t}{2m}} \left[\cos\left(\sqrt{\frac{k}{m} - \frac{\zeta^2}{4m^2}} t\right) - \frac{\zeta \sin\left(\sqrt{\frac{k}{m} - \frac{\zeta^2}{4m^2}} t\right)}{2m\sqrt{\frac{k}{m} - \frac{\zeta^2}{4m^2}}} \right] \quad (1.14)$$

1.2.2 Case 2: $\frac{\zeta^2}{4m^2} > \frac{k}{m}$

If $\frac{\zeta^2}{4m^2} \gg \frac{k}{m}$, then the matrix exponential $e^{\mathbf{A}t}$ has the following form:

$$e^{\mathbf{A}t} = e^{-\frac{\zeta t}{2m}} \begin{bmatrix} \cosh\left(\sqrt{\frac{\zeta^2}{4m^2} - \frac{k}{m}} t\right) + \frac{\zeta \sinh\left(\sqrt{\frac{\zeta^2}{4m^2} - \frac{k}{m}} t\right)}{2m\left(\sqrt{\frac{\zeta^2}{4m^2} - \frac{k}{m}}\right)} & \frac{\sinh\left(\sqrt{\frac{\zeta^2}{4m^2} - \frac{k}{m}} t\right)}{\sqrt{\frac{\zeta^2}{4m^2} - \frac{k}{m}}} \\ -\frac{k \sinh\left(\sqrt{\frac{\zeta^2}{4m^2} - \frac{k}{m}} t\right)}{m\sqrt{\frac{\zeta^2}{4m^2} - \frac{k}{m}}} & \cosh\left(\sqrt{\frac{\zeta^2}{4m^2} - \frac{k}{m}} t\right) - \frac{\zeta \sinh\left(\sqrt{\frac{\zeta^2}{4m^2} - \frac{k}{m}} t\right)}{2m\sqrt{\frac{\zeta^2}{4m^2} - \frac{k}{m}}} \end{bmatrix} \quad (1.15)$$

Such that, the solution now becomes:

$$x(t) = x(0)e^{-\frac{\zeta t}{2m}} \left[\cosh\left(\sqrt{\frac{\zeta^2}{4m^2} - \frac{k}{m}} t\right) + \frac{\zeta \sinh\left(\sqrt{\frac{\zeta^2}{4m^2} - \frac{k}{m}} t\right)}{2m\left(\sqrt{\frac{\zeta^2}{4m^2} - \frac{k}{m}}\right)} \right] + v(0) \frac{e^{-\frac{\zeta}{2m}t} \sinh\left(\sqrt{\frac{\zeta^2}{4m^2} - \frac{k}{m}} t\right)}{\sqrt{\frac{\zeta^2}{4m^2} - \frac{k}{m}}} + h(t) \quad (1.16)$$

$$v(t) = -x(0)e^{-\frac{\zeta t}{2m}} \frac{k \sinh\left(\sqrt{\frac{\zeta^2}{4m^2} - \frac{k}{m}} t\right)}{m\sqrt{\frac{\zeta^2}{4m^2} - \frac{k}{m}}} + v(0)e^{-\frac{\zeta t}{2m}} \left[\cosh\left(\sqrt{\frac{k}{m} - \frac{\zeta^2}{4m^2}} t\right) - \frac{\zeta \sinh\left(\sqrt{\frac{\zeta^2}{4m^2} - \frac{k}{m}} t\right)}{2m\sqrt{\frac{\zeta^2}{4m^2} - \frac{k}{m}}} \right] + g(t) \quad (1.17)$$

where,

$$h(t) = e^{-\frac{\zeta}{2m}t} \int_0^t e^{\frac{\zeta}{2m}\tau} \frac{\sinh\left(\sqrt{\frac{\zeta^2}{4m^2} - \frac{k}{m}}(t - \tau)\right)}{\sqrt{\frac{\zeta^2}{4m^2} - \frac{k}{m}}} f(\tau) d\tau \quad (1.18)$$

$$g(t) = e^{-\frac{\zeta}{2m}t} \int_0^t e^{\frac{\zeta}{2m}\tau} \left[\cosh\left(\sqrt{\frac{\zeta^2}{4m^2} - \frac{k}{m}}(t - \tau)\right) + \frac{\zeta \sinh\left(\sqrt{\frac{\zeta^2}{4m^2} - \frac{k}{m}}(t - \tau)\right)}{2m\sqrt{\frac{\zeta^2}{4m^2} - \frac{k}{m}}} \right] f(\tau) d\tau \quad (1.19)$$

The time correlation functions now become:

$$\langle x(t)x(0) \rangle = \langle x^2 \rangle e^{-\frac{\zeta t}{2m}} \left[\cosh\left(\sqrt{\frac{\zeta^2}{4m^2} - \frac{k}{m}} t\right) + \frac{\zeta \sinh\left(\sqrt{\frac{\zeta^2}{4m^2} - \frac{k}{m}} t\right)}{2m\left(\sqrt{\frac{\zeta^2}{4m^2} - \frac{k}{m}}\right)} \right] \quad (1.20)$$

$$\langle v(t)v(0) \rangle = \langle v^2 \rangle e^{-\frac{\zeta t}{2m}} \left[\cosh\left(\sqrt{\frac{\zeta^2}{4m^2} - \frac{k}{m}} t\right) - \frac{\zeta \sinh\left(\sqrt{\frac{\zeta^2}{4m^2} - \frac{k}{m}} t\right)}{2m\sqrt{\frac{\zeta^2}{4m^2} - \frac{k}{m}}}\right] \quad (1.21)$$

In this case, we can extract the diffusivity easily by assuming that $\frac{\zeta^2}{4m^2} \gg \frac{k}{m}$ such that the evaluation of the mean square displacement $\langle (x(t) - x_0)^2 \rangle$ can be simplified.

$$\langle (x(t) - x_0)^2 \rangle = \langle h(t)^2 \rangle \quad (1.22)$$

With:

$$\langle h(t)^2 \rangle = \frac{m^2}{\zeta^2} \int_0^t \int_0^t \left(1 - e^{-\frac{\zeta}{m}(t-\tau_1)}\right) \left(1 - e^{-\frac{\zeta}{m}(t-\tau_2)}\right) \langle f(\tau_1)f(\tau_2) \rangle d\tau_1 d\tau_2 \quad (1.23)$$

$\langle f(\tau_1)f(\tau_2) \rangle = 2k_b T \frac{\zeta}{m^2} \delta(\tau_1 - \tau_2)$. This is going to give us:

$$\langle h^2(t) \rangle = \frac{2k_b T}{\zeta} t - \frac{3k_b T m}{\zeta^2} + \frac{4k_b T m}{\zeta^2} e^{-\frac{\zeta}{m}t} - \frac{k_b T m}{\zeta^2} e^{-\frac{2\zeta}{m}t} \quad (1.24)$$

As time tends to infinity, we then have:

$$\lim_{t \rightarrow \infty} \langle (r - r_0)^2 \rangle = \frac{2k_b T t}{\zeta} \quad (1.25)$$

Therefore, $D = \frac{k_b T}{\zeta}$, where D is the diffusivity of the classical particle.

1.2.3 Brownian Dynamics

In BD, the equation of motion is even much easier as the inertia term is neglected. Consider the same case of a 1D classical particle subjected to a harmonic potential.

$$\zeta \frac{dx}{dt} = -kx \quad (1.26)$$

This can be solved even more straightforwardly.

$$x(t) = x(0)e^{-\frac{k}{\zeta}t} \quad (1.27)$$

Even though we will not be able to get the velocity time correlation function from BD, when the system is only subjected to a stochastic force, the diffusivity can be calculated. With the stochastic force $f(t)$ only, we have the following equation of motion:

$$\zeta \frac{dx}{dt} = f(t) \quad (1.28)$$

Such that the stochastic force has a normal distribution with $\langle f(t) \rangle = 0$ and $\langle f(t)f(t') \rangle = 2\zeta k_b T \delta(t - t')$. The solution is as follows:

$$x(t) = x(0) + \int_0^t \frac{f(\tau)}{\zeta} d\tau \quad (1.29)$$

To derive the diffusivity, the mean square displacement $\langle x^2(t) \rangle$ has to be known.

$$\langle x^2(t) \rangle = \langle x^2(0) \rangle + \int_0^t \int_0^t d\tau_1 d\tau_2 \frac{\langle f(\tau_1)f(\tau_2) \rangle}{\zeta^2} \quad (1.30)$$

This gives us:

$$\langle x^2(t) \rangle = \frac{2k_b T}{\zeta} t = 2Dt \quad (1.31)$$

1.3 Statistical mechanics and distribution function theory of simple liquid

1.3.1 Canonical Ensemble and Classical Statistical Thermodynamics

It is also pertinent to introduce the fundamental concept of statistical mechanics of simple liquid (i.e., derivation of statistical weight and partition function of a canonical ensemble.) before any detailed discussion of radial distribution function and pressure equation.

Consider a box as depicted in Figure 1.1 with many compartments having the same number of particles, volume and temperature. The walls of the box are adiabatic, rigid and impermeable, whereas the walls separating compartments are diathermal, rigid and impermeable. The energy of each compartment is different in this case. And say each compartment possesses a certain energy level of E_i , then the total energy of the box is:

$$E_{total} = \sum_i E_i a_i \quad (1.32)$$

a_i is the number of compartments at the energy state E_i , such that the total number of compartments is:

$$A_{total} = \sum_i a_i \quad (1.33)$$

The total number of ways of arranging these a_i compartments at different energy level E_i s (W) is then:

$$W(\mathbf{a}) = \frac{\mathcal{A}_{total}!}{a_1!a_2!a_3!\dots} \quad (1.34)$$

where $\mathbf{a} = [a_1 \ a_2 \ a_3 \ a_4 \ \dots]^T$. As $\mathcal{A}_{total} \rightarrow \infty$, there exists a particular distribution \mathbf{a}^* , which maximizes $W(\mathbf{a})$. Subjected to Equation (1.32) and Equation (1.33), we have:

$$\frac{\partial \ln W(\mathbf{a})}{\partial a_i^*} - \alpha_1 - \beta E_i^* = 0 \quad (1.35)$$

With Stirling approximation, we know that $\frac{\partial \ln W(\mathbf{a})}{\partial a_i^*} = -1 - \ln a_i^*$, leading to:

$$a_i^* = \exp(-1 - \alpha_1 - \beta E_i^*) \quad (1.36)$$

A macroscopic property \mathcal{M} can be then determined.

$$\mathcal{M} = \frac{\sum_i a_i m_i}{\sum_i a_i} = \frac{\sum_i m_i \exp(-\beta E_i)}{\sum_i \exp(-\beta E_i)} \quad (1.37)$$

In classical mechanics, m_i and E_i are both functions of positions and momenta of the particles, which can be denoted as $m(\mathbf{p}, \mathbf{q})$ and $E(\mathbf{p}, \mathbf{q})$, such that Equation (1.37) can be rewritten as:

$$\mathcal{M} = \frac{\int \dots \int m(\mathbf{p}, \mathbf{q}) \exp[-\beta E(\mathbf{p}, \mathbf{q})] d\mathbf{p} d\mathbf{q}}{\int \dots \int \exp[-\beta E(\mathbf{p}, \mathbf{q})] d\mathbf{p} d\mathbf{q}} \quad (1.38)$$

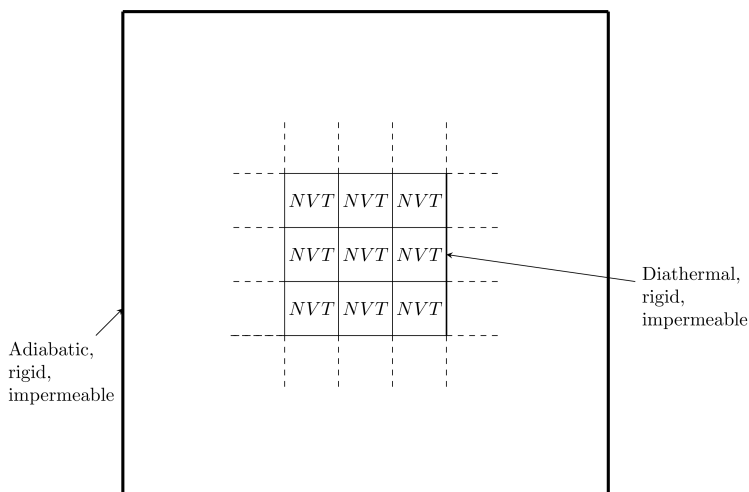


Figure 1.1: A box containing multiple compartments with the same N , V and T .

1.3.2 Radial Distribution Function

Thus, if we consider a system of all atoms interacting with one another with a total potential energy of U_N , the probability of finding atom 1 at $d\mathbf{r}_1$, atom 2 at $d\mathbf{r}_2$, ... , atom N at $d\mathbf{r}_N$ is:

$$P^{(N)}(\mathbf{r}_1, \mathbf{r}_2, \dots, \mathbf{r}_N)d\mathbf{r}_1d\mathbf{r}_2\dots d\mathbf{r}_N = \exp(-\beta U_N)d\mathbf{r}_1d\mathbf{r}_2\dots d\mathbf{r}_N/Z_N \quad (1.39)$$

Z_N is the partition function of the canonical ensemble, which has the form:

$$Z_N = \int \dots \int \exp(-\beta U_N)d\mathbf{r}_1d\mathbf{r}_2\dots d\mathbf{r}_N \quad (1.40)$$

Therefore, the probability of finding atom 1 at $d\mathbf{r}_1$, atom 2 at $d\mathbf{r}_2$, ..., atom n $d\mathbf{r}_n$ is:

$$P^{(n)}(\mathbf{r}_1, \mathbf{r}_2, \dots, \mathbf{r}_n)d\mathbf{r}_1d\mathbf{r}_2\dots d\mathbf{r}_n = \left[\int \dots \int \exp(-\beta U_N)d\mathbf{r}_{n+1}d\mathbf{r}_{n+2}\dots d\mathbf{r}_N/Z_N \right] d\mathbf{r}_1d\mathbf{r}_2\dots d\mathbf{r}_n \quad (1.41)$$

The probability density of finding any atom at $d\mathbf{r}_1, d\mathbf{r}_2, \dots, d\mathbf{r}_n$ is then:

$$\rho^{(n)} = \frac{N!}{(N-n)!Z_N} \int \dots \int \exp(-\beta U_N)d\mathbf{r}_{n+1}\dots d\mathbf{r}_N \quad (1.42)$$

Let us define a function $g^{(n)}$ as follows:

$$g^{(n)} = \frac{\rho^{(n)}}{\rho^n} \quad (1.43)$$

ρ is the number density of the atoms. The simplest form is $n = 1$, which is related to the probability of finding any atom in the system. We have:

$$\rho = \frac{1}{V} \int_0^\infty \rho^{(1)} 4\pi r^2 dr = \frac{N}{V} \quad (1.44)$$

This implies that $g^{(1)} = 1$. This is only true for single monoatomic particle. If the molecule is a polymer, then $g^{(1)}(r)$ is a function of r (See Chapter 8 for derivation of a Gaussian chain).

When $n = 2$,

$$g^{(2)} = \frac{V^2(N-1)}{NZ_N} \int \dots \int \exp(-\beta U_N) d\mathbf{r}_3 \dots d\mathbf{r}_N \quad (1.45)$$

$g^{(2)}$ is a function of our main interest as it is related to the probability of finding a molecule 1 in $d\mathbf{r}_1$ given a molecule 2 in $d\mathbf{r}_2$. It is an extremely useful function as the interaction potential in simple liquid is typical pairwise.

1.3.3 Pressure Equation

Consider the following coordinate transformation:

$$x_k = V^{1/3}x'_k \quad (1.46)$$

This implies that:

$$\mathbf{r}_k = V\mathbf{r}'_k \quad (1.47)$$

And the partition function Z_N is expressed as follows:

$$Z_N = V^N \int_0^1 \dots \int_0^1 \exp(-\beta U_N) d\mathbf{r}'_1 d\mathbf{r}'_2 \dots d\mathbf{r}'_N \quad (1.48)$$

Taking derivative with respect to V .

$$\left(\frac{\partial Z_N}{\partial V}\right)_{N,T} = \frac{\partial}{\partial V} \int_0^1 \dots \int_0^1 \exp(-\beta U_N) V^N d\mathbf{r}'_1 d\mathbf{r}'_2 \dots d\mathbf{r}'_N \quad (1.49)$$

$$\left(\frac{\partial Z_N}{\partial V}\right)_{N,T} = \int_0^1 \dots \int_0^1 \exp(-\beta U_N) \left[NV^{N-1} - V^N \beta \left(\frac{\partial U_N}{\partial V}\right) \right] d\mathbf{r}'_1 d\mathbf{r}'_2 d\mathbf{r}'_3 \dots d\mathbf{r}'_N \quad (1.50)$$

In which we have, if the interaction potential is pairwise addition:

$$\left(\frac{\partial U_N}{\partial V}\right) = \sum_{1 \leq i < j \leq N} \frac{\partial u_{ij}}{\partial r_{ij}} \cdot \frac{\partial r_{ij}}{\partial V} = \sum_{1 \leq i < j \leq N} \frac{r_{ij}}{3V} \frac{\partial u_{ij}}{\partial r_{ij}} \quad (1.51)$$

As $p = k_b T \frac{\partial \ln Z_N}{\partial V}$, we can obtain the pressure equation with the following:

$$\begin{aligned} \frac{\partial \ln Z_N}{\partial V} &= \frac{1}{Z_N} \frac{\partial Z_N}{\partial V} \\ &= \frac{N}{V} - \frac{\beta}{3V} \frac{N(N-1)}{2Z_N} \int_0^1 \dots \int_0^1 r_{ij} \frac{\partial u_{ij}}{\partial r_{ij}} \exp(-\beta U_N) d\mathbf{r}'_1 d\mathbf{r}'_2 d\mathbf{r}'_3 \dots d\mathbf{r}'_N \\ &= \frac{N}{V} - \frac{2\pi\beta}{3V} \int_0^\infty r_{12} \frac{\partial u_{12}}{\partial r_{12}} \rho^{(2)}(\mathbf{r}_1, \mathbf{r}_2) d\mathbf{r}_1 d\mathbf{r}_2 \end{aligned}$$

By transformation into spherical coordinate, we finally have:

$$\boxed{p\beta = \rho - \frac{2\pi\beta\rho^2}{3} \int_0^\infty r_{12}^3 \frac{\partial u_{12}}{\partial r_{12}} g^{(2)} dr_{12}} \quad (1.52)$$

1.3.4 Percus-Yevick Equation

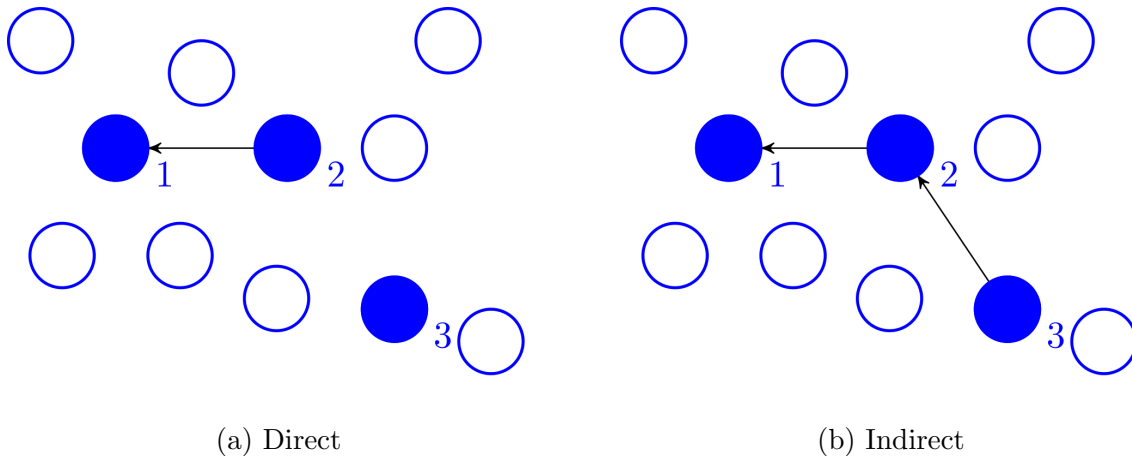


Figure 1.2: (a) Direct and (b) indirect interactions between particle 1 and particle 2 in a many-body system. Particle 3 can influence the motion of particle 1 by indirectly interacting with particle 2.

The problem of determining the pressure in a simple liquid then becomes obtaining $g(r)$ (also known as $g^{(2)}$), which allows us to quantify the many-body effect. With $h(r) = g(r) - 1$ and the direct correlation function $c(r)$, Ornstein and Zernike proposed the following:

$$h(r_{12}) = c(r_{12}) + \rho \int c(r_{13})h(r_{23})d\mathbf{r}_3 \quad (1.53)$$

The key idea behind such equation is illustrated in Figure 1.2. In Figure 1.2, they argued that $g(r)$ can be divided into direct and indirect parts. The direct part accounts for the influence from atom 2 on atom 1, whereas the indirect part includes the influence from atom 3 on atom 2, which results in indirect influence on atom 1, as these particles interact with one another through a particular potential, such as hard-sphere potential or 6-12 Lennard-Jones (LJ) potential.

However, Equation (1.53) is not useful as there are two unknowns. Percus and Yevick then proposed a closure relation along with Equation (1.53):

$$\begin{aligned} c(r) &= g_{total} - g_{indirect} \\ &\approx \exp(-\beta w(r)) - \exp(-\beta[w(r) - u(r)]) \end{aligned}$$

Let $y(r) = \exp(-\beta[w(r) - u(r)])$, such that $g(r) = \exp[-\beta u(r)]y(r)$.

$$c(r) = \left\{ \exp[-\beta u(r)] - 1 \right\} y(r) = f(r)y(r) \quad (1.54)$$

The Percus-Yevick Equation was finally obtained as:

$$y_{12} = 1 + \rho \int f_{13} y_{13} [e^{-\beta u_{23}} y_{23} - 1] d\mathbf{r}_3 \quad (1.55)$$

1.3.5 Fourier Transform Method

To solve Equation (1.53), it is simplified to a scalar algebraic equation when it is transformed to the Fourier space:

$$\hat{h}(k) = \hat{c}(k) + \rho \hat{c}(k) \hat{h}(k) \quad (1.56)$$

k is the wavevector. $\hat{h}(k)$ can be therefore easily calculated with:

$$\hat{h}(k) = \frac{\hat{c}(k)}{1 - \rho \hat{c}(k)} \quad (1.57)$$

The Fourier Transform is three dimensional. The position vector in Cartesian coordinate is firstly rewritten in spherical coordinate.

$$\begin{bmatrix} x \\ y \\ z \end{bmatrix} = \begin{bmatrix} r \sin(\theta) \cos(\psi) \\ r \sin(\theta) \sin(\psi) \\ r \cos(\theta) \end{bmatrix} \quad (1.58)$$

The corresponding Jacobian matrix is therefore as follows:

$$\mathbf{J} = \begin{bmatrix} \sin \theta \cos \psi & r \cos \psi \cos \theta & -r \sin \theta \sin \psi \\ \sin \theta \sin \psi & r \cos \theta \sin \psi & r \sin \theta \cos \psi \\ \cos \theta & -r \sin \theta & 0 \end{bmatrix} \quad (1.59)$$

Determinant of such matrix is $r^2 \sin \theta$. Secondly, if we look at the integral in the Fourier Transformation:

$$\int dx \int dy \int dz e^{-i(k_x x + k_y y + k_z z)} g(x, y, z) \quad (1.60)$$

Coordinate transformation gives us:

$$\int_0^{2\pi} d\psi \int_0^\infty \int_0^\pi e^{-ikr \cos \theta} g(r) r^2 \sin \theta d\theta dr \quad (1.61)$$

Consider the integral:

$$\begin{aligned} \int_0^\pi e^{-ikr \cos \theta} \sin \theta d\theta &= - \int_1^{-1} e^{-ikr \cos \theta} d \cos \theta \\ &= - \left[\frac{e^{-ikr \cos \theta}}{-ikr} \right]_1^{-1} \\ &= \frac{2i \sin kr}{ikr} = 2 \frac{\sin kr}{kr} \end{aligned}$$

Finally, the Fourier transform of property $A(r)$ is defined as:

$$\hat{A}(k) = 4\pi \int_0^\infty A(r)r^2 \frac{\sin(kr)}{kr} dr \quad (1.62)$$

With these, Equation (1.56) was solved numerically along with the Percus-Yevick closure relation, and the solutions with different ρ s are shown in Figure 1.3 with $u(r)$ being 6-12 LJ potential. As expected, when ρ decreases, the amplitude of the first peak decreases until $g(r) \rightarrow \exp[-\beta u(r)]$ as $\rho \rightarrow 0$.

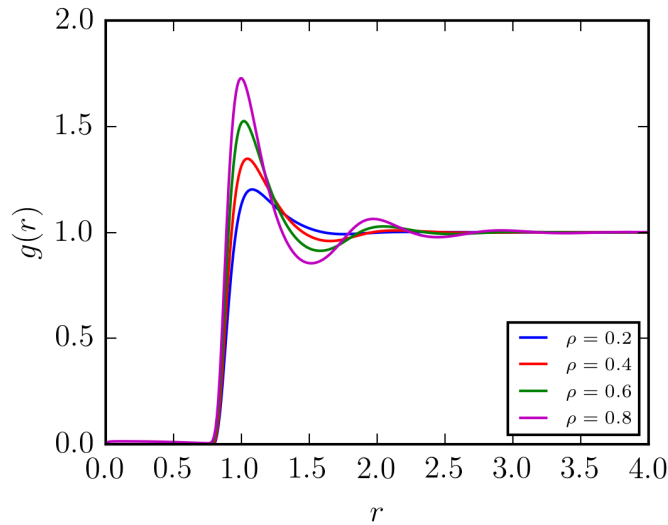


Figure 1.3: Radial distribution function of monatomic liquid at different number densities.

The compressibility factor, which is defined as $\frac{p\beta}{\rho}$, can be then evaluated using the pressure equation that we have derived earlier. The results are shown in Figure 1.4. In ideal gas, the compressibility factor should be constant, but in monoatomic liquid, atoms interact with one another and they have finite sizes. Therefore, the compressibility factor increases nonlinearly with ρ . The reader is going to see that this computation is important in the approximation of mean free volume and effective pressure of a polymer melt.

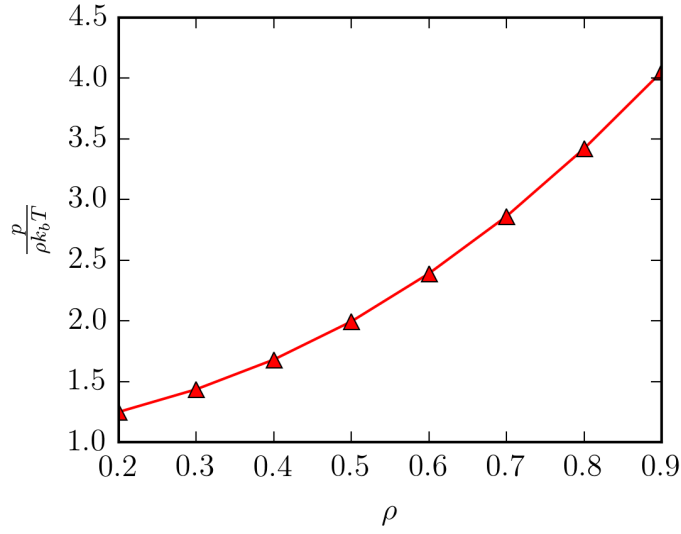


Figure 1.4: Calculated pressure as a function of number density.

1.4 Maxwell-Boltzmann Distribution and Transport Coefficients of Dilute Gas

1.4.1 Derivation of Boltzmann Distribution and Mean-Free Path

Consider a phase space function $f_j(\mathbf{v}_j, \mathbf{r}_j, t)$ of a particle j , which is a function of the velocity (\mathbf{v}_j) and position (\mathbf{r}_j) of particle j . Infinitesimal change in \mathbf{v}_j and \mathbf{r}_j can be expressed in terms of dt that $d\mathbf{v}_j = \frac{\mathbf{F}_j}{m_j} dt$ and $d\mathbf{r}_j = \mathbf{v}_j dt$.

$$df_j = \left[\left(\frac{\partial f_j}{\partial t} \right) + \mathbf{v}_j \cdot \nabla_{\mathbf{r}} f_j + \frac{\mathbf{F}_j}{m_j} \cdot \nabla_{\mathbf{v}_j} f_j \right] dt \quad (1.63)$$

We have:

$$\left(\frac{\partial f_j}{\partial t} \right) + \mathbf{v}_j \cdot \nabla_{\mathbf{r}} f_j + \frac{\mathbf{F}_j}{m_j} \cdot \nabla_{\mathbf{v}_j} f_j = \left(\frac{df_j}{dt} \right) \quad (1.64)$$

$\frac{df_j}{dt}$ can be known by understanding the collision between gas particles because the gain and the loss of f_j with time is dependent on the scattering due to collisions. With the normalization to the number density of particle j :

$$\int_{-\infty}^{\infty} f_j d\mathbf{v}_j = \rho_j \quad (1.65)$$

As the term df_j/dt is related to the collisions among particles. Equation (1.64) can be rewritten as:

$$\frac{\partial f_j}{\partial t} + \mathbf{v}_j \cdot \nabla_{\mathbf{r}} f_j + \frac{\mathbf{F}_j}{m_j} \cdot \nabla_{\mathbf{v}_j} f_j = \sum_i \Gamma_{ij}^+ - \Gamma_{ij}^- \quad (1.66)$$

Γ_{ij}^+ and Γ_{ij}^- are the gain and loss in the phase space distribution function of particle j due to its collision with particle i , respectively. Before analyzing the expressions for Γ_{ij}^+ and Γ_{ij}^- , consider two particles collide with one another, assuming that the collision is elastic, we can write equations for mass, momentum and energy balance.

$$m_1 + m_2 = m'_1 + m'_2 \quad (1.67)$$

Without any reaction, then $m_1 = m'_1$ and $m_2 = m'_2$. Then, the momentum balance gives us:

$$m_1 \mathbf{v}_1 + m_2 \mathbf{v}_2 = m_1 \mathbf{v}'_1 + m_2 \mathbf{v}'_2 \quad (1.68)$$

$$0.5m_1 v_1^2 + 0.5m_2 v_2^2 = 0.5m'_1 v'^2_1 + 0.5m'_2 v'^2_2 \quad (1.69)$$

To make our lives easier, the velocities can be rewritten in terms of relative velocity (\mathbf{v}_r) and center-of-mass velocity (\mathbf{v}_c), with the following definitions:

$$\mathbf{v}_c = \frac{m_1 \mathbf{v}_1 + m_2 \mathbf{v}_2}{m_1 + m_2} \quad (1.70)$$

$$\mathbf{v}_r = \mathbf{v}_1 - \mathbf{v}_2 \quad (1.71)$$

Consider the momentum balance and energy balance:

$$m_1 \mathbf{v}_1 + m_2 \mathbf{v}_2 = m_1 \mathbf{v}'_1 + m_2 \mathbf{v}'_2$$

$$m_1 \mathbf{v}_1 + m_2 \mathbf{v}_2 = m_1 \left(\mathbf{v}_c + \frac{m_2}{m_1 + m_2} \mathbf{v}_r \right) + m_2 \left(\mathbf{v}_c - \frac{m_1}{m_1 + m_2} \mathbf{v}_r \right) = (m_1 + m_2) \mathbf{v}_c$$

This proves that $\mathbf{v}_c = \mathbf{v}'_c$. Consider the following definition of \mathbf{v}_1 and \mathbf{v}_2 :

$$\mathbf{v}_1 = \mathbf{v}_c + \frac{m_2}{m_1 + m_2} \mathbf{v}_r \quad (1.72)$$

$$\mathbf{v}_2 = \mathbf{v}_c - \frac{m_1}{m_1 + m_2} \mathbf{v}_r \quad (1.73)$$

$$v_1^2 = v_c^2 + \frac{m_2}{m_1 + m_2} \mathbf{v}_c \cdot \mathbf{v}_r + \frac{m_2^2}{(m_1 + m_2)^2} v_r^2 \quad (1.74)$$

$$v_2^2 = v_c^2 - \frac{m_1}{m_1 + m_2} \mathbf{v}_c \cdot \mathbf{v}_r + \frac{m_1^2}{(m_1 + m_2)^2} v_r^2 \quad (1.75)$$

The energy balance equation then becomes:

$$\frac{1}{2}m_1v_1^2 + \frac{1}{2}m_2v_2^2 = \frac{1}{2}(m_1 + m_2)v_c^2 + \frac{1}{2}\mu v_r^2$$

where $\mu = \frac{m_1m_2}{m_1+m_2}$. This means that $v_r = v_r'$. In conclusion, during an elastic collision, the magnitude of v_c and v_r remain unchanged. Only the direction of \mathbf{v}_r has changed, such that $\mathbf{v}_r \cdot \mathbf{v}_r' = v_r^2 \cos \chi$. The angle χ is dependent on the potential of interaction between two particles, which will be discussed in details in the forthcoming section.

Assumed that particle i is now traveling through a medium, in which all other particles j are fixed. This means that particle i travels with a velocity of $v_r = |\mathbf{v}_i - \mathbf{v}_j|$. Then, the total number of collisions (n_{col}) experienced by one particle j in a unit time is:

$$n_{col} = \int_0^{2\pi} d\psi \int_{-\infty}^{\infty} \int_0^{\infty} f_i' v_r' b db d\mathbf{v}_i' = 2\pi \sum_i \int_{-\infty}^{\infty} \int_0^{\infty} f_i' v_r' b db d\mathbf{v}_i' \quad (1.76)$$

f_i' is function of v_i' , which is the velocity of particle i after the collision. The phase space distribution function of particle j for the gain due to collision is f_j' , which is also a function of velocity of particle j after collision (v_j'). Therefore:

$$\sum_i \Gamma_{ij}^+ = 2\pi \sum_i \int_{-\infty}^{\infty} \int_0^{\infty} f_i' f_j' v_r' b db d\mathbf{v}_i' \quad (1.77)$$

Similarly, for $\sum_i \Gamma_{ij}^-$, we consider f_i and f_j , which are functions of velocities before collision.

$$\sum_i \Gamma_{ij}^- = 2\pi \sum_i \int_{-\infty}^{\infty} \int_0^{\infty} f_i f_j v_r b db d\mathbf{v}_i \quad (1.78)$$

Let the following to represent the net gain contribution due to collision:

$$\left(\frac{\partial f_j}{\partial t}\right)_{col} = \sum_i \Gamma_{ij}^+ - \Gamma_{ij}^- \quad (1.79)$$

In a volume element with $d\mathbf{r}$, the probable number of particles j in the range of \mathbf{v}_j to $\mathbf{v}_j + d\mathbf{v}_j$ is $f_j d\mathbf{r} d\mathbf{v}_j$. Similarly, we have $f_j' d\mathbf{r} d\mathbf{v}_j'$ for the post-collisional term. Then, for the gain and loss terms, we have:

$$\sum_i \Gamma_{ij}^+ d\mathbf{v}_j' d\mathbf{r} = 2\pi \sum_i \int_{-\infty}^{\infty} \int_0^{\infty} f_i' f_j' v_r' b db d\mathbf{v}_i' d\mathbf{v}_j' d\mathbf{r} \quad (1.80)$$

$$\sum_i \Gamma_{ij}^- d\mathbf{v}_j d\mathbf{r} = 2\pi \sum_i \int_{-\infty}^{\infty} \int_0^{\infty} f_i f_j v_r b db d\mathbf{v}_i d\mathbf{v}_j d\mathbf{r} \quad (1.81)$$

In a binary collision event, magnitude of \mathbf{v}_r remains unchanged and \mathbf{v}_c does not change. Consider the following Jacobian matrix for coordinate transformation from $d\mathbf{v}_i'd\mathbf{v}_j'$ to $d\mathbf{v}_r'd\mathbf{v}_c'$ for one component system:

$$\mathbf{J} = \begin{bmatrix} \frac{\partial \mathbf{v}_1}{\partial \mathbf{v}_c} & \frac{\partial \mathbf{v}_1}{\partial \mathbf{v}_r} \\ \frac{\partial \mathbf{v}_2}{\partial \mathbf{v}_c} & \frac{\partial \mathbf{v}_2}{\partial \mathbf{v}_r} \end{bmatrix} = \begin{bmatrix} 1 & 0.5 \\ 1 & -0.5 \end{bmatrix} \quad (1.82)$$

The absolute value of determinant is one, therefore $d\mathbf{v}_i'd\mathbf{v}_j' = d\mathbf{v}_c d\mathbf{v}_r'$ and $d\mathbf{v}_i d\mathbf{v}_j = d\mathbf{v}_c d\mathbf{v}_r$. Note that we have used $\mathbf{v}_c = \mathbf{v}_c'$. If we define $d\mathbf{v}_r$ and $d\mathbf{v}_r'$ in spherical coordinate, we find that they are equivalent. See that:

$$d\mathbf{v}_r' = v_r'^2 \sin \theta d\theta d\psi dv_r' = d\mathbf{v}_r = v_r^2 \sin \theta d\theta d\psi dv_r \quad (1.83)$$

This then gives us $d\mathbf{v}_i'd\mathbf{v}_j' = d\mathbf{v}_i d\mathbf{v}_j$, and it leads to the conclusion:

$$\sum_i \Gamma_{ij}^+ - \Gamma_{ij}^- = 2\pi \sum_i \int_{-\infty}^{\infty} \int_0^{\infty} (f_i' f_j' - f_i f_j) v_r b db d\mathbf{v}_i \quad (1.84)$$

Rewriting again for the Boltzmann Equation, we get:

$$\frac{\partial f_j}{\partial t} + \mathbf{v}_j \cdot \nabla_{\mathbf{r}} f_j + \frac{\mathbf{F}_j}{m_j} \cdot \nabla_{\mathbf{v}_j} f_j = 2\pi \sum_i \int_{-\infty}^{\infty} \int_0^{\infty} (f_i' f_j' - f_i f_j) v_r b db d\mathbf{v}_i \quad (1.85)$$

Now consider the phase space distribution of all particles, which are identical to one another such that we have a one-component system. In this case, we can drop the summation operator \sum_i and all the subscripts j and change the subscript i to 1, such that we have:

$$\frac{\partial f}{\partial t} + \mathbf{v} \cdot \nabla_{\mathbf{r}} f + \frac{\mathbf{F}}{m} \cdot \nabla_{\mathbf{v}} f = 2\pi \int_{-\infty}^{\infty} \int_0^{\infty} (f_1' f' - f_1 f) v_r b db d\mathbf{v}_1 \quad (1.86)$$

We then write the following H function:

$$H(t) = \int_{-\infty}^{\infty} \int_{-\infty}^{\infty} f \ln f d\mathbf{r} d\mathbf{v} \quad (1.87)$$

Taking time derivative of both sides:

$$\frac{dH(t)}{dt} = \int_{-\infty}^{\infty} \int_{-\infty}^{\infty} \left(\ln f \frac{\partial f}{\partial t} + \frac{\partial f}{\partial t} \right) d\mathbf{r} d\mathbf{v} \quad (1.88)$$

As total number of points in phase space does not change with time, we can write:

$$\int_{-\infty}^{\infty} \int_{-\infty}^{\infty} \frac{\partial f}{\partial t} d\mathbf{r} d\mathbf{v} = \frac{\partial}{\partial t} \int_{-\infty}^{\infty} \int_{-\infty}^{\infty} f d\mathbf{r} d\mathbf{v} = 0 \quad (1.89)$$

We know that:

$$\begin{aligned} \int_{-\infty}^{\infty} \int_{-\infty}^{\infty} (\ln f) \mathbf{v} \cdot \nabla_{\mathbf{r}} f d\mathbf{r} d\mathbf{v} &= \sum_{k=x,y,z} \int_{-\infty}^{\infty} \int_{-\infty}^{\infty} v_k (\ln f) \frac{\partial}{\partial k} f dk dv_k \\ &= \sum_{k=x,y,z} \int_{-\infty}^{\infty} v_k \left[f \ln f \Big|_{-\infty}^{\infty} - \int_{-\infty}^{\infty} df \right] dv_k = 0 \end{aligned}$$

Similarly, we also know that:

$$\begin{aligned} \int_{-\infty}^{\infty} \int_{-\infty}^{\infty} (\ln f) \frac{\mathbf{F}}{m} \cdot \nabla_{\mathbf{v}} f d\mathbf{r} d\mathbf{v} &= \sum_{k=x,y,z} \int_{-\infty}^{\infty} \int_{-\infty}^{\infty} \frac{F_k}{m} (\ln f) \frac{\partial}{\partial v_k} f dk dv_k \\ &= \sum_{k=x,y,z} \int_{-\infty}^{\infty} \frac{F_k}{m} \left[f \ln f \Big|_{-\infty}^{\infty} - \int_{-\infty}^{\infty} df \right] dk = 0 \end{aligned}$$

With these, we can write:

$$\frac{dH(t)}{dt} = \int_{-\infty}^{\infty} \int_{-\infty}^{\infty} \left[2\pi (\ln f) \int_{-\infty}^{\infty} \int_0^{\infty} (f'_1 f' - f_1 f) v_r b db d\mathbf{v}_1 \right] d\mathbf{r} d\mathbf{v} \quad (1.90)$$

The collision integral is reversible:

$$\int_{-\infty}^{\infty} \int_{-\infty}^{\infty} \int_{-\infty}^{\infty} \int_0^{\infty} (\ln f) (f'_1 f' - f_1 f) v_r b db d\mathbf{v}_1 d\mathbf{r} d\mathbf{v} = - \int_{-\infty}^{\infty} \int_{-\infty}^{\infty} \int_{-\infty}^{\infty} \int_0^{\infty} (\ln f') (f'_1 f' - f_1 f) v_r b db d\mathbf{v}_1 d\mathbf{r} d\mathbf{v} \quad (1.91)$$

\mathbf{v}_1 and \mathbf{v} , as well as \mathbf{v}'_1 and \mathbf{v}' , are treated as the pre-collisional velocities on the left and right hand sides of the above equation, respectively. Then we have:

$$\int_{-\infty}^{\infty} \int_{-\infty}^{\infty} \int_{-\infty}^{\infty} \int_0^{\infty} (\ln f) (f'_1 f' - f_1 f) v_r b db d\mathbf{v}_1 d\mathbf{r} d\mathbf{v} = \frac{1}{2} \int_{-\infty}^{\infty} \int_{-\infty}^{\infty} \int_{-\infty}^{\infty} \int_0^{\infty} \left(\ln \frac{f}{f'} \right) (f'_1 f' - f_1 f) v_r b db d\mathbf{v}_1 d\mathbf{r} d\mathbf{v} \quad (1.92)$$

Similarly for f_1 :

$$\int_{-\infty}^{\infty} \int_{-\infty}^{\infty} \int_{-\infty}^{\infty} \int_0^{\infty} (\ln f_1) (f'_1 f' - f_1 f) v_r b db d\mathbf{v}_1 d\mathbf{r} d\mathbf{v} = \frac{1}{2} \int_{-\infty}^{\infty} \int_{-\infty}^{\infty} \int_{-\infty}^{\infty} \int_0^{\infty} \left(\ln \frac{f_1}{f'_1} \right) (f'_1 f' - f_1 f) v_r b db d\mathbf{v}_1 d\mathbf{r} d\mathbf{v} \quad (1.93)$$

As we only have one component, an interchange of the f and f_1 is not going to affect the value of the integral [10], we then have:

$$\begin{aligned} &\int_{-\infty}^{\infty} \int_{-\infty}^{\infty} \int_{-\infty}^{\infty} \int_0^{\infty} (\ln f) (f'_1 f' - f_1 f) v_r b db d\mathbf{v}_1 d\mathbf{r} d\mathbf{v} \\ &= \frac{1}{4} \int_{-\infty}^{\infty} \int_{-\infty}^{\infty} \int_{-\infty}^{\infty} \int_0^{\infty} \ln \left(\frac{f_1 f}{f'_1 f'} \right) (f'_1 f' - f_1 f) v_r b db d\mathbf{v}_1 d\mathbf{r} d\mathbf{v} \end{aligned}$$

At equilibrium, $dH(t)/dt = 0$. This suggests that:

$$\ln f + \ln f_1 = \ln f' + \ln f'_1 \quad (1.94)$$

This bears a close resemblance with conservation law in collisional motion, which leads to the result that $\ln f$ should be a linear combination of m , $m\mathbf{v}$ and $\frac{1}{2}mv^2$ as these quantities are conserved.

$$\ln f = c_1 m + m\mathbf{c}_2 \cdot \mathbf{v} - \frac{c_3}{2}mv^2 \quad (1.95)$$

c_1 , \mathbf{c}_2 and c_3 are constants. f should have the following form:

$$f = c \exp \left[-\frac{c_3}{2}m\left(\mathbf{v} - \frac{\mathbf{c}_2}{c_3}\right)^2 \right] \quad (1.96)$$

where $c = \exp[c_1 m + mc_2^2/(2c_3)]$. These constants can be found as follows:

$$\rho = \int_{-\infty}^{\infty} f d\mathbf{v} \quad (1.97)$$

$$c = \left(\frac{c_3 m}{2\pi}\right)^{1.5} \rho(\mathbf{r}, t) \quad (1.98)$$

$$\mathbf{v}_0 = \frac{1}{\rho} \int_{-\infty}^{\infty} \mathbf{v} f d\mathbf{v} \quad (1.99)$$

$$v_{0,k} = \int_{-\infty}^{\infty} v_k \left(\frac{c_3 m}{2\pi}\right)^{0.5} \exp \left[-\frac{c_3 m}{2}\left(v_k - \frac{c_{2,k}}{c_3}\right)^2 \right] dv_k \quad (1.100)$$

$$\mathbf{v}_0 = \frac{\mathbf{c}_2}{c_3} \quad (1.101)$$

$$(\mathbf{v} - \mathbf{v}_0)^2 = \int_{-\infty}^{\infty} (\mathbf{v} - \mathbf{v}_0)^2 \left(\frac{c_3 m}{2\pi}\right)^{1.5} \exp\left[-\frac{c_3}{2}m(\mathbf{v} - \mathbf{v}_0)^2\right] d\mathbf{v} \quad (1.102)$$

$$= \int_0^{\infty} 4\pi \left(\frac{c_3 m}{2\pi}\right)^{1.5} (v - v_0)^4 \exp \left[-\frac{c_3 m}{2}(\mathbf{v} - \mathbf{v}_0)^2 \right] d(v - v_0) = \frac{3}{c_3 m} \quad (1.103)$$

As we know that $\frac{m(\mathbf{v}-\mathbf{v}_0)^2}{2} = \frac{3k_b T}{2}$, $c_3 = \frac{1}{k_b T}$. This implies:

$$f = \rho \left(\frac{m}{2\pi k_b T}\right)^{1.5} \exp \left[-\frac{m(\mathbf{v} - \mathbf{v}_0)^2}{2k_b T} \right] \quad (1.104)$$

By knowing the velocity distribution as well as the mean free path of a monoatomic particle, viscosity and diffusivity can be easily calculated as these information allow us to approximate the collisional probability. This analysis is important because it allows us to calculate the diffusivity of one single bead in the polymer melt. We have:

$$f(v_x, v_y, v_z) dv_x dv_y dv_z = \rho \left(\frac{m}{2\pi k_b T}\right)^{3/2} \exp \left[-\frac{m(v_x^2 + v_y^2 + v_z^2)}{2k_b T} \right] dv_x dv_y dv_z \quad (1.105)$$

which is equivalent to:

$$f(v) dv = 4\pi \rho v^2 \left(\frac{m}{2\pi k_b T}\right)^{3/2} \exp \left[-\frac{mv^2}{2k_b T} \right] dv \quad (1.106)$$

It can then be shown that the mean value of velocity $\langle v \rangle$ is:

$$\langle v \rangle = \int_0^\infty \left(\frac{m}{2\pi k_b T} \right)^{3/2} 4\pi v^3 \exp \left[-\frac{mv^2}{2k_b T} \right] dv = \sqrt{\frac{8k_b T}{\pi m}} \quad (1.107)$$

And the mean square velocity $\langle v^2 \rangle$ is:

$$\langle v^2 \rangle = \frac{3k_b T}{m} \quad (1.108)$$

For the mean free path, the simplest way to calculate it is to firstly assume the monoatomic particle as hard sphere, and then quantify the probability of collision. The number of collision that a particle encounters per unit time is:

$$\int_0^\sigma \rho 2\pi \langle v \rangle b db = \rho \pi \sigma^2 \langle v \rangle \quad (1.109)$$

ρ and σ are the number density and hard sphere diameter of the particle. (σ here is not to be confused with the statistical weight in Section 1.5). The distance traveled by the particle in a unit time is $\langle v \rangle$ if there is no collision. Therefore, the mean free path is finally obtained as:

$$l = \frac{\langle v \rangle}{\rho \pi \sigma^2 \langle v \rangle} = \frac{1}{\rho \pi \sigma^2} \quad (1.110)$$

With these, we can approximate viscosity and diffusion coefficient.

1.4.2 Viscosity

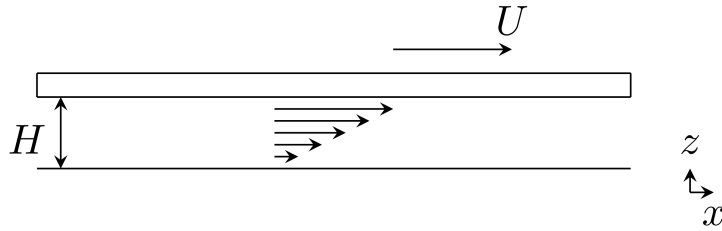


Figure 1.5: A plate on the top of the fluid moving with a velocity of U , leading to a velocity gradient. It is argued that the momentum can transfer along the z direction, and most of the momentum transfer is from above as the velocity of the particle near the top is faster.

Figure 1.5 shows a moving plate on the top with velocity U , with a distance of H above the bottom of the fluid. The gradient of momentum along the z direction is:

$$G(z) = \frac{mUz}{H}$$

The last collision occurred at a height of $z' = z - \frac{v_z l}{v}$. In a unit time, the average number of molecules in a layer passing through a horizontal plane at z can be calculated as:

$$|v_z| f(v_x, v_y, v_z) dv_x dv_y dv_z \quad (1.111)$$

with the assumption that the plate has an unit area. The flow of momentum $\psi(z)$:

$$\psi(z) = \int_{-\infty}^{\infty} \int_{-\infty}^{\infty} \int_{-\infty}^{\infty} G(z') v_z f(v_x, v_y, v_z) dv_x dv_y dv_z \quad (1.112)$$

By Taylor expansion,

$$G(z') = G(z) - \frac{v_z l}{v} G'(z) \quad (1.113)$$

Equation (1.112) then becomes:

$$\psi(z) = -\frac{mUl}{a} \int_{-\infty}^{\infty} \int_{-\infty}^{\infty} \int_{-\infty}^{\infty} \frac{v_z^2}{v} f(v_x, v_y, v_z) dv_x dv_y dv_z \quad (1.114)$$

$$\psi(z) = -\frac{mUl}{a} \int_{-\infty}^{\infty} \int_{-\infty}^{\infty} \int_{-\infty}^{\infty} \frac{v}{3} f(v_x, v_y, v_z) dv_x dv_y dv_z \quad (1.115)$$

$$\psi(z) = -\frac{\rho mUl \langle v \rangle}{3a} = -\frac{\rho ml \langle v \rangle}{3} \frac{dv}{dz} \quad (1.116)$$

We can find η by juxtaposing this final form with the formula of shear stress:

$$\sigma_{xz} = -\eta \frac{dv}{dz} \quad (1.117)$$

$$\boxed{\eta = \frac{\rho ml \langle v \rangle}{3}} \quad (1.118)$$

1.4.3 Diffusion Coefficient

Similarly, for diffusion coefficient, the flow of mass can be calculated.

$$\phi(z) = \int_{-\infty}^{\infty} \int_{-\infty}^{\infty} \int_{-\infty}^{\infty} \frac{\rho(z')}{\rho} v_z f(v_x, v_y, v_z) dv_x dv_y dv_z \quad (1.119)$$

$$\rho(z') = \rho(z) - \frac{v_z l}{v} \frac{d\rho}{dz} \quad (1.120)$$

$$\phi(z) = -l \frac{d\rho}{dz} \int_{-\infty}^{\infty} \int_{-\infty}^{\infty} \int_{-\infty}^{\infty} \frac{v_z^2}{\rho v} f(v_x, v_y, v_z) dv_x dv_y dv_z \quad (1.121)$$

$$\phi(z) = -\frac{l \langle v \rangle}{3} \frac{d\rho}{dz} \quad (1.122)$$

With the knowledge of the mass flux being:

$$J = -D \frac{d\rho}{dz} \quad (1.123)$$

one can then write:

$$\boxed{D = l\langle v \rangle / 3} \quad (1.124)$$

This analysis of viscosity and diffusivity is simple, but elegant. It allows one to directly evaluate these transport coefficients without solving any sophisticated equations and knowing the gradient of momentum and mass accurately. Nonetheless, it was found that Equation (1.118) and Equation (1.124) underestimate these transport coefficients. As demonstrated in the forthcoming section, with the Chapman-Enskog method, these transport coefficients were expressed in terms of weighed integrals of the angle of deflection, which were found to agree better with experimental values.

1.4.4 A More Rigorous Approximation of Transport Coefficient

As mentioned above, a more rigorous calculation of transport coefficient, such as diffusivity requires the knowledge of the deflection angle χ in collision between particles.

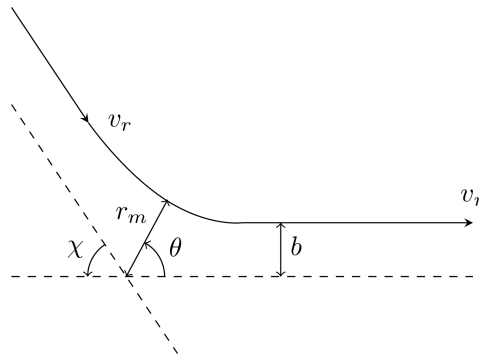


Figure 1.6: An illustration of one particle traveling at a velocity of v_r , colliding with another stationary particle. Collision is elastic in this case, that the magnitude of v_r does not change after the collision.

If a particle is traveling with v_r , then it can be said that the particle is moving as if other particles in its surrounding do not move at all. Such scenario is depicted in Figure 1.6. The

energy during the collision is equal to that before or after the collision. In polar coordinate, we obtain:

$$\frac{1}{2}\mu v_r^2 = \frac{1}{2}\mu(\dot{r}^2 + r^2\dot{\theta}^2) + u(r) \quad (1.125)$$

$u(r)$ is the interaction potential between two particles. Angular momentum before or after the collision is $\mu b v_r = \mu r^2 \dot{\theta}$.

$$\mu v_r^2 = \mu \dot{r}^2 + \mu v_r^2 (b^2/r^2) + 2u(r) \quad (1.126)$$

This leads to Equation (1.127).

$$\dot{r} = \sqrt{v_r^2 \left(1 - \frac{b^2}{r^2}\right) - \frac{2u(r)}{\mu}} \quad (1.127)$$

We know that $\dot{\theta} = \frac{b v_r}{r^2}$.

$$\frac{dr}{d\theta} = \frac{r^2}{b v_r} \sqrt{v_r^2 \left(1 - \frac{b^2}{r^2}\right) - \frac{2u(r)}{\mu}} \quad (1.128)$$

An expression for θ is then obtained.

$$\int_0^{\theta_m} d\theta = \int_{r_m}^{\infty} \frac{b v_r}{r^2 \sqrt{v_r^2 \left(1 - \frac{b^2}{r^2}\right) - \frac{2u(r)}{\mu}}} dr \quad (1.129)$$

The deflection angle (χ) is related to θ_m that $\chi = \pi - 2\theta_m$. χ can be calculated using the following:

$$\chi = \pi - 2 \int_{r_m}^{\infty} \frac{b v_r}{r^2 \sqrt{v_r^2 \left(1 - \frac{b^2}{r^2}\right) - \frac{2u(r)}{\mu}}} dr \quad (1.130)$$

It is impossible to solve the integral in Equation (1.130) analytically if the potential $u(r)$ is a 6-12 LJ potential. But analytical form of χ exists for a hard sphere potential. For hard sphere potential, r_m is always greater than σ . The key of evaluating the integral is to let $\sqrt{1 - \frac{b^2}{r^2}} = \cos \alpha$, and $\frac{b}{r} = \sin \alpha$, such that $dr = -b \frac{\cos \alpha}{\sin^2 \alpha} d\alpha$. As $r \rightarrow \infty$, $\alpha \rightarrow 0$, and as $r \rightarrow r_m$, $\alpha \rightarrow \arcsin(\frac{b}{r_m})$.

$$\int_{r_m}^{\infty} \frac{b}{r^2 \sqrt{\left(1 - \frac{b^2}{r^2}\right)}} dr = \int_{r_m}^{\infty} \frac{\sin^2 \alpha}{b \cos \alpha} dr = - \int_{\arcsin(b/r_m)}^0 d\alpha = \arcsin\left(\frac{b}{r_m}\right) \quad (1.131)$$

Substitute this result into Equation (1.130), we get:

$$\chi = \pi - 2 \arcsin\left(\frac{b}{r_m}\right) = 2 \arccos\left(\frac{b}{r_m}\right) \quad (1.132)$$

When $b \leq \sigma$, $\chi = 2 \arccos(\frac{b}{\sigma})$, otherwise $\chi = 0$. Now, let us consider the change in momentum of particle 1:

$$\Delta(m_1 \mathbf{v}_1) = m_1(\mathbf{v}_1' - \mathbf{v}_1) \quad (1.133)$$

By Equation (1.72), Equation (1.133) can be rewritten as:

$$\Delta(m_1 \mathbf{v}_1) = \mu_{12}(\mathbf{v}_r' - \mathbf{v}_r) \quad (1.134)$$

Then, with Equation (1.72), we can consider the momentum of particle 1:

$$m_1 \mathbf{v}_1 = m_1(\mathbf{v}_c + \frac{m_2}{m_1 + m_2} \mathbf{v}_r) \quad (1.135)$$

Combining the results of Equation (1.133) and Equation (1.134), we have:

$$m_1 \mathbf{v}_1 \cdot \Delta(m_1 \mathbf{v}_1) = v_r^2 \mu_{12}^2 (\cos \chi - 1) + m_1 \mu_{12} \mathbf{v}_c \cdot (\mathbf{v}_r' - \mathbf{v}_r) \quad (1.136)$$

The averaged change of this quantity with respect to time is therefore:

$$\left\langle \frac{m_1 \mathbf{v}_1 \cdot \Delta(m_1 \mathbf{v}_1)}{\Delta t} \right\rangle = 2\pi \rho_2 \left(\frac{\mu_{12}}{2\pi k_b T} \right)^{1.5} \int_0^\infty \int_0^\sigma v_r^3 \mu_{12}^2 (\cos \chi - 1) \exp\left(-\frac{\mu_{12} v_r^2}{2k_b T}\right) b db d\mathbf{v}_r \quad (1.137)$$

With:

$$4\pi \left(\frac{\mu_{12}}{2\pi k_b T} \right)^{1.5} \int_0^\infty v_r^5 \exp\left(-\frac{\mu_{12} v_r^2}{2k_b T}\right) dv_r = \frac{8k_b T}{\mu_{12}} \sqrt{\frac{2k_b T}{\mu_{12} \pi}} \quad (1.138)$$

And:

$$2\pi \int_0^\infty (\cos \chi - 1) b db = -\pi \sigma^2 \quad (1.139)$$

if we assume that the particle is hard-sphere. We then simplify Equation (1.137) to the following:

$$\left\langle \frac{m_1 \mathbf{v}_1 \cdot \Delta(m_1 \mathbf{v}_1)}{\Delta t} \right\rangle = -\frac{8k_b T}{\mu_{12}} \sqrt{\frac{2k_b T \pi}{\mu_{12}}} \rho_2 \sigma^2 \mu_{12}^2 \quad (1.140)$$

This is important as we know that the velocity correlation function has this form:

$$\langle \mathbf{v}_1(t) \cdot \mathbf{v}_1(0) \rangle = \langle v_1^2 \rangle e^{-at} \quad (1.141)$$

Taking derivative of Equation (1.141) with time at $t = 0$ gives us:

$$a = -\frac{\langle \mathbf{v}_1(0) \cdot \left(\frac{d\mathbf{v}_1(t)}{dt}\right)_{t=0} \rangle}{\langle v_1^2 \rangle} \quad (1.142)$$

This implies that:

$$a = - \lim_{\Delta t \rightarrow 0} \frac{\langle \left(\frac{\Delta \mathbf{v}_1(t)}{\Delta t} \right)_{t=0} \cdot \mathbf{v}_1(0) \rangle}{\langle v_1^2 \rangle} \quad (1.143)$$

The diffusion coefficient can then be written as:

$$D = -k_b T \left[\left\langle \frac{m_1 \mathbf{v}_1 \cdot \Delta(m_1 \mathbf{v}_1)}{\Delta t} \right\rangle \right]^{-1} m_1 \langle v_1^2 \rangle \quad (1.144)$$

This is because:

$$D = \frac{1}{3} \int_0^\infty \langle \mathbf{v}_1(t) \cdot \mathbf{v}_1(0) \rangle dt \quad (1.145)$$

It is known that from the Maxwell-Boltzmann distribution, $\langle v_1^2 \rangle = \frac{3k_b T}{m_1}$. Thus, by using these results, we can write:

$$D = \frac{3}{8\rho_2\sigma^2} \sqrt{\frac{k_b T}{2\pi\mu_{12}}} \quad (1.146)$$

If particle 1 and particle 2 share the same mass m , then the expression is further simplified as:

$$D = \frac{3}{8\rho_2\sigma^2} \sqrt{\frac{k_b T}{\pi m}} \quad (1.147)$$

Interestingly, Equation (1.147) can also be obtained by solving the Boltzmann Equation hierarchically using Chapman-Enskog method as well as Sonine polynomial [10]. Similarly, we can determine η using this approach.

$$\eta = \frac{m^2}{k_b T V} \int_0^\infty \langle v_x(t)v_x(0) \rangle \langle v_y(t)v_y(0) \rangle dt \quad (1.148)$$

The velocity correlation function $v_x(t)v_x(0)$ can be assumed as this form:

$$\langle v_x(t)v_x(0) \rangle = \langle v_y(t)v_y(0) \rangle = \frac{k_b T}{m} e^{-at} \quad (1.149)$$

For which, $a = \frac{8\rho_1\sigma^2}{3} \sqrt{\frac{\pi k_b T}{m}}$. Hence:

$$\eta = \frac{m^2}{k_b T V} \cdot \frac{k_b^2 T^2}{m^2} \cdot \frac{3\sqrt{m}}{16\rho_1\sigma^2\sqrt{\pi k_b T}} = \frac{3}{16\sigma^2} \sqrt{\frac{m k_b T}{\pi}} \quad (1.150)$$

This result is lower by a factor of 1.67 than that obtained by Chapman-Enskog method along with Sonine polynomial.

1.5 Static properties of polymers

This section aims to introduce the fundamentals of rotational isomeric state model derived by Flory [11] with reference to the book written by Mattice and Suter [12]. We have used this model to study the conformational properties, such as characteristic ratio, end-to-end vector as well as mean-squared end-to-end distance, of polyethylene with different degree of polymerization. The initial configuration of polymer chain in the MD simulation was also prepared using this model. It is worthwhile to note that unlike the other sections, in which vector quantities are represented by boldface letters, they are highlighted by a right arrow only in this section for clarity.

It is well-known that the conformation of a polymer chain can be characterized using the end-to-end distance, which can be computed theoretically using the freely-joint chain, free rotation and independent hindered rotation models [13, 14, 15]. Consider a polymer chain consists of C-C backbone with a C-C bond length l and with n of this bond, armed with the knowledge of vector calculus, the end-to-end vector \vec{r} can be expressed as below:

$$\vec{r} = \sum_i^n \vec{l}_i \quad (1.151)$$

To determine the magnitude of \vec{r} , we would have to evaluate the dot product of \vec{r} with itself.

$$\langle \vec{r} \cdot \vec{r} \rangle = nl^2 + \left\langle \sum_i^n \sum_{j \neq i}^n \vec{l}_i \cdot \vec{l}_j \right\rangle \quad (1.152)$$

n is the number of C-C bonds, which is not to be confused the number of particles N in Section 1.3 and Chapter 2, with the number of carbon atoms of polyethylene from Chapter 3 to Chapter 9. Depending on our assumptions, there are different ways to handle the second term in Equation (1.152) (i.e. $\langle \sum_i^n \sum_{j \neq i}^n \vec{l}_i \cdot \vec{l}_j \rangle$)[13, 14, 15]. Table 1.2 summarizes ways to compute $\langle r^2 \rangle$ using different aforementioned models[13, 14, 15]. In Table 1.2, θ is defined as the subtraction of 180° from the bond angle (for example, for polyethylene, $\theta = 180^\circ - 112^\circ = 68^\circ$) and ϕ is the torsion angle of the C-C backbone bond.

As observed in Table 1.2, for different models, nl^2 is multiplied by a different prefactor. As $n \rightarrow \infty$, we can then write:

$$\langle r^2 \rangle = C_\infty nl^2 \quad (1.153)$$

Table 1.2: Formulae of $\langle r^2 \rangle$ for different model chains.

Model	$\langle r^2 \rangle$
Freely-joint chain	nl^2
Freely-rotating chain	$\left(\frac{1+\cos\theta}{1-\cos\theta}\right)nl^2$
Hindered-rotating chain	$\left(\frac{1+\cos\theta}{1-\cos\theta}\right)\left(\frac{1+\langle\cos\phi\rangle}{1-\langle\cos\phi\rangle}\right)nl^2$

C_∞ is the characteristic ratio as $n \rightarrow \infty$. It is pertinent to note that $\langle \cos \phi \rangle$ in the independent hindered rotation model (cf., Table 1.2) can be calculated using Boltzmann's statistics with the knowledge of the energy of a *trans* (t) state (i.e. $\phi = 180^\circ$) and a *gauche plus* state (g^+) or *gauche minus* state (g^-) (i.e. $\phi = 60^\circ$ or 300°). To make our lives easier, in this paper, we are going to limit our discussion on a three-state model, that there are only three minima in the torsional energy curve. Furthermore, such a curve is symmetrical. Therefore, $\langle \cos \phi \rangle$ for the independent hindered rotation model can be easily computed by Equation (1.154).

$$\langle \cos \phi \rangle = \frac{1}{Z} \cos \phi_t + 2 \frac{\exp\left(-\frac{E_g - E_t}{RT}\right)}{Z} \cos \phi_g \quad (1.154)$$

Z is the partition function, E_t and E_g are the energy of t state and g^+/g^- state, and R is the ideal gas constant. And Z in this case can be calculated by Equation (1.155).

$$Z = 1 + 2 \exp\left(-\frac{E_g - E_t}{RT}\right) \quad (1.155)$$

The independent hindered rotation model does not account for the fact that for bond i to be in a particular state would affect the probability of bond $i + 1$ to be in another state, owing to a second-order interaction. In other words, as there are correlation between a bond and its adjacent neighbour, the possible states for the case of a pentane molecule that have to be included in the Boltzmann statistical calculation are tt , tg^+ , tg^- , g^+g^- , g^-g^+ , g^+g^+ and g^-g^- . In this sense, evaluation of Z has become a daunting task for macromolecule.

1.5.1 Partition Function and Probability

An expression that evaluates Z straightforwardly consists of multiplication of matrix and arrays [16, 12].

$$Z = \mathbf{U}_1 \mathbf{U}_i^{(n-2)} \mathbf{U}_n \quad (1.156)$$

Let us first define a matrix \mathbf{U}_i that contains the statistical weight of all the possible states for $1 < i < n$:

$$\mathbf{U}_i = \begin{bmatrix} 1 & \sigma & \sigma \\ 1 & \sigma & \sigma\omega \\ 1 & \sigma\omega & \sigma \end{bmatrix}_i \quad (1.157)$$

$\sigma = \exp(-\frac{E_g - E_t}{RT})$ and $\omega = \exp(-\frac{\varepsilon}{RT})$. ε is the energy involved in the second-order interaction in either g^+g^- or g^-g^+ states. In the multiplication of the matrix, that is going to be shown, we would find that the rows and columns of \mathbf{U}_i corresponds to t , g^+ and g^- for bond $i - 1$ and bond i respectively. By realizing the fact that for $n=3$, Equation (1.155) can be applied and $Z = 1 + 2\sigma$, \mathbf{U}_1 and \mathbf{U}_n are defined as below:

$$\mathbf{U}_1 = [1 \quad 0 \quad 0] \quad (1.158)$$

$$\mathbf{U}_n = [1 \quad 1 \quad 1]^T \quad (1.159)$$

To simplify Equation (1.156), we solve for the eigenvalues of \mathbf{U}_i such that Equation (1.156) can be rewritten as follows:

$$Z = \mathbf{U}_1 \mathbf{B} \mathbf{\Lambda}^{(n-2)} \mathbf{B}^{-1} \mathbf{U}_n \quad (1.160)$$

As we know that,

$$\mathbf{U}_i^{(n-2)} = \mathbf{B} \mathbf{\Lambda}^{(n-2)} \mathbf{B}^{-1} \quad (1.161)$$

$\mathbf{\Lambda}$ is a diagonal matrix with eigenvalues of \mathbf{U}_i , and \mathbf{B} is a matrix containing the corresponding eigenvectors. We can solve for $\mathbf{\Lambda}$ and \mathbf{B} by realizing the fact that $\det(\mathbf{U}_i - \mathbf{\Lambda}) = 0$ and $\mathbf{v}_j = \mathbf{U}_i - \lambda_j \mathbf{I}$, where \mathbf{v}_j is the eigenvector corresponding to λ_j . And these can be solved analytically by the assumption that the torsional energy curve is symmetrical that \mathbf{U}_i can be reduced to a 2×2 matrix, and \mathbf{U}_1 and \mathbf{U}_n become arrays with two elements.

$$\mathbf{U}_i = \begin{bmatrix} 1 & 2\sigma \\ 1 & \sigma(1 + \omega) \end{bmatrix}_i \quad (1.162)$$

$$\mathbf{U}_1 = [1 \quad 0] \quad (1.163)$$

$$\mathbf{U}_n = [1 \quad 1]^T \quad (1.164)$$

Therefore, the eigenvalues λ can be determined by Equation (1.165) and Equation (1.166).

$$\lambda^2 - [\sigma(1 + \omega) + 1]\lambda - 2\sigma = 0 \quad (1.165)$$

$$\lambda = \frac{\sigma(1 + \omega) + 1 \pm \sqrt{[1 - \sigma(1 + \omega)]^2 + 8\sigma}}{2} \quad (1.166)$$

With a little mathematical trick, one will find that:

$$\mathbf{B} = \begin{bmatrix} \lambda_1 - \sigma(1 + \omega) & \lambda_2 - \sigma(1 + \omega) \\ 1 & 1 \end{bmatrix} \quad (1.167)$$

$$\mathbf{B}^{-1} = \frac{1}{\lambda_1 - \lambda_2} \begin{bmatrix} 1 & \sigma(1 + \omega) - \lambda_2 \\ -1 & \lambda_1 - \sigma(1 + \omega) \end{bmatrix} \quad (1.168)$$

$$\mathbf{B}\mathbf{\Lambda}^{(n-2)}\mathbf{B}^{-1} = \frac{1}{\lambda_1 - \lambda_2} \begin{bmatrix} \lambda_1^{n-2}(\lambda_1 - \sigma(1 + \omega)) - \lambda_2^{n-2}(\lambda_2 - \sigma(1 + \omega)) & H_{1,2} \\ H_{2,1} & H_{2,2} \end{bmatrix} \quad (1.169)$$

As revealed in Equation (1.160), Z is in fact the summation of the elements of the first row of $\mathbf{B}\mathbf{\Lambda}^{(n-2)}\mathbf{B}^{-1}$. Therefore, the exact values of $H_{2,1}$ and $H_{2,2}$ are unimportant and $H_{1,2}$ is expressed as below:

$$H_{1,2} = [\lambda_1 - \sigma(1 + \omega)][\lambda_1^{(n-2)}\sigma(1 + \omega) - \lambda_2\lambda_1^{(n-2)}] + [\lambda_2 - \sigma(1 + \omega)][\lambda_2^{(n-2)}\lambda_1 - \lambda_2^{(n-2)}\sigma(1 + \omega)] \quad (1.170)$$

With these, Z can be evaluated by:

$$Z = \frac{1}{\lambda_1 - \lambda_2} [\lambda_1^{n-2}(\lambda_1 - \sigma(1 + \omega)) - \lambda_2^{n-2}(\lambda_2 - \sigma(1 + \omega)) + H_{1,2}] \quad (1.171)$$

With algebraic rearrangement, we find that:

$$Z = \frac{\lambda_1^{n-1}(1 - \lambda_2) + \lambda_2^{n-1}(\lambda_1 - 1)}{\lambda_1 - \lambda_2} + \frac{[\sigma(1 + \omega)(\lambda_2^{(n-2)} - \lambda_1^{(n-2)}) - \lambda_2^{(n-1)} + \lambda_1^{(n-1)} + \lambda_2\lambda_1^{(n-2)} - \lambda_2^{(n-2)}\lambda_1]}{\lambda_1 - \lambda_2} + \frac{\sigma^2(1 + \omega)^2(\lambda_2^{(n-2)} - \lambda_1^{(n-2)})}{\lambda_1 - \lambda_2} \quad (1.172)$$

As the first term is much greater than the sum of the second and third terms. Equation (1.172) can be simplified as below:

$$Z \approx \frac{\lambda_1^{n-1}(1 - \lambda_2) + \lambda_2^{n-1}(\lambda_1 - 1)}{\lambda_1 - \lambda_2} \quad (1.173)$$

To test if Equation (1.173) is a good approximation of Z , we have computed Z using both Equations (1.172) and (1.173), as well as obtained the percentage error for different n . They are reported in Table 1.3, which shows the calculated Z as a function of n with $\sigma = 0.543$ and $\omega = 0.088$. Our results agree with that of Mattice and Suter [12]. The probability of bond i in a particular state η , $p_{i;\eta}$, can be calculated by starting with the postulation that Z can be expanded as presented in Equation (1.174).

$$Z = A + \sigma_{\eta;i} \left(\frac{\partial Z}{\partial \sigma_{\eta;i}} \right) \quad (1.174)$$

n	Z	Percentage Error (%)
4	3.795	2.76×10^{-15}
9	83.119	1.11×10^{-14}
30	3.52×10^7	5.00×10^{-15}
100	2.00×10^{26}	7.08×10^{-15}

Table 1.3: Z as a function of n for $\sigma = 0.543$ and $\omega = 0.088$.

As in Equation (1.174), Z is expressed as the sum of statistical weights, A , and the sum of statistical weights, where bond i is in state η . Therefore, the probability for bond i to be in the state of η can be determined:

$$p_{\eta;i} = \frac{\sigma_{\eta;i}}{Z} \frac{\partial Z}{\partial \sigma_{\eta;i}} \quad (1.175)$$

$\sigma_{\eta;i} \frac{\partial Z}{\partial \sigma_{\eta;i}}$ can be explicitly expressed as below:

$$\sigma_{\eta;i} \frac{\partial Z}{\partial \sigma_{\eta;i}} = \mathbf{U}_1 \mathbf{U}_2 \dots \mathbf{U}'_{\eta;i} \dots \mathbf{U}_n \quad (1.176)$$

$$\mathbf{U}'_{g^+;i} = \mathbf{U}'_{g^-;i} = \frac{1}{2} \begin{bmatrix} 0 & 2\sigma \\ 0 & (1 + \omega)\sigma \end{bmatrix}_i \quad (1.177)$$

The matrix is multiplied by $\frac{1}{2}$ due to our assumption that the torsional energy curve is symmetrical. $p_{\eta;i}$ was evaluated for different bond i using Equation (1.175) and Equation (1.176). Figure 1.7 shows $p_{g^+;i}$ at different i and n . It is intriguing to point that $p_{g^+;i}$ for the bond near the chain end is slightly higher than that of others. And intuitively, $p_{t;i}$ can be calculated by $p_{t;i} = 1 - p_{g^+;i} - p_{g^-;i}$. The fraction of bonds in η state, p_η , in the polymer chain can be calculated using Equation (1.178).

$$p_\eta = \frac{1}{n-2} \sum_{i=2}^{n-1} p_{\eta;i} \quad (1.178)$$

1.5.2 Exact Calculation of End-to-End Vector

Armed with the knowledge of computing Z and $p_{\eta;i}$, we can proceed to the exact evaluation of $\langle \vec{r} \rangle$. The evaluation of $\langle \vec{r} \rangle$ with reference to the book written by Flory as well as that by Mattice and Suter is achieved by expressing it in terms of the local coordinate of the first bond vector, $\vec{l} = [l, 0, 0]$. It is well-known that rotation of a particular vector in a 3D space can be achieved by multiplying it with rotation matrices \mathbf{T}_1 and \mathbf{T}_i (for $i > 1$), respectively.

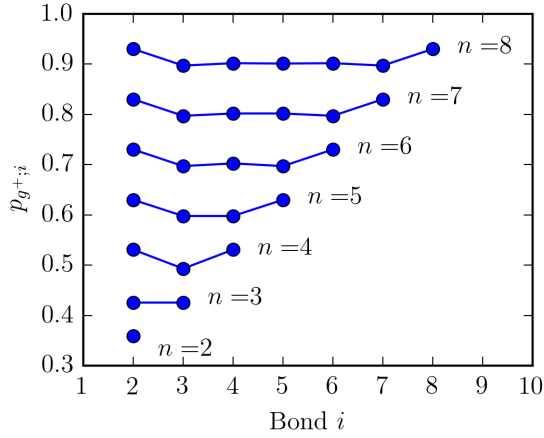


Figure 1.7: $p_{g^{+};i}$ of different bond i and different n . The $p_{g^{+};i}$ for $n > 2$ is shifted up for better presentation purpose.

$$\mathbf{T}_1 = \begin{bmatrix} \cos \theta & \sin \theta & 0 \\ \sin \theta & -\cos \theta & 0 \\ 0 & 0 & -1 \end{bmatrix} \quad (1.179)$$

$$\mathbf{T}_i = \begin{bmatrix} \cos \theta & \sin \theta & 0 \\ -\sin \theta \cos \phi & \cos \theta \cos \phi & -\sin \phi \\ -\sin \theta \sin \phi & \cos \theta \sin \phi & \cos \phi \end{bmatrix}_i \quad (1.180)$$

θ and ϕ are the bond angle and torsional angle for bond i in \mathbf{T}_i . It is therefore obvious that:

$$\vec{l}_i^S = \left[\prod_{m=0}^{i-1} \mathbf{T}_m \right] \vec{l} \quad (1.181)$$

Note that \mathbf{T}_0 is an identity matrix and $\vec{l} = [l, 0, 0]$. The superscript S of \vec{l}_i^S reminds us that the components of the vector are expressed in terms of global coordinates. \vec{r} can be then evaluated by Equation (1.182).

$$\vec{r} = \sum_{i=1}^n \vec{l}_i^S = \sum_{i=1}^n \left[\prod_{m=0}^{i-1} \mathbf{T}_m \right] \vec{l} \quad (1.182)$$

To make life easier, Mattice and Suter defines a transformation matrix \mathbf{R}_i for bond i that it is a 3×4 matrix with the form:

$$\mathbf{R}_i = \left[\prod_{m=0}^{i-1} \mathbf{T}_m \quad r_{0i}^{\vec{l}} \right] \quad \text{for } i > 1 \quad (1.183)$$

And,

$$\mathbf{R}_1 = \left[\mathbf{T}_1 \quad \vec{l}_1 \right] \quad \text{for } i = 1 \quad (1.184)$$

\vec{r}_{0i} is the vector from the first bond to bond i . And a 4×4 matrix, \mathbf{A}_i , for $1 < i < n$, and a 4×1 array, \mathbf{A}_n , are defined as below,

$$\mathbf{A}_i = \begin{bmatrix} \mathbf{T}_i & \vec{l} \\ \mathbf{0} & 1 \end{bmatrix}_i \quad (1.185)$$

$$\mathbf{A}_n = \begin{bmatrix} \vec{l}^T & 1 \end{bmatrix}^T \quad (1.186)$$

Such that,

$$\mathbf{R}_i = \mathbf{R}_{i-1} \mathbf{A}_i \quad (1.187)$$

As we can see from above, the last column of the matrix \mathbf{R}_i is the most valuable as it is \vec{r} . Therefore, \vec{r} can be simply expressed in Equation (1.188).

$$\vec{r} = \mathbf{R}_1 \prod_{i=2}^n \mathbf{A}_i \quad (1.188)$$

With $\mathbf{A}_1 = \mathbf{R}_1$, Equation (1.188) can be rewritten.

$$\vec{r} = \prod_{i=1}^n \mathbf{A}_i \quad (1.189)$$

Free and Independent Hindered Rotation

For free rotation and independent hindered rotation, we can simply use $\langle \mathbf{A}_i \rangle$, which is constructed using $\langle \mathbf{T}_i \rangle$, to calculate $\langle \vec{r} \rangle$ by Equation (1.189). $\langle \mathbf{T}_i \rangle$ are identical for bond $1 < i < n$ that the $\cos \phi$ and $\sin \phi$ terms in Equation (1.180) are substituted by $\langle \cos \phi \rangle$ and $\langle \sin \phi \rangle$, which can be calculated using Equation (1.154) for independent hindered rotation model and they are zero for free rotation model. Figure 1.8 (a) and (b) show the x and y components of $\langle \vec{r} \rangle$ at different n for polyethylene with free rotation model (i.e. $\langle \cos \phi \rangle = 0$) and independent hindered rotation model, respectively. As $n \rightarrow \infty$, we found that x and y components converge to a particular value that $\langle \vec{r} \rangle_{n \rightarrow \infty}$ can be calculated using Equation (1.190).

$$\langle \vec{r} \rangle_{n \rightarrow \infty} = \frac{l}{(1 - \cos \theta)(1 + \langle \cos \phi \rangle)} \begin{bmatrix} 1 - \cos \theta \langle \cos \phi \rangle \\ \sin \theta \\ 0 \end{bmatrix} \quad (1.190)$$

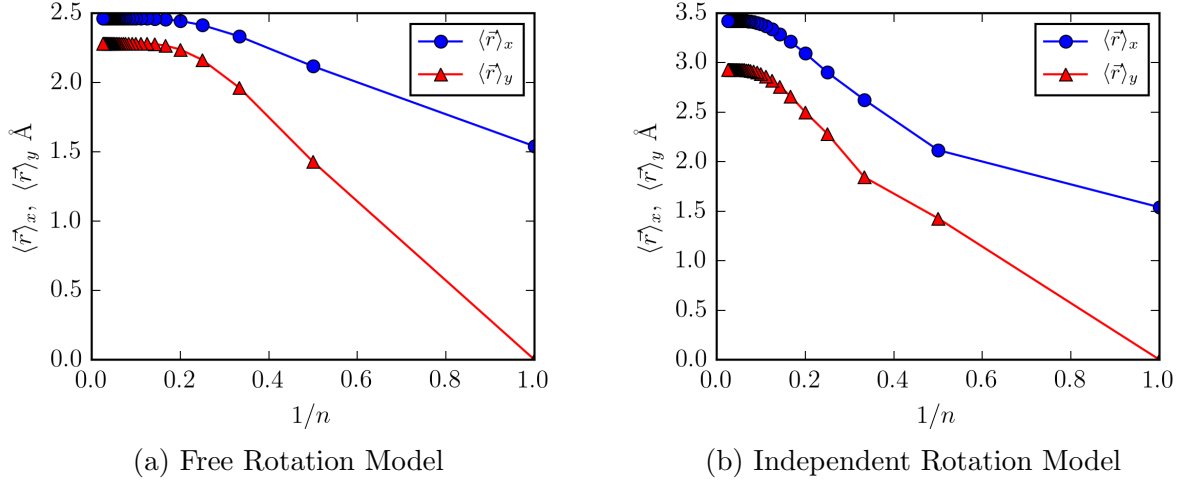


Figure 1.8: x and y components of $\langle \vec{r} \rangle$ evaluated using Equation (1.188) at different n .

Interdependent Hindered Rotation

For interdependent hindered rotation, $\langle \vec{r} \rangle$ would be an ensemble-average of \vec{r}_κ of a polymer chain in different κ states.

$$\langle \vec{r} \rangle = \sum_{\kappa} p_{\kappa} \vec{r}_{\kappa} \quad (1.191)$$

Alternatively, Equation (1.191) can be written in terms of Z and the statistical weight w_i of each bond i .

$$\langle \vec{r} \rangle = \frac{1}{Z} \sum_{\kappa} \left(\prod_{i=1}^n w_i \mathbf{A}_i \right)_{\kappa} \quad (1.192)$$

As demonstrated in the calculation of Z , the summation of w_i can be simplified with the use of matrix \mathbf{U}_i . In the same sense, the term $\sum_{\kappa} \left(\prod_{i=1}^n w_i \mathbf{A}_i \right)_{\kappa}$ can be simplified with the use of matrix \mathbf{U}_i . With the definition of \mathbf{U}_i in Equation (1.157), we define a 1×12 array \mathcal{A}_1 , a 12×12 matrix \mathcal{A}_i (for $1 < i < n$) as well as a 12×1 array \mathcal{A}_n .

$$\mathcal{A}_1 = [\mathbf{A}_1 \quad \mathbf{0} \quad \mathbf{0}] \quad (1.193)$$

$$\mathcal{A}_i = \begin{bmatrix} \mathbf{A}_t & \sigma \mathbf{A}_{g^+} & \sigma \mathbf{A}_{g^-} \\ \mathbf{A}_t & \sigma \mathbf{A}_{g^+} & \sigma \omega \mathbf{A}_{g^-} \\ \mathbf{A}_t & \sigma \omega \mathbf{A}_{g^+} & \sigma \mathbf{A}_{g^-} \end{bmatrix}_i \quad \text{for } 1 < i < n \quad (1.194)$$

$$\mathcal{A}_n = [\mathbf{A}_n \quad \mathbf{A}_n \quad \mathbf{A}_n]^T \quad (1.195)$$

Now, Equation (1.192) can be simplified to a large extent (cf., Equation (1.196)).

$$\langle \vec{r} \rangle = \frac{1}{Z} \prod_{i=1}^n \mathcal{A}_i \quad (1.196)$$

Figure 1.9 shows the x and y components of $\langle \vec{r} \rangle$ at different n for polyethylene, which has $\theta = 68^\circ$, $\phi_t = 180^\circ$, $\phi_{g^+} = 60^\circ$, $\phi_{g^-} = 300^\circ$ and $l = 1.54\text{\AA}$. Our calculation results again agree with that mentioned by Mattice and Suter [12].

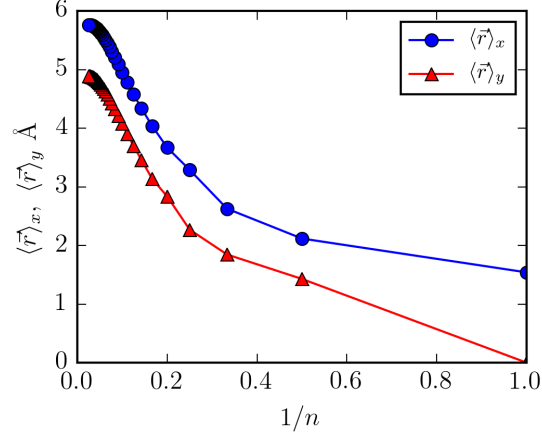


Figure 1.9: x and y components of $\langle \vec{r} \rangle$ at different n for polyethylene in interdependent hindered rotation model.

1.5.3 Exact Calculation of Mean-Square End-to-End Distance and Characteristic Ratio

Nevertheless, in order to obtain C_n at different n for interdependent hindered rotation model, $\langle r^2 \rangle$ has to be obtained using similar procedures to that of $\langle \vec{r} \rangle$. Analogous to the use of \mathbf{A}_i in the evaluation of \vec{r} , we define a 1×5 array \mathbf{G}_1 , a 5×5 matrix \mathbf{G}_i and a 5×1 array \mathbf{G}_n for calculating r^2 .

$$\mathbf{G}_1 = [1 \quad l \cos \theta \quad l \sin \theta \quad 0 \quad l^2] \quad (1.197)$$

$$\mathbf{G}_i = \begin{bmatrix} 1 & 2\vec{l}^T \mathbf{T} & l^2 \\ \mathbf{0} & \mathbf{T}_i & \vec{l} \\ 0 & \mathbf{0} & 1 \end{bmatrix}_i \quad \text{for } 1 < i < n \quad (1.198)$$

$$\mathbf{G}_n = [l^2 \quad \vec{l}^T \quad 1]^T \quad (1.199)$$

In this way, r^2 can be calculated using Equation (1.200).

$$r^2 = \prod_{i=1}^n \mathbf{G}_i \quad (1.200)$$

Free Rotation and Independent Rotation Models

Similar to what have been done for $\langle \vec{r} \rangle$, we use $\langle \mathbf{G}_i \rangle$, which is constructed using $\langle \mathbf{T}_i \rangle$ to calculate $\langle r^2 \rangle$ using Equation (1.200). Note that $\langle \mathbf{G}_i \rangle$ is identical for $1 < i < n$.

Interdependent Rotation Model

For interdependent hindered rotation model, \mathcal{G}_1 , \mathcal{G}_i and \mathcal{G}_n are 1×15 array, 15×15 matrix as well as 15×1 array, respectively, which are constructed using \mathbf{G}_i in a similar fashion as that of \mathcal{A}_i (cf., Equations (1.193), (1.194) and (1.195)). It seems to be superfluous to explicitly write the expression for \mathcal{G}_1 , \mathcal{G}_i and \mathcal{G}_n in this paper. $\langle r^2 \rangle$ is then computed using Equation (1.201).

$$\langle r^2 \rangle = \frac{1}{Z} \prod_{i=1}^n \mathcal{G}_i \quad (1.201)$$

The characteristic ratio, C_n , for different models can be now evaluated as a function of n using Equation (1.202). Figure 1.10 shows the dependence of C_n on n for polyethylene for free rotation model, independent hindered rotation model as well as interdependent hindered rotation model.

$$C_n = \frac{\langle r^2 \rangle}{nl^2} \quad (1.202)$$

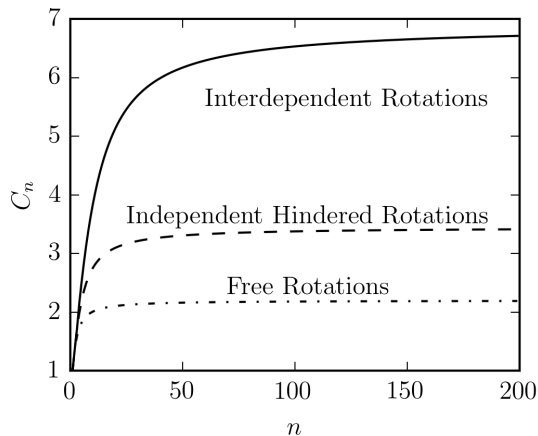


Figure 1.10: C_n at different n for polyethylene for free rotation model, independent hindered rotation model as well as interdependent hindered rotation model.

1.6 Summary

In the first part of this chapter, we have explored the dynamics as well as statistical mechanics of monoatomic liquid and ideal gas. The radial distribution function $g(r)$ is a key function in the pressure equation. It was also demonstrated that the Maxwell-Boltzmann distribution can be derived using the Boltzmann H-theorem, and such distribution allows us to obtain different transport coefficients of ideal gas. Alternatively, transport coefficients of ideal gas can be obtained by integration of different time correlation functions, such as the time correlation function of velocity.

In the second part of this chapter, the rotational isomeric model has been presented, which is crucial in generating the initial configuration of the polymer for MD simulation. Such model has taken into account of the bond length, bond angle as well as torsion angle in the calculation of the characteristic ratio of polymer.

Chapter 2

Molecular Dynamics, Numerical Simulations and Numerical Analysis

In Chapter 1, we have dealt with linear equations of motion. But in many-body system, the equation of motion is highly nonlinear due to the nonlinear bonded and non-bonded forces acting upon the atoms. This is particularly true in the case of MD simulation of polymer chain when we would like to evaluate the many-chain effect on the dynamics of a polymer chain. In such case, the equation of motion can only be solved numerically.

2.1 MD Simulation

Equation of motion for MD simulation:

$$m_i \ddot{\mathbf{r}}_i = \mathbf{F}_i \quad (2.1)$$

The force acting on the i th atom can be a function of the positions of other particles and it is nonlinear (you should expect some square term or even higher order exponent term of the positions in \mathbf{F}_i). Due to the absence of a friction term in Equation (2.1), one may argue that there is no damping in the system and therefore, the system never relaxes. In fact, the friction term will come into play, when we consider the temperature coupling of the equation of motion.

2.1.1 Temperature and Pressure Coupling: Nonholonomic Constraints of the Equation of Motion

With respect to the temperature and pressure coupling in equation of motion, Gauss proposed the following curvature function, which is a function of $\ddot{\mathbf{r}}_i$ [17]:

$$C(\ddot{\mathbf{r}}) = \frac{1}{2} \sum_{i=1}^N m_i \left(\ddot{\mathbf{r}}_i - \frac{\mathbf{F}_i}{m_i} \right)^2 \quad (2.2)$$

Here, N is the total number of atoms. If the system is not subjected to any constraint, then it should evolve according to Equation (2.1), and $C = 0$. To couple the system to a particular temperature, the following constraint function is defined:

$$g(\dot{\mathbf{r}}) = \left(\sum_{i=1}^N \frac{m_i}{2} \dot{\mathbf{r}}_i^2 \right) - \frac{3}{2} N k_b T = 0 \quad (2.3)$$

To make $g(\dot{\mathbf{r}})$ only a function of $\ddot{\mathbf{r}}$, we take the derivative of $g(\dot{\mathbf{r}})$ with respect to time:

$$G(\ddot{\mathbf{r}}) = \sum_{i=1}^N m_i \dot{\mathbf{r}}_i \cdot \ddot{\mathbf{r}}_i = 0 \quad (2.4)$$

We then subject $C(\ddot{\mathbf{r}})$ to the constraint function $G(\ddot{\mathbf{r}})$, and then minimize it as follows, which will give us the equation of motion:

$$\frac{\partial}{\partial \ddot{\mathbf{r}}} [C(\ddot{\mathbf{r}}) - \lambda G(\ddot{\mathbf{r}})] = 0 \quad (2.5)$$

The equation of motion of particle i is then:

$$\ddot{\mathbf{r}}_i = \lambda \dot{\mathbf{r}}_i + \frac{\mathbf{F}_i}{m_i} \quad (2.6)$$

Resubstitute this back to Equation (2.4) to get λ :

$$\lambda = - \frac{\sum_{i=1}^N \dot{\mathbf{r}}_i \cdot \mathbf{F}_i}{\sum_{i=1}^N m_i \dot{\mathbf{r}}_i^2} \quad (2.7)$$

The Lagrange multiplier acts like a friction coefficient. For pressure coupling, the idea is very similar, we can start with the following constraint function:

$$g(\dot{\mathbf{r}}) = \left(\sum_{i=1}^N \frac{m_i \dot{\mathbf{r}}_i^2}{2} + \sum_{i<j} \mathbf{F}_{ij} \cdot \mathbf{r}_{ij} \right) - \frac{3}{2} p V = 0 \quad (2.8)$$

This gives $G(\ddot{\mathbf{r}})$ in the following form.

$$G(\ddot{\mathbf{r}}) = \sum_{i=1}^N m_i \dot{\mathbf{r}}_i \cdot \ddot{\mathbf{r}}_i + \sum_{i<j} (\mathbf{F}_{ij} \cdot \dot{\mathbf{r}}_{ij} + \dot{\mathbf{F}}_{ij} \cdot \mathbf{r}_{ij}) = 0 \quad (2.9)$$

Taking derivative of $G(\ddot{\mathbf{r}})$ with respect to $\ddot{\mathbf{r}}_i$ gives us the same equation of motion as that in Equation (2.7). But λ is now written as:

$$\lambda = - \frac{\sum_{i=1}^N \mathbf{F}_i \cdot \dot{\mathbf{r}}_i + \sum_{i<j} (\mathbf{F}_{ij} \cdot \dot{\mathbf{r}}_{ij} + \dot{\mathbf{F}}_{ij} \cdot \mathbf{r}_{ij})}{\sum_{i=1}^N m_i \dot{\mathbf{r}}_i^2} \quad (2.10)$$

These are the simplest ways of maintaining temperature and pressure of the system at a constant value, and the key concepts behind the derivation of a Nosé-Hoover thermostat and Parrinello-Rahman barostat.

2.1.2 Integration of the Equation of Motion

The equation of motion of all the particles can be rewritten as follows:

$$\boxed{\frac{d^2 \mathbf{r}}{dt^2} + \xi \frac{d\mathbf{r}}{dt} = \frac{\mathbf{F}(\mathbf{r})}{m}} \quad (2.11)$$

\mathbf{R} and \mathbf{F} are vectors containing the positions of particles and the force acting upon them, respectively. Both of them have a dimension of $3N \times 1$. To be explicit, they have the form:

$$\mathbf{r} = [r_{0,x} \quad \dots \quad r_{N-1,x} \quad r_{0,y} \quad \dots \quad r_{N-1,y} \quad r_{0,z} \quad \dots \quad r_{N-1,z}]^T \quad (2.12)$$

$$\mathbf{F} = [F_{0,x} \quad \dots \quad F_{N-1,x} \quad F_{0,y} \quad \dots \quad F_{N-1,y} \quad F_{0,z} \quad \dots \quad F_{N-1,z}]^T \quad (2.13)$$

In fact, Equation (2.11) can be solved analytically in the case of Rouse chain. In the case that the force term \mathbf{F} can be highly nonlinear, Equation (2.11) has to be solved numerically using Leapfrog Algorithm, which can be summarized in the following two equations:

$$\mathbf{v}(t + \frac{\Delta t}{2}) = \mathbf{v}(t - \frac{\Delta t}{2}) + \left[\frac{\mathbf{F}(t)}{m} - \xi \mathbf{v}(t - \frac{\Delta t}{2}) \right] \Delta t \quad (2.14)$$

$$\mathbf{r}(t + \Delta t) = \mathbf{r}(t) + \mathbf{v}(t + \frac{\Delta t}{2}) \Delta t \quad (2.15)$$

where \mathbf{v} contains the velocities of the particles in all three directions, such that:

$$\mathbf{v} = [v_{0,x} \quad \dots \quad v_{N-1,x} \quad v_{0,y} \quad \dots \quad v_{N-1,y} \quad v_{0,z} \quad \dots \quad v_{N-1,z}]^T \quad (2.16)$$

Therefore, the most crucial point to focus on is the evaluation of \mathbf{F} , which depends on the forcefield. In this work, we applied the TraPPE forcefield [18, 19] because we are only interested in polyethylene. In TraPPE forcefield, methyl and methylene groups were coarse-grained into a single united atoms such that these single united atoms interact with one another through bonded and non-bonded interactions. The bond stretching potential is a simple harmonic potential.

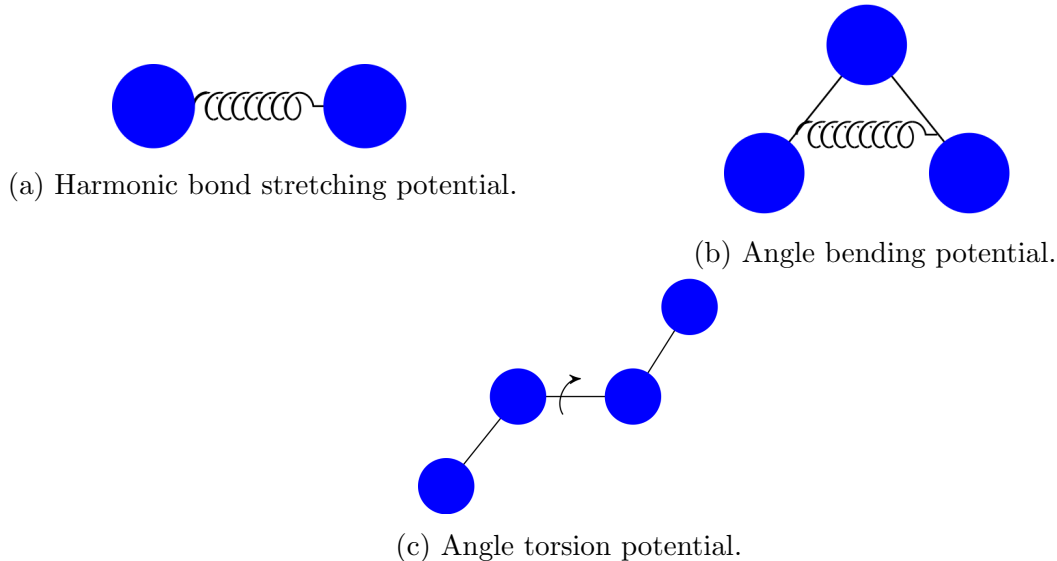


Figure 2.1: Different bonded potentials, such as (a) harmonic bond stretching potential, (b) angle bending potential and (c) angle torsion potential, in MD simulation. (cf., Equation (2.17), Equation (2.18) and Equation (2.19))

$$u_b(r_{ij}) = \frac{1}{2}k(r_{ij} - l)^2 \quad (2.17)$$

$l = 1.54$ nm and k is the spring constant. (The value of k is not given in TraPPE forcefield, which assumes that the beads are always separated from one another by a distance of l . In this work, we used the value of k for alkane in either OPLS-all atom forcefield or the MM2 forcefield.) r_{ij} is the distance between two bonded united atoms. The angle bending potential is of the form:

$$u_{bending}(\theta) = k_\theta(\theta - \theta_0)^2 \quad (2.18)$$

and was used for every bond angle θ consists of methylene group and methyl group united atoms with $k_\theta = 519$ kJ/(mole rad²) and $\theta_0 = 114^\circ$, whereas for the bond angle CH₂-C-CH₂,

$\theta_0 = 109.5^\circ$. Each torsional angle ϕ , which is defined with $\phi_{trans} = 180^\circ$, is modeled as:

$$u_{torsion}(\phi) = \sum_{p=0}^3 c_p \cos^p(\phi - 180^\circ) \quad (2.19)$$

with $c_0 = 8.397$ kJ/mol, $c_1 = 16.786$ kJ/mole, $c_2 = 1.134$ kJ/mole, $c_3 = -26.318$ kJ/mole for all torsion angles, except for $\text{CH}_2\text{-CH}_2\text{-C-CH}_2$ and $\text{CH}_2\text{-C-CH}_2\text{-CH}_2$, $c_0 = 1.917$ kJ/mol, $c_1 = 5.753$ kJ/mole, $c_2 = 0.000$ kJ/mole, $c_3 = -7.671$ kJ/mole. Intermolecular interaction was modeled using 12-6 Lennard Jones potential:

$$u_{LJ} = 4\varepsilon \left[\left(\frac{\sigma}{r} \right)^{12} - \left(\frac{\sigma}{r} \right)^6 \right] \quad (2.20)$$

with $\varepsilon = 0.0042$ kJ/mole and $\sigma = 0.640$ nm, $\varepsilon = 0.38$ kJ/mol and $\sigma = 0.395$ nm, as well as $\varepsilon = 0.81$ kJ/mole and $\sigma = 0.375$ nm for a carbon atom, methylene group and methyl group, respectively. r is the distance between any two united atoms. In the simulation, the cut-off distance was set at 1.4 nm. Electrostatic potential were neglected as polyethylene is non-polar. From these potentials, the force acting upon the i th united atom can be easily evaluated by taking the negative gradient of the potential V :

$$\mathbf{F}_i = - \frac{\partial u}{\partial \mathbf{r}_i} \quad (2.21)$$

Additionally, in the MD simulation, the united atoms are confined in a square box with periodic boundary condition. The definition of periodic boundary condition is illustrated in Figure 2.2. Subjected to such condition, when a particle in the box passes through one wall of the box, its duplicate is going to come into the same box from another side. The effect of the periodic boundary condition on the MD simulation results can be minimized by increasing the size of the simulation box. It was found that the effect of periodic boundary condition on our work is minimal. For instance, in Chapter 5, the diffusivity of linear polyethylene with $N = 405$ does not change much with the size of the box.

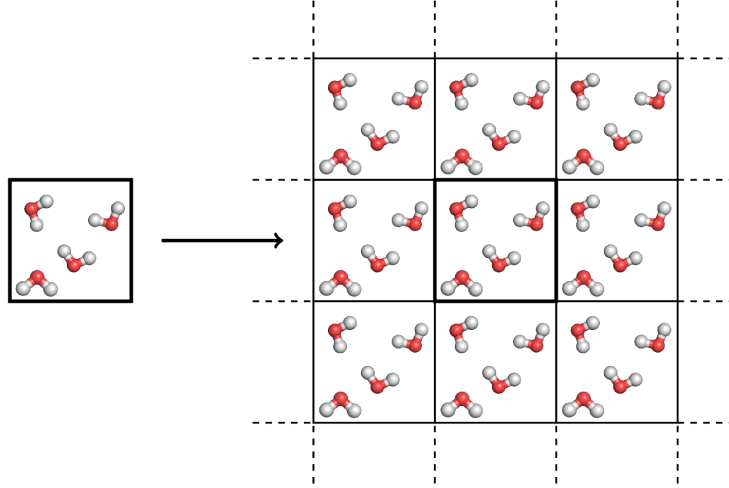


Figure 2.2: Illustration of periodic boundary condition in MD simulation. (This figure was created by Germain Salvato-Vallverdu and the corresponding source file can be found on <http://www.texample.net/tikz/examples/periodic-boundaries-conditions/>.)

2.2 Implicit Euler Method

In the forthcoming sections of this thesis, the reader is going to see that the implicit Euler method was also used to integrate non-linear equation of motion that is simpler than that in MD simulation. Compared to the Leapfrog algorithm, the implicit Euler method is more robust in a way that stability is guaranteed regardless of the size of the time step. Nonetheless, it is a much more daunting task to implement the implicit Euler method as the positions in the future time step have to be calculated based on the positions in the previous time steps. This leads to a system of non-linear equations, which have to be solved numerically.

To illustrate this more explicitly, we are going to consider a molecule consisting of two beads, which are connected to one another through a harmonic spring with a finite length b , in a two dimensional space. Without the inertia term, the equation of motion is explicitly written as follows:

$$\frac{dx_0}{dt} = \frac{k}{\zeta} [\sqrt{(x_0 - x_1)^2 + (y_0 - y_1)^2} - b] \cdot \frac{(x_1 - x_0)}{\sqrt{(x_0 - x_1)^2 + (y_0 - y_1)^2}} \quad (2.22)$$

$$\frac{dx_1}{dt} = \frac{k}{\zeta} [\sqrt{(x_0 - x_1)^2 + (y_0 - y_1)^2} - b] \cdot \frac{(x_0 - x_1)}{\sqrt{(x_0 - x_1)^2 + (y_0 - y_1)^2}} \quad (2.23)$$

Similarly, in y direction:

$$\frac{dy_0}{dt} = \frac{k}{\zeta} [\sqrt{(x_0 - x_1)^2 + (y_0 - y_1)^2} - b] \cdot \frac{(y_1 - y_0)}{\sqrt{(x_0 - x_1)^2 + (y_0 - y_1)^2}} \quad (2.24)$$

$$\frac{dy_1}{dt} = \frac{k}{\zeta} [\sqrt{(x_0 - x_1)^2 + (y_0 - y_1)^2} - b] \cdot \frac{(y_0 - y_1)}{\sqrt{(x_0 - x_1)^2 + (y_0 - y_1)^2}} \quad (2.25)$$

For i th particle in the q direction, discretization gives us:

$$q_i(t + \Delta t) - q_i(t) - F_{iq}(t + \Delta t)\Delta t = 0 \quad (2.26)$$

where F_{iq} is the force acting on the i th particle in the q direction. And by juxtaposing Equation (2.26) and Equations (2.22) to (2.25), we know that for $i < 1$:

$$F_{iq} = \frac{k}{\zeta} [\sqrt{(x_i - x_{i+1})^2 + (y_i - y_{i+1})^2} - b] \cdot \frac{(q_{i+1} - q_i)}{\sqrt{(x_i - x_{i+1})^2 + (y_i - y_{i+1})^2}} \quad (2.27)$$

And for $i = 1$:

$$F_{iq} = \frac{k}{\zeta} [\sqrt{(x_i - x_{i-1})^2 + (y_i - y_{i-1})^2} - b] \cdot \frac{(q_{i-1} - q_i)}{\sqrt{(x_i - x_{i-1})^2 + (y_i - y_{i-1})^2}} \quad (2.28)$$

This indicates that at each time step, one has to solve systems of non-linear equations numerically (cf., Equation (2.26)). This can be attained by using the Newton-Gauss method, which is initiated by inputting an initial guess such that Equation (2.26) is rewritten as follows:

$$q_i^{(k)}(t + \Delta t) - q_i^{(k)}(t) - F_{iq}^{(k)}(t + \Delta t)\Delta t = \mathcal{R}_{iq} \quad (2.29)$$

The superscript (k) indicates the k th iteration. \mathcal{R}_{iq} is the residue, which is initially much greater than zero. An initial guess of $q_0^{(0)}(t + \Delta t)$ was input. The problem then becomes how to update the value of $q_0(t + \Delta t)$ until the magnitude of \mathcal{R}_{iq} is minimized. To solve this, it is firstly important to build up the Jacobian matrix \mathbf{J} , which has a dimension of 4×4 in this example.

$$\mathbf{J} = \begin{bmatrix} \frac{\partial \mathcal{R}_{0x}}{\partial x_0} & \frac{\partial \mathcal{R}_{0x}}{\partial x_1} & \frac{\partial \mathcal{R}_{0x}}{\partial y_0} & \frac{\partial \mathcal{R}_{0x}}{\partial y_1} \\ \frac{\partial \mathcal{R}_{1x}}{\partial x_0} & \frac{\partial \mathcal{R}_{1x}}{\partial x_1} & \frac{\partial \mathcal{R}_{1x}}{\partial y_0} & \frac{\partial \mathcal{R}_{1x}}{\partial y_1} \\ \frac{\partial \mathcal{R}_{0y}}{\partial x_0} & \frac{\partial \mathcal{R}_{0y}}{\partial x_1} & \frac{\partial \mathcal{R}_{0y}}{\partial y_0} & \frac{\partial \mathcal{R}_{0y}}{\partial y_1} \\ \frac{\partial \mathcal{R}_{1y}}{\partial x_0} & \frac{\partial \mathcal{R}_{1y}}{\partial x_1} & \frac{\partial \mathcal{R}_{1y}}{\partial y_0} & \frac{\partial \mathcal{R}_{1y}}{\partial y_1} \end{bmatrix} \quad (2.30)$$

Then $q_i^{(k)}(t + \Delta t)$ can be updated to $q_i^{(k+1)}(t + \Delta t)$ by the following until the residue has become a very small number (in the order of $\sim 10^{-5}$):

$$\begin{bmatrix} x_0 \\ x_1 \\ y_0 \\ y_1 \end{bmatrix}^{(k+1)} = \begin{bmatrix} x_0 \\ x_1 \\ y_0 \\ y_1 \end{bmatrix}^{(k)} - [(\mathbf{J}^T \mathbf{J})^{-1} \mathbf{J}^T \begin{bmatrix} \mathcal{R}_{0x} \\ \mathcal{R}_{1x} \\ \mathcal{R}_{0y} \\ \mathcal{R}_{1y} \end{bmatrix}]^{(k)} \quad (2.31)$$

2.3 Numerical Analysis of the Trajectory

2.3.1 Proper Orthogonal Decomposition

The proper orthogonal decomposition (POD) analysis generates a reduced order model of the MD trajectory. Basically, it gives us different eigenmodes based on the numerical solution to the highly nonlinear equation of motion in the MD simulation, which may not be obtained analytically. In such analysis, the deviation of the positions of different atoms (q) of a molecule in a particular direction (either x , y or z) of the same molecule from its center-of-mass at different time (q') is calculated. The components of a correlation matrix \mathbf{C} in a particular direction are then evaluated by the following:

$$C_{ij} = \frac{1}{N_{snap}} \sum_{t'=0}^{T'} q'_i(t') q'_j(t') \quad (2.32)$$

N_{snap} is the number of snapshot of the MD trajectory and $q'_i(t)$ is the deviation of the position of atom i from the center-of-mass of the molecule at time t .

$$q'_i(t) = q_i(t) - \frac{1}{N} \sum_{i=0}^{N-1} q_i(t) \quad (2.33)$$

To be more explicit, if the number of atoms consisting a molecule (N) is three, then the correlation matrix is:

$$\mathbf{C} = \begin{bmatrix} C_{00} & C_{01} & C_{02} \\ C_{10} & C_{11} & C_{12} \\ C_{20} & C_{21} & C_{22} \end{bmatrix} \quad (2.34)$$

The eigenvectors of \mathbf{C} are the eigenmodes. The number of the eigenmodes derived from a correlation matrix in a particular direction is N . As there are three directions, there are in total $3N$ normalized eigenmodes ($\tilde{\psi}_{pq}$), for which p ranges from 0 to $N - 1$. With the eigenmodes in different directions, transformation of the Cartesian coordinates of the atoms can be achieved, which is expressed as follows:

$$X'_{pq}(t) = \sum_{i=0}^{N-1} q'_i(t) \tilde{\psi}_{pq} \quad (2.35)$$

The relaxation times of different eigenmodes (τ_p) can be then extracted from the time correlation functions of these transformed coordinate ($\mu_p(t)$) by fitting it to a stretched exponential

function.

$$\mu_p(t) = \frac{\langle X'_{px}(t)X'_{px}(0) + X'_{py}(t)X'_{py}(0) + X'_{pz}(t)X'_{pz}(0) \rangle}{\langle X'_{px}(t)^2 + X'_{py}(t)^2 + X'_{pz}(t)^2 \rangle} \approx \exp[-(t/\tau_p)^{\beta_p}] \quad (2.36)$$

where β_p is the stretching factor. From the above equation, we know that a molecule with size N has N relaxation times.

2.3.2 Time Correlation Function and Mean Square Displacement

In many-body system of polymers, for example, we are interested in the time correlation function of the end-to-end vector \mathbf{R} , which is $\langle \mathbf{R}(t) \cdot \mathbf{R}(0) \rangle$. The bracket indicates that it is indeed an average property, and to calculate such time correlation function, one has to average over the number of chains and time. It is intuitive to understand the average over the number of chains that if there are ten chains in the simulation, the time correlation functions for each individual chain can be obtained and then summed up altogether, followed by the division by the chain numbers. But the fact that $\langle \mathbf{R}(t) \cdot \mathbf{R}(0) \rangle$ is also a time average property may not be straightforwardly understood. To be exact, the time correlation function is a function of *duration*, not a function of time. For simplicity, let us consider a trajectory with only five time steps with an increment of 1 ps as depicted in Figure 2.4. Then, one can count the number of samples corresponding to a certain amount of duration. For instance, if we consider a duration of 1 ps, we have five samples: $\mathbf{R}(1) \cdot \mathbf{R}(0)$, $\mathbf{R}(2) \cdot \mathbf{R}(1)$, $\mathbf{R}(3) \cdot \mathbf{R}(2)$, $\mathbf{R}(4) \cdot \mathbf{R}(3)$, $\mathbf{R}(5) \cdot \mathbf{R}(4)$. The time correlation function at a duration of 1 ps can be individually evaluated and then averaged over these five samples. Similarly, if we consider a duration of 5 ps, we only have one sample, i.e. $\mathbf{R}(5) \cdot \mathbf{R}(0)$.

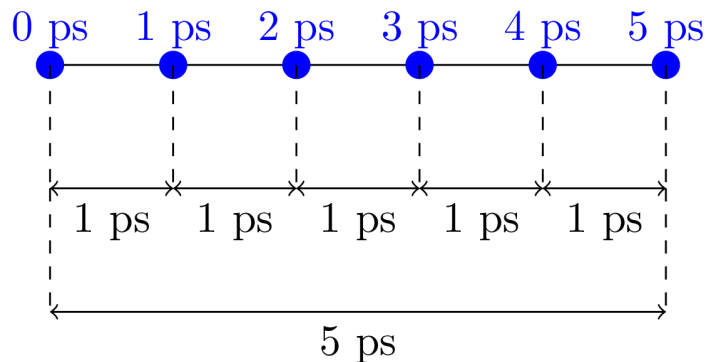


Figure 2.3: Illustration of sampling for time averaging of time correlation function and mean-square-displacement for a MD trajectory with six snapshots from 0 ps to 5 ps (represented by the blue circle).

This also applies to the calculation of mean-square-displacement of the center-of-mass of the polymer molecules. As explained above, the number of samples for time averaging decreases with increasing duration. Owing to this, the mean-square-displacement values near the end of the simulation are typically excluded from the calculation of the diffusivity.

2.3.3 Voronoi Tessellation

Voronoi tessellation is a mathematical method of evaluating the free space available to multiple points in a two dimensional or three dimensional space. This is particularly useful in the analysis of probability for a particle getting free volume, which relies on the knowledge of the distribution of free volume. This is because the size distribution of the Voronoi cell is related to distribution of free volume, and the cumulative function of such distribution function is the probability for a particle getting certain amount of free volume. The procedures of Voronoi Tessellation is as follows:

Consider four points randomly distributed in a two dimensional space, point A is then connected to its closest neighbours, which are points B, C and D. They are connected to one another by dashed lines as depicted in Figure 2.4. The Voronoi cell for point A, which is the free space available to point A, is then constructed by drawing solid lines, subjected to the constraint that these lines must be perpendicular to the blue dashed lines and that the solid line has to intersect with the dashed line at the mid-point of the dashed line. In

the case as depicted in Figure 2.4, the Voronoi cell for point A is a triangle with the solid lines as boundaries. In a more complicated case of many points, different sizes of Voronoi cells can be obtained using exactly the same procedures. (cf., Figure 2.5) The same logic can be applied to three dimensional space that after connecting the points to their closest neighbour, surfaces with their normal vectors perpendicular to these lines are constructed.

Alternatively, one can also construct Voronoi cells using the so-called Delaunay triangulation. In such method, each point is again connected to all its closest neighbours, which creates multiple triangles, such as the one as shown in Figure 2.4. With such triangle, one can obtain the center of the circumcircle of such triangle. Finally, by connecting the centers of all the circumcircles, one can then be able to obtain different Voronoi cells. In three dimensional space, it would have been a sphere instead of a circle.

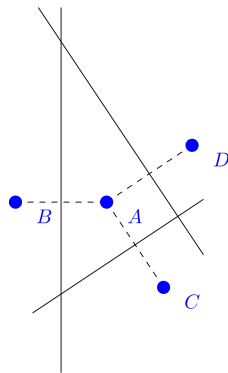


Figure 2.4: Voronoi tessellation of a 2D system with only four points.

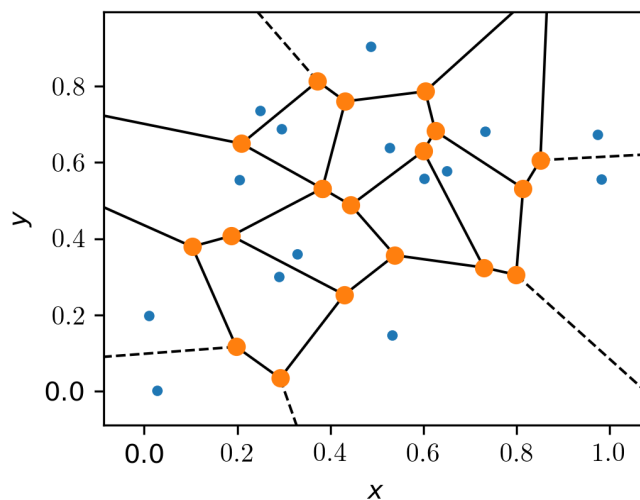


Figure 2.5: A more complicated example of Voronoi tessellation in two dimensional space.

One limitation of Voronoi Tessellation in MD simulation is that Voronoi Tessellation does not take into account of the fact when the particles or beads of different polymer molecules interact with one another through a soft core potential, such as Lennard-Jones potential, instead of hard-sphere potential. Voronoi Tessellation assumes that the Lennard-Jones particles are points and thus it neglects the excluded volume. Hence, as demonstrated in Chapter 5 and Chapter 6, when the probability is extracted from the size distribution of Voronoi cells, such excluded volume effect is considered.

Chapter 3

Velocity Time Correlation Function of a Rouse Chain¹

3.1 Introduction

The dynamics of unentangled linear polymer in a melt has been successfully predicted by the Rouse model, which was developed by Rouse back in 1953 [20]. In such a simple and elegant model, a Gaussian chain is modelled as beads connected by springs, and is under the influence of a random force, which has a normal distribution. Without accounting for the inertia of the chain, if a Langevin equation for each individual bead is written, one will end up with a system of coupled linear first order ordinary differential equations. Such a system of equations with the positions of the beads as the states, can be easily solved by hand if we consider the continuous approach introduced in Doi and Edwards' book [21], in which the difference $\mathbf{R}_{n+1} - 2\mathbf{R}_n + \mathbf{R}_{n-1} \approx \frac{\partial^2 \mathbf{R}_n}{\partial n^2}$ and $\mathbf{R}_n - \mathbf{R}_{n-1} \approx \frac{\partial \mathbf{R}_n}{\partial n}$. Clearly, the eigenvalues (λ) of the operator $\partial^2/\partial n^2$ are related to the relaxation time of different modes of the polymer chain and coordinate transformation can be easily achieved with the knowledge of the eigenfunctions (ψ). Even though such an eigenfunction may not be true in highly nonlinear equation of motion, the behavior of chain relaxation [22, 23], and the shear relaxation modulus [8], can be still reasonably predicted for unentangled chain. Nevertheless, to our knowledge, one may not be able to obtain accurately the velocity correlation function of the polymer and to study the short time dynamic behavior of the polymer chain in the

¹A version of this chapter has been published in *Comput. Mater. Sci.*, 2018, 155, 320-324.

melt as the inertia term is neglected.

In this paper, we consider the simple case, in which the friction coefficient is constant for every bead (i.e., no hydrodynamic interaction). We logically started from the inclusion of an inertia term in the Langevin equation for a single particle and then extended it to the Rouse model for unentangled polymer melts, which enables us to obtain the velocity time correlation function for different normal modes of a Rouse chain. To confirm our analytical results, the velocity time correlation function was also numerically obtained using Langevin dynamics simulation.

3.2 Numerical Simulation Details

To perform such a numerical simulation, the implicit Euler method was implemented in a C++ program (cf., Supporting Information). The advantage of using implicit Euler method is that the stability is unconditionally guaranteed regardless of the size of Δt . Discretization of the Langevin equation of motion would lead to a system of linear equations in each of the three directions at each time step:

$$-\mathbf{q}(t) - \frac{\mathbf{g}(t + \Delta t)}{m} \Delta t = \mathcal{A} \mathbf{q}(t + \Delta t) \quad (3.1)$$

\mathbf{q} is a vector with $2N$ components, in which N of its components being the positions of the beads and other N components being the velocities of the beads in one particular direction. \mathbf{g} is also a vector with $2N$ components, in which the first N elements in this vector are zeros, and the remaining components are stochastic force $g_{i,q}$ acting on the bead with $\langle g(t) \rangle = 0$ and $\langle g(t)g(t') \rangle = 2k_b T \zeta \delta(t - t')$. m is the mass of the bead and ζ is the friction coefficient. To be explicit:

$$\mathbf{q} = [R_{0,q} \ \dots \ R_{N-1,q} \ V_{0,q} \ \dots \ V_{N-1,q}]^T \quad (3.2)$$

$R_{i,q}$ and $V_{i,q}$ are the position and velocity of i th bead in the q direction, respectively.

$$\mathbf{g} = [0 \ \dots \ 0 \ g_{0,q} \ \dots \ g_{N-1,q}]^T \quad (3.3)$$

\mathcal{A} is a $2N \times 2N$ matrix created by blocks of $N \times N$ matrices:

$$\mathcal{A} = \begin{bmatrix} \mathbf{0} & \mathbf{I} \\ \mathbf{A} & \mathbf{\Sigma} \end{bmatrix} \Delta t - \begin{bmatrix} \mathbf{I} & \mathbf{0} \\ \mathbf{0} & \mathbf{I} \end{bmatrix} \quad (3.4)$$

Note that \mathbf{I} is a $N \times N$ identity matrix and $\mathbf{\Sigma} = -\xi\mathbf{I}$ and $\xi = \zeta/m$. And \mathbf{A} , which is a $N \times N$ matrix, has the following form:

$$\mathbf{A} = \frac{k}{m} \begin{bmatrix} -1 & 1 & 0 & 0 & \dots & 0 \\ 1 & -2 & 1 & 0 & \dots & 0 \\ 0 & 1 & -2 & 1 & \dots & 0 \\ 0 & 0 & \ddots & \ddots & \ddots & 0 \\ 0 & 0 & \dots & 1 & -2 & 1 \\ 0 & 0 & \dots & 0 & 1 & -1 \end{bmatrix} \quad (3.5)$$

k is the spring constant. By solving the system of matrix equation as expressed in Equation (3.1), the positions and velocities of the beads in the next time step were obtained. For the studies in long time scale motion (normal mode $p = 1$) and in short time scale motion (normal mode $p = 6$), a time step of $\Delta t = 0.01$ ps and $\Delta t = 0.001$ ps was chosen with the number of time steps set at 3500 and 6000, respectively.

The initial conformation of the chain was generated using rotational isomeric state model, which was originally developed by Flory [16] and further extended by Mattice and Suter [12], in which the assignment of torsional angle of different segments is achieved by evaluating the interdependent probability of having a particular configurational state (i.e. tt , tg^+ , tg^- , g^+g^- , g^+g^+ as well as g^-g^-). These procedures have been implemented in a Python 3.5 program (cf., Supporting Information).

3.3 Preliminaries

3.3.1 Langevin Dynamics of a Single Particle: without Inertia Term

Equation (3.6) is a one dimensional Langevin equation for a single particle without the inertia term, in which x is the position of the particle and $f(t)$ is the random force with a normal distribution with $\langle f(t) \rangle = 0$, and $\langle f(\tau_1)f(\tau_2) \rangle = \sigma^2\delta(\tau_1 - \tau_2)$.

$$\frac{dx}{dt} = \frac{f(t)}{\zeta} \quad (3.6)$$

This is easily solved:

$$x = x(0) + \frac{1}{\zeta} \int_0^t f(t)dt \quad (3.7)$$

From Equation (3.7), we found that x is only a linear combination of the normal distribution $f(t)$, therefore x by itself is also a normal distribution with $\langle x \rangle = 0$, and $\langle x^2 \rangle$ is expressed as follows:

$$\langle x^2 \rangle = \frac{1}{\zeta^2} \int_0^t \int_0^t \langle f(\tau_1) f(\tau_2) \rangle d\tau_1 d\tau_2 = \frac{\sigma^2 t}{\zeta^2} \quad (3.8)$$

The next step is to determine σ^2 and the velocity of the particle.

3.3.2 Langevin Dynamics of a Single Particle: with Inertia Term

Inclusion of the inertia term leads to the following equation:

$$\frac{d^2 x}{dt^2} = -\xi \frac{dx}{dt} + \frac{f(t)}{m} \quad (3.9)$$

As $\frac{dx}{dt} = v(t)$, which is the velocity, the equation can be arranged in matrix form:

$$\frac{d}{dt} \begin{bmatrix} x \\ v \end{bmatrix} = \begin{bmatrix} 0 & 1 \\ 0 & -\xi \end{bmatrix} \begin{bmatrix} x \\ v \end{bmatrix} + \begin{bmatrix} 0 \\ f(t)/m \end{bmatrix} \quad (3.10)$$

With matrix \mathbf{C} to be as follows:

$$\mathbf{C} = \begin{bmatrix} 0 & 1 \\ 0 & -\xi \end{bmatrix}$$

The solution is therefore:

$$\begin{bmatrix} x \\ v \end{bmatrix} = e^{\mathbf{C}t} \begin{bmatrix} x_0 \\ v_0 \end{bmatrix} + \int_0^t e^{\mathbf{C}(t-\tau)} \begin{bmatrix} 0 \\ f(\tau)/m \end{bmatrix} d\tau \quad (3.11)$$

To evaluate the matrix exponential, inverse laplace transformation can be applied:

$$\begin{aligned} e^{\mathbf{C}t} &= \mathcal{L}^{-1}[(s\mathbf{I} - \mathbf{C})^{-1}] \\ &= \mathcal{L}^{-1} \begin{bmatrix} \frac{1}{s} & \frac{1}{s(\xi+s)} \\ 0 & \frac{1}{s+\xi} \end{bmatrix} \\ &= \begin{bmatrix} 1 & \frac{2}{\xi} e^{-\frac{\xi}{2}t} \sinh(\frac{\xi}{2}t) \\ 0 & e^{-\xi t} \end{bmatrix} \end{aligned}$$

We have the following:

$$\begin{aligned} x(t) &= x(0) + \frac{v(0)}{\xi} (1 - e^{-\xi t}) + \int_0^t \frac{1}{m\xi} (1 - e^{-\xi(t-\tau)}) f(\tau) d\tau \\ v(t) &= v(0) e^{-\xi t} + \frac{1}{m} \int_0^t e^{-\xi(t-\tau)} f(\tau) d\tau \end{aligned}$$

Now, we have to firstly obtain σ^2 . It is known that from the equipartition theorem, $\langle v^2 \rangle = \frac{k_b T}{m}$, where k_b is the Boltzmann constant and T is the temperature, therefore,

$$\langle v^2(t) \rangle = \langle v^2 \rangle e^{-2\xi t} + \frac{1}{m^2} \int_0^t \int_0^t e^{-\xi(2t-\tau_1-\tau_2)} \langle f(\tau_1) f(\tau_2) \rangle d\tau_1 d\tau_2 \quad (3.12)$$

As time approaches infinity, the second term becomes much larger than the first term in Equation (3.12), we end up with the following integral equation:

$$\int_0^t \int_0^t e^{-\xi(2t-\tau_1-\tau_2)} \sigma^2 \delta(\tau_1 - \tau_2) d\tau_1 d\tau_2 = m k_b T \quad (3.13)$$

From this we obtain $\sigma^2 = 2k_b T m \xi = 2k_b T \zeta$. The velocity correlation function for a single particle is as follows:

$$\langle v(t) v(0) \rangle = \frac{k_b T}{m} e^{-\xi t} \quad (3.14)$$

In the case of three dimension, the variance $\langle v(t) v(0) \rangle$ in x , y and z directions are uncorrelated to each other. This gives us:

$$\langle \mathbf{v}(t) \cdot \mathbf{v}(0) \rangle = \frac{3k_b T}{m} e^{-\xi t} \quad (3.15)$$

3.3.3 Rouse Dynamics: without Inertia Term

For a Rouse chain, if we neglect the inertial term,

$$\frac{d\mathbf{R}_n}{dt} = \frac{k}{\zeta} [\mathbf{R}_{n+1} - 2\mathbf{R}_n + \mathbf{R}_{n-1}] + \frac{\mathbf{f}_n(t)}{\zeta} \quad (3.16)$$

Equation (3.16) is a system of first order coupled ordinary differential equations. $\mathbf{f}_n(t)$ is a normal distribution, which has $\langle \mathbf{f}_n \rangle = \mathbf{0}$ and the covariance matrix $\Sigma = 2k_b T \zeta \delta(\tau_1 - \tau_2) \mathbf{I}$. In the continuous limit, this equation can be rewritten as a second order parabolic partial differential equation,

$$\frac{\partial \mathbf{R}_n}{\partial t} = \frac{k}{\zeta} \frac{\partial^2 \mathbf{R}_n}{\partial n^2} + \frac{\mathbf{f}_n}{\zeta} \quad (3.17)$$

Subjected to the following boundary conditions:

$$\frac{\partial \mathbf{R}_0}{\partial n} = 0, \quad \frac{\partial \mathbf{R}_N}{\partial n} = 0$$

By separation of variables, $\mathbf{R}_n(t) = \mathbf{A}(t)\psi(n)$, this lead us to the following:

$$\frac{1}{\mathbf{A}} \frac{d\mathbf{A}}{dt} = \frac{k}{\zeta \psi} \frac{d^2 \psi}{dn^2} = -\lambda^2$$

With the boundary conditions, $\psi_p = \cos(p\pi\frac{n}{N})$ for $p = 0, 1, 2, 3 \dots N - 1$. The solution is therefore:

$$\mathbf{R}_n(t) = \frac{2}{N} \left\{ \sum_{p=1}^{N-1} e^{-\lambda_p^2 t} \left[\mathbf{A}_p + \int_0^t e^{\lambda_p^2 \tau} \int_0^N \frac{\mathbf{f}_{n'}}{\zeta} \cos(p\pi\frac{n'}{N}) dn' d\tau \right] \cos(p\pi\frac{n}{N}) \right\} + \frac{1}{N} \left[\mathbf{A}_0 + \int_0^t \int_0^N \frac{\mathbf{f}_{n'}}{\zeta} dn' d\tau \right]$$

\mathbf{A}_0 and \mathbf{A}_p are related to the initial condition $\mathbf{R}(n, 0)$. We then let the following:

$$\mathbf{X}_0(t) = \frac{1}{N} \left[\mathbf{A}_0 + \int_0^t \int_0^N \frac{\mathbf{f}_n}{\zeta} dnd\tau \right] \quad (3.18)$$

$$\mathbf{X}_p(t) = \frac{1}{N} e^{-\lambda_p^2 t} \left[\mathbf{A}_p + \int_0^t e^{\lambda_p^2 \tau} \int_0^N \frac{\mathbf{f}_n}{\zeta} \cos(p\pi\frac{n}{N}) dnd\tau \right] \quad (3.19)$$

The solution is simplified to a large extent:

$$\mathbf{R}_n = \mathbf{X}_0 + 2 \sum_{p=1}^{N-1} \mathbf{X}_p \cos(p\pi\frac{n}{N})$$

Inverse transformation can be achieved easily by firstly multiply both size by $\cos(q\pi\frac{n}{N})$ and integrate with respect to n .

$$\int_0^N \mathbf{R}_n \cos(q\pi\frac{n}{N}) dn = \int_0^N \left[\mathbf{X}_0 + 2 \sum_{p=1}^{N-1} \mathbf{X}_p \cos(p\pi\frac{n}{N}) \right] \cos(q\pi\frac{n}{N}) dn$$

If $q = p$ and $q > 0$, with orthonormality, we have:

$$\mathbf{X}_p = \frac{1}{N} \int_0^N \mathbf{R}_n \cos(p\pi\frac{n}{N}) dn$$

If $p = q = 0$,

$$\mathbf{X}_0 = \frac{1}{N} \int_0^N \mathbf{R}_n dn$$

This is essentially the center-of-mass of the Rouse chain. We can study the dynamics of the center-of-mass of the Rouse chain by taking derivative of Equation (3.18) with respect to time.

$$\dot{\mathbf{X}}_0(t) = \dot{\mathbf{X}}_0(0) + \int_0^t \int_0^N \frac{\dot{\mathbf{f}}_n}{N\zeta} dnd\tau \quad (3.20)$$

This is similar to Equation (3.7).

3.4 Velocity Time Correlation Function of a Rouse Chain

3.4.1 Rouse Dynamics: with Inertia Term

Center-of-Mass of the Chain ($p = 0$)

Alternatively, we can also directly incorporate the inertia term in Equation (3.17).

$$m \frac{\partial^2 \mathbf{R}_n}{\partial t^2} + \zeta \frac{\partial \mathbf{R}_n}{\partial t} = k \frac{\partial^2 \mathbf{R}_n}{\partial n^2} + \mathbf{f}_n \quad (3.21)$$

Separation of variables implies that $\mathbf{R}_n = \mathbf{A}(t)\psi(n)$, which leads to:

$$\frac{m}{k\mathbf{A}} \frac{d^2 \mathbf{A}}{dt^2} + \frac{\zeta}{k\mathbf{A}} \frac{d\mathbf{A}}{dt} = \frac{1}{\psi} \frac{\partial^2 \psi}{\partial n^2} = -\lambda^2 \quad (3.22)$$

We then solve for $\mathbf{A}(t)$:

$$\frac{d^2 \mathbf{A}}{dt^2} + \frac{\zeta}{m} \frac{d\mathbf{A}}{dt} = -\frac{\lambda^2 k}{m} \mathbf{A} \quad (3.23)$$

That for different modes:

$$\mathbf{A}_p(t) = \mathbf{c}_{1p} \exp \left[\left(-0.5\xi + 0.5\sqrt{\xi^2 - 4\lambda_p^2 k/m} \right) t \right] + \mathbf{c}_{2p} \exp \left[\left(-0.5\xi - 0.5\sqrt{\xi^2 - 4\lambda_p^2 k/m} \right) t \right] \quad (3.24)$$

As demonstrated above, as $p = 0$ ($\lambda_p = 0$), it corresponds to the dynamics of the center-of-mass of the Rouse's chain.

$$\mathbf{A}_0(t) = \mathbf{c}_{10} + \mathbf{c}_{20} \exp(-\xi t) \quad (3.25)$$

With:

$$\mathbf{X}_0(t) = \frac{1}{N} [\mathbf{c}_{10} + \mathbf{c}_{20} \exp(-\xi t)] + \frac{1}{Nm\xi} \int_0^t [1 - e^{-\xi(t-\tau)}] \int_0^N \mathbf{f}_n dnd\tau \quad (3.26)$$

The initial conditions can be used to find the parameters \mathbf{c}_{10} and \mathbf{c}_{20} :

$$\mathbf{X}_0(0) = \frac{1}{N} [\mathbf{c}_{10} + \mathbf{c}_{20}] \quad (3.27)$$

$$\mathbf{V}_0(0) = \frac{1}{N} [-\xi \mathbf{c}_{20}] \quad (3.28)$$

Putting this back to Equation (3.26) gives us:

$$\mathbf{X}_0(t) = \mathbf{X}_0(0) + \frac{\mathbf{V}_0(0)}{\xi} [1 - e^{-\xi t}] + \frac{1}{Nm\xi} \int_0^t [1 - e^{-\xi(t-\tau)}] \int_0^N \mathbf{f}_n dnd\tau \quad (3.29)$$

If we assume the center-of-mass of the chain is at the origin at $t = 0$:

$$\mathbf{V}_0(t) = \mathbf{V}_0(0)e^{-\xi t} + \frac{1}{Nm} \int_0^t e^{-\xi(t-\tau)} \int_0^N \mathbf{f}_n dnd\tau \quad (3.30)$$

The velocity correlation function is therefore:

$$\langle \mathbf{V}_0(t) \cdot \mathbf{V}_0(0) \rangle = \frac{3k_b T}{Nm} e^{-\xi t} \quad (3.31)$$

For which, $\langle V_0^2 \rangle = \frac{3k_b T}{Nm}$. Alternatively, we can obtain the velocity for the center-of-mass of the Rouse chain ($\mathbf{V}_0(t)$), based on Equation (3.20):

$$\frac{d^2 \mathbf{X}_0}{dt^2} + \xi \frac{d\mathbf{X}_0}{dt} = \frac{1}{Nm} \int_0^N \mathbf{f}_n dn \quad (3.32)$$

Similar to the procedures in the previous section, we can easily obtain $\mathbf{V}_0(t)$ as

$$\mathbf{V}_0(t) = \mathbf{V}_0(0)e^{-\xi t} + \frac{1}{Nm} \int_0^t e^{-\xi(t-\tau)} \int_0^N \mathbf{f}_n(\tau) dnd\tau \quad (3.33)$$

The velocity correlation function is therefore:

$$\boxed{\langle \mathbf{V}_0(t) \cdot \mathbf{V}_0(0) \rangle = \frac{3k_b T}{Nm} e^{-\xi t}} \quad (3.34)$$

This is analogous to the case for a single particle (cf., Equation (3.15)). Integration of Equation (3.34) from $t = 0$ to ∞ gives us the diffusion coefficient of the center-of-mass of the chain.

$$D_{cm} = \frac{1}{3} \int_0^\infty \frac{3k_b T}{Nm} e^{-\xi t} dt = \frac{k_b T}{N\xi} \quad (3.35)$$

Other Different Normal Modes ($p = 1, 2, 3, \dots, N - 1$)

For convenience, we let the following:

$$\omega = \frac{\sqrt{\xi^2 - 4\lambda_p^2 k/m}}{2} \quad (3.36)$$

Interestingly, if $4\lambda_p^2 k/m < \xi^2$, ω is a real number, whereas if $4\lambda_p^2 k/m > \xi^2$, ω is an imaginary number. The reader will find that the velocity correlation function is oscillatory in the latter case.

Case 1: ω is a real number and $4\lambda_p^2 k/m < \xi^2$

$$\mathbf{X}_{\mathbf{p}}(t) = \frac{e^{-\frac{\xi}{2}t}}{N} \left\{ \mathbf{c}_{1\mathbf{p}} e^{\omega t} + \mathbf{c}_{2\mathbf{p}} e^{-\omega t} \right\} + \mathbf{H}_{\mathbf{p}}(t) \quad (3.37)$$

For which, we let $\mathbf{H}_{\mathbf{p}}(t)$ as:

$$\mathbf{H}_{\mathbf{p}}(t) = \frac{1}{2\omega Nm} \int_0^t \left[e^{(-\frac{\xi}{2}+\omega)(t-\tau)} - e^{(-\frac{\xi}{2}-\omega)(t-\tau)} \right] \int_0^N \mathbf{f}_{\mathbf{n}} \cos(p\pi \frac{n}{N}) dn d\tau \quad (3.38)$$

The initial conditions can be used to find the parameters $\mathbf{c}_{1\mathbf{p}}$ and $\mathbf{c}_{2\mathbf{p}}$.

$$\mathbf{X}_{\mathbf{p}}(0) = \frac{1}{N} [\mathbf{c}_{1\mathbf{p}} + \mathbf{c}_{2\mathbf{p}}] \quad (3.39)$$

$$\mathbf{V}_{\mathbf{p}}(0) = \mathbf{X}_{\mathbf{p}}(0) \left[-\frac{\xi}{2} + \omega \right] - \frac{\mathbf{c}_{2\mathbf{p}} 2\omega}{N} \quad (3.40)$$

This leads to:

$$\mathbf{X}_{\mathbf{p}}(t) = \mathbf{X}_{\mathbf{p}}(0) e^{(-\frac{\xi}{2}+\omega)t} - \frac{e^{-\frac{\xi}{2}t}}{2\omega} \left[\mathbf{V}_{\mathbf{p}}(0) - \mathbf{X}_{\mathbf{p}}(0) \left(-\frac{\xi}{2} + \omega \right) \right] \left[e^{-\omega t} - e^{\omega t} \right] + \mathbf{H}_{\mathbf{p}}(t) \quad (3.41)$$

The normal mode correlation function is therefore:

$$\langle \mathbf{X}_{\mathbf{p}}(t) \cdot \mathbf{X}_{\mathbf{p}}(0) \rangle = \langle X_p^2 \rangle e^{(-\frac{\xi}{2}+\omega)t} + \frac{\langle X_p^2 \rangle e^{-\frac{\xi}{2}t}}{2\omega} \left(-\frac{\xi}{2} + \omega \right) \left(e^{-\omega t} - e^{\omega t} \right) \quad (3.42)$$

The normal mode velocity is computed as:

$$\mathbf{V}_{\mathbf{p}}(t) = \mathbf{X}_{\mathbf{p}}(0) \left(-\frac{\xi}{2} + \omega \right) e^{(-\frac{\xi}{2}+\omega)t} + \mathbf{V}_{\mathbf{p}}(0) \left\{ \frac{-\xi + 2\omega}{\xi + 2\omega} e^{(-\frac{\xi}{2}+\omega)t} + e^{(-\frac{\xi}{2}-\omega)t} \right\} + \mathbf{G}_{\mathbf{p}}(t) \quad (3.43)$$

For which, we let $\mathbf{G}_{\mathbf{p}}(t)$ as:

$$\mathbf{G}_{\mathbf{p}}(t) = \frac{1}{Nm} \int_0^t e^{-\frac{\xi}{2}(t-\tau)} \left[\cosh(\omega(t-\tau)) - \frac{\xi}{2\omega} \sinh(\omega(t-\tau)) \right] \int_0^N \mathbf{f}_{\mathbf{n}} \cos(p\pi \frac{n}{N}) dn d\tau \quad (3.44)$$

The transformation from $\mathbf{v}_{\mathbf{n}}$ to $\mathbf{V}_{\mathbf{p}}$ is expressed as:

$$\mathbf{V}_{\mathbf{p}} = \frac{1}{N} \int_0^N \mathbf{v}_{\mathbf{n}} \cos(p\pi \frac{n}{N}) dn \quad (3.45)$$

The velocity correlation function for different normal modes is therefore:

$$\langle \mathbf{V}_{\mathbf{p}}(t) \cdot \mathbf{V}_{\mathbf{p}}(0) \rangle = \langle V_p^2 \rangle \cdot \frac{e^{-\frac{\xi}{2}t}}{(-2\omega)} \left[e^{-\omega t} \left(-\frac{\xi}{2} - \omega \right) - e^{\omega t} \left(-\frac{\xi}{2} + \omega \right) \right] \quad (3.46)$$

Case 2: ω is an imaginary number and $4\lambda_p^2 k/m > \xi^2$

Now, we let the following:

$$\tilde{\omega} = \frac{\sqrt{4\lambda_p^2 k/m - \xi^2}}{2} \quad (3.47)$$

Such that $\omega = i \cdot \tilde{\omega}$ with $i = \sqrt{-1}$. The solution now becomes:

$$\mathbf{X}_p(t) = \frac{e^{-\frac{\xi}{2}t}}{N} \left\{ \mathbf{d}_{1p} \cos(\tilde{\omega}t) + \mathbf{d}_{2p} \sin(\tilde{\omega}t) \right\} + \mathbf{H}_p(t) \quad (3.48)$$

$\mathbf{H}_p(t)$ is expressed as:

$$\mathbf{H}_p(t) = \frac{1}{\tilde{\omega}Nm} \int_0^t e^{-\frac{\xi}{2}(t-\tau)} \sin(\tilde{\omega}(t-\tau)) \int_0^N \mathbf{f}_n \cos(p\pi \frac{n}{N}) dnd\tau \quad (3.49)$$

With $\mathbf{d}_{1p} = (\mathbf{c}_{1p} + \mathbf{c}_{2p})$ and $\mathbf{d}_{2p} = i(\mathbf{c}_{1p} - \mathbf{c}_{2p})$. We then used the initial conditions to evaluate \mathbf{d}_{1p} as well as \mathbf{d}_{2p} . It was obtained:

$$\mathbf{X}_p(t) = e^{-\frac{\xi}{2}t} \left[\mathbf{X}_p(0) \cos(\tilde{\omega}t) + \frac{\xi}{2\tilde{\omega}} \mathbf{X}_p(0) \sin(\tilde{\omega}t) + \frac{\mathbf{V}_p(0)}{\tilde{\omega}} \sin(\tilde{\omega}t) \right] + \mathbf{H}_p(t) \quad (3.50)$$

This gives us the following:

$$\langle \mathbf{X}_p(t) \cdot \mathbf{X}_p(0) \rangle = \langle X_p^2 \rangle e^{-\frac{\xi}{2}t} \left[\cos(\tilde{\omega}t) + \frac{\xi}{2\tilde{\omega}} \sin(\tilde{\omega}t) \right] \quad (3.51)$$

The normal mode velocity is:

$$\mathbf{V}_p(t) = \mathbf{X}_p(0) e^{-\frac{\xi}{2}t} \left[-\frac{\xi^2}{4\tilde{\omega}} - \tilde{\omega} \right] \sin(\tilde{\omega}t) + \mathbf{V}_p(0) e^{-\frac{\xi}{2}t} \left[\cos(\tilde{\omega}t) - \frac{\xi}{2\tilde{\omega}} \sin(\tilde{\omega}t) \right] + \mathbf{G}_p(t) \quad (3.52)$$

$\mathbf{G}_p(t)$ reads:

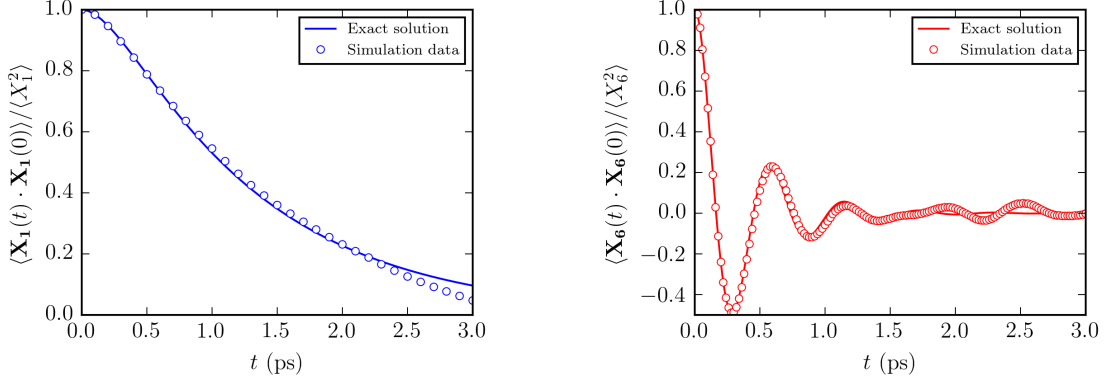
$$\mathbf{G}_p(t) = \frac{1}{Nm} \int_0^t \left[e^{-\frac{\xi}{2}(t-\tau)} (\cos(\tilde{\omega}(t-\tau)) - \frac{\xi}{2\tilde{\omega}} \sin(\tilde{\omega}(t-\tau))) \right] \int_0^N \mathbf{f}_n \cos(p\pi \frac{n}{N}) dnd\tau \quad (3.53)$$

The velocity time correlation function is therefore:

$$\langle \mathbf{V}_p(t) \cdot \mathbf{V}_p(0) \rangle = \langle V_p^2 \rangle \cdot e^{-\frac{\xi}{2}t} \left[\cos(\tilde{\omega}t) - \frac{\xi}{2\tilde{\omega}} \sin(\tilde{\omega}t) \right] \quad (3.54)$$

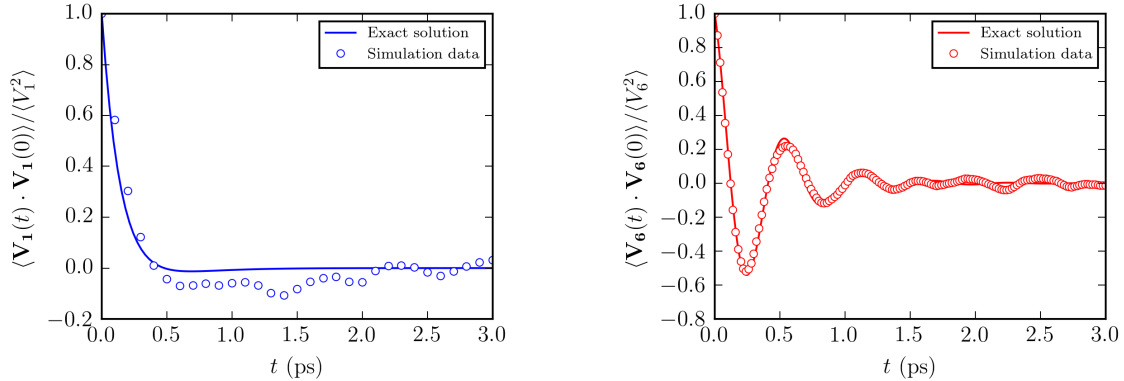
Intriguingly, the velocity time correlation function for $4\lambda_p^2 k/m > \xi^2$ is a damped oscillatory function of t . Figure 3.1a and Figure 3.1b show plots of Equation (3.42) and (3.51) compared with numerical simulation results, respectively. Figure 3.2a and Figure 3.2b show plots of Equation (3.46) and (3.54) compared with numerical simulation results, respectively. The

parameters are chosen as: $\xi = 5 \text{ ps}^{-1}$, $k/m = 900 \text{ ps}^{-2}$, $\lambda_p^2 = p^2\pi^2/N^2$. The exact solution was confirmed by the numerical simulation.



(a) Normal mode time correlation function in case 1 ($p = 1$). (b) Normal mode time correlation function in case 2 ($p = 6$).

Figure 3.1: Normal mode time correlation functions for different cases.



(a) Velocity time correlation function in case 1 ($p = 1$). (b) Velocity time correlation function in case 2 ($p = 6$).

Figure 3.2: Velocity time correlation functions for different cases.

As demonstrated above, there are multiple modes of relaxation in polymeric system due to the fact that there are multiple eigenvalues $-\lambda_p^2$ for $p = 0, 1, 2, 3, \dots, N - 1$ to the operator $\partial^2/\partial n^2$. Under any meaningful condition, depending on the values of these multiple eigenvalues $-\lambda_p^2$, the longer wavelength motion (i.e., when p is small) should always be overdamped (case 1), whereas it is possible that the relatively shorter wavelength motion (i.e., when p is large) can be underdamped (case 2). But ultimately, the time correlation function of the

end-to-end vector ($\mathbf{R} = \mathbf{R}_{N-1} - \mathbf{R}_0$) and the velocity of a bead (\mathbf{v}_n), which can be constructed using all the time correlation functions of normal modes from both case 1 and case 2, are still overdamped relaxation as they are dominated by the longer wavelength motion (cf., Equation (3.55), Equation (3.56) and Figure 3.3).

$$\langle \mathbf{R}(t) \cdot \mathbf{R}(0) \rangle = 16 \sum_{p=1, \text{odd}}^{N-1} \langle \mathbf{X}_p(t) \cdot \mathbf{X}_p(0) \rangle \quad (3.55)$$

$$\langle \mathbf{v}_n(t) \cdot \mathbf{v}_n(0) \rangle = \langle \mathbf{V}_0(t) \cdot \mathbf{V}_0(0) \rangle + 4 \sum_{p=1}^{N-1} \langle \mathbf{V}_p(t) \cdot \mathbf{V}_p(0) \rangle [\cos(p\pi \frac{n}{N})]^2 \quad (3.56)$$

These analytical expressions as presented in Equation (3.55) and Equation (3.56) are also in good agreement with simulation data.²

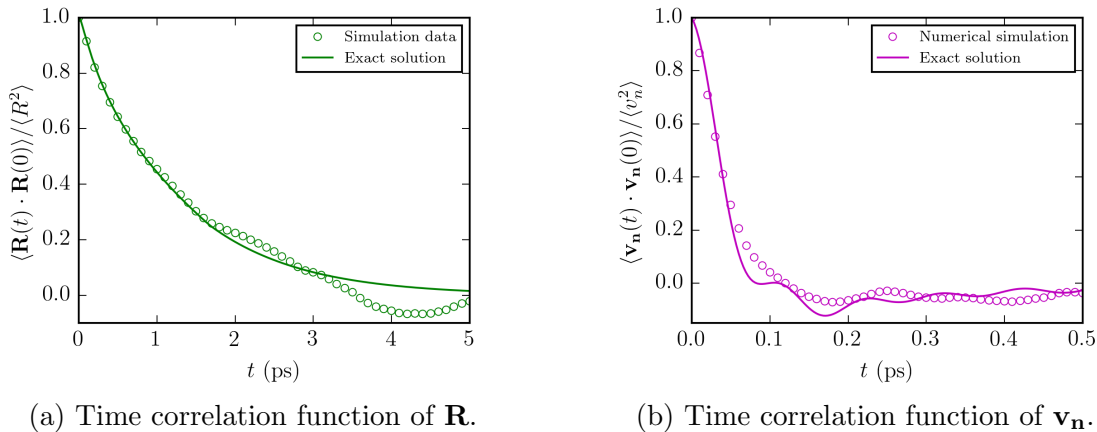


Figure 3.3: Time correlation functions of \mathbf{R} and \mathbf{v}_n .

3.5 Conclusion

In summary, we have shown the velocity time correlation function for different normal modes under the consideration that there is no hydrodynamic interaction. As $p = 0$, which corresponds to the dynamics of the center-of-mass of the chain, the velocity correlation function of the chain has an analytical form similar to that of a single particle. Integration of the

²The aforementioned analysis was also applied in ring polymer in Appendix A. In addition, as mentioned in the future plan, such analysis allows us to derive the viscosity of polymer with the consideration of the kinetic contribution. (cf., Chapter 9)

velocity time correlation function gives the same diffusion coefficient when the inertia term is ignored. For $p = 1, 2, 3, \dots, N - 1$, there are two different cases for the correlation functions:

1. ω is a real number and $4\lambda_p^2 k/m < \xi^2$: The correlation function is an exponential decay function of t .
2. ω is an imaginary number and $4\lambda_p^2 k/m > \xi^2$: The correlation function is a damped oscillatory function of t .

This is also confirmed by our simulation data.

Chapter 4

Analysis of Brownian Dynamics and Molecular Dynamics Data of Unentangled Polymer Melts Using Proper Orthogonal Decomposition¹

4.1 Introduction

The Rouse model [20], a Brownian dynamics (BD) based model, is the simplest molecular level model that one can use it to describe the dynamics of unentangled polymer melts. In the Rouse model, beads are held together by harmonic springs with a spring constant $k = 3k_bT/b^2$ where k_b , T and b are the Boltzmann constant, temperature and equilibrium spring (step or bond) length, respectively. The beads are also under the influence of friction ($-\zeta \frac{d\mathbf{R}_n}{dt}$) and stochastic ($\mathbf{f}_n(t)$) forces. Here, ζ is the friction coefficient and \mathbf{R}_n is the position of the n th bead. The equation of motion for the n th bead is given as

$$\zeta \frac{d\mathbf{R}_n}{dt} = k(\mathbf{R}_{n-1} - \mathbf{R}_n) + k(\mathbf{R}_{n+1} - \mathbf{R}_n) + \mathbf{f}_n(t) = k(\mathbf{R}_{n+1} - 2\mathbf{R}_n + \mathbf{R}_{n-1}) + \mathbf{f}_n(t) \quad (4.1)$$

It is obvious from Equation (4.1) that the inertia term and hydrodynamic interaction are neglected in the Rouse model. Another simplification of the model, which is seldom

¹A version of this chapter has been published in *Macromol. Theory Simul.*, 2019, 28, 1800072.

pointed out explicitly, is that the equilibrium length of the springs is set to zero. It is worth pointing out that according to Equation (4.1), forces due to the springs on the beads are zero when the beads overlap. Obviously, this is unphysical. However, setting the equilibrium spring length to zero makes it straightforward to solve the above linear stochastic differential equation analytically. And the solution is typically expressed in terms of normal modes (Rouse modes). In this way, the relaxation of the polymer chain with different molecular structures can be easily determined. For instance, Ghosh used the Rouse model to study the dynamics of branched polymer melt [24]. Another noteworthy point is that the Rouse model was originally developed for dilute polymer solutions (no chain-chain interaction). However, it turns out that the model yields correct prediction on the chain length dependence of the dynamics of polymer melts.

In this work, we propose to incorporate a finite value for the equilibrium spring length in the Rouse model so that two beads connected by the same harmonic spring are prevented from overlapping with each other. To determine what value of b that should be used, we followed the idea of Hiemenz and Lodge. [13] In their work, they defined an effective bond length to describe chain dimensions such that in their words, “the real chain with local constraints has an end-to-end distance, which is the same as that of a freely jointed chain with the same number of links, but with a different (larger) step length.” Here, C_∞ and b_0 are the characteristic ratio and the carbon-carbon bond length. In other words, inclusion of b implicitly incorporates the chain rigidity (i.e., bond angle and torsion angle correlations) in the model. However, doing so makes the resultant equation of motion non-linear and it can only be solved numerically. As a result, Rouse modes and time correlation functions cannot be easily obtained. To address this issue, we propose to use the technique of proper orthogonal decomposition (POD) to analyze the data (see further discussion below).

Another reason that the Rouse model is so popular is that when the Rouse modes are expressed in stretched exponential functions, they can be used to elucidate the dynamics of entangled polymer melts [25, 8, 26, 22, 23, 27] even though one can argue that Rouse modes do not actually exist for such non-linear systems. In fact, this issue has been pointed out by various authors. In the work of Padding and Briels [8], they mentioned that “For realistic polymer chains, however, it is not expected that the Rouse modes are the normal modes (in a dynamic sense; the static cross-correlations are zero), because the non-bonded interactions

and un-crossibility constraints modify the equations of motion and make them highly non-linear.” Shaffer [26] clearly stated that “If the basic Rouse model is modified to include excluded volume interactions or topological constraints, the governing Langevin equations become highly non-linear and can no longer be diagonalized by the Rouse coordinates.” In the work of Kalathi *et al.*, [22, 23] they even attempted to address the issue why they used the Rouse modes instead of the true normal modes. This can be seen in the conclusion section of their paper: “One question is why we choose to use the Rouse modes of the chains to describe motion rather than true normal modes, which are guaranteed to be orthogonal to each other.” In addition, the stress analysis work of Vladkov and Barrat [28] also requires the assumption that the Rouse modes are applicable to non-linear systems before any meaningful conclusion could be drawn.

In light of the above discussion, it is clear that when a BD based model contains non-linear force terms, validity of Rouse modes is questionable. Therefore, we propose to use the concept of eigenmodes derived from the proper orthogonal decomposition (POD) for the analysis of the numerical solution of the non-linear BD equation of motion. The POD analysis is commonly used in the areas of process control and fluid dynamics simulation [29, 30, 31]. To the best of our knowledge, we are the first ones to apply the POD to analyze dynamics data of polymer melts. The essence of POD analysis is to construct functions of interest based upon a reduced order model of the numerical simulation data. Generally, in the POD analysis, a correlation matrix is constructed using the fluctuation in the positions of beads at various time steps. The resulting eigenvectors of the correlation matrix are the eigenmodes (analogous to the Rouse modes), which are useful for the reconstruction of time correlation functions. The main difference between Rouse modes and eigenmodes is that Rouse modes are the same in x , y and z directions, whereas eigenmodes in these three directions can be different because the correlation matrix is different in the three directions.

To illustrate that the non-linear BD model that we propose can be easily implemented on different molecular structures, we applied it to unentangled polyethylene melts with linear, ring and star structures. The equilibrium spring length b used was set to 4.42 Å which is derived from a C_∞ value of 8.23 at $T = 450$ K as reported by Foteinopoulou *et al.* [32], The POD will be used to obtain the time correlation functions of the end-to-end vector, the m -to- n vector and the arm vector, as well as the zero-shear viscosity (η_0), of the aforementioned

molecular structures. Nonetheless, the Rouse model results of the same systems (i.e., $b = 0$) were also obtained and are presented in the Supporting Information file. To illustrate that the non-linear BD model yields consistent results, we also carried out molecular dynamics (MD) simulations on comparable molecular systems. Obviously, MD simulation, by nature, includes all intra and intermolecular interactions. We also applied the POD to analyze the corresponding MD results.

4.2 BD Simulation Details

Consider the force due to the harmonic bond stretching potential is expressed as follows:

$$\mathbf{F}_n = k(d_{nm} - b) \frac{\mathbf{d}_{nm}}{d_{nm}} \quad (4.2)$$

Given that:

$$d_{nm} = \sqrt{(x_m - x_n)^2 + (y_m - y_n)^2 + (z_m - z_n)^2} \quad (4.3)$$

And,

$$\mathbf{d}_{nm} = \begin{bmatrix} x_m - x_n \\ y_m - y_n \\ z_m - z_n \end{bmatrix} \quad (4.4)$$

b is the equilibrium length of the spring. Let q_n be the position of the n th bead that q can be either x , y or z . The position of each bead of a system containing N beads can be arranged in a vector \mathbf{q} .

$$\mathbf{q} = [x_0 \ \dots \ x_{N-1} \ y_0 \ \dots \ y_{N-1} \ z_0 \ \dots \ z_{N-1}]^T \quad (4.5)$$

If $b = 0$, Rouse model is recovered; If $b = \sqrt{C_\infty} b_0 = 4.42 \text{ \AA}$, the BD equation of motion becomes non-linear. The harmonic bond stretching force in Equation (4.2) can sufficiently avoid overlapping of the beads because in the BD simulation, as $d_{nm} = 0$, a repulsive force with magnitude of kb is always resulted, which is much greater than the stochastic force. In fact, such harmonic bond stretching force is also commonly used in MD simulation for reliable evaluation of static properties, such as radius of gyration, and dynamic properties, such as diffusion coefficient, of linear and ring polyethylene [2, 3] as well as the surface structure of polymethylene [33].

As mentioned, the equation of motion becomes non-linear by including a finite statistical length in the stretching potential. Now, if we would like to solve the non-linear equation of

motion numerically with the implicit Euler method, we have to solve a system of non-linear equations at each time step j by the Newton-Gauss method. Similar numerical procedures were presented by Fixman [34]. The equation of motion is as follows:

$$\frac{d\mathbf{q}_n}{dt} = \frac{1}{\zeta}(\mathbf{F}_n + \mathbf{g}_n) \quad (4.6)$$

\mathbf{g}_n is the stochastic force acting on the n th bead with $\langle g_n \rangle = 0$ and $\langle g_n(t)g_n(t') \rangle = 2k_b T \zeta \delta(t - t')$. After that, we need to know the Jacobian matrix \mathbf{J} , which has a dimension of $3N \times 3N$ and it can be obtained by taking the gradient of the \mathbf{F}_n , which is the force due to bond stretching potential acting on the n th bead, and it is expressed as:

$$\mathbf{F}_n = [F_{n,x} \quad F_{n,y} \quad F_{n,z}]^T \quad (4.7)$$

The derivative of $F_{n,q}$, which is the force acting on the n th bead in q direction, with respect to s_n . (s_n can be x_n , y_n or z_n , which are the positions of the n th bead at x , y or z direction, respectively.) If $q = s$:

$$\frac{\partial F_{n,q}}{\partial q_n} = -k \cdot \frac{(d_{nm} - b)}{d_{nm}} + k \cdot \frac{(q_m - q_n)^2 (d_{nm} - b)}{d_{nm}^3} - k \cdot \frac{(q_m - q_n)^2}{d_{nm}^2} \quad (4.8)$$

If $q \neq s$:

$$\frac{\partial F_{n,q}}{\partial s_n} = k \cdot \frac{(q_m - q_n)(s_m - s_n)(d_{nm} - b)}{d_{nm}^3} - k \cdot \frac{(q_m - q_n)(s_m - s_n)}{d_{nm}^2} \quad (4.9)$$

k is the spring constant. With this, we can immediately write:

$$\frac{\partial F_{n,q}}{\partial q_m} = -\frac{\partial F_{n,q}}{\partial q_n} \quad (4.10)$$

$$\frac{\partial F_{n,q}}{\partial s_m} = -\frac{\partial F_{n,q}}{\partial s_n} \quad (4.11)$$

We then let, in the case of linear polyethylene:

$$\mathbf{J}_{\mathbf{q}s} = \frac{\Delta t}{\zeta} \begin{bmatrix} \frac{\partial F_{0,q}}{\partial s_0} & \frac{\partial F_{0,q}}{\partial s_1} & 0 & 0 & \dots & 0 \\ \frac{\partial F_{1,q}}{\partial s_0} & \frac{\partial F_{1,q}}{\partial s_1} & \frac{\partial F_{1,q}}{\partial s_2} & 0 & \dots & 0 \\ 0 & \frac{\partial F_{2,q}}{\partial s_1} & \frac{\partial F_{2,q}}{\partial s_2} & \frac{\partial F_{2,q}}{\partial s_3} & \dots & 0 \\ 0 & 0 & \ddots & \ddots & \ddots & 0 \\ 0 & 0 & \dots & \frac{\partial F_{N-2,q}}{\partial s_{N-3}} & \frac{\partial F_{N-2,q}}{\partial s_{N-2}} & \frac{\partial F_{N-2,q}}{\partial s_{N-1}} \\ 0 & 0 & \dots & 0 & \frac{\partial F_{N-1,q}}{\partial s_{N-2}} & \frac{\partial F_{N-1,q}}{\partial s_{N-1}} \end{bmatrix} \quad (4.12)$$

ζ is the friction coefficient and Δt is the integration time step. The Jacobian matrix can be then constructed using blocks of $\mathbf{J}_{\mathbf{q}s}$:

$$\mathbf{J} = \begin{bmatrix} \mathbf{J}_{\mathbf{xx}} - \mathbf{I} & \mathbf{J}_{\mathbf{xy}} & \mathbf{J}_{\mathbf{xz}} \\ \mathbf{J}_{\mathbf{yx}} & \mathbf{J}_{\mathbf{yy}} - \mathbf{I} & \mathbf{J}_{\mathbf{yz}} \\ \mathbf{J}_{\mathbf{zx}} & \mathbf{J}_{\mathbf{zy}} & \mathbf{J}_{\mathbf{zz}} - \mathbf{I} \end{bmatrix} \quad (4.13)$$

At each time step, the initial guess of the positions of the beads at the next time step was set at that of the present time step, and \mathbf{q}_{j+1} was updated in the internal iteration of the Newton-Gauss method based on Equation (4.14) until the tolerance, which is the norm of the residual \mathbf{r} , is less than 10^{-10} .

$$\mathbf{q}_{j+1}^{(a+1)} = \mathbf{q}_j^{(a)} - \left[(\mathbf{J}^T \mathbf{J})^{-1} \mathbf{J}^T \mathbf{r} \right]^{(a)} \quad (4.14)$$

The superscripts (a) and $(a + 1)$ indicate the present and next iteration, respectively. \mathbf{r} has components expressed as:

$$\mathbf{r} = [r_{0,x} \ \dots \ r_{N-1,x} \ r_{0,y} \ \dots \ r_{N-1,y} \ r_{0,z} \ \dots \ r_{N-1,z}]^T \quad (4.15)$$

$$r_{n,q} = \left[F_{n,q}(t + \Delta t) + g_{n,q}(t + \Delta t) \right] \cdot \frac{\Delta t}{\zeta} - q_n(t + \Delta t) + q_n(t) \quad (4.16)$$

A C++ program is presented in the Supporting Information.

In all numerical simulations, $T = 450$ K, $k = 3k_b T / b^2$ and $\zeta = l\sqrt{mk_b T}$, where l is the bead size, which is taken to be 2 \AA . And Δt was set at 0.63 ps. Numerical stability is still guaranteed despite a large Δt as integration was achieved by the implicit Euler method. The number of beads in linear and ring structures, as well as star structure with four arms ranged from $N = 30$ to $N = 73$, respectively. The range of N was chosen such that they are below the entanglement chain length. The simulation was allowed to run for $3 \cdot 10^5$ steps. Initial conformations of all structures were constructed using free software Avogadro. CPU time in this case was approximately $0.013 - 0.020$ hr/ns in a computer with Intel(R) Xeon(R) CPU E5-2630 v2 at 2.60 GHz.

4.3 MD Simulation Details

Molecular dynamics simulation was also performed by explicitly including the many-chain effect, and more detailed bonded interactions, such as torsion angle potential as well as angle bending potential in the equation of motion. The forcefield we considered is coarse-grained without electrostatic interaction. The forcefield parameters were taken from the work by Martin and Siepmann [19, 18], which is also known as the TraPPE forcefield. The most daunting task in such simulation was the preparation of a good initial configuration, which

ensures stability of the subsequent simulation. With regard to this, many of the chains, which was prepared using Avogadro, were packed in a box such that the distance between one united atom of one chain and another was at least 4 nm. This was achieved using the free software PACKMOL [35]. Alternatively, for ring polymer, as such procedure may lead to concatenation of the ring polymers, they were randomly distributed in a much larger box. In equilibration, the system was compressed by NPT simulation with a Nosé-Hoover thermostat with a time constant of 0.2 ps to maintain the time-averaged temperature at 450 K and a Berendsen barostat with reference at room pressure and time constant of 0.5 ps. After such procedure, the density of the system reached approximately $700 \text{ kg}\cdot\text{m}^{-3}$. In the production run, a 20 ns of canonical ensemble (NVT) MD simulation was then performed. Systems with $N = 30-73$ were used. The number of chains used in this study was varied such that the total number of united atoms is 800 for $N \leq 50$ and it was fixed at 40 for $N > 50$. The equation of motion was integrated using leapfrog algorithm. Periodic boundary conditions were imposed in all cases. These simulations were performed using the free software GROMACS 5.1.4 [36]. Figure 4.1 shows the final configurations of polyethylene with different structures after the NVT MD simulation. CPU time in this case was approximately 0.035 – 0.080 hr/ns in a computer with Intel(R) Xeon(R) CPU E5-2630 v2 at 2.60GHz. Note that the CPU time taken in MD simulation is 4 times longer than that in BD simulation.

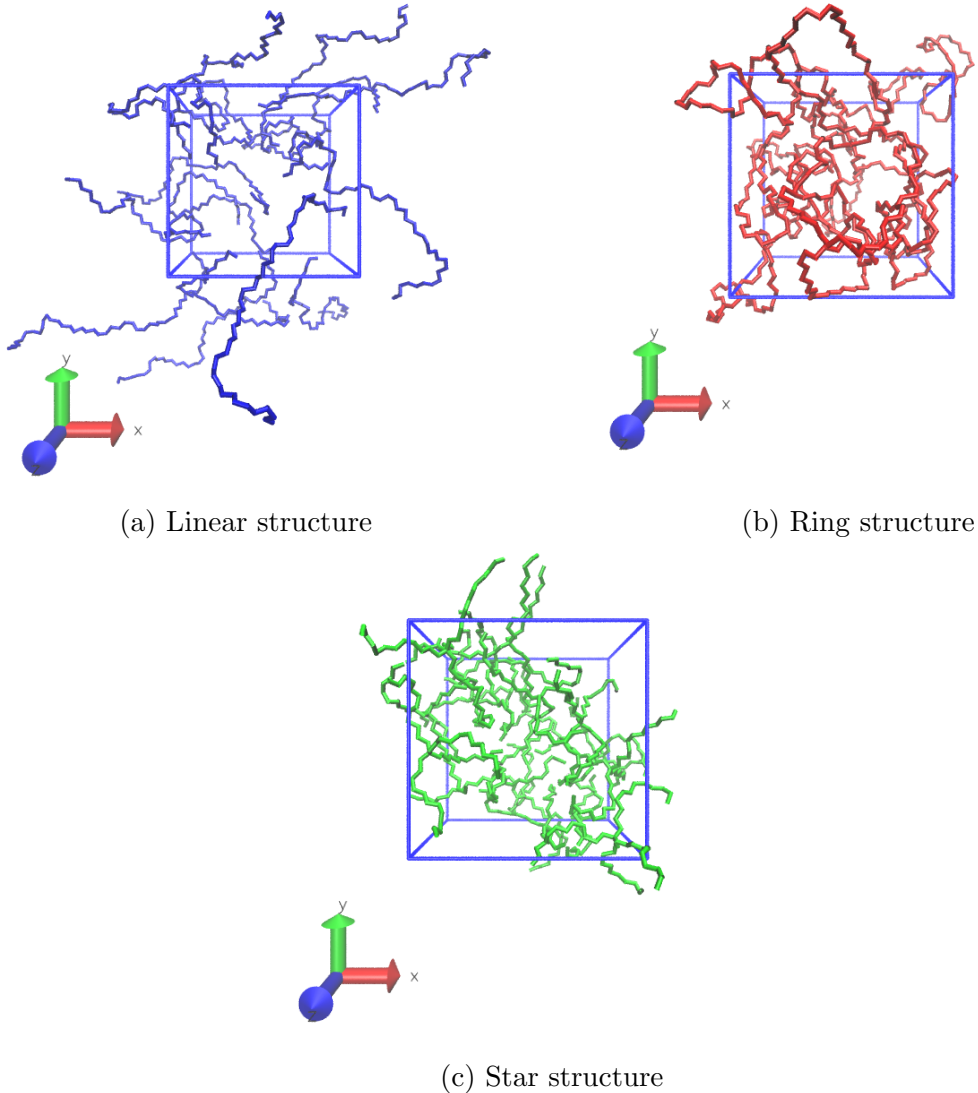


Figure 4.1: Final configurations of polyethylene with different structures after the NVT MD simulation. ($N = 50$ for linear and ring structures, and $N = 49$ for star structure)

To show that our MD data are reliable, we have also evaluated the center-of-mass diffusion coefficient (D_{cm}) as well as the root-mean-square radius of gyration ($\sqrt{\langle R_g^2 \rangle}$) of polyethylene with different structures to check if the corresponding N dependence is in good qualitative agreement with that reported in the literature. Such calculation results are presented in the Supporting Information. In addition, to prove that the finite size effect due to periodic boundary condition is not significant, we have performed one more MD simulation run of 40 linear chains with $N = 50$, i.e. a total number of 2000 united atoms. In this case, we found that the change in the longest relaxation time (τ_1) and η_0 is small with only 5% – 7%. τ_1

changes from 468 ps to 432 ps, while η_0 changes from $1.09 \cdot 10^{-3}$ Pa · s to $1.04 \cdot 10^{-3}$ Pa · s when the number of chains increases by 2.5 times. This is in good agreement with Sen *et al.* [37], in which they found that for linear chain with $N = 120$, the viscoelastic properties were unchanged even if they doubled the number of chains used in the MD simulation. Therefore, we conclude that the finite size effect does not significantly influence the calculated results of τ_1 and η_0 in the MD simulation of this work. And it should be expected that such effect is even more trivial for ring and star polymers because their radii of gyration are even shorter than that of linear chains (cf., Supporting Information).

4.4 Proper Orthogonal Decomposition

As the equation is non-linear, the POD analysis should be performed to obtain the eigenmodes. The time averaged position of different beads/unit atoms of polyethylene in a particular direction (either x , y or z) was computed.

$$\bar{q}(t) = \frac{1}{N} \sum_{i=0}^{N-1} q_i(t) \quad (4.17)$$

The fluctuation in the position q'_i can be then calculated as follows:

$$q'_i(t) = q_i(t) - \bar{q}(t) \quad (4.18)$$

The correlation matrix ($N \times N$), denoted as \mathbf{C} , can be then formed using the following equation:

$$C_{i,j} = \frac{1}{N_{snap}} \sum_{t=0}^{N_{snap}-1} q'_i(t) q'_j(t) \quad (4.19)$$

\mathbf{C} is symmetrical and the eigenvectors of \mathbf{C} are the eigenmodes, which is denoted as $\psi_p^q(n)$, such that $\psi_p^q(n)$ is the p th eigenmode in direction q with dimension of $N \times 1$. N_{snap} is the number of snapshots taken from the trajectory, and it was set at a range of $N_{snap} = 4000 - 5000$. If one would like to obtain the high frequency eigenmode, a larger value of N_{snap} was preferred. Nevertheless, as we are mainly interested in the large scale motion (up to a maximum of 7 modes), a large value of N_{snap} may not be necessary. As the correlation matrix \mathbf{C} can be different in the three directions, this also implies that the eigenmodes can

be slightly different in x , y and z directions. Normalization of ψ_p^q was achieved by:

$$\tilde{\psi}_p^q = \frac{\psi_p^q}{\left\{ \sum_{n=0}^{N-1} [\psi_p^q(n)]^2 \right\}^{0.5}} \quad (4.20)$$

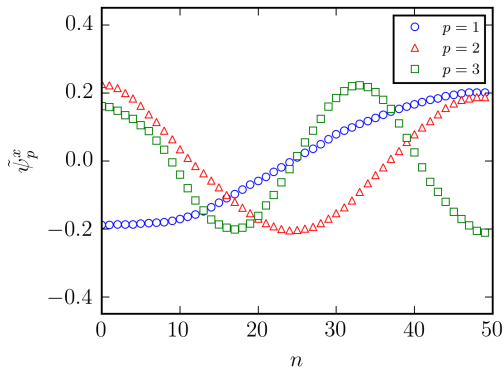
To obtain the normal coordinate, the coordinate transformation in this case is therefore,

$$X'_{p,q} = \sum_{n=0}^{N-1} q_n \tilde{\psi}_p^q(n) \quad (4.21)$$

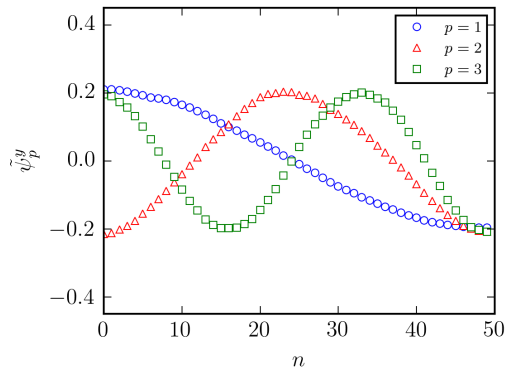
This analysis was performed using a Python 3.5 program attached in the Supporting Information.

4.5 Non-Linear BD of Polyethylene with $b = \sqrt{C_\infty} b_0$

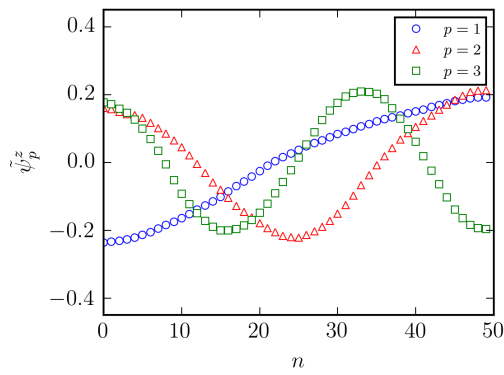
The non-linear equation of motion was solved numerically with $b = 4.42 \text{ \AA}$. As the equation of motion is non-linear and positions of the beads in different direction are coupled to each other. Rouse mode is no longer applicable, and the normal mode in each direction has to be approximated with the POD analysis. Figure 4.2, Figure 4.3 and Figure 4.4 show the first three most dominant eigenmodes obtained from the POD analysis in three directions for polyethylene with different molecular structures. It was found that these eigenmodes are almost the same in three directions. However, they are slightly different from Rouse modes, which are described by perfect cosine and sine functions: $\cos(p\pi n/N)$, and $\cos(2p\pi n/N)$ as well as $\sin(2p\pi n/N)$, with the continuous approach introduced by Doi and Edwards [21] in the case of linear polymer and ring polymer but not for star structure (a more detailed derivation can be found in the Supporting Information).



(a) Direction x

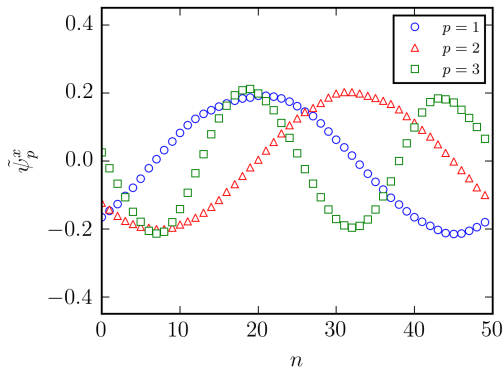


(b) Direction y

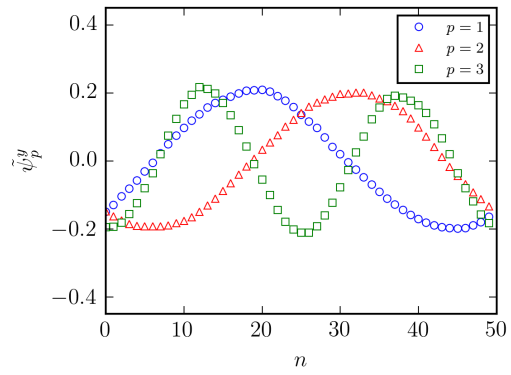


(c) Direction z

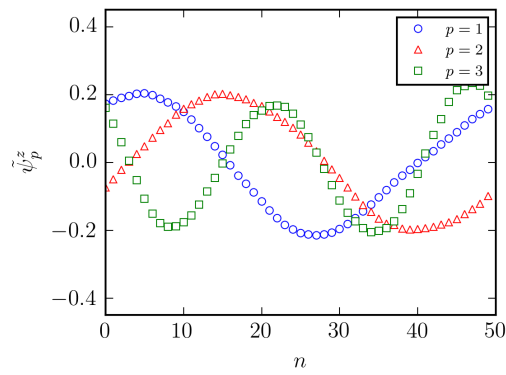
Figure 4.2: The first three most dominant eigenmodes in different directions obtained from the POD analysis in linear structure.



(a) Direction x (ring structure)



(b) Direction y (ring structure)



(c) Direction z (ring structure)

Figure 4.3: The first three most dominant eigenmodes in different directions obtained from the POD analysis in the ring structure.

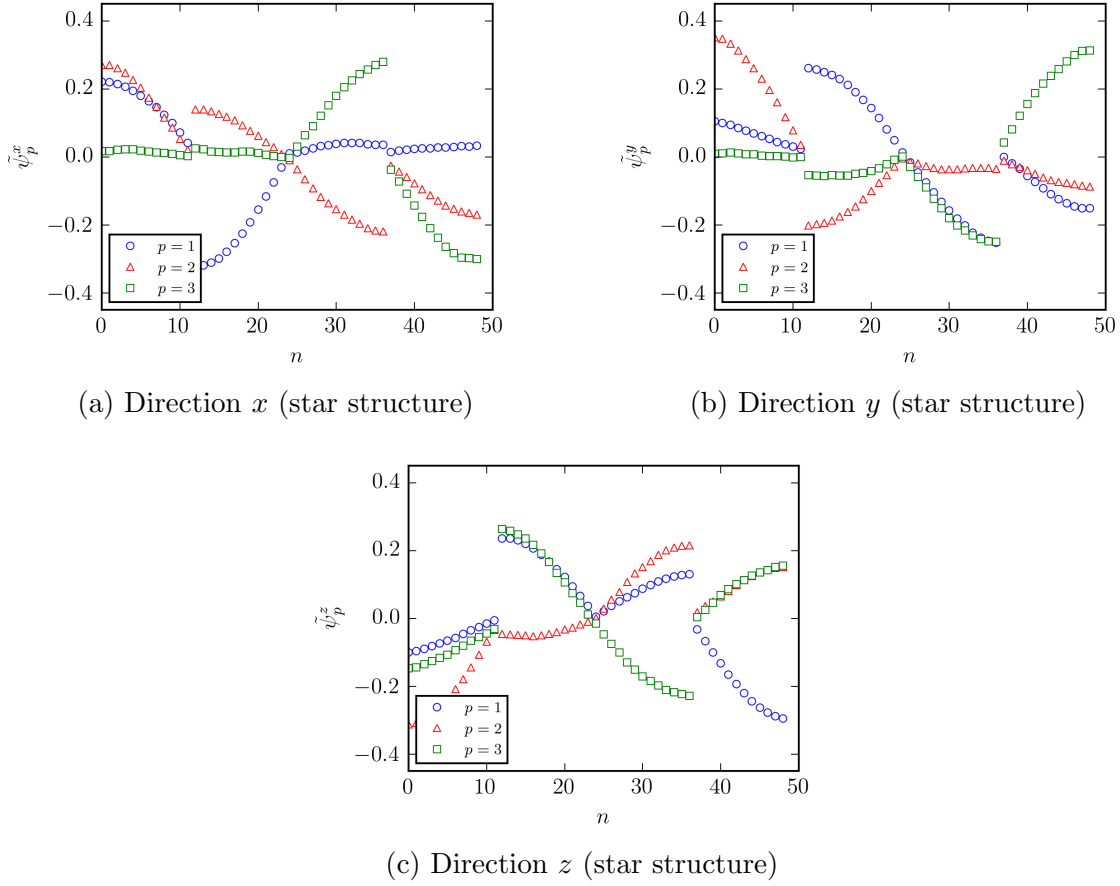


Figure 4.4: The first three most dominant eigenmodes in different directions obtained from the POD analysis in the star structure.

We then applied the coordinate transformation as stated in Equation (4.21), and the corresponding time correlation functions $\mu_p(t)$ of different eigenmodes were evaluated and fitted to a stretched exponential function.

$$\mu_p(t) = \frac{\langle X'_{p,x}(t) \cdot X'_{p,x}(0) + X'_{p,y}(t) \cdot X'_{p,y}(0) + X'_{p,z}(t) \cdot X'_{p,z}(0) \rangle}{\langle X'^2_{p,x} + X'^2_{p,y} + X'^2_{p,z} \rangle} \approx \exp[-(t/\tau_p^*)^{\beta_p}] \quad (4.22)$$

The effective relaxation time of the p th mode (τ_p) is determined as follows:

$$\tau_p = \frac{\tau_p^*}{\beta_p} \cdot \Gamma(1/\beta_p) \quad (4.23)$$

In Figure 4.5, $-\ln \mu_p(t)$ is plotted as a function of time for the three different molecular structures, such that the time correlation functions appear as linear curves, in which the y -intercept is related to τ_p , and the slope is β_p . Interestingly, as mentioned above and

demonstrated in the Supporting Information, there are two and three eigenfunctions sharing the same relaxation time for ring and star structures, respectively (cf., Figure 4.5(b) and Figure 4.5(c)). Among these molecular structures, it was found that τ_1 of linear polymer is the longest (cf., Table 8.1). And β_p was within the range of $0.97 - 1.05$, indicating the constraint on the motion of the polymer is small because the β_p does not deviate much from unity [8, 26].

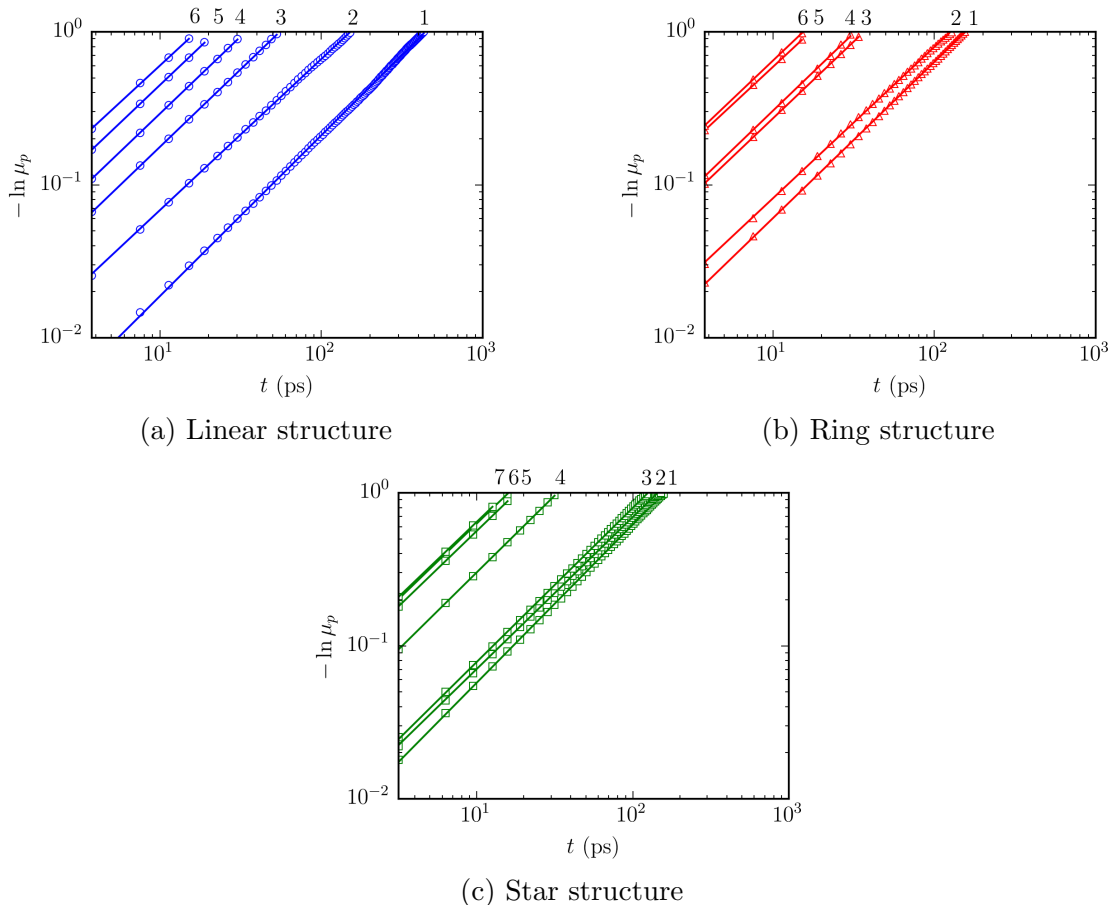


Figure 4.5: Time correlation functions of different eigenmodes in BD simulation. ($N = 50$ for linear and ring structures, and $N = 49$ for star structure)

Table 4.1: β_1 and τ_1 of the most dominant eigenmodes in BD simulation, and τ_1^R in the classic Rouse model as presented in the Supporting Information. ($N = 50$ for linear and ring structures, and $N = 49$ for star structure)

Structures	β_1	τ_1 (ps)	τ_1^R (ps)
Linear ($N = 50$)	1.051	432	159
Ring ($N = 50$)	1.021	155	40
Star ($N = 49$)	1.034	157	40

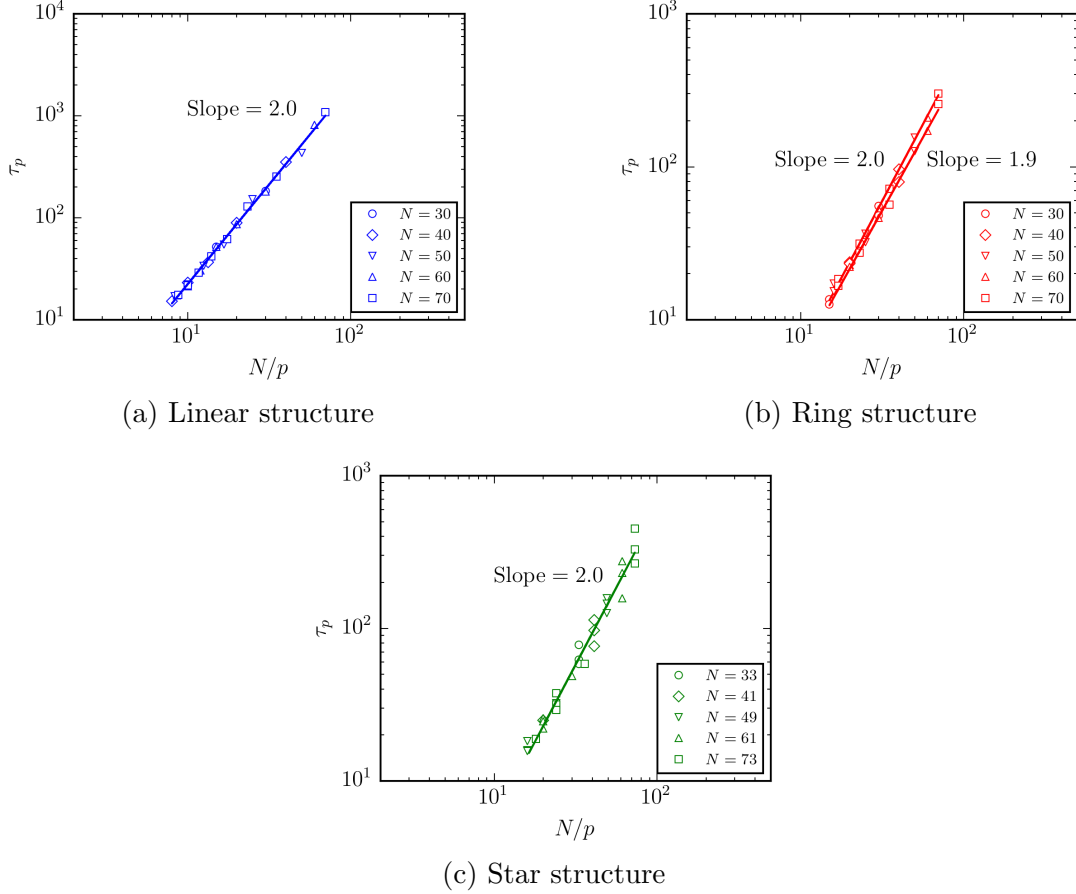


Figure 4.6: N/p dependence of τ_p for polyethylene with different structures. (BD)

τ_p obtained from these time correlation functions are then plotted as a function of N/p in Figure 4.6. In Figure 4.6, note that for ring structure, two linear curves were fitted to the data as two eigenmodes can share roughly the same relaxation time, whereas for star structure, as three eigenmodes can share similar magnitude of relaxation time, the data points were shifted accordingly and was fitted to one single linear curve. As expected, $\tau_p \sim N^2/p^2$. This confirms that the eigenmodes derived from the POD analysis are reliable. The longest relaxation time of linear polymer is longer by a factor of 2.8 than those of ring and star structures (cf., Table 8.1). Furthermore, compared to the relaxation time in classic Rouse model (τ_1^R), τ_1 derived from the BD simulation data is longer as expected (cf., Table 8.1).

Finally, we analyzed the time correlation functions of different vectors (cf., Figure 4.8), which has a longer relaxation time compared to that in Rouse model. With τ_p obtained from the above time correlation functions of different eigenmodes, it is possible to get a reasonable

approximation of the time correlation functions of these vectors (cf., Figure 4.8).

$$\langle \mathbf{R}(t) \cdot \mathbf{R}(0) \rangle \approx \sum_{p=1}^9 \frac{e^{-t/\tau_p}}{3} \left[\sum_{q=x,y,z} \langle X_{p,q}^2 \rangle (\tilde{\psi}_p^q(m) - \tilde{\psi}_p^q(n))^2 \right] \quad (4.24)$$

Note that m and n are the index labels of any two beads of the polymer. The choice of m and n is simply determined by which two beads the researchers are interested in. In the linear chain, we are interested in the end-to-end vector, therefore, $m = N - 1$ and $n = 0$, which refers to the two beads/unit atoms at the two ends of the linear chain. \mathbf{R} is the vector joining these two points (i.e. m and n beads) (cf., Figure 4.7(a)). For ring structure, we are interested in the vector joining $m = N/2 - 1$ and $n = 0$ (cf., Figure 4.7(b)); for star structure, we are interested in the vector joining $m = (N - 1)/2$ and $n = 0$ (cf., Figure 4.7(c)), which corresponds to the arm vector.

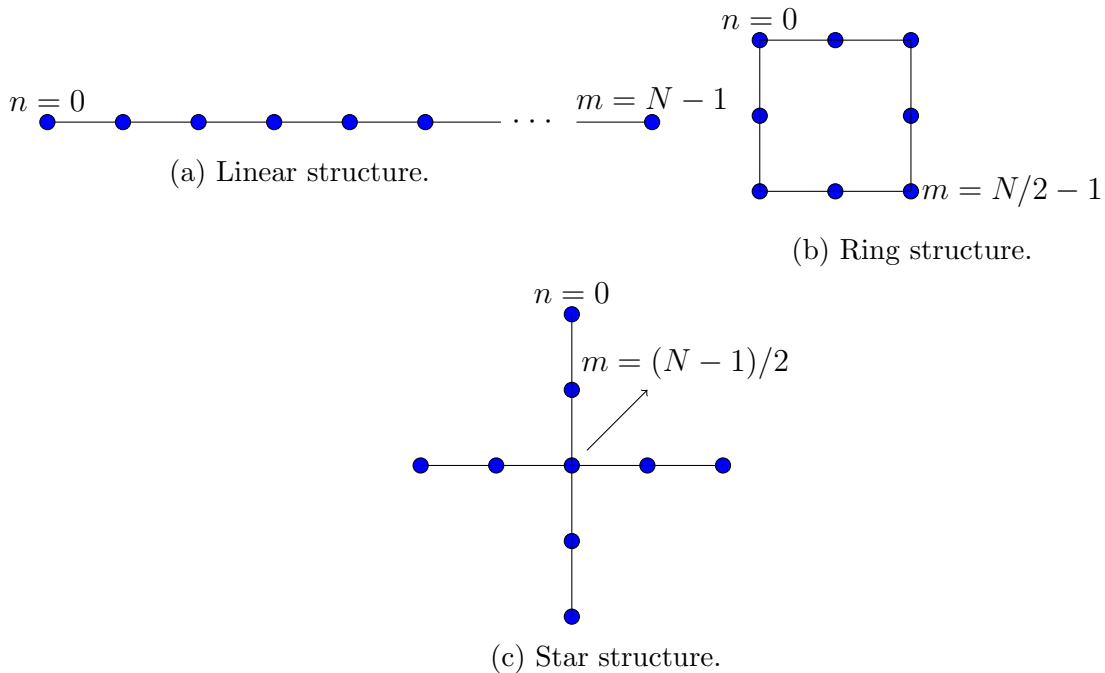


Figure 4.7: Nomenclature of different bead in polyethylene with different structures.

To check if the harmonic bond stretching force in Equation (4.2) was able to avoid overlapping of the beads and generate correct static properties of the polymer, the root-mean-square values of these vectors ($\sqrt{\langle R^2 \rangle}$) were also evaluated and compared with the value calculated by $\sqrt{\langle R^2 \rangle} = \sqrt{NC_\infty}b_0$ as presented in the Supporting Information. We found that the nu-

merical values of $\sqrt{\langle R^2 \rangle}$ are always slightly higher than that of $\sqrt{NC_\infty b_0}$ and $\sqrt{\langle R^2 \rangle} \sim N^{0.5}$ in BD simulation (cf., Supporting Information).

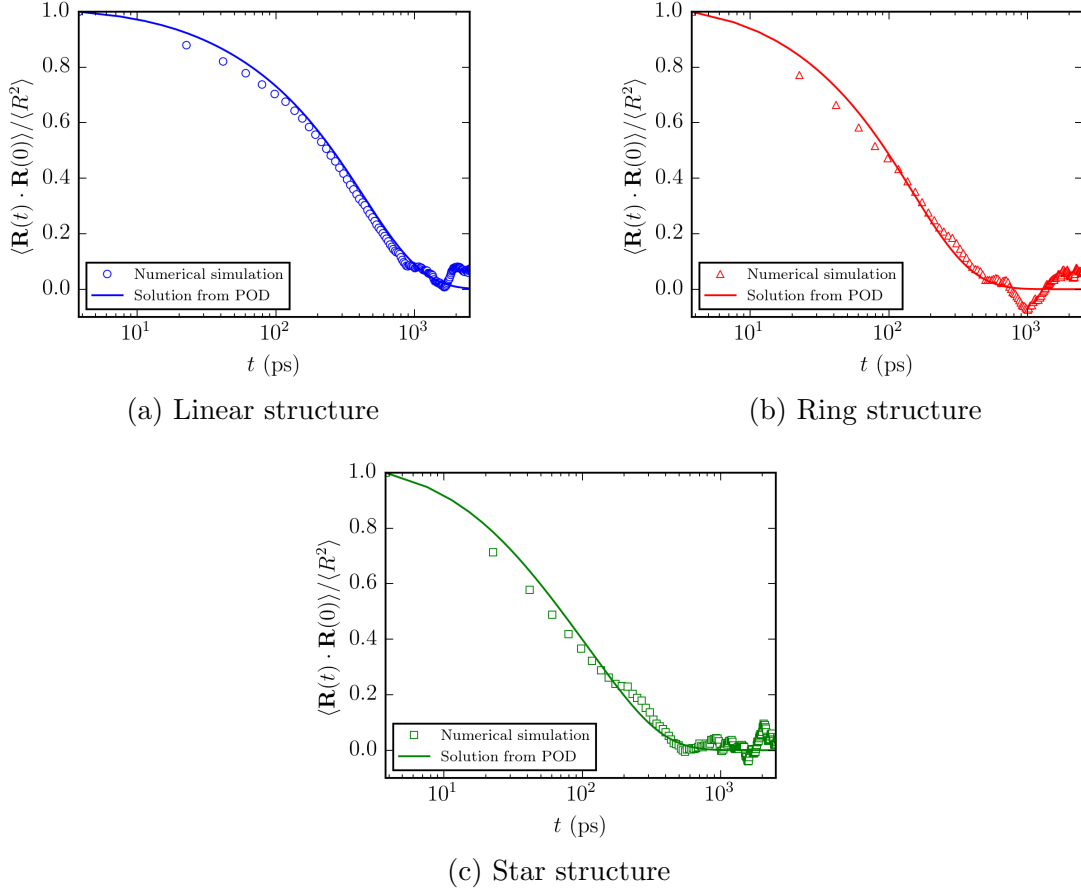


Figure 4.8: Time correlation functions of different vectors of linear, ring and star structures ($b = 4.42 \text{ \AA}$) ($N = 50$ for linear and ring structures, and $N = 49$ for star structure).

4.6 MD Simulation

Same procedures of POD analysis were repeated for the MD simulation data of polyethylene with linear, ring and star structures. Figure 4.9 shows the first three most dominant eigenmodes of one of the many chains in x direction for the linear and ring structures with $N = 50$, and star structure with $N = 49$. Data for y and z directions are not shown here as they resemble to those of x direction. As expected, with the incorporation of the effect of many-chain interaction and stiffness, the eigenmodes are similar to those of the eigenmodes found in the BD simulation. This may be because the force derived from the harmonic potential

of the bond stretching is much larger than other inter/intra-molecular force and forces from other bonded interaction potentials in the TraPPE forcefield [19, 18]. In TraPPE forcefield [19, 18], the spring constant in bond stretching potential is $k_b = 502416 \text{ kJ} \cdot \text{mol}^{-1} \cdot \text{nm}^2$, whereas that in angle bending and torsional potential are $k_\theta = 519 \text{ kJ} \cdot \text{mol}^{-1} \cdot \text{rad}^2$ and $k_\psi = 1.134 - 26.318 \text{ kJ} \cdot \text{mol}^{-1}$. The depth of the potential well in Lennard-Jones potential for a carbon atom, methylene group and methyl group are $\varepsilon = 0.831 \text{ kJ} \cdot \text{mol}^{-1}$, $\varepsilon = 0.382 \text{ kJ} \cdot \text{mol}^{-1}$ and $\varepsilon = 0.815 \text{ kJ} \cdot \text{mol}^{-1}$, respectively. k_b is 10^3 times larger than k_θ , 10^4 times larger than k_ψ and 10^5 times larger than ε . Therefore, it is not surprising that any fluctuation in the positions of the united atom is mainly contributed by the bond stretching force.

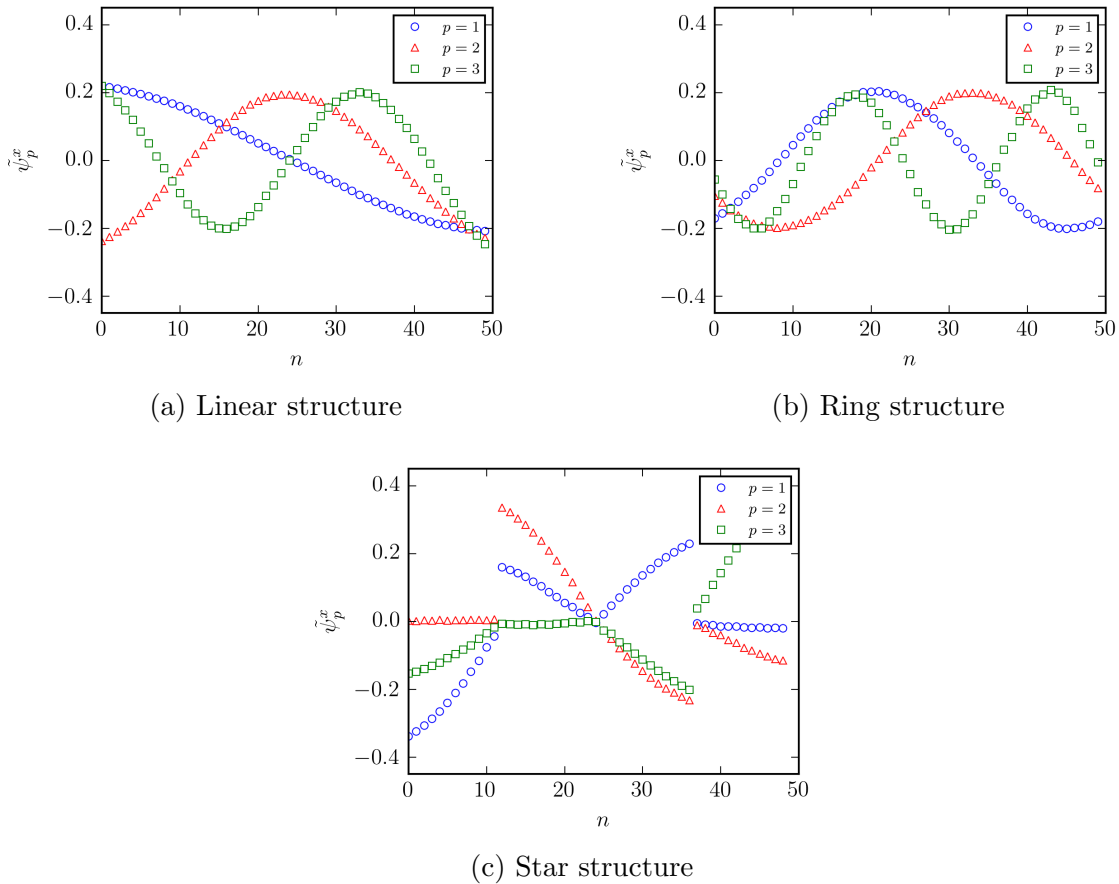


Figure 4.9: First three most dominant eigenmodes of one of the many chains in x direction for different molecular structures of polyethylene.

Figure 4.10 shows the log-log plot of $-\ln \mu_p$ with time for linear and ring structures

with $N = 50$, and star structure with $N = 49$. The simulation data were fitted to a stretched exponential function (cf., Equation (4.22)) and τ_p were obtained using Equation (4.23). Unlike the case that eigenmodes were extracted using only a single macromolecule in BD simulation, μ_p was averaged over all the macromolecules in addition to the time-averaging in MD simulation. Due to the kinetic constraints imposed by the torsion potential and angle bending potential in the bonded interaction, as well as the intermolecular potential in the non-bonded interaction, μ_p is now a relatively more stretched exponential function of time with values of β_p ranging from 0.82 – 0.93. This is in line with the findings of Faller and Müller-Plathe [38] as well as Bulacu and van der Giessen [27], which suggest that in addition to many-chain effect, increased chain stiffness can lead to stronger reptation and more severe kinetic constraints.

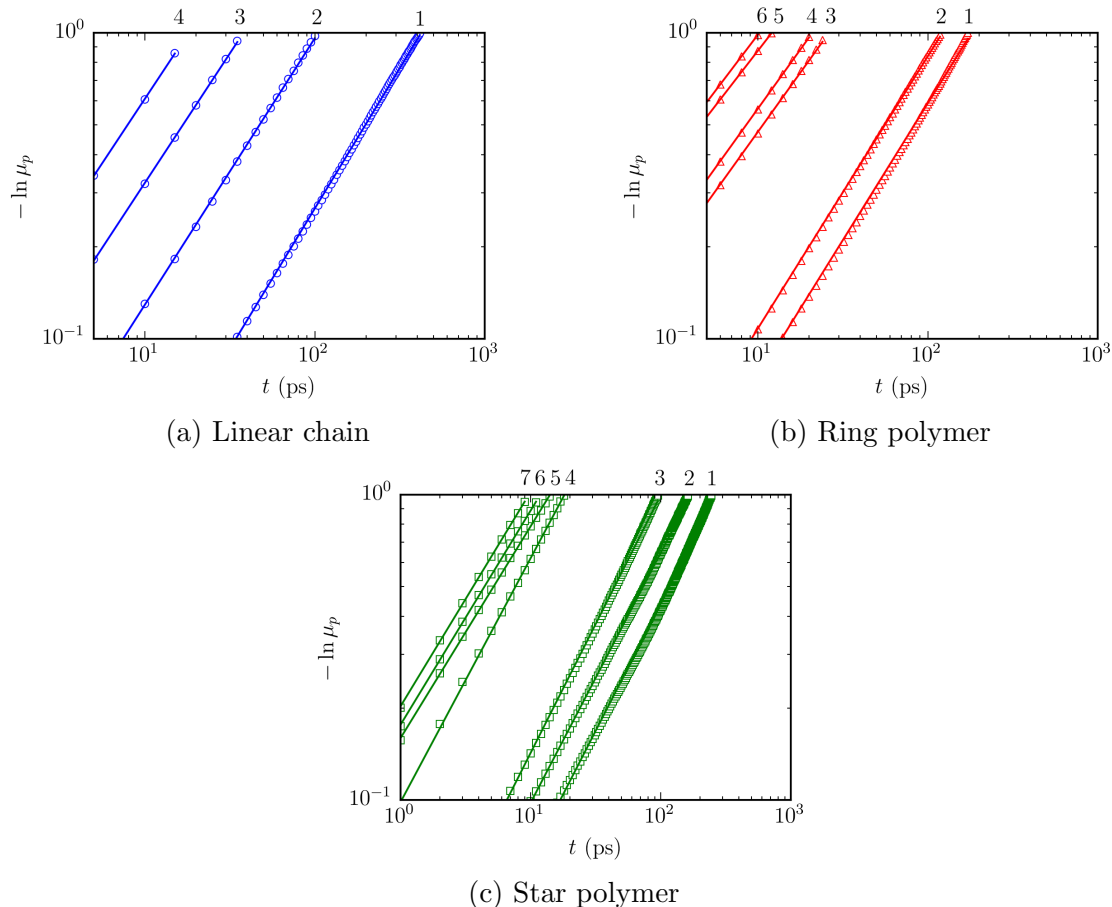


Figure 4.10: Time correlation functions of different eigenmodes in many-chain systems of linear, ring and star polyethylene. ($N = 50$ for linear and ring structures, and $N = 49$ for star structure)

Table 4.2: β_1 and τ_1 of the most dominant eigenmodes in MD simulation. ($N = 50$ for linear and ring structures, and $N = 49$ for star structure)

Structures	β_1	τ_1 (ps)
Linear ($N = 50$)	0.913	468
Ring ($N = 50$)	0.894	191
Star ($N = 49$)	0.833	296

Interestingly, once the many-chain effect and stiffness are explicitly included, τ_1 of star polymer becomes longer than that of the ring polymer, with τ_1 of linear structure being longer than that of star and ring polymer by factors of 2.4 and 1.6, respectively (cf., Table 8.2). Compared with the BD simulation results (cf., Table 8.1), we found that τ_1 s of all structures in BD simulation agree well with those in MD simulation, except for star structure (cf., Table 8.1 and Table 8.2). It was found that D_{cms} of star polymers are slightly lower than that of linear polymers in MD simulation, whereas they are roughly the same in BD simulation (cf., Supporting Information). This indicates that the resulting ζ of star polymers is slightly higher than that of linear polymers in MD simulation, whereas this was held fixed at $\zeta = l\sqrt{mk_bT}$ for all different structures in BD simulation (cf., BD Simulation Details). The obvious consequence is therefore the slowing down of relaxation dynamics of the star polymers in the MD simulation, compared to that in BD simulation.

Relaxation times of different eigenmodes (τ_p) are also plotted as a function of N/p in Figure 4.11 similar to that depicted in Figure 4.6. Dependence of τ_p on N/p from the MD simulation results is slightly stronger (i.e., $\tau_p \sim (N/p)^{2.3}$) than that from the BD simulation results (i.e., $\tau_p \sim (N/p)^{2.0}$). We speculate that this stronger dependence is attributed to the fact that the equation of motion in MD simulation is more non-linear than that in BD simulation. Kremer *et al.* [39, 25] and Kalathi *et al.* [22] applied the Rouse mode in the analysis of the simulation data of linear chain with many-chain effect, and they observed that in the unentangled regime, $\tau_p \sim (N/p)^2$, which is slightly weaker than our MD simulation results. This shows that the POD analysis is sensitive to the non-linearity of the system when compared to the Rouse mode. Yet, the model in Padding *et al.* [8], Harnau *et al.* [40] as well as Kavassalis and Noolandi [41], however, with Rouse mode analysis, suggested that in the unentangled regime, the dependence is stronger with $\tau_p \sim (N/p)^4$. Nonetheless, these models are derived based on Langevin dynamics with uncrossibility constraints or Lagrange

multiplier, and are therefore different from MD simulation: “Uncrossibility” and stiffness are explicitly achieved by including Lennard Jones potential, as well as angle bending and torsional potential, respectively, in MD simulation.

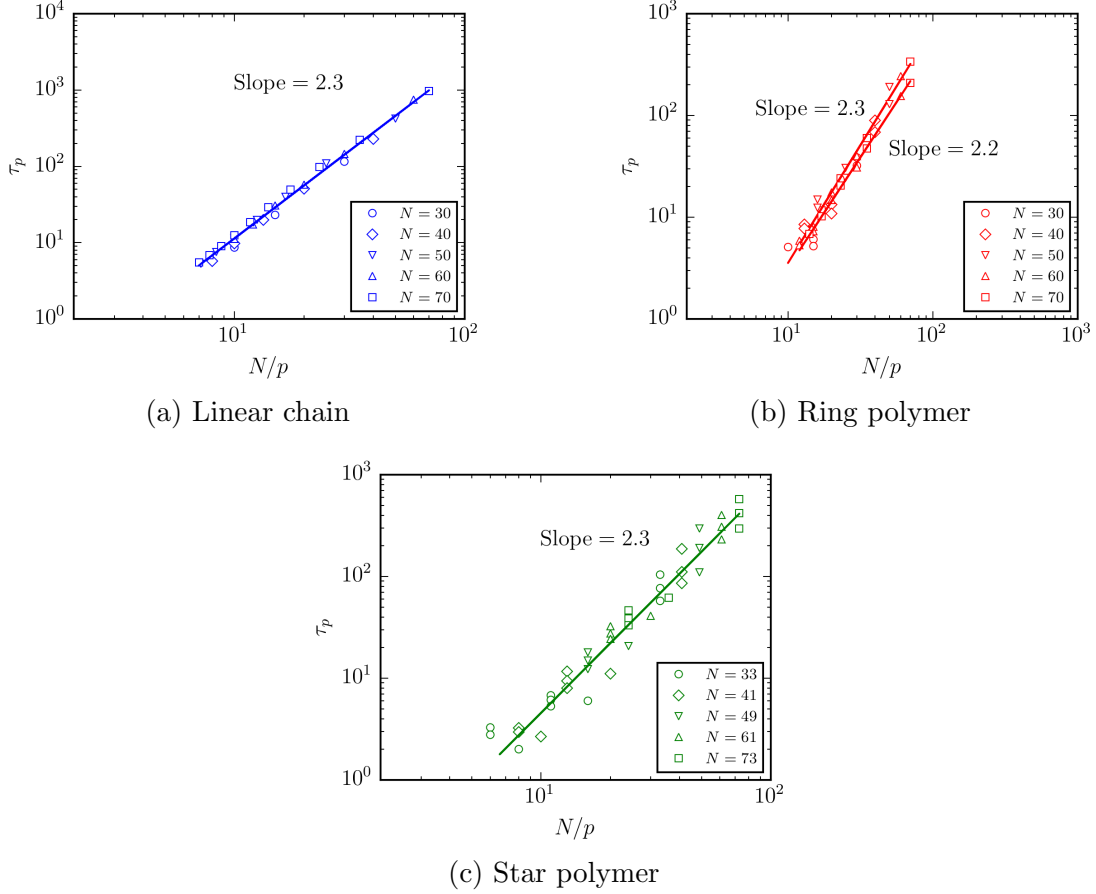


Figure 4.11: N/p dependence of τ_p for polyethylene with different structures. (MD simulation)

With these, we can reconstruct the time correlation function of different vectors based on the eigenmodes using the following Equation (4.25):

$$\langle \mathbf{R}(t) \cdot \mathbf{R}(0) \rangle \approx \left\langle \sum_{p=1}^{p'} \frac{\exp \left[- (t/\tau_p^*)^{\beta_p} \right]}{3} \left[\sum_{q=x,y,z} \langle X_{p,q}^{r2} \rangle (\tilde{\psi}_p^q(m) - \tilde{\psi}_p^q(n))^2 \right] \right\rangle \quad (4.25)$$

Note that p' is the number of eigenmodes being used in the construction of POD solution. In linear structure, $m = N - 1$ and $n = 0$; in ring structure, $m = N/2 - 1$ and $n = 0$; in star structure, $m = (N - 1)/2$ and $n = 0$. The big angled bracket in Equation (4.25) indicates

that the correlation function is also averaged over all the chains in the system. As shown in Figure 4.12, the POD solutions are in line with the simulation data.

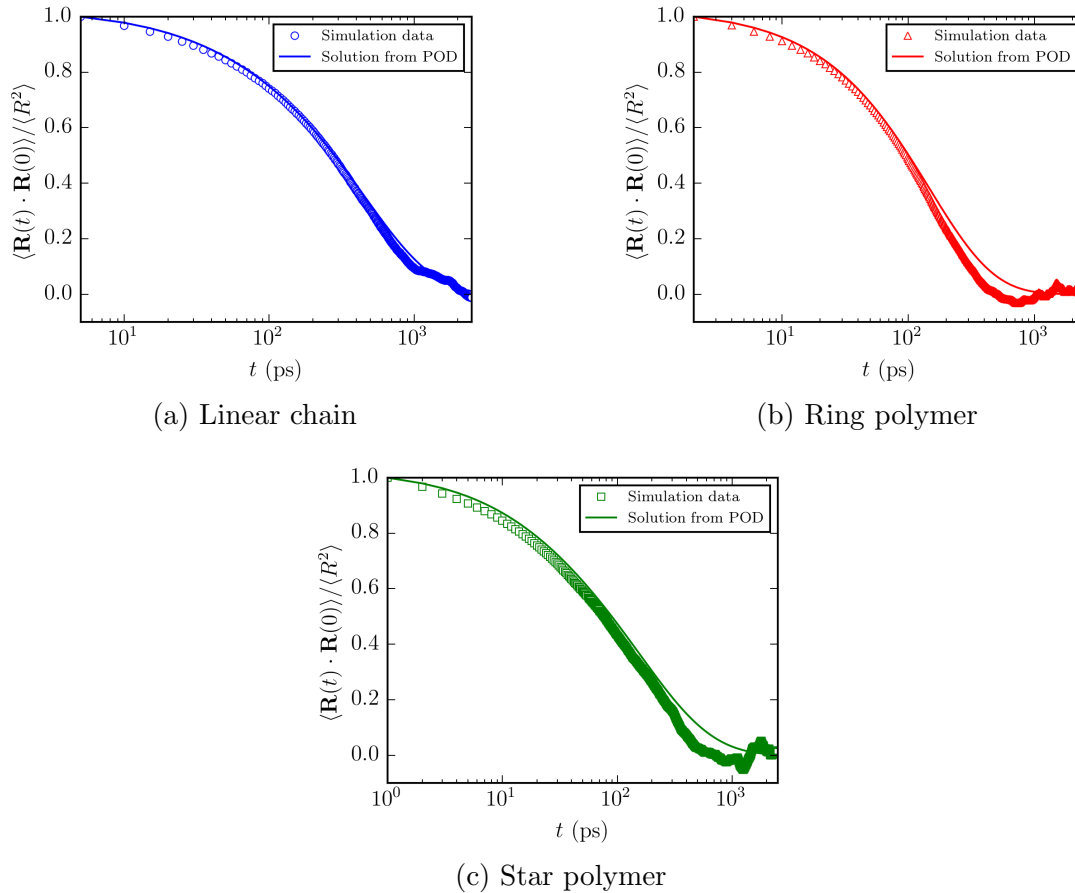


Figure 4.12: Time correlation functions of different vectors ($N = 50$ for linear and ring structures, and $N = 49$ for star structure) (MD simulation).

As indicated in Equation (4.24) and Equation (4.25), since the time correlation functions of different vectors are linear combinations of time correlation functions of different eigenmodes, for the purpose of comparison of the results in Figure 4.8 and Figure 4.12, we define a relaxation time τ_v , which is the time such that $\langle \mathbf{R}(\tau_v) \cdot \mathbf{R}(0) \rangle / \langle R^2 \rangle = e^{-1}$. Table 8.6 shows the τ_v of linear, ring and star structures in Rouse model, BD simulation and MD simulation.

Table 4.3: τ_v of time correlation functions of different vectors in Rouse model, BD simulation and MD simulation. ($N = 50$ for linear and ring structures, and $N = 49$ for star structure)

Structures	τ_v (ps) (Rouse model)	τ_v (ps) (BD simulation)	τ_v (ps) (MD simulation)
Linear ($N = 50$)	138	389	410
Ring ($N = 50$)	32	147	154
Star ($N = 49$)	31	113	155

As shown in Table 8.6, τ_v s of all structures in BD simulation are in good agreement with that in MD simulation. On the contrary, the values of τ_v s derived from the Rouse model were significantly lower than that of MD simulation. This demonstrates that incorporation of a finite equilibrium spring length in the Rouse model gives a relaxation time that resembles more to the realistic value.

4.7 Zero-Shear Viscosity from BD and MD Simulations

With the time autocorrelation functions of different eigenmodes, it is possible to obtain the shear relaxation modulus ($G(t)$), which is a linear combination of the square of $\mu_p(t)$ (cf., Equation (4.26)). Integration of $G(t)$ with respect to time will give us the zero-shear viscosity (η_0). The corresponding $G(t)$ can be therefore estimated as follows²:

$$G(t) \approx \frac{\rho RT}{M} \sum_{p=1}^{N-1} \exp \left[-2(t/\tau_p^*)^{\beta_p} \right] \quad (4.26)$$

ρ is the mass density, and R is the ideal gas constant. The justification for using Equation (4.26) for $G(t)$ is that the harmonic bond stretching force is much larger than other forces acting upon the bead/unit atom in the simulation. η_0 can be indirectly obtained with:

$$\eta_0 = \int_0^{\infty} G(\tau) d\tau \quad (4.27)$$

The time integration in Equation (4.27) can be numerically achieved using trapezoidal rule. As $G(t)$ is dependent on ρ (cf., Equation (4.26)), this indicates that η_0 can be influenced by many-chain effect. Therefore, we anticipate η_0 from BD data should deviate slightly from that of MD data. Due to the fact that in BD simulation, ρ cannot be obtained numerically, we

²Equation (4.26) is a modification of the shear relaxation modulus derived in the Rouse model as shown in Appendix A.

assumed $\rho \approx 700 \text{ g/m}^3$ for the evaluation of η_0 in BD simulation, whereas in MD simulation, ρ can be directly obtained from the MD data as many-chain effect has been included. Figure 4.13 shows plots of η_0 with N for polyethylene with different structures derived from BD and MD simulations, and comparison with the literature data. For linear and ring structures, the N dependence of η_0 is slightly stronger in the MD simulation than that in the BD simulation, whereas for star structure, η_0 s from BD and MD simulations are in excellent agreement with one another. Furthermore, for both linear and ring structures, η_0 derived from MD simulation agrees well with the results by Tsolou *et al.* [4] and Mondello *et al.* [42], in which they have also found that as N is small, the exponent of N dependence of η_0 is larger than unity (cf., Figure 4.13). For linear structure, we found that our data analysis procedures correctly reproduce the experimentally observed N dependence of η_0 by Pearson *et al.*[7] (i.e. $\eta_0 \sim N^{1.8}$) (cf., Figure 4.13).

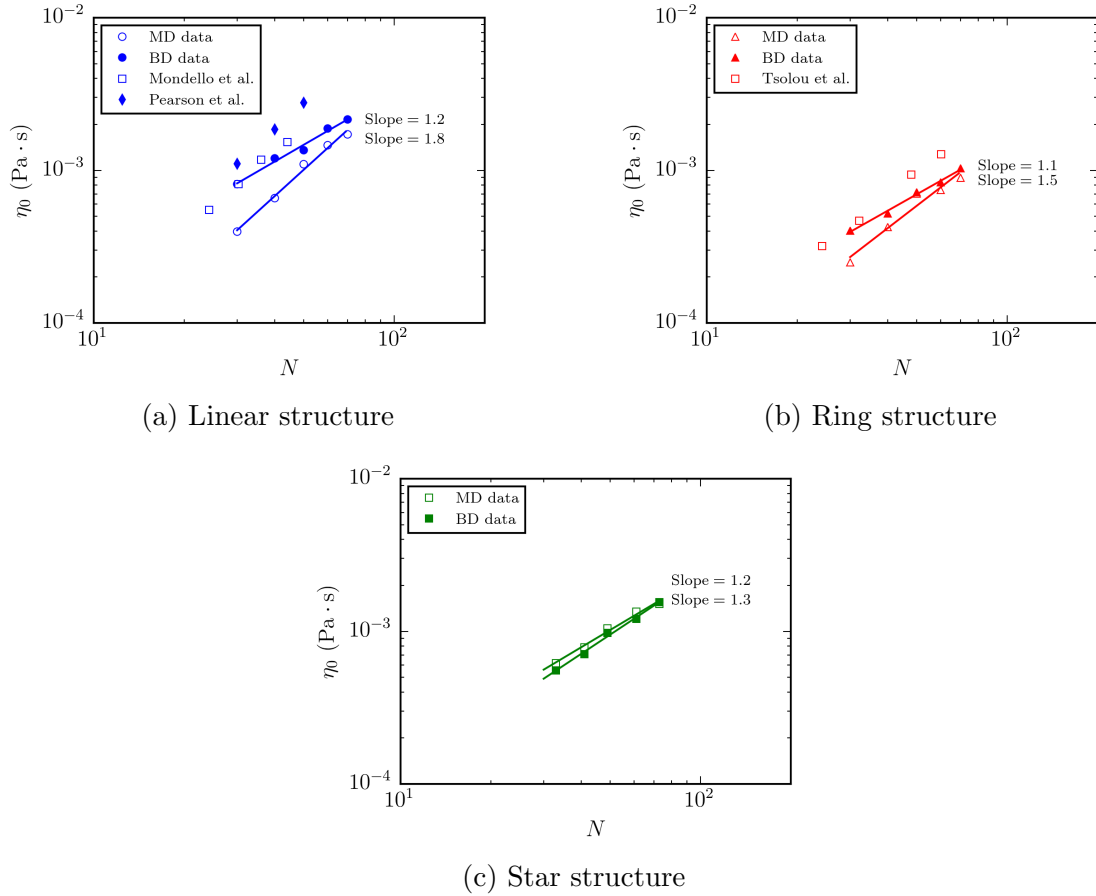


Figure 4.13: η_0 of polyethylene with linear, ring and star structures in BD and MD simulations, and comparison with the literature data.

4.8 Conclusions

We performed BD numerical simulation and MD simulation for unentangled polyethylene melts with linear, ring and star structures at 450 K. In the BD models, an equilibrium spring length ($b = 4.42\text{\AA}$) was included. Inclusion of a finite value for b prevents beads connected by the same harmonic spring from overlapping and brings the rigidity of the polymer chain into the BD simulation implicitly. The POD, which is known for analyzing the dynamics of non-linear systems, was used to analyze both BD and MD data. POD provides a method to obtain the eigenmodes of the non-linear systems, thereby the time correlation functions of different structural vectors. The eigenmodes obtained from the POD analysis in the MD simulation are similar to those in BD simulation. They are also similar in x , y and z directions. This demonstrates that even in many-chain systems, the macromolecular motion is still very Rouse-like probably because the most dominant force in the equation of motion is the bond stretching force derived from the harmonic potential.

τ_1 of linear polymer is longer than that of ring and star structures by a factor of 4 in the Rouse model. This factor decreases to 2.8 and about 1.6-2.4 based on the BD simulation results and MD simulation results, respectively. The dependence of τ_p on N/p obtained from the POD analysis of unentangled polyethylene in MD simulation (i.e., $\tau_p \sim (N/p)^{2.3}$) are stronger than that in BD simulation (i.e., $\tau_p \sim (N/p)^{2.0}$). This may be attributed to the fact that the equation of motion in MD simulation is more non-linear. Furthermore, relaxation times of vectors and zero-shear viscosity derived from BD simulation are in good agreement with those in MD simulation for all structures.

Chapter 5

A Free Volume Theory on the Chain Length Dependence of the Diffusivity of Linear Polymers¹

5.1 Introduction

The chain length dependence of the dynamics of polymer melts has been extensively studied both experimentally [43, 7, 44, 45, 46] and numerically [47, 39, 48, 49]. It was demonstrated in the log–log plot of the center-of-mass diffusion coefficient (D_{cm}) as a function of molecular weight (M) that the slopes are more negative than -1 below the critical molecular weight (M_c), which was observed by von Meerwall *et al.* [1] that the exponent of the N dependence of D_{cm} of n -alkane with $N = 9 - 60$ can be as negative as -1.85 at 170 °C, and approximately -2.4 above M_c . It is well-known that below M_c , the behavior can be qualitatively predicted by the Rouse model [20] after elimination of the chain end effect, in which the beads are modeled as Brownian particles connected by harmonic springs experiencing a stochastic force, whereas above M_c , the behavior is well described by the reptation theory developed by Doi and Edwards [21], as well as de Gennes [50] with the consideration of tube length fluctuation [51, 52, 53].

In the reptation theory, entanglements and topological constraints imposed by surrounding chains on a given chain have substantially hindered its transverse motion, such that it is

¹A version of this chapter has been published in *Soft Matter*, 2019, 15, 9300-9309.

as if the chain is reptating in a confined tube. With this, one can then solve the diffusion equation for segments of the chain in the tube, which obeys the Rouse dynamics, to obtain the mean-square-displacement of the center-of-mass of the chain as well as the probability of segments staying in the tube [21]. The repton theory, which is also known as the discretized reptation theory, introduced by Rubinstein presents a more accurate description of tube length fluctuation, and agrees better with the experimental results [53]. Nevertheless, the mathematical formulation and the molecular structures of entanglements have not yet been clearly elucidated, although there were few attempts to quantify this property for the determination of the entanglement length [54, 55, 56, 32]. To our knowledge, there are very few alternatives to the entanglement theory in the understanding of the unusual behavior of the self-diffusion of long chains. In addition, the concept of entanglement has become more complicated when it comes to the understanding of the dynamics of non-linear polymers (e.g., ring polymers).

The free volume theory has successfully predicted the diffusion in polymer–solvent systems as well as the temperature dependence of the diffusion coefficient in oligomers [57, 58, 59, 60]. Notably, von Meerwall *et al.* explained the pulse-gradient NMR measurement of self-diffusion of oligomers by considering the flip frequency of the segments [60], in which they proved that the amount of free volume present in oligomer melts can influence their dynamic properties. Nonetheless, one of the most impressive attempts is the modified free volume theory proposed by Sabbagh and Eu [61], which can be applied to polymer melts. In their version of modified free volume theory, which is essentially an extension of the Cohen-Turnbull free volume theory, parameters, such as mean free volume, are calculated using the generic van der Waals equation of state [62, 63, 64] and solving the system of coupled integral equations with Percus-Yevick closure relations for polymer melt systems in a way that is similar to their previous work on simple liquid [65, 66, 67]. Their proposed theory [61] is not, however, entirely free of adjustable parameters as the theory was developed under the assumption that the critical free volume for each bead follows a stretched exponential distribution, for which any justification for this proposition is not adequate and as a result of this, three empirical parameters are introduced in their theory.

In this work, we will improve and consolidate such proposition that the self-diffusion coefficients of polymer can be evaluated by knowing free volume available to each bead of the

chain and their corresponding distributions. The intermolecular radial distribution function ($g(r)$) and intramolecular radial distribution function ($g^{intra}(r)$) of the polymer melts were obtained accurately by molecular dynamics (MD) simulation, in which detailed bonded and non-bonded potential were included in the equation of motion. The critical free volume for activation of diffusion, and the mean free volume can be then obtained from $g(r)$ and $g^{intra}(r)$, as well as the generic van der Waals (GvdW) equation of state developed by Eu [64]. Furthermore, Voronoi tessellation of the MD simulation data of linear chains with different N was performed, which gave us the exact probability distribution of the volume available to a bead.

In the literature, detailed atomistic and coarse-grained simulations have been used to study the dynamics of polyethylene systems [68, 69, 70, 8]. For instance, Zhu *et al.* introduced a highly coarse-grained model to simulate the entangled polymer melts, which can reflect the characteristics of entanglements and simulate the dynamics correctly [68]. Harmandaris *et al.* [69] demonstrated a clear crossover (at C_{154}) from the Rouse regime to the entangled regime for the D_{cm} of linear polyethylene chains in the melt state using MD simulation along with a united atom model. Tsolou *et al.* [70] adopted the non-bonded and bonded parameter sets used by Harmandaris *et al.* [69] for poly(butadiene) and showed that the crossover for the polymer was around 2,600 g/mol. With these, we used MD simulation as well as a free volume theory to demonstrate that the crossover in the N dependence of D_{cm} of linear polyethylene melts can be accurately described.

5.2 The Free Volume Theory of Polymers

The self-diffusion of simple liquids is well described by the free volume theory of Cohen and Turnbull, which is shown as follows:

$$D = D_0 \exp\left(-\frac{\alpha v^+}{\langle v_f \rangle}\right) \quad (5.1)$$

where α is the overlapping factor of the free volume, αv^+ is the critical free volume, above which diffusion occurs and $\langle v_f \rangle$ is the mean free volume. D_0 is the Chapman-Enskog self-diffusion coefficient. In this simple theory, it is postulated that the self-diffusion coefficient is proportional to the probability of finding αv^+ . And such probability has the following

distribution:

$$P = \frac{\alpha}{\langle v_f \rangle} \exp\left(-\frac{\alpha v}{\langle v_f \rangle}\right) \quad (5.2)$$

Therefore, to extend the free volume theory to polymers, we should consider the probability for a certain number of beads having sufficient free volume because the diffusion of polymer relies on the motion of a collection of beads. The probability (F_{ct}) for a single bead to obtain a certain critical volume in the form of Cohen and Turnbull can be calculated as follows:

$$F_{ct} = \exp\left(-\frac{N\alpha v_i^+}{\langle v_f \rangle}\right) \quad (5.3)$$

where v_i^+ is the critical volume for activating the diffusive movement of the i th bead, N is the chain length. Nonetheless, in positron annihilation lifetime spectroscopy experiments [71], the free volume distribution in polymers was found to be more accurately described by the gamma distribution. The probability for a bead to have free volume greater than or equal to αv_i^+ for the activation of its diffusive movement (F) can be then approximated by:

$$F = 1 - \frac{1}{\Gamma(b)} \int_0^{\alpha v_i^+} x^{b-1} e^{-x} dx \quad (5.4)$$

$\Gamma(b)$ is the gamma function with b as the argument:

$$\Gamma(b) = \int_0^{\infty} x^{b-1} e^{-x} dx \quad (5.5)$$

The parameter a and b are defined as follows:

$$a = \frac{b}{\langle v_{f,i} \rangle} \quad (5.6)$$

$$b = \frac{\langle v_{f,i} \rangle^2}{\langle v_{f,i}^2 \rangle - \langle v_{f,i} \rangle^2} \quad (5.7)$$

b is the regularity factor, which is the ratio of the mean value to the variance of the gamma distribution, and it is a dimensionless parameter (cf., Equation (5.7)), whereas a has a unit of nm^{-3} (cf., Equation (5.6)). It should be noted here that this exact distribution can be determined using Voronoi tessellation (VT), which will be discussed in the forthcoming section.

Considering the fact that diffusion of a polymer chain as the motion of a collection of beads, some of the beads in the chain, which have $v_{f,i} < \alpha v_i^+$ may, perhaps, still be activated

by the motion of its neighbours, which have $v_{f,i} \geq \alpha v_i^+$. In other words, a chain may only require a particular fraction of beads having $v_{f,i} \geq \alpha v_i^+$ (ϕ^+) such that diffusion of its center-of-mass can be activated. This is similar to the idea in the reptation theory that diffusion of an extremely long chain relies on one another bead (i.e., a cooperative motion) to reptate through the highly dense polymer melt.

To evaluate the distribution of bead having $v_{f,i} \geq \alpha v_i^+$ in the polymer chain, the probability that a polymer may displace (P_d) is related to the probability of finding n_f beads having $v_{f,i} \geq \alpha v_i^+$ and $(N - n_f - 2)$ beads not having.

$$P_d \sim F^{n_f} (1 - F)^{N - n_f - 2} \quad (5.8)$$

In Equation (5.8), as for the bead of the chain end, the probability for them to have $v_{f,i} \geq \alpha v_i^+$ is assumed to be unity in order to simplify this problem to a large extent. There are $\frac{(N-2)!}{n_f!(N-n_f-2)!}$ different possible ways to arrange n_f beads in a polymer (cf., Equation (5.9)).

$$P_d = \frac{(N-2)!}{n_f!(N-n_f-2)!} F^{n_f} (1 - F)^{N - n_f - 2} \quad (5.9)$$

We can then apply the Stirling approximation that $N! \approx \sqrt{2\pi N} \left[\frac{N^N}{\exp(N)} \right]$.

$$\ln P_d = (N-2) \ln \left[\frac{(N-2)(1-F)}{N-n_f-2} \right] + n_f \ln \left[\frac{(N-n_f-2)F}{n_f(1-F)} \right] + \frac{1}{2} \ln \left[\frac{N-2}{2\pi n_f(N-n_f-2)} \right] \quad (5.10)$$

The number fraction (ϕ) of the beads possessing $v_{f,i} \geq \alpha v_i^+$ is then introduced, such that $\phi = n_f/(N-2)$. Also, to ensure numerical stability, Equation (5.10) reads:

$$\ln P_d = (N-2) \ln \left[\left(\frac{1-F}{1-\phi+\varepsilon} \right)^{1-\phi} \left(\frac{F}{\phi+\varepsilon} \right)^\phi \right] - \frac{1}{2} \ln \left[2\pi(N-2)\phi(1-\phi) + \exp\left[-\frac{\phi^2}{\varepsilon^2}\right] + \exp\left[-\frac{(\phi-1)^2}{\varepsilon^2}\right] \right] + \ln(c) \quad (5.11)$$

where ε is a very small number ($\sim 10^{-5}$), which ensures the denominators in Equation (5.11) are not zero, and the second term of Equation (5.11) is 0 for $\phi = 0$ and $\phi = 1$. c is the normalization constant such that $\int_0^1 P_d d\phi = 1$ and it was obtained numerically. As $N \rightarrow \infty$, Equation (5.11) becomes a normal distribution function of ϕ . The probability that the chain has $\phi \geq \phi^+$ (\mathcal{P}) can be found as follows:

$$\mathcal{P}(\phi^+, \alpha v_i^+, N) = \int_{\phi^+}^1 P_d d\phi \quad (5.12)$$

Polymer chain is a collection of beads that the diffusion of polymer chain is governed by connectivity and the cooperative motion. Consider a chain without any cooperative motion, the motion of the beads within the chain is uncorrelated to one another. The center-of-mass ($\mathbf{r}_{\text{cm}}(t)$) of a polymer chain can be calculated as follows:

$$\mathbf{r}_{\text{cm}}(t) = \frac{1}{N} \sum_{i=0}^{N-1} \mathbf{r}_i(t) \quad (5.13)$$

Without any cooperative motion, $\mathbf{r}_i(t)$ is Gaussian distribution and the mean-square displacement of all beads of the chain are identical that $\langle r_i^2(t) \rangle = \langle r_b^2(t) \rangle$. $\langle r_b^2(t) \rangle$ is the mean-square-displacement of a single bead. Then, it follows that $\mathbf{r}_{\text{cm}}(t)$ is a linear combination of Gaussian distributions. This leads to the following:

$$\langle r_{\text{cm}}^2(t) \rangle = \frac{1}{N^2} \sum_{i=0}^{N-1} \langle r_i^2(t) \rangle = \frac{\langle r_b^2(t) \rangle}{N} \quad (5.14)$$

By Einstein's relation and from Equation (5.14), it can be deduced that: $6D'_{\text{cm}}t = 6Dt/N$, which implies that $D'_{\text{cm}} = D/N$. D'_{cm} is the center-of-mass diffusion coefficient of a polymer chain without any cooperative motion.

The cooperative motion of the chain in diffusion has been studied in the above analysis, which leads to Equation (5.11) as well as Equation (5.12). We then follow the rationale of Cohen-Turnbull theory: the polymer chain can only diffuse when $\phi \geq \phi^+$, otherwise D_{cm} is zero. Therefore, when we average over all possible values of ϕ , we have:

$$D_{\text{cm}} = \int_{\phi^+}^1 \frac{D}{N} P_d d\phi = \frac{D}{N} \int_{\phi^+}^1 P_d d\phi \quad (5.15)$$

The center-of-mass diffusion coefficient in the polymer melt can be therefore calculated:

$$\boxed{D_{\text{cm}} = \frac{D}{N} \int_{\phi^+}^1 P_d d\phi} \quad (5.16)$$

Given that P_d has a form of Poisson distribution (cf., Equation (5.9)), Equation (5.16) can be also written as:

$$\boxed{D_{\text{cm}} = \frac{D}{N} \left[1 - \exp \left[- (N-2)F \right] \sum_{i=0}^{(N-2)\phi^+} \frac{\left((N-2)F \right)^i}{i!} \right]} \quad (5.17)$$

It was found that numerically, Equation (5.16) was able to generate a smooth curve of N dependence of D_{cm} , but a slight fluctuation in the predicted values of D_{cm} was resulted if Equation (5.17) was used. This is because Equation (5.16) is a continuous approximation, whereas Equation (5.17) is a discrete form. Similar to Sabbagh and Eu [61], with $g(r)$ and $g^{intra}(r)$ in polymer melts, $\langle v_f \rangle$ can be directly calculated using the GvdW equation of state. Nonetheless, in their work [61], the parameters, such as v_i^+ and α , were not accurately determined from $g(r)$ and $g^{intra}(r)$ as the potential in their case is a simple square well potential, whereas these parameters can be readily obtained from our MD simulation data as the beads interact with one another through 6-12 Lennard-Jones potential.

Finally, the parameter ϕ^+ can be determined with the following. It is well-known that the typical Arrhenius form relation can describe accurately the temperature dependence of the diffusion coefficient of polyethylene [1]. With the use of experimental data, the apparent activation energy (E_a^{app}) was found to be dependent on the chain length [1]. Sabbagh and Eu [61] pointed out that E_a^{app} can be evaluated with the effective pressure (p_{eff}) from the GvdW equation of state as well as the critical free volume, along with the adjustable parameters. Nonetheless, Macedo and Litovitz [72], as well as von Meerwall *et al.* [1] pointed out that E_a^{app} includes two contributions: 1. thermal activation energy responsible for the growing free volume at higher temperatures 2. the energetic cost for performing diffusive motion (E_a). Based on this, von Meerwall [1] modified the Arrhenius equation to a hybrid equation for D_{cm} :

$$D_{cm} \sim N^{-1} \exp\left(-\frac{E_a}{RT}\right) \exp\left(-\frac{1}{f}\right) \quad (5.18)$$

where f is the fractional free volume, having the form $f = \rho_b \langle v_{f,i} \rangle$. von Meerwall *et al.* applied such analysis on n -alkane and found that $E_a \approx 0.81 \pm 0.25$ kcal/mole [1]. With these findings, ϕ^+ can be directly calculated as it is related to E_a , which is the energy that is necessary for the activation of diffusion. Similar to Sabbagh and Eu [61], E_a can be interpreted as the energy required for creating a certain critical volume in the polymer melt such that the diffusive motion of the chain is activated. E_a can be therefore determined as follows:

$$E_a = p_{eff} \cdot [\phi^+ \alpha v_i^+ + (1 - \phi^+) \langle v_{f,i} \rangle] \quad (5.19)$$

p_{eff} can be obtained from the GvdW equation of state.

5.3 Molecular Dynamics (MD) Simulation

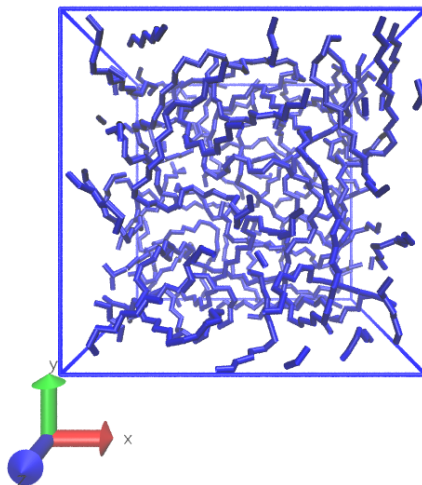


Figure 5.1: Final configuration of $N = 105$ linear chains with imposed periodic boundary condition in MD simulation.

In our simulation, the initial configuration of a coarse-grained polyethylene chain was firstly generated using rotational isomeric state (RIS) model [12, 16], in which a methyl group or a methylene group is treated as a bead. The problem with RIS model, nevertheless, is that it does not account for any excluded volume effect that as chain length increases, several segments can overlap with each other. Owing to this, we performed a subsequent geometry optimization using free software Avogadro. Many chains were then packed into a box using the PACKMOL software [35] such that the intermolecular distance between any two atoms of any two chains was equal to or greater than 40 Å. The system was relaxed using NVT simulation for 1 ns, and then compressed to the correct density using NPT simulation for 10 ns, in which the temperature was maintained at 450 K by the Nosé-Hoover thermostat and the pressure at 1.01325 bar using the Parrinello-Rahman barostat with time constants of 0.2 ps and 2 ps, respectively. The pressure coupling only serves to give us a reasonable mean density. The cut-off distance for intermolecular interaction was 1.4 nm. Finally, a NPT simulation for another 20-400 ns was performed. Periodic boundary conditions were applied in three directions. Equation of motion was integrated using the Leapfrog algorithm with a time step of $\Delta t = 1$ fs and the TraPPE forcefield [19, 18] was used. Figure 5.1 shows the final configuration of linear chains $N = 105$ after the final 200 ns NPT MD simulation. All

the simulations were performed using open source GROMACS-5.1.4 [36]. Figure 5.2 shows the number densities of the beads (ρ_b) as a function of N . As expected, it was found that the behavior can be reasonably described by the function: $\rho_b = \rho_{b,\infty} - \frac{C_1}{N}$ with $\rho_{b,\infty} = 32.760 \text{ nm}^{-3}$ and $C_1 = 83.759 \text{ nm}^{-3}$.

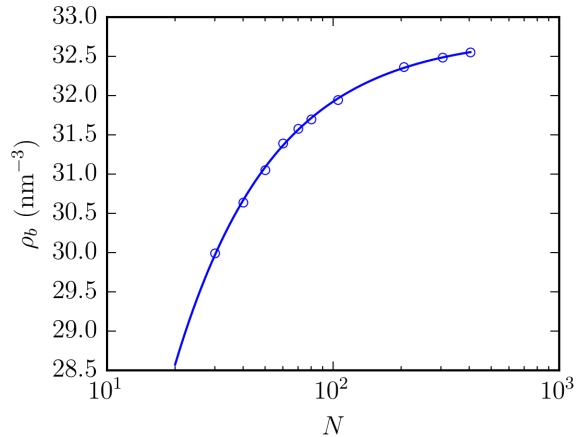


Figure 5.2: Number density of the bead in the system with different N fitted to an empirical function: $\rho_b = \rho_{b,\infty} - \frac{C_1}{N}$ with $\rho_{b,\infty} = 32.760 \text{ nm}^{-3}$ and $C_1 = 83.759 \text{ nm}^{-3}$.

The number of chains used in the simulation is stated in Table 5.1.

Table 5.1: Number of chains, box dimension and root-mean-square radius of gyration in the MD simulation for systems with different N .

N	30	40	50	60	70	80	105	205	305	405
Number of chains	26	20	16	40	40	40	10	10	10	10
L (nm)	2.91	2.96	2.98	4.28	4.49	4.67	3.17	3.98	4.52	5.00
$\sqrt{\langle R_g^2 \rangle}$ (nm)	0.780	0.946	1.100	1.241	1.363	1.465	1.732	2.579	3.236	3.367

The effect of finite-size on the calculated D_{cm} is negligible. Firstly, it was found that our calculated values of D_{cm} s are in good agreement with the experimental values. Secondly, the dimension of the box (L) is at least 1.5 times greater than the root-mean-square radius of gyration of the chains ($\sqrt{\langle R_g^2 \rangle}$). Finally, to be more explicit, we increased the number of chains used in the MD simulation for polymer chains with $N = 30$ from 26 to 40 and that with $N = 405$ from 10 to 20 in order to evaluate if there is any influence on D_{cm} . Figure 5.3 shows plots of mean-square displacement as a function of time in these two cases. It was

found that regardless of the increase in the number of chains used in the MD simulation, the mean-square displacement does not change much. The D_{cm} s found in these cases are as follows: for $N = 30$, D_{cm} s were found to be $1.34 \cdot 10^{-9} \text{ m}^2 \cdot \text{s}^{-1}$ and $1.67 \cdot 10^{-9} \text{ m}^2 \cdot \text{s}^{-1}$ for 26 chains and 40 chains, respectively; for $N = 405$, D_{cm} s were found to be $7.84 \cdot 10^{-12} \text{ m}^2 \cdot \text{s}^{-1}$ and $7.19 \cdot 10^{-12} \text{ m}^2 \cdot \text{s}^{-1}$ for 10 chains and 20 chains, respectively. These differences are not significant enough to affect our conclusions derived from our MD simulation results.

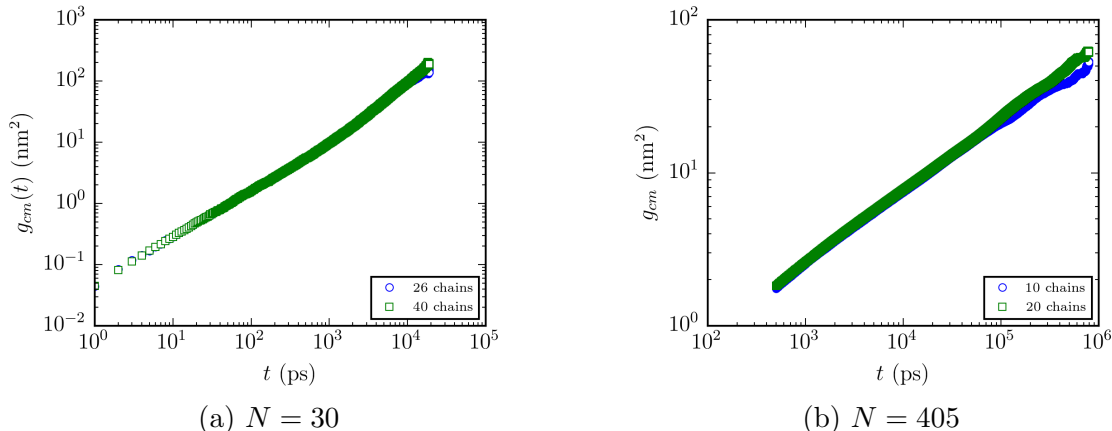


Figure 5.3: Mean-square displacements for different numbers of polymer chains used in the MD simulations with (a) $N = 30$ and (b) $N = 405$.

5.4 Results and Discussion

5.4.1 Free Volume Analysis

Determination of α and v_i^+ Based on $g(r)$ from MD Data

In the MD simulation of polyethylene, the intermolecular interaction between beads of two different chains is governed by the 6-12 Lennard-Jones potential ($u(r)$):

$$u(r) = 4\varepsilon \left[\left(\frac{\sigma}{r} \right)^{12} - \left(\frac{\sigma}{r} \right)^6 \right] \quad (5.20)$$

where ε is the magnitude of the potential well, r is the distance between two beads of two different chains and σ is the distance, which has a value of $\sigma = 0.395 \text{ nm}$, between these two beads such that the potential is zero. As $u(r)$ is a pairwise interaction potential, different properties of the simulation system can be readily obtained with the knowledge of

the radial distribution function ($g(r)$), which is essentially the probability to find another bead at a distance r from the reference bead. The pressure equation for a polymer melt can be explicitly written as follows:

$$\frac{p\beta}{\rho_b} = 1 - \frac{2\pi\beta\rho_b}{3} \left\{ \int_0^\infty r^3 \frac{du}{dr} \left[g(r) + \frac{2\omega(r)}{\rho_b} \right] dr \right\} - \frac{4\pi\beta}{3} \left[\int_0^\infty \omega_{bond}(r) r^3 \frac{du_{bond}}{dr} dr \right] \quad (5.21)$$

And:

$$\omega(r) = \frac{1}{NV} \left[\sum_{\alpha=1}^{N-4} \sum_{\gamma=\alpha+4}^N \omega^{\alpha,\gamma}(r) \right] \quad (5.22)$$

$$\omega_{bond}(r) = \frac{1}{NV} \left[\sum_{\varepsilon=1}^{N-1} \omega_{bond}^{\varepsilon,\varepsilon+1}(r) \right] \quad (5.23)$$

$V = \frac{4}{3}\pi r_{max}^3$, where r_{max} is the maximum sampling radius for the evaluation of the intramolecular radial distribution function per unit volume and per bead due to 6-12 Lennard Jones potential ($\omega(r)$) as well as bond stretching potential ($\omega_{bond}(r)$) in the MD simulation trajectory. r_{max} is related to the dimension of the simulation box in a way that $r_{max} \approx 3L$ (cf., Table 5.1), which is always greater than the cut-off distance for 6-12 Lennard-Jones potential. In addition, when $\omega(r)$ and $\omega_{bond}(r)$ were input into Equation (5.21), they must be normalized by factors of $4\pi \int_0^\infty \omega(r)r^2 dr$ and $4\pi \int_0^\infty \omega_{bond}(r)r^2 dr$, respectively. In the calculation of intramolecular radial distribution functions, the periodic boundary conditions were removed from the trajectory after the MD simulation by shifting the coordinates of the corresponding beads such that a chain crossing the boundary of the simulation box would not be ‘truncated’. u_{bond} is harmonic bond stretching potential between bead i and bead $i + 1$ of the same chain.

$$u_{bond} = \frac{1}{2} k_{bond} (r - l_0)^2 \quad (5.24)$$

k_{bond} is the spring constant, which has a value of $132506 \text{ kJ} \cdot \text{mole}^{-1} \cdot \text{nm}^{-2}$ obtained from molecular mechanics 2 forcefield. And l_0 is the equilibrium bond length. It should be also noted that as the TraPPE forcefield only gives us $l_0 = 0.154 \text{ nm}$ without defining a value for k_{bond} , which is crucial in the calculation of free volume. $\omega^{\alpha,\gamma}(r)$ and $\omega_{bond}^{\varepsilon,\varepsilon+1}$ are the intramolecular radial distribution functions between sites α and γ , as well as sites ε and $\varepsilon + 1$, respectively, within the same chain. Note that $\omega(r)$ and $\omega_{bond}(r)$ as expressed in Equation (5.22) and Equation (5.23) only include the interaction between the reference bead and the bead that is separated by four bonds and one bond away from the reference bead, respectively. In this case, Equation (5.21) only accounts for the contribution of the intermolecular

and intramolecular interaction through 6-12 Lennard-Jones potential and bond stretching potential to the pressure. The contribution of angle bending and torsion potential to the pressure is negligible, which has been demonstrated by Honnell *et al.* [73]. Honnell *et al.* [73] stated that the contribution of the angle bending and torsion potential would be reflected in the $g(r)$.

With these, as Laghaei *et al.* [65] proposed, for simple liquids, the work required to move the surrounding beads near the reference bead per 4π ($W(R)$) by a diameter of R can be calculated as follows:

$$W(R) = \int_0^R \left[-r^3 \frac{du}{dr} g(r) \right] dr \quad (5.25)$$

Equation (5.25) can be applied in our case if we consider the energy of the bead of the polymer chain overcoming the intermolecular and intramolecular Lennard-Jones force in the polymer melts.

$$W(R) = \int_0^R -r^3 \frac{du}{dr} \left[g(r) + \frac{2\omega(r)}{\rho_b} \right] dr \quad (5.26)$$

Laghaei *et al.* [65] then proposed that important length scales, such as diameters of the hard-core sphere and cavity, can be derived from the plot of the integrand with distance in Equation (5.25). These length scales can be used to deduce the parameters in our free volume theory (cf., Equation (5.4)). To obtain these length scales, a function $I(r)$ can be defined as:

$$I(r) = -r^3 \frac{du}{dr} \left[g(r) + \frac{2\omega(r)}{\rho_b} \right] \quad (5.27)$$

Figure 5.4 shows plots of $g(r)$, $\omega_{bond}(r)$, $\omega(r)$ as well as that of integrand $I(r)$ with r from a MD simulation of polyethylene with $N = 405$. Interestingly, in our simulation, the position of the first peak of $g(r)$ is slightly greater than σ , having a value of 0.5 nm due to the screening effect of the collective motion of the beads within a chain. This makes the bead appears to be larger from the perspective of the bead of another chain. Also, when compared to the case in simple monatomic liquid, the amplitude of the first peak of $g(r)$ is significantly lower despite the fact that ρ_b is higher than density of simple liquid (Note that ‘simple liquid’ means Lennard-Jones monoatomic liquid, and typically, the values of $\rho_b \sigma^3$ of Lennard-Jones monoatomic liquid are typically below 1.0 at $T = 450$ K, whereas for polymer melts, $\rho_b \sigma^3 \approx 1.8 - 2.0$). As for $\omega(r)$, it was found that there are strong peaks at 0.44 nm and 0.52 nm, which correspond to the 6-12 Lennard-Jones potential and force minima, respectively. (cf., Figure 5.4) As expected, a strong peak at $l_0 = 0.154$ nm in $\omega_{bond}(r)$ was observed (cf., Figure 5.4).

Four length scales can be deduced from Figure 5.4(d). With the same notation used by Laghaei *et al.* [65], the four length scales are r_c , r^+ , r_{fm} and r_{pm} as depicted in Figure 5.4(d). r_c is the levitation diameter, r^+ is the diameter of the cavity, and r_{pm} as well as r_{fm} correspond to the length scales at the potential and force minima, respectively. The physical significance of r_c and r^+ is as follows: r_c can be taken as the diameter of a hard sphere, which is the minimum possible and incompressible diameter of the bead. At r^+ , it has the highest probability that two beads of different chains experience a strong repulsive force. The experience of the bead in such situation is as if a hard sphere being placed in a cavity that the hard sphere never touches the wall of the cavity. In other words, the hard sphere in the cavity can be said to be ‘levitated’ in such cavity. The volume of the cavity with diameter r^+ can be then interpreted as v_i^+ . In MD simulation, for $N = 405$, $r_c = 0.314$ nm, $r^+ = 0.366$ nm, $r_{pm} = 0.444$ nm and $r_{fm} = 0.524$ nm. With the calculated values of r^+ , v_i^+ can be easily obtained with $v_i^+ = \frac{\pi}{6}r^{+3}$, which is the critical free volume of a bead. The hard-core (also known as levitation) volume of a bead v_c can be evaluated with $v_c = \frac{\pi}{6}r_c^3$. It was found that in the simulation, $v_i^+ = 0.0257$ nm³ and $v_c = 0.0162$ nm³. In addition, according to Laghaei *et al.* [65], the overlap parameter α can be approximated by the following:

$$\alpha = \left(1 - \frac{|r_{pm} - r_{fm}|}{r^+}\right)^3 \quad (5.28)$$

It was found that in our case, $\alpha \approx 0.50$.

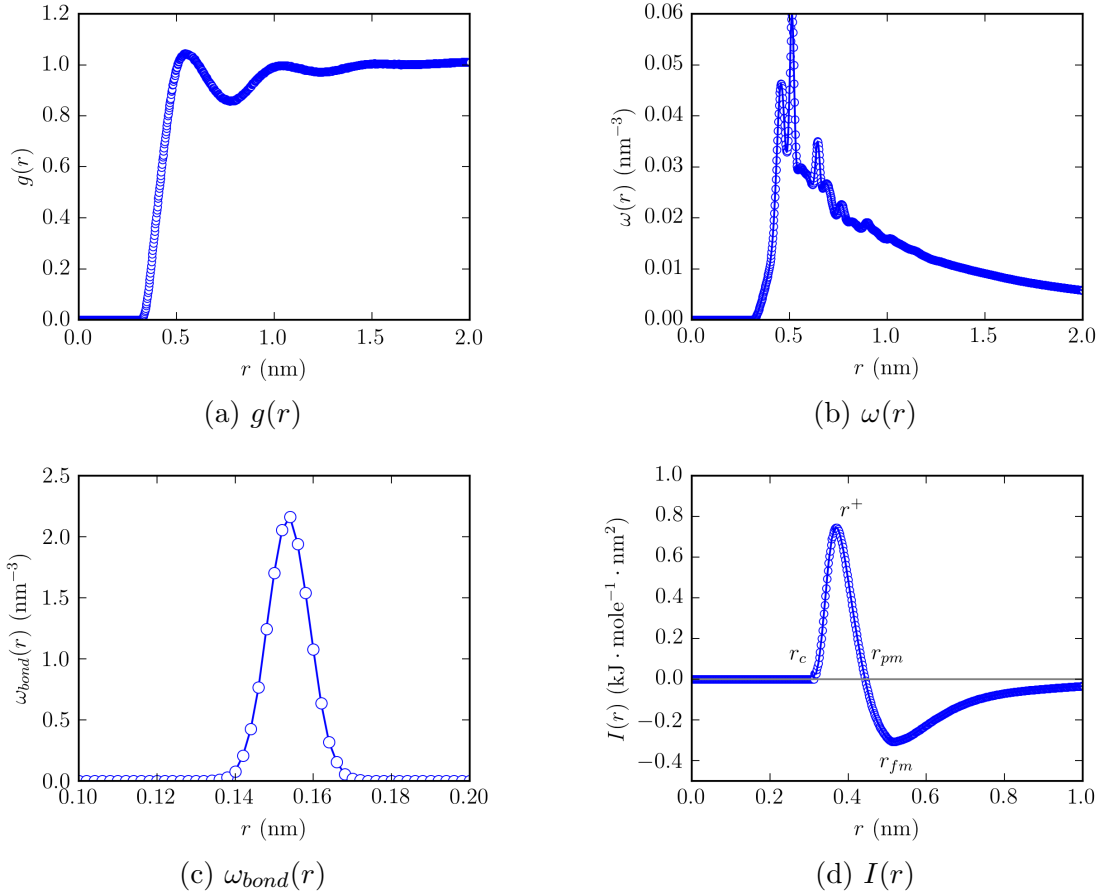


Figure 5.4: $g(r)$, $\omega(r)$, $\omega_{bond}(r)$ and $I(r)$ as a function of r for polyethylene chain with $N = 405$ obtained in MD simulation.

Determination of $\langle v_f \rangle$ from the GvdW Equation of State and ϕ^+ from Activation Energy

Equation (5.21) can be recast into the van der Waals equation, which has been proposed by Eu [64, 63, 62]. The van der Waals equation in such case is called the Gvdw equation of state, which has been applied in many different studies of transport coefficients of liquid [61, 65, 67, 66]. The excluded volume in the polymer melt can be easily determined using the GvdW equation of state. The GvdW equation of state is expressed as follows:

$$(p + A\rho_b^2)(N - B\rho_b) = \rho_b\beta^{-1} \quad (5.29)$$

$A(\rho, \beta)$ and $B(\rho, \beta)$ are GvdW parameters:

$$A(\rho, \beta) = -\frac{2\pi}{3} \left[\int_{r^+}^{\infty} I(r) dr + \int_{l_b}^{\infty} I_b(r) dr \right] \quad (5.30)$$

And,

$$B(\rho, \beta) = \frac{\frac{N-1}{\rho_b} + \frac{2\pi\beta N}{3} [\int_0^{r^+} I(r)dr + \int_0^{l_b} I_b(r)dr]}{1 + \frac{2\pi\beta\rho_b}{3} [\int_0^{r^+} I(r)dr + \int_0^{l_b} I_b(r)dr]} \quad (5.31)$$

With,

$$I_b(r) = -r^3 \frac{du_{bond}}{dr} \frac{2\omega_{bond}(r)}{\rho_b} \quad (5.32)$$

$l_b = 0.148$ nm, which corresponds to the maximum positive value of $I_b(r)$. $B(\rho, \beta)$ gives a measure of mean excluded volume. The integral term $\int_0^{l_b} I_b(r)dr$ captures the excluded volume effect due to the harmonic bond stretching potential. The mean free volume per chain ($\langle v_f \rangle$) is then given by:

$$\langle v_f \rangle = \frac{1}{\rho} [N - B\rho_b] \quad (5.33)$$

The values of $\langle v_f \rangle$ as well as B , which are the mean free volume and a measure of the excluded volume of the whole chain, respectively, obtained using GvdW are plotted as a function of N in Figure 5.5. The fraction of free volume of the chain, which is defined as $f = \rho_b \langle v_{f,i} \rangle$, is approximately 0.3. Local correlation lattice model developed by White and Lipson, which shows that the fractional free volume in polyethylene melt at 425 K and 1 atm is slightly lower at around 15% [74]. Our values are in better agreement with the empirical relation found by von Meerwall *et al.* [1], which has the form $f = 0.1 + 0.0007T(^{\circ}\text{C})$, it can be deduced that f in n -alkane at $T = 450$ K is approximately 0.22.

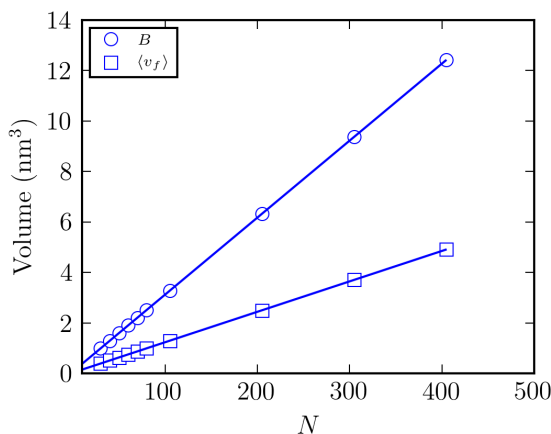


Figure 5.5: N dependence of $\langle v_f \rangle$ and B as determined from the GvdW.

p_{eff} can be then determined using parameter A in Equation (5.29) that $p_{eff} = p + A\rho_b^2$, which can be then used to evaluate E_a (cf., Equation (5.19)). Figure 5.6 shows that with

$\phi^+ = 0.22$, $E_a \approx 0.88 - 0.89$ kcal/mole, which is in excellent agreement with the range of 0.81 ± 0.25 kcal/mole as experimentally measured by von Meerwall *et al.* [1]. As shown in Figure 5.6, E_a is independent of chain length, therefore, ϕ^+ is constant.

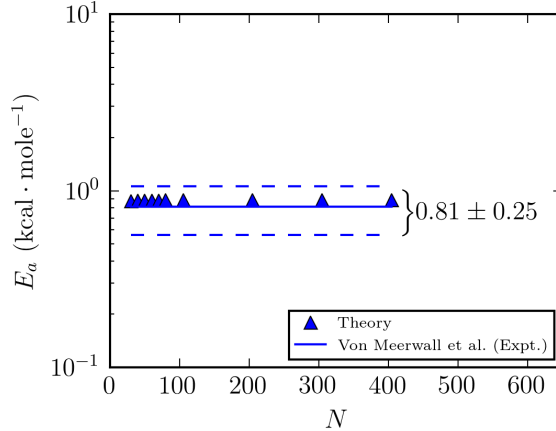


Figure 5.6: Determined value of E_a in this work, compared with that of von Meerwall *et al.* [1] at $T = 450$ K and $\phi^+ = 0.22$.

Free Volume Distribution as Determined by the Voronoi Tessellation (VT) on the MD Data

To evaluate b in Equation (5.4) and the exact free volume distribution, the Voronoi cell volume for each bead in the polymer with different N was also calculated using the voro++ code [75], in which the box in MD simulation at each time step was tessellated into different so-called Voronoi cells. The obtained Voronoi cell distribution was shifted in a way that $v_i - v_{i,min}$, where $v_{i,min}$ is the minimum Voronoi cell volume and should be the hard-core volume of the bead. $v_{i,min}$ was found to be 0.017 nm^3 , which is in good agreement with the above statistical mechanical calculation that $v_c = 0.016 \text{ nm}^3$. In this way, the shifted distribution of Voronoi cell volume represents the distribution of volume, excluding the hard-core volume only. Although the VT method does not tell us exactly the distribution of the free volume and holes in the polymer melt, the distribution derived from it is related to the distribution of the free volume. In particular, the probability F can be therefore calculated from the distribution of Voronoi cell volume given the knowledge of v_i^+ , $\langle v_{f,i} \rangle$ and α , which have been already determined using GvdW equation of state.

Figure 5.7(a) and (b) show the distribution of $v_i - v_{i,min}$ from the VT analysis, and its corresponding cumulative distribution function. As expected, peak width of the distribution decreases as N increases as a result of a lower number density of chain ends in longer polymer chain, and the distribution of free volume in the polymer melt are not perfectly symmetrical due to the presence of the supernumerary free volume at the chain ends, which are in good agreement with Liu *et al.* [71] (cf., Figure 5.7(a)). The distribution was then fitted to a gamma distribution to obtain b in Equation (5.4) (cf., Figure 5.7(a)). It was found that $b = 4.976 - 5.760$ and $a = 354.7 - 465.1 \text{ nm}^{-3}$ (cf., Table 8.1). As depicted in Figure 5.7(a), the fitting to the gamma distribution is better as $N \rightarrow \infty$, whereas as N decreases, the distribution has a longer tail due to the chain end effect, for which the gamma distribution cannot capture entirely. Figure 5.7(b) shows a plot of the corresponding cumulative distribution function. As the Voronoi cell distribution was shifted by $v_i - v_{i,min}$. The shifted Voronoi cell volume only excludes the hard-core volume as a result of 6-12 Lennard Jones potential, but it neglects the contribution from the soft-core nature of the intermolecular potential. As demonstrated in the previous section, r^+ is the effective diameter instead of r_c . Therefore, in the evaluation of F , the upper limit of the integral in Equation (5.4) has to be slightly modified that:

$$F = 1 - \frac{1}{\Gamma(b)} \int_0^{\alpha v_i^*} x^{b-1} e^{-x} dx \quad (5.34)$$

Such that:

$$v_i^* = \alpha v_i^+ + \frac{1}{\rho_b} (1 - N + B\rho_b) - v_c \approx v_c \quad (5.35)$$

With b derived from the distribution of v_i , $F(v_i)$ can be accurately calculated using Equation (5.34). It was found that $F(v_i^*)$ is dependent on N in MD simulation that can be described by the empirical relation $F = C_1 + C_2/N$ similar to that of the N dependence of ρ_b (cf., Figure 5.2 and Figure 5.8). $F_{ct}(\alpha v_i^+)$ was also computed using the simpler form as represented by Equation (5.3) for comparison, but its values are slightly higher than that from Equation (5.34) (cf., Figure 5.8). Only the values obtained from Equation (5.34), which is the more exact one, were used in the calculations of the diffusion coefficient in the forthcoming section.

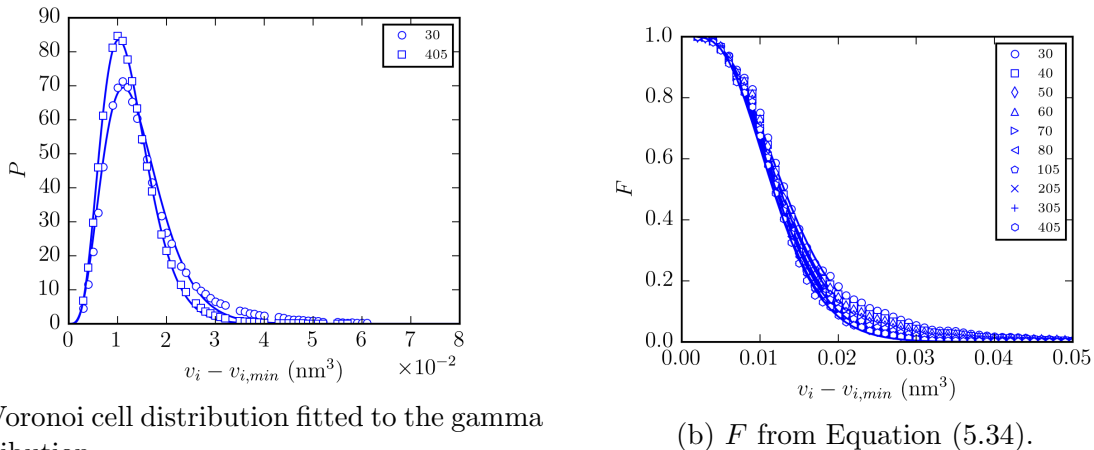


Figure 5.7: (a) Distribution of Voronoi cell volume in linear chain with different N . (b) F derived from the Voronoi cell analysis and the solid line is Equation (5.34).

Table 5.2: Fitting results of the parameters a and b in the gamma distribution

N	30	40	50	60	70	80	105	205	305	405
a (nm^{-3})	354.7	379.1	395.7	414.3	420.3	423.4	434.4	454.6	458.4	465.1
b	4.976	5.141	5.299	5.409	5.450	5.461	5.556	5.684	5.700	5.760

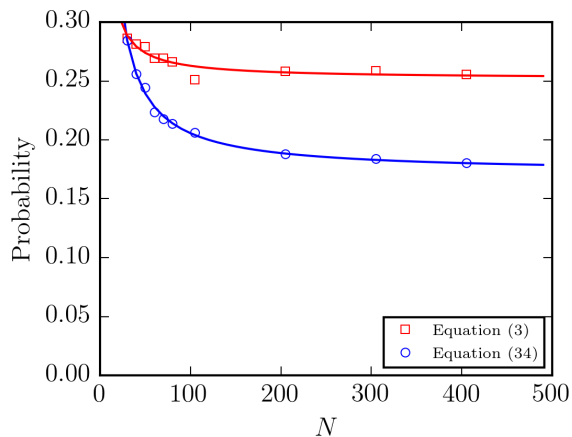


Figure 5.8: Dependence of the probability of finding the critical volume upon N . The solid line is the empirical function: $C_1 + C_2/N$ with $C_1 = 0.252$ and $C_2 = 1.10$ determined by Equation (5.3), as well as $C_1 = 0.172$ and $C_2 = 3.38$ determined by Equation (5.34).

More importantly, VT of the MD data also enables us to calculate the exact P_d distribution by counting n_f based on the snapshot of the MD trajectory at each time step, which allows us

to test the validity of Equation (5.11). Figure 5.9 shows the comparison of the P_d distribution directly obtained from VT of the MD data with that approximated by Equation (5.11) using F derived from Equation (5.34). As expected, with the probability derived from Equation (5.34), the distribution derived from Equation (5.11) is in good agreement with the exact one as shown in Figure 5.9. This indicates that the distribution of free volume along the polymer chain is similar to the Poisson distribution (cf., Equation (5.11)).

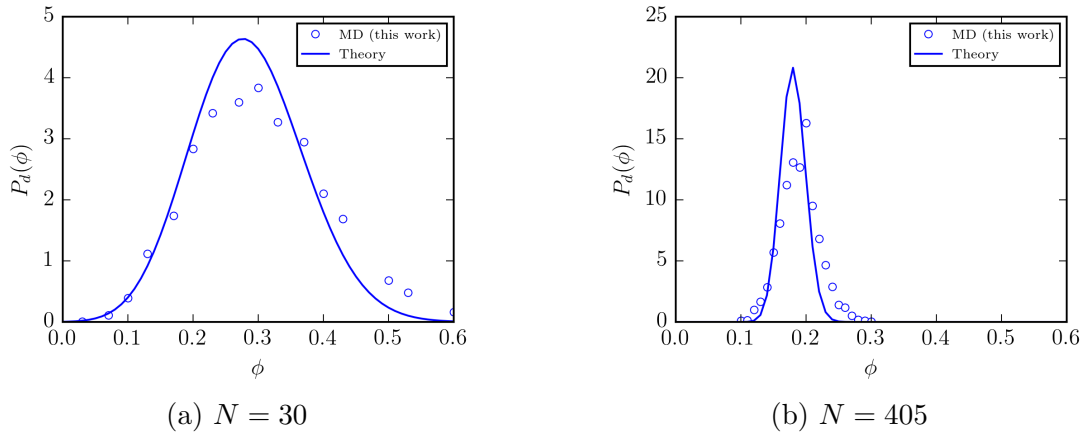


Figure 5.9: P_d distribution extracted directly from VT of the MD data and compared with the approximation using Equation (5.11).

5.4.2 Center-of-mass Diffusion Coefficient of Polyethylene

The calculation of D_{cm} of a polymer from MD simulation is well-known that it can be derived from the mean-square-displacement of the center-of-mass of the polymer given the time is long enough (cf., Equation (5.36)). The factor of 6 in Equation (5.36) is attributed to the fact that the system is three dimensional.

$$g_{cm}(t) = \lim_{t \rightarrow \infty} \langle [\mathbf{r}_{cm}(t) - \mathbf{r}_{cm}(0)]^2 \rangle = 6D_{cm}t \quad (5.36)$$

The dynamic behavior of $g_{cm}(t)$ with respect to t is not of our interest in the framework of our free volume theory, which is an nonequilibrium statistical mechanical theory of polymer. Therefore, our main focus is on the regime that $g_{cm}(t) \sim t$. Figure 5.10 shows a log-log plot of D_{cm} at different N in linear polymers. A clear crossover from unentangled regime to entangled regime at $N_c = 105$ was observed that $D_{cm} \sim N^{-1.46 \pm 0.06}$ in the unentangled regime and $D_{cm} \sim N^{-2.23 \pm 0.20}$ in the entangled regime. Qualitatively, the exponent in the

unentangled regime and entangled regime are slightly higher than the classic Rouse model [20] as well as the reptation theory [21], respectively. In particular, in the unentangled regime, we found that the exponent in $D_{cm} \sim N^{-1.46 \pm 0.06}$ is slightly less negative than that of $D_{cm} \sim N^{-1.8}$ in von Meerwall *et al.* [1] as the temperature in our MD simulation is slightly lower. Quantatively, D_{cm} obtained from our MD simulation data agree well with the experimental results of polyethylene melt by Pearson *et al.* [7] and McCall *et al.* [43], which is in the range of $10^{-9} - 10^{-11}$ m²/s (cf., Figure 5.10). We also compared our MD simulation data with the simulation data of polyethylene melt in Harmandaris *et al.* [69]. Our simulation data are in good agreement with that of Harmandaris *et al.* [69] (cf., Figure 5.10).

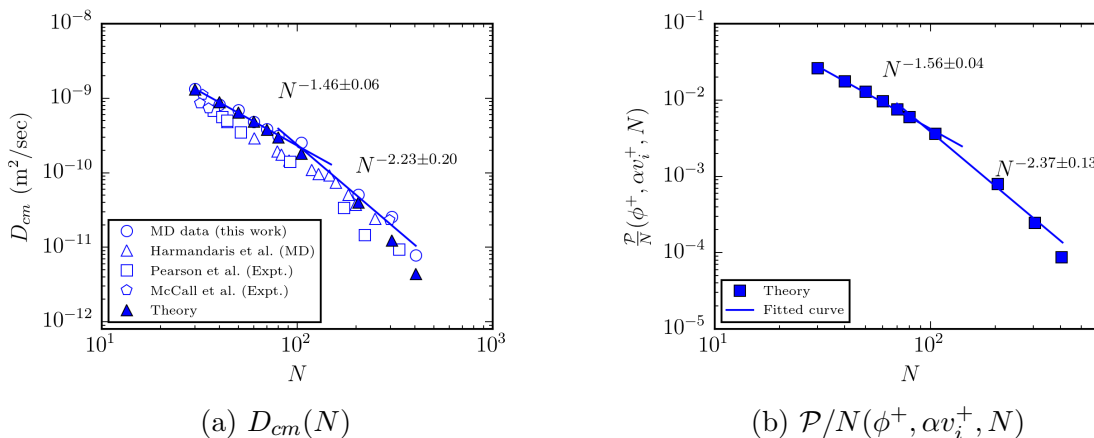


Figure 5.10: N dependence of (a) D_{cm} as well as (b) \mathcal{P} in linear polymer with MD simulation data and other literature data compared with our theory (cf., Equation (5.4)).

We then compare the simulation data as well as other literature data with Equation (5.16) using parameters found earlier (i.e., α , v_i^+ , $\langle v_f \rangle$ and ϕ^+) (cf., Figure 5.10). With the determined parameters, we found that Equation (5.16) successfully describes all the data presented in Figure 5.10(a). Our free volume theory is capable of describing the crossover from unentangled regime to entangled regime. Furthermore, \mathcal{P}/N was also plotted as a function of N as depicted in Figure 5.10(b). Notably, in the unentangled regime as shown in Figure 5.10(b), \mathcal{P}/N has a slightly stronger N dependence (i.e., $D_{cm} \sim N^{-1.56 \pm 0.04}$) than that in the Rouse model (i.e., $D_{cm} \sim N^{-1}$), indicating that our model captures the free volume effect, which has been observed experimentally, but it was not taken into account by the Rouse model [69, 60, 1]. In the entangled regime, the exponent for N dependence of

\mathcal{P}/N is slightly stronger ($\mathcal{P}/N \sim N^{-2.37 \pm 0.13}$) than that determined in the MD simulation ($D_{cm} \sim N^{-2.23 \pm 0.20}$). In addition, contrary to the model in Sabbagh and Eu [61], which has three adjustable parameters, our theory only has one empirical parameter ϕ^+ and is able to account for the distribution of the free volume along the whole chain molecule.

5.5 Conclusion

In summary, a free volume theory for polymer melt was derived. Parameters in this theory, such as v_i^+ , $\langle v_{f,i} \rangle$, α and ϕ^+ , can be evaluated using theoretical approaches, such as MD simulation, as well as experimental measurement of E_a . With these parameters, it was found that our free volume theory is successful in describing the crossover of the center-of-mass diffusion of linear polymer melt from unentangled regime ($D_{cm} \sim N^{-1.46 \pm 0.06}$) to entangled regime ($D_{cm} \sim N^{-2.23 \pm 0.20}$). This is appealing in systems, such as ring polymer, in which the concept of reptation and entanglements are not clearly understood.

Chapter 6

On the Diffusivity of Ring Polymers¹

6.1 Introduction

The Rouse model [20] and reptation model [21, 50] are the two famous theories to describe the self diffusion of linear polyethylene (PE) melts. These two separate theories were developed to account for the crossover in the N dependence of center-of-mass diffusion coefficient (D_{cm}) from $D_{cm} \sim N^{-1}$ to $D_{cm} \sim N^{-2}$, in the so-called unentangled and entangled regimes, respectively [20, 21]; these have also been proven experimentally [7] and numerically [8, 39]. Nonetheless, more careful experimental measurement later reveals that the exponent of the N dependence of D_{cm} is indeed slightly more negative with: $D_{cm} \sim N^{-1.5}$ in the unentangled regime [1] and $D_{cm} \sim N^{-2.3}$ in the entangled regime [44] at $T = 450$ K. In the reptation model, it was postulated that the diffusive motion of a polymer chain is as if it is reptating through an environment of obstacles [21], which mimicks the many-chain effect experienced by the polymer chain. An important parameter defined in the reptation model is the entanglement length, which is related to the number of obstacles experienced by the chain. It has been demonstrated that these obstacles can be identified by geometric transformation of the snapshots of linear polymer chains obtained from either Monte Carlo (MC) simulation or molecular dynamics (MD) simulation into a primitive path [55, 56, 76, 77].

Dynamics of ring polymers in an environment of fixed obstacles have been proposed by Rubinstein [78]. Rubinstein stated that the dynamics of ring polymers can be mapped to

¹A version of this chapter has been published in *Soft Matter*, 2020, 16, 2350-2362.

that of a randomly branched polymer, in which the concept of entanglement can be readily applied [78]. In the case of ring polymer melt, in which obstacles are not fixed, diffusion of smaller loop into a larger loop has to be considered so as to explain the absence of plateau modulus in ring polymer melts [79]. The mathematical formulation of the obstacle, and the appearance and disappearance of obstacle is not intuitive for non-concatenated ring polymer melts as the ‘first’ and the ‘last’ repeat units cannot be clearly defined, which have to be fixed in the algorithm developed by Kröger [77] in order to obtain the primitive path. Robertson and Smith [80] and Chapman *et al.* [81] also demonstrated a peculiar trend observed in the diffusivities of cyclic and linear DNAs. Given the fact that solution is highly concentrated and the size of the biopolymer is large, the diffusivity of cyclic DNAs can drop when it is surrounded by many linear DNAs, but the reverse is true as linear DNA is surrounded by its circular counterparts. These unusual dynamic behaviours are then attributed to the fact that linear DNAs are more capable of forming entanglements, and the effect of entanglement disappears as the concentration or the chain length of linear DNAs decreases [80, 81].

It is well-known that transport coefficients, such as diffusion coefficients, of dilute gas can be calculated by non-equilibrium statistical mechanics, i.e., by knowing its collision probability, velocity distribution and the mean free path. When the system becomes more dense and thus is a simple liquid, the Cohen-Turnbull theory [82], which includes the probability of finding a certain amount of free volume, can be applied. The concept of free volume was also used in the William-Landel-Ferry equation [83], which describes the temperature dependence of viscosities of impure ring polystyrene [84]. But Hiemenz and Lodge [13] pointed out that despite the fact that it is easy to discuss free volume, a numerical value of free volume has to be well defined from first principles. Furthermore, this approach has never been widely applied in determining D_{cm} of polymers as a function of N .

To our knowledge, this was firstly attempted by Sabbagh and Eu [61] and then our group [85] for determining the crossover in the N dependence of D_{cm} of linear polymers. The distribution function theory of polymeric liquid and generic van der Waals’ (GvdW) equation of state [64] allow us to obtain the mean free volume ($\langle v_f \rangle$), and thus the probability of finding certain free volume in a polymer melt. In our previous work, we have demonstrated that the distribution of the free volume along a linear chain is related to the crossover of the center-of-mass diffusion coefficient from unentangled regime to entangled regime, i.e., the

exponent associated with the N dependence of D_{cm} changes from -1.5 to -2.3 . Parameters were theoretically determined based on the intermolecular and intramolecular radial distribution functions, as well as the activation energy that is derived from the temperature dependence curve of D_{cm} s of linear polymers in our free volume theory. The advantage of this analytical approach is that the concept of entanglement is completely unnecessary. This in particular is very useful in more complex system, such as ring polymers, in which the concept of entanglement cannot be straightforwardly applied.

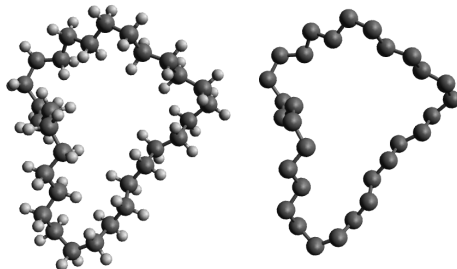


Figure 6.1: The methylene groups of a ring PE (left) are coarse-grained to beads (right) in all our calculations.

In this work, we are going to use this non-equilibrium statistical mechanics approach to determine the D_{cm} s of ring PE melts. In all the calculations, the ring PE is coarse-grained such that each methylene group is modeled as bead with interaction parameters derived by Martin *et al.* [19] (cf., Figure 6.1). The radial distribution functions of ring PE are obtained by the integral equation method, i.e., the polymer reference interaction site model (PRISM) [86] and more accurately the molecular dynamics (MD) simulation, in which all the details of bonded and non-bonded interactions are explicitly included. The calculation in the former case is less sophisticated, computationally inexpensive, and the solution is free of any finite size effect, whereas the radial distribution function derived from the latter case is explicitly computed from the numerical solution to the highly non-linear equations of motion of atoms, which is much more computationally expensive, but more accurate. In the latter case, the probability for a bead to find a certain amount of free volume can be precisely determined by Voronoi tessellation [87], in which the space available to a bead is mathematically determined from the MD trajectory. The activation energy for the diffusion of ring PE was also determined by varying the temperature in the MD simulation.

6.2 Preliminary: Free Volume Theory Revisited

In our free volume theory, it is postulated that for a linear chain, the distribution of free volume along the chain is:

$$P_d = \frac{(N-2)!}{n_f!(N-n_f-2)!} F^{n_f} (1-F)^{N-n_f-2} \quad (6.1)$$

where n_f is the number of beads having free volume ($v_{f,i}$) greater than or equal to αv_i^+ , α is the overlapping parameter and v_i^+ is the effective volume of the bead. F is the probability for a single bead having $v_{f,i} \geq \alpha v_i^+$. For ring polymers, the expression for such distribution in the absence of chain ends is:

$$P_d = \frac{N!}{n_f!(N-n_f)!} F^{n_f} (1-F)^{N-n_f} \quad (6.2)$$

Equation (6.2) can be rewritten as:

$$\ln P_d = N \ln \left[\left(\frac{1-F}{1-\phi+\varepsilon} \right)^{1-\phi} \left(\frac{F}{\phi+\varepsilon} \right)^\phi \right] - \frac{1}{2} \ln \left[2\pi N \phi (1-\phi) + \exp\left[-\frac{\phi^2}{\varepsilon^2}\right] + \exp\left[-\frac{(\phi-1)^2}{\varepsilon^2}\right] \right] + \ln(c) \quad (6.3)$$

Note that $\phi = n_f/N$, which is the number fraction of beads having $v_{f,i} \geq \alpha v_i^+$. ε is a very small number ($\sim 10^{-5}$), which ensures the denominators in Equation (6.3) are not zero, and the second term of Equation (6.3) is 0 for $\phi = 0$ and $\phi = 1$. c is the normalization constant such that $\int_0^1 P_d d\phi = 1$ and it was obtained numerically. Following the rationale of the Cohen-Turnbull theory [82], F in such sense (F_{ct}) can be expressed as follows:

$$F_{ct}(\alpha v_i^+) = \exp\left(-\frac{N\alpha v_i^+}{\langle v_f \rangle}\right) \quad (6.4)$$

α is the overlapping parameter, v_i^+ is the effective volume of the i th bead and $\langle v_f \rangle$ is the mean free volume of the whole macromolecule. It was found that a more precise expression for F is indeed a gamma distribution, which has been verified experimentally by positron annihilation experiment [71], as follows:

$$F(\alpha v_i^+) = 1 - \frac{1}{\Gamma(b)} \int_0^{\alpha v_i^+} x^{b-1} e^{-x} dx \quad (6.5)$$

where $\Gamma(b)$ is the gamma function with b as the argument:

$$\Gamma(b) = \int_0^\infty x^{b-1} e^{-x} dx \quad (6.6)$$

The parameters a and b are defined as follows:

$$a = \frac{b}{\langle v_{f,i} \rangle} \quad (6.7)$$

$$b = \frac{\langle v_{f,i} \rangle^2}{\langle v_{f,i}^2 \rangle - \langle v_{f,i} \rangle^2} \quad (6.8)$$

The parameter a has a unit of nm^{-3} and the parameter b , also known as the regularity factor, is dimensionless. With these, D_{cm} of ring polymers with different N can be computed as:

$$D_{cm} = \frac{D}{N} \int_{\phi^+}^1 P_d d\phi \quad (6.9)$$

Note that:

$$D = D_0 \exp\left(-\frac{\alpha v_1^+}{\langle v_{f,1} \rangle}\right) \quad (6.10)$$

D_0 is the diffusion coefficient of dilute monoatomic gas determined by Chapman-Enskog method. v_1^+ and $\langle v_{f,1} \rangle$ are the critical volume and mean free volume, respectively, as $N = 1$. D is therefore the diffusion coefficient of a dense monoatomic liquid, for which it was found that $D = 4.42 \times 10^{-8} \text{ m}^2 \cdot \text{s}^{-1}$ at $T = 450 \text{ K}$ using the parameters obtained by MD simulation. (Note that $D = 4.98 \times 10^{-8} \text{ m}^2 \cdot \text{s}^{-1}$ in our previous work of linear PE [85].) ϕ^+ is the fraction of beads in a single ring polymer having $v_{f,i} \geq \alpha v_i^+$, such that the integral $\int_{\phi^+}^1 P_d d\phi$ gives us the probability of finding $\phi \geq \phi^+$ of the whole macromolecule having sufficient free volume for the activation of diffusion. The value of ϕ^+ used in Equation (6.9) can be inferred from the activation energy of the macromolecule (E_a), which can be directly obtained by evaluating D_{cm} from MD simulation at different temperatures.

6.3 Calculation Details

6.3.1 Integral Equation Theory of Ideal Ring Polymers

It is well-known that for simple monoatomic liquid, its intermolecular radial distribution function ($g(r)$) can be evaluated with the Ornstein-Zernike Equation, which was proposed a century ago. They argued that $g(r)$ can be divided into direct and indirect parts. The direct part accounts for the influence from atom 2 on atom 1, whereas the indirect part includes the influence from atom 3 on atom 2, which results in indirect influence on atom

1, as these particles interact with one another through a particular potential, such as hard-sphere potential or 6-12 Lennard-Jones (LJ) potential. The Ornstein-Zernike equation has the following form:

$$h(r_{12}) = c(r_{12}) + \rho \int c(r_{13})h(r_{23})d\mathbf{r}_3 \quad (6.11)$$

$h(r) = g(r) - 1$ and $c(r)$ is the direct correlation function. This equation is simplified to an algebraic equation when it is transformed to the fourier space:

$$\hat{h}(k) = \hat{c}(k) + \rho\hat{c}(k)\hat{h}(k) \quad (6.12)$$

k is the wavevector. For polymer, the expression becomes a matrix equation, known as the polymer reference interaction site model (PRISM) equation. In real space, it is expressed as:

$$\mathbf{H}(r) = \int \int d\mathbf{r}_1 d\mathbf{r}_2 \mathbf{\Omega}(|\mathbf{r} - \mathbf{r}_1|) \mathbf{C}(|\mathbf{r}_1 - \mathbf{r}_2|) [\mathbf{\Omega}(r_2) + \rho \mathbf{H}(r_2)] \quad (6.13)$$

$\mathbf{\Omega}$ is a matrix containing the intramolecular correlation functions of different sites, and ρ is the number density of the whole macromolecule. In polymer melts, translational invariance can be applied such that all sites along the polymer chain are equivalent. Equation (6.13) can be then simplified as:

$$h(r) = \int \int d\mathbf{r}_1 d\mathbf{r}_2 \omega(|\mathbf{r} - \mathbf{r}_1|) c(|\mathbf{r}_1 - \mathbf{r}_2|) [\omega(r_2) + \rho_b h(r_2)] \quad (6.14)$$

$\rho_b = \rho/N$ such that ρ_b is the number density of bead. In the Fourier's space, we have:

$$\hat{h}(k) = \hat{\omega}(k)^2 \hat{c}(k) + \rho_b \hat{\omega}(k) \hat{c}(k) \hat{h}(k) \quad (6.15)$$

In order to solve the equation self-consistently, the Percus-Yevick closure relation is applied:

$$c^{new}(r) = \{\exp[-\beta u(r)] - 1\} [h^{old}(r) + 1 - c^{old}(r)] \quad (6.16)$$

The superscripts *new* and *old* indicate that a new $c(r)$ is generated based on $h(r)$ and $c(r)$ from the previous iteration step [88]. The intermolecular interaction potential $u(r)$ is the 6-12 LJ potential, which has the following form:

$$u(r) = 4\varepsilon \left(\frac{\sigma^{12}}{r^{12}} - \frac{\sigma^6}{r^6} \right) \quad (6.17)$$

$\sigma = 0.395$ nm and $\varepsilon = 380$ J/mole, which are parameters for ring PE. For a Gaussian ring,

$$\hat{\omega}(k) = 1 + 2N^{-1} \sum_{i=1}^{N-1} (N-i) \exp \left[\frac{-k^2 d^2 i(N-i)}{6N} \right] \quad (6.18)$$

d is the contact diameter of the segment and it is assumed to be equal to the statistical segmental length. The PRISM equation was solved using a Python 3.6 program with the Fourier transformation procedures as described in Martin *et al.* [88] (cf., Supporting Information).

6.3.2 Molecular Dynamics Simulation

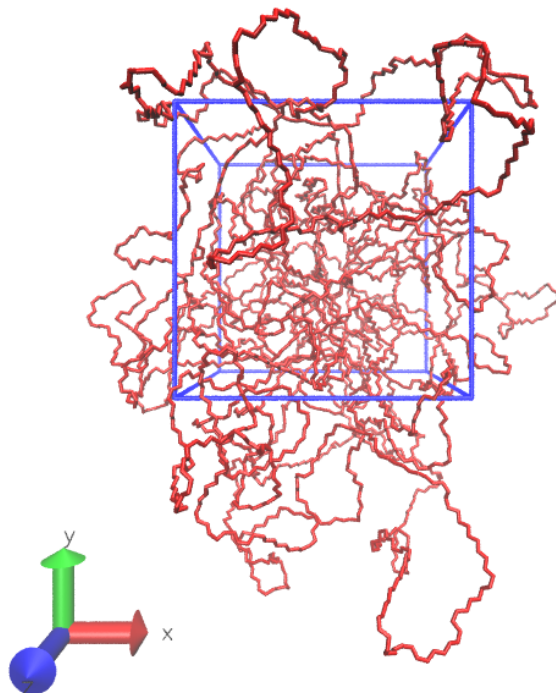


Figure 6.2: Final snapshot of MD simulation of ring PE with $N = 305$ at $T = 450$ K.

Similar to the PRISM calculation, in the MD simulation, the methylene groups of the ring PE were coarse-grained to beads, with unique forcefield interaction parameters, which were the TraPPE forcefield parameters reported by Martin *et al.* [19]. The equation of motion was solved numerically by leapfrog integration with a discrete time step of 1 fs. Temperature and pressure coupling, at 450 K and ambient pressure, were achieved using Nosé-Hoover thermostat as well as Parrinello-Rahman barostat, respectively. The time constants of the thermostat and barostat were set at 0.2 ps and 2 ps, respectively, unless otherwise mentioned. All MD simulations were performed using GROMACS-5.1.4 free software [36].

Generation of MD data involved three steps: initial configuration preparation, equilibration and production. The procedures of initial configuration preparation for ring PE are very similar to that of linear PE, and described in our previous papers [9, 85]. With the rotational isomeric state model [16, 12], a linear chain was first constructed, followed by joining the two ends of the polymer chain to form a ring. The excluded volume effect due to the

intramolecular interaction was then introduced by geometry optimization in the Avogadro software [89]. Identical ring PE molecules were then randomly distributed in a simulation box and the energy was minimized with the force tolerance set at $100 \text{ kJ} \cdot \text{mol}^{-1} \cdot \text{nm}^{-1}$.

The equilibration as well as the production steps were the same as described in our previous work of linear PE [85], except that the time constant of barostat was set at 0.5 ps and the NPT MD simulation was allowed to run for a duration of 20 – 650 ns, in the equilibration and production runs. Figure 6.2 shows the final snapshot of MD simulation of ring PE with $N = 305$ at $T = 450 \text{ K}$. Figure 6.3 shows the N dependence of number density of beads (ρ_b) at $T = 450 \text{ K}$, the fitting curve is $C_1 - C_2/N$ with $C_1 = 32.7 \text{ nm}^{-3}$ and $C_2 = 23.8 \text{ nm}^{-3}$. This allows us to approximate ρ_b as $N \rightarrow 1$ for calculation of D (cf., Equation (6.10)). In our previous work of linear PE, the extrapolated ρ_b is a negative value as $N \rightarrow 1$ that ρ_b corresponding to $N = 4$ was used for calculation of D in linear PE [85]. The fact that ρ_b of ring PE melts is dependent on N is not surprising as this has been reported by von Meerwall *et al.* [90] and Alatas *et al.* [91]. Additionally, to investigate the effect of periodic boundary condition, the number of rings used in simulation was doubled for $N = 405$. At $T = 450 \text{ K}$, it was found that the resultant D_{cm} are $1.47 \times 10^{-11} \text{ m}^2 \cdot \text{sec}^{-1}$ and $1.59 \times 10^{-11} \text{ m}^2 \cdot \text{sec}^{-1}$ when 10 rings and 20 rings were used, respectively. This shows that finite size effect is negligible.

As mentioned in the Introduction, we would also like to know the effect of temperature on the diffusivity of ring PE. To do so, the temperature of the NPT simulation of ring PE was decreased from 450 K to 370 K with an increment of 10 K. Each temperature was kept constant for 20 – 50 ns and 200 ps was allowed for the cooling from one temperature to another. The number of rings used in the simulation, the dimension of the box in the final snapshot of the MD trajectory (L) and the root-mean-square radius of gyration of ring PE ($\sqrt{\langle R_g^2 \rangle}$) are listed in Table 6.1.

Table 6.1: Number of rings, dimension of the box and root-mean-square radius of gyration of ring PE melts.

N	30	40	50	60	70	80	105	205	305	405	405
Number of rings	26	20	16	40	40	40	10	10	10	10	20
L (nm)	2.914	2.938	2.912	4.201	4.431	4.585	3.189	4.0352	4.544	5.103	6.291
$\sqrt{\langle R_g^2 \rangle}$ (nm)	0.530	0.657	0.772	0.870	0.954	1.033	1.199	1.661	1.971	2.204	2.216

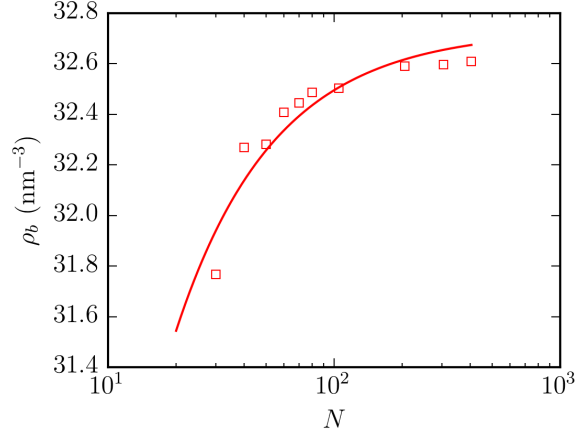


Figure 6.3: Number density of beads at different N at $T = 450$ K. The data are fitted to the empirical relation $C_1 - C_2/N$ with $C_1 = 32.7 \text{ nm}^{-3}$ and $C_2 = 23.8 \text{ nm}^{-3}$.

6.4 Results and Discussion

6.4.1 PRISM Theory

Pressure Equation and GvdW Equation of State for Ideal Rings

For ideal ring polymers, the pressure equation is written as follows:

$$\frac{p\beta}{\rho_b} = 1 - \frac{2\pi\beta\rho_b}{3} \left[\int_0^\infty r^3 \frac{du}{dr} g(r) dr \right] \quad (6.19)$$

Figure 6.4(a) shows the $g(r)$ of ideal ring PE with $N = 405$ evaluated by the PRISM theory. As expected, the first peak is relatively lower than that of a monoatomic fluid, due to the screening effect from the intramolecular interaction within the ideal ring polymer. Different

length scales can be then deduced by defining a function $I(r)$ with the following form:

$$I(r) = -r^3 \frac{du}{dr} g(r) \quad (6.20)$$

As the 6-12 LJ potential is a soft-core potential, unlike the hard-sphere potential in which only one length scale can be obtained, four lengths can be determined from the former case: $r_c = 0.306$ nm, $r^+ = 0.355$ nm, $r_{pm} = 0.444$ nm and $r_{fm} = 0.524$ nm (cf., Figure 6.4(b)). Despite the 6-12 LJ potential being a soft-core potential, it has a corresponding hard-core diameter r_c , which is the minimum possible incompressible size of the bead. r^+ is the cavity diameter. With the 6-12 LJ potential, the situation can be imagined as placing a hard-sphere with diameter of r_c in a cavity with diameter of r^+ . It is highly probable for the bead to experience a strong repulsive force at r^+ . Finally, r_{pm} and r_{fm} correspond to the lengths at potential and force minima, respectively.

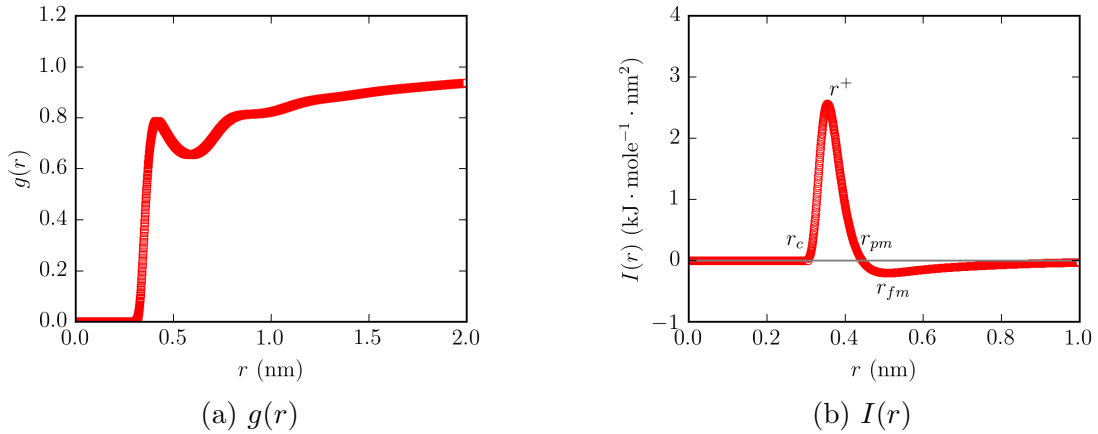


Figure 6.4: $g(r)$ and $I(r)$ of ring PE with $N = 405$ from the PRISM theory.

With these length scales, the critical volume of a bead is $v_i^+ = \frac{\pi r^{+3}}{6} = 0.0234$ nm³ and the overlap parameter (α) can be evaluated with the following:

$$\alpha = \left(1 - \frac{|r_{fm} - r_{pm}|}{r^+}\right)^3 \approx 0.46 \quad (6.21)$$

This formula was derived by Laghaei *et al.* [65] to quantify the overlapping of free volume in LJ fluids. The excluded volume in the polymer melt can be quantified using the GvdW equation of state:

$$(p + A\rho_b^2)(N - B\rho_b) = \rho_b\beta^{-1} \quad (6.22)$$

By juxtaposing the GvdW equation of state with Equation (6.19), one can deduce that:

$$A = -\frac{2\pi}{3} \int_{r^+}^{\infty} I(r) dr \quad (6.23)$$

And:

$$B = \frac{1}{\rho_b} \left[N - \frac{1}{1 + \frac{2\pi\beta\rho_b}{3} \int_0^{r^+} I(r) dr} \right] \quad (6.24)$$

The parameter B actually gives a measure of the excluded volume. The mean free volume of the whole ideal ring PE $\langle v_f \rangle_{ideal}$ can be then evaluated as follows:

$$\langle v_f \rangle_{ideal} = \frac{1}{\rho} [N - B\rho_b] \quad (6.25)$$

Figure 6.5(a) and Figure 6.5(b) show a plot of the compressibility factor and the GvdW parameter B and $\langle v_f \rangle_{ideal}$, respectively, as a function of N . As expected, the compressibility factor is inversely proportional to N as observed by Sabbagh and Eu [61], and Gan and Eu [92]. The GvdW parameter B increases with N as the excluded volume of the macromolecule increases with its size. The fraction of free volume (f) in ring PE melt is approximately 0.45. The probability for a bead having free volume greater than or equal to αv_i^+ can be then easily evaluated using Equation (6.4).

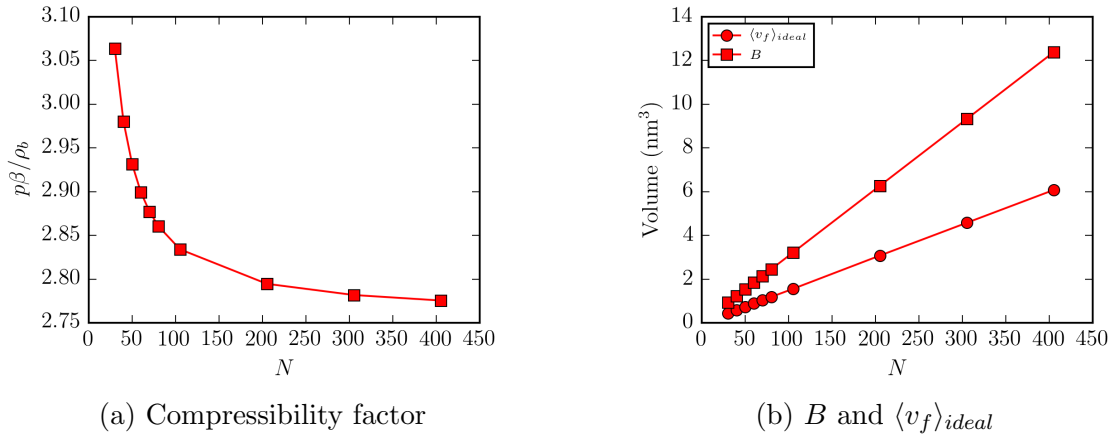


Figure 6.5: Compressibility factor, B and $\langle v_f \rangle_{ideal}$ as a function of N . The solid lines depicted are guides only.

Temperature Dependence of the Free Volume

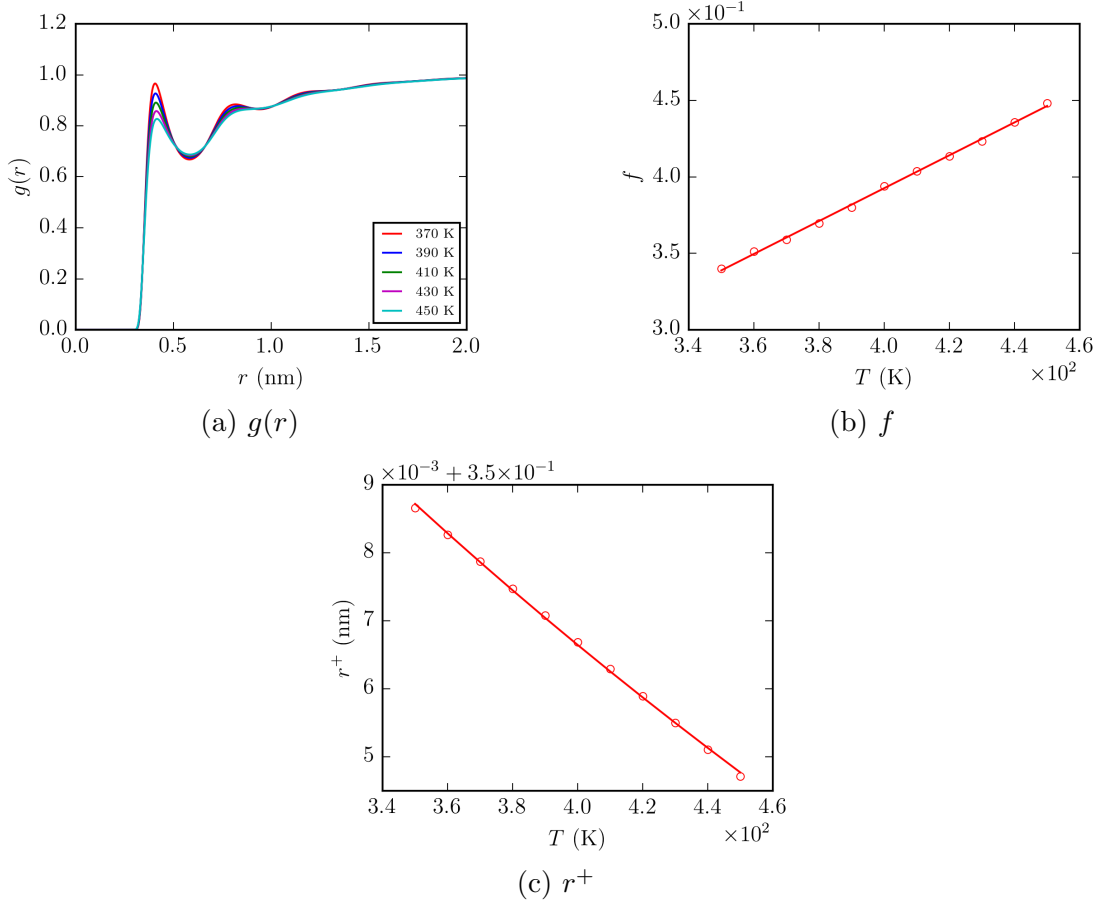


Figure 6.6: Temperature dependence of (a) $g(r)$, (b) f and (c) r^+ for ring PE with $N = 80$ obtained by the PRISM theory. The data reported in (b) were fitted to the relation $f = C_1 + C_2T$ with $C_1 = -0.0373$ and $C_2 = 0.00107 \text{ K}^{-1}$. The data in (c) were fitted to Equation (6.26) with $d_0 = 0.404 \text{ nm}$ and $d_1 = 0.0563 \text{ K}^{-0.5}$.

Using ρ_{bs} obtained at different temperatures from MD simulation, $g(r)$ s of an ideal ring PE with $N = 80$ at different temperatures were computed using the PRISM theory as depicted in Figure 6.6(a). As expected, the first peak of $g(r)$ decreases with increasing temperature as the system becomes less dense at higher temperatures.

The effect of temperature on the f can be then investigated for ring PE with $N = 80$ as the mean free volume can be calculated straightforwardly using the procedures above. Figure 6.6(b) shows the temperature dependence of f for ring PE with $N = 80$ for all temperatures. As expected, f increases with T , and the data were fitted to a linear curve $f = C_1 + C_2T$,

with $C_1 = -0.0373$, $C_2 = 0.00107 \text{ K}^{-1}$. Our results agree qualitatively with the studies of excluded volume and free volume in simple monoatomic LJ fluids conducted by Laghaei *et al.* [65]. C_2 obtained in this case is the thermal expansion coefficient of the fractional free volume. The extrapolated thermal expansion coefficient of cyclic alkane as $N \rightarrow \infty$ based on the data of cyclic alkane with $N = 5 - 10$ from Huang *et al.*[93] is approximately $8 \times 10^{-4} \text{ K}^{-1}$, and is higher than that determined by the PRISM theory as the ring PE is assumed to be ideal such that beads of the same macromolecule are allowed to overlap. Owing to this, the prediction of temperature dependence of D_{cm} , which will be discussed in more details in Section 4.3.2, is not that successful using the PRISM theory.

In addition, we found that the parameter r^+ obtained from the PRISM theory is slightly dependent on temperature in that it decreases with increasing temperature (cf., Figure 6.6(c)), as also observed by Laghaei *et al.* [65] in the case of simple monoatomic fluids. The temperature dependence of r^+ can be described by the following equation:

$$r^+ = d_0(1 + d_1\sqrt{T})^{-\frac{1}{6}} \quad (6.26)$$

It was found that $d_0 = 0.404 \text{ nm}$ and $d_1 = 0.0563 \text{ K}^{-0.5}$ (cf., Figure 6.6(c)). With these, we can know the probability of finding αv_i^+ at different temperatures in ideal ring polymer melts using Equation (6.4).

6.4.2 Molecular Dynamics Simulation

Pressure Equation and GvdW Equation of State

A more accurate approach to obtain the radial distribution function as well as the mean free volume is the MD simulation, in which all intramolecular interactions, such as bond angle, torsional angle, and intermolecular interactions, such as 6-12 LJ potential, are explicitly taken into account in the equation of motion. For MD simulation, the pressure equation can be expressed in a more precise way:

$$\frac{p\beta}{\rho_b} = 1 - \frac{2\pi\beta\rho_b}{3} \int_0^\infty r^3 \frac{du}{dr} g(r) dr - \frac{4\pi\beta}{3} \int_0^\infty r^3 \frac{du_{bond}}{dr} \omega_{bond}(r) dr - \frac{4\pi\beta}{3} \int_0^\infty r^3 \frac{du}{dr} \omega(r) dr \quad (6.27)$$

Equation (6.27) was originally derived by Honnell *et al.* [73]. In Equation (6.27), the direct contributions from angle bending and torsional potentials to the pressure are neglected because the derivative of the bond angle and torsional angle with respect to the volume is zero as shown by Honnell *et al.* [73]. The influences of the angle bending and torsional angle potential are indirectly reflected in the radial distribution functions [73]. Also, it is worthwhile to note that when $\omega(r)$ and ω_{bond} are input in Equation (6.27), they have to be normalized by factors of $4\pi \int_0^\infty \omega(r)r^2 dr$ and $4\pi \int_0^\infty \omega_{bond}(r)r^2 dr$, respectively. Figure 6.7(a) shows the $g(r)$ of ring polymer with $N = 405$ from MD simulation. $g(r)$ in this case is less suppressed than that of the PRISM theory (cf., Figure 6.4(a)), indicating that the actual effect of the intramolecular interaction on the intermolecular interaction is not that strong. We have the bond stretching potential $u_{bond}(r)$:

$$u_{bond}(r) = \frac{1}{2}k_{bond}(r - l_0)^2 \quad (6.28)$$

l_0 is the equilibrium bond length having a value of 0.154 nm and k_{bond} is the spring constant of the harmonic bond stretching potential. $k_{bond} = 132506 \text{ kJ} \cdot \text{mole}^{-1} \cdot \text{nm}^{-2}$, which is obtained from molecular mechanics (MM2) forcefield. $\omega_{bond}(r)$ in Equation (6.27) is:

$$\omega_{bond}(r) = \frac{1}{NV} \left[\omega_{bond}^{0,N-1}(r) + \sum_{\varepsilon=1}^{N-2} \omega_{bond}^{\varepsilon,\varepsilon+1}(r) \right] \quad (6.29)$$

$\omega_{bond}^{\alpha,\gamma}(r)$ is the intramolecular radial distribution function between two sites interacting with one another through $u_{bond}(r)$. As for the intramolecular 6-12 LJ potential interactions between the beads separated by four bonds within the same polymer, we have:

$$\omega(r) = \frac{1}{NV} \sum_{\alpha=1}^{N-6} \sum_{\gamma=\alpha+4}^{\alpha+N-4} \omega^{\alpha,\gamma}(r) + \frac{1}{NV} \sum_{\alpha=N-5}^{N-4} \sum_{\gamma=\alpha+4}^N \omega^{\alpha,\gamma}(r) \quad (6.30)$$

$\omega^{\alpha,\gamma}(r)$ is the intramolecular radial distribution function between two sites due to 6-12 LJ potential. In Equation (6.29) and Equation (6.30), V is the volume of the sampling sphere for different radial distribution functions, i.e., $V = \frac{4}{3}\pi r_{max}^3$. $r_{max} \approx 3L$ and it is the maximum radius used in the calculation of radial distribution function based on the MD trajectory. Figure 6.7(b) and Figure 6.7(c) show the plots of $\omega(r)$ and $\omega_{bond}(r)$, respectively. Three main peaks at 0.46 nm, 0.51 nm and 0.65 nm, were observed in $\omega(r)$, whereas there is only one peak at l_0 in $\omega_{bond}(r)$. These results are similar to that of its linear counterpart from our previous MD simulation [85].

Similar to the above analysis of an ideal ring polymer, four different length scales can be derived by defining a function $I(r)$. (Figure 6.7(d))

$$I(r) = -r^3 \frac{du}{dr} g(r) - 2r^3 \frac{du}{dr} \frac{\omega(r)}{\rho_b} \quad (6.31)$$

Figure 6.7(d) shows a plot of $I(r)$ and the corresponding length scales read: $r_c = 0.316$ nm, $r^+ = 0.368$ nm, $r_{pm} = 0.444$ nm and $r_{fm} = 0.524$ nm. This indicates that $v_i^+ = \frac{\pi}{6} r^{+3} = 0.0260$ nm³, and $\alpha = 0.48$. Compared to the case of ideal ring polymer, in MD simulation, v_i^+ is slightly larger because the position of the first peak of $g(r)$ in MD simulation is relatively higher (cf., Figure 6.4(a) and Figure 6.7(a)).

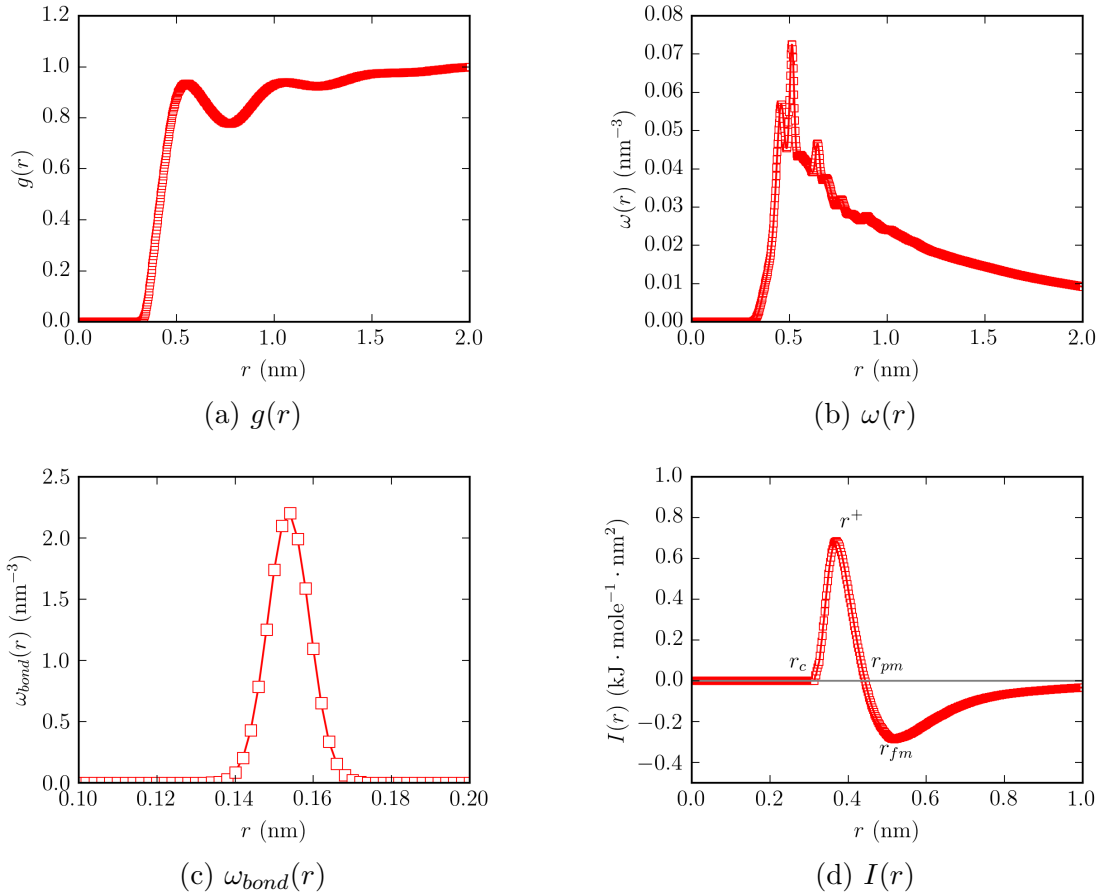


Figure 6.7: $g(r)$, $\omega(r)$, $\omega_{bond}(r)$ and $I(r)$ of ring polymer with $N = 405$ from MD simulation.

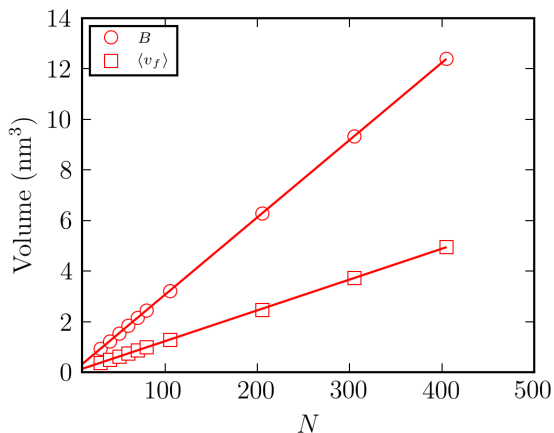


Figure 6.8: N dependence of B and $\langle v_f \rangle$. The solid lines depicted are guides only.

For MD simulation, A and B are defined as follows:

$$A = -\frac{2\pi}{3} \left[\int_{r^+}^{\infty} I(r) dr + \int_{l_0}^{\infty} I_b(r) dr \right] \quad (6.32)$$

And:

$$B = \frac{1}{\rho_b} \left[N - \frac{1}{1 + \frac{2\pi\beta\rho_b}{3} \left(\int_0^{r^+} I(r) dr + \int_0^{l_0} I_b(r) dr \right)} \right] \quad (6.33)$$

where $I_b(r)$ is in the following form:

$$I_b(r) = -\frac{2r^3 \omega_{bond}(r)}{\rho_b} \frac{du_{bond}}{dr} \quad (6.34)$$

The integral term $\int_0^{l_0} I_b(r) dr$ captures the excluded volume effect due to repulsion experienced by the bead in the harmonic bond stretching potential. The corresponding mean free volume per ring PE and values of parameter B are shown in Figure 6.8. The fractional free volume is approximately 0.3.

Free Volume Distribution for Different Ring Sizes

A more accurate approach of calculating the probability distribution of free volume in the polymer melt is by Voronoi tessellation of the MD trajectory. In Voronoi tessellation, the free space available to each united atom in the MD simulation trajectory is calculated using the free software voro++ [75] and the volume of the so-called Voronoi cell can be then obtained.

Although Voronoi tessellation does not give us the exact amount of free volume in the system, the size distribution of the Voronoi cell should be directly related to that of the free volume per bead.

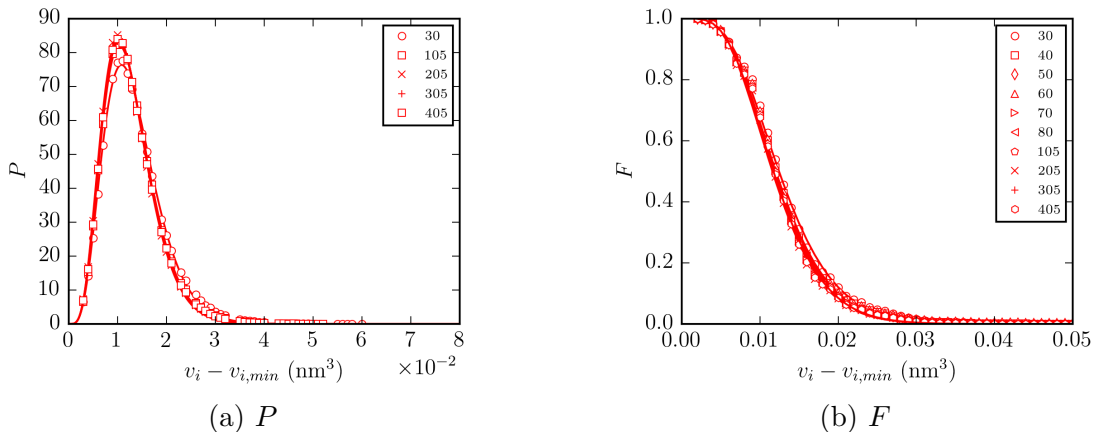


Figure 6.9: Probability distribution functions of the free volume in the ring PE melts as determined by the Voronoi tessellation for $N = 30$, $N = 105$, $N = 205$, $N = 305$ and $N = 405$, and the cumulative distribution functions for all ring PEs. The data in (a) and (b) were fitted to probability distribution function and cumulative distribution function of the gamma distribution, respectively, with the parameters as shown in Table 8.1.

Table 6.2: Fitting results of the parameters a and b in the gamma distribution.

N	30	40	50	60	70	80	105	205	305	405
a (nm ⁻³)	411.3	437.1	443.3	448.1	453.7	455.1	454.0	468.3	464.7	462.4
b	5.444	5.586	5.644	5.665	5.710	5.703	5.706	5.759	5.764	5.752

It was found that the minimum Voronoi cell volume $v_{i,min}$ for a bead is 0.018 nm³, which is close to the value of the hard-core volume of the bead $v_c = \frac{\pi}{6}r_c^3 = 0.0165$ nm³. The distribution was shifted by $v_{i,min}$ as shown in Figure 6.9 and was then fitted to a gamma distribution. a and b were therefore obtained from the data, which have values of $a = 411.3 - 462.4$ nm⁻³ and $b = 5.444 - 5.752$. The distribution of $(v_i - v_{min,i})$ is equivalent to the distribution of the volume excluding the effect of the hard-core nature of the LJ potential. Nonetheless, the Voronoi tessellation method does not take into account of the soft-core nature of the LJ potential, which results in the cavity diameter r^+ . Therefore, if Equation (6.5) is applied to the distributions as depicted in Figure 6.9, to account for the fact that each bead has an effective diameter of r^+ instead of r_c , the critical volume

$v_i^* = \alpha v_i^+ + \frac{1}{\rho_b}(1 - N + B\rho_b) - v_c$ should be used instead of $v_i^* = \alpha v_i^+$. The probability of finding v_i^* ($F(v_i^*)$) evaluated for ring PE melts with different N is shown in Figure 6.10. The data were fitted to an empirical function $C_1 + C_2/N$ that describes the N dependence of $F(v_i^*)$, which is similar to the form describing the N dependence of ρ_b (cf., Figure 6.3). This allows us to easily calculate F_{ct} as $N \rightarrow 1$, which is necessary for the calculation of D (cf., Equation (6.10)). In addition, the probability determined by Voronoi tessellation is lower than that calculated by the classic form in Equation (6.4) (cf., Figure 6.10).

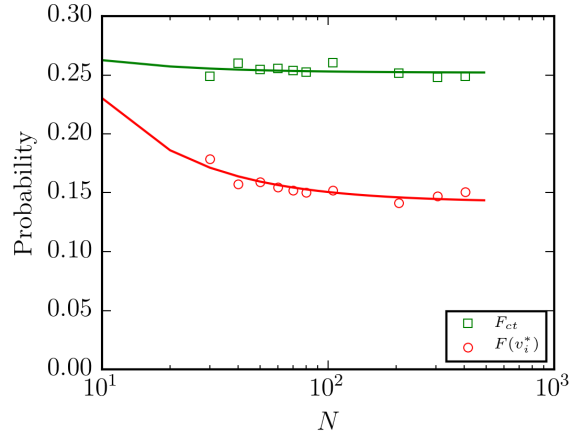


Figure 6.10: Probability of finding v_i^* for ring PE with different N . The data were fitted to the relation: $F = C_1 + C_2/N$ and $F_{ct} = C_{1,ct} + C_{2,ct}/N$. The values of the parameters are $C_1 = 0.141$ and $C_2 = 0.886$, as well as $C_{1,ct} = 0.252$ and $C_{2,ct} = 0.107$.

The Voronoi tessellation method also allows us to directly compute the distribution of free volume along the chain (i.e., $P_d(\phi)$ distribution) as we can explicitly count the number n_f as presented in Equation (6.3) at any specific time in a MD simulation trajectory. Figure 6.11 shows the $P_d(\phi)$ distribution derived from the MD simulation and the theory for ring polymers with $N = 105$ and $N = 405$. The obtained data can be then juxtaposed with that theoretically calculated using Equation (6.3) and the determined values of $F(v_i^*)$ (cf., Figure 6.10). As shown in Figure 6.11, the $P_d(\phi)$ obtained from MD simulation is slightly broader. This is because in our free volume theory, the $P_d(\phi)$ distribution, which is the distribution of fraction of beads of ring PE having enough free volume for the activation of diffusion, was derived based on the assumption that each bead of the ring PE always has the same probability of getting critical volume at each time step and the probability is independent of the bead's ‘memory’ of how often it had sufficient free volume. The slightly broader $P_d(\phi)$

distribution indicates that such assumption is not entirely valid. It seems that the bead that possessed more free volume in the past may have a greater opportunity of getting more free volume in the future.

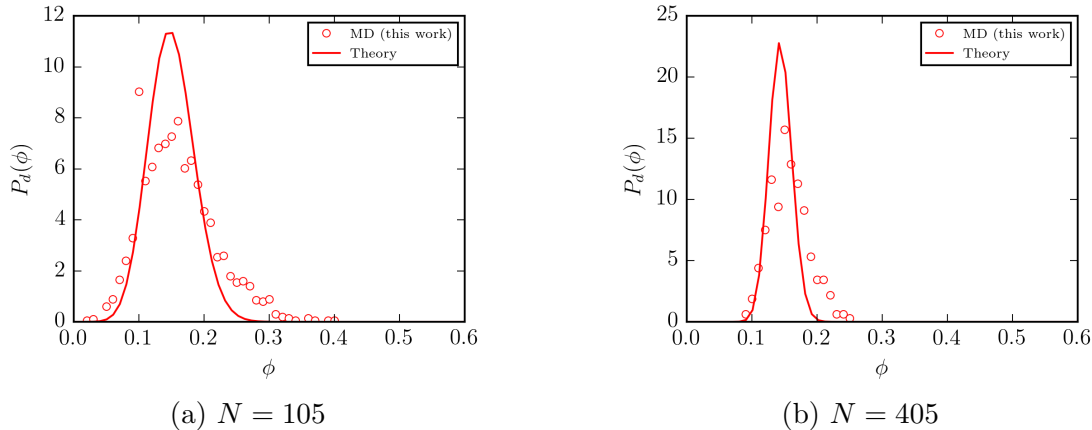


Figure 6.11: $P_d(\phi)$ distribution extracted directly from VT of the MD data and compared with the approximation using Equation (6.3) for (a) $N = 105$ and (b) $N = 405$.

Temperature Dependence of Fractional Free Volume

Similar to the analysis in the previous section of using the solution of the integral equation for obtaining the temperature dependence of fractional free volume, we are also interested in the temperature dependence of $g(r)$ and f from MD simulation. In the MD simulation of ring PE with $N = 80$, the temperature of the system gradually decreased from $T = 450$ K to $T = 370$ K. The procedures were exactly the same as the previous section, i.e., to determine f as a function of T using intermolecular and intramolecular radial distribution functions, as well as the GvdW equation of state. In the calculation of the temperature dependence of f of ring PE with $N = 80$ from MD data, as the integral $\int_0^{l_b} I_b(r)dr$ can completely mask the contribution from $\int_0^{r^+} I(r)dr$ when temperature changes, it was neglected in Equation (6.33) and a volume of $\frac{\pi r_c^2 l_0}{4}$ is subtracted from the resultant $\langle v_{f,i} \rangle$. Figure 6.12 shows the temperature dependence of $g(r)$ as well as f in ring PE with $N = 80$. Interestingly, in such way, the resultant f is still close to that determined using Equation (6.33) when the integral $\int_0^{l_0} I_b(r)dr$ is included, which is approximately $f = 0.35$ at $T = 450$ K. It was found that the temperature dependence of $g(r)$ in MD simulation is similar to that of the PRISM theory, that the first peak of $g(r)$ decreases with temperature as ρ_b decreases with

temperature, whereas the data of f were fitted to $f = C_1 + C_2T$ with $C_1 = -0.04$ and $C_2 = 8.74 \times 10^{-4} \text{ K}^{-1}$. Compared with the PRISM theory, f is a slightly weaker function of temperature in MD simulation. Notably, $C_2 = 8.74 \times 10^{-4} \text{ K}^{-1}$ (cf., Figure 6.12(b)), which is the thermal expansion coefficient, obtained from the MD data is closer to the extrapolated value (i.e. $8 \times 10^{-4} \text{ K}^{-1}$ as mentioned in Section 4.1.2) from Huang *et al.* [93].

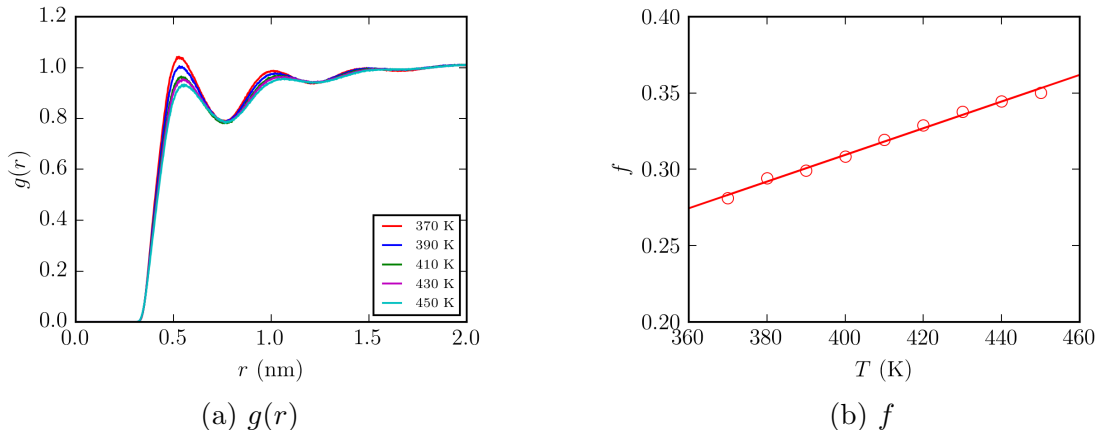


Figure 6.12: Temperature dependence of (a) $g(r)$ as well as (b) f of ring PE with $N = 80$ obtained from MD simulation. The data reported in (b) were fitted to the relation $f = C_1 + C_2T$ with $C_1 = -0.04$ and $C_2 = 8.74 \times 10^{-4} \text{ K}^{-1}$.

6.4.3 Center-of-Mass Diffusion Coefficient

In the MD simulation, evaluation of D_{cm} is achieved by analyzing the mean-square displacement (MSD) of the center-of-mass of the ring PE in the regime that $g_{cm}(t) \sim t$.

$$g_{cm}(t) = \lim_{t \rightarrow \infty} \langle [\mathbf{r}_{cm}(t) - \mathbf{r}_{cm}(0)]^2 \rangle = 6D_{cm}t \quad (6.35)$$

Log-log plots of $g_{cm}(t)$ of the center-of-mass of the ring PEs with $N = 30$ and $N = 405$ are shown in Figure 6.13. The linear curve as shown in the plot then allows us to extract D_{cm} , which is related to the y -intercept of the linear curve. The slopes in the cases of $N = 30$ and $N = 405$ are 1.00 and 1.04, respectively, which was also observed by several other groups [6, 94, 2]. It is important to note that in the curve fitting, only the data points from 10 ns to 15 ns, as well as from 400 ns to 510 ns were used. This is because as indicated in Equation (6.35), $g_{cm}(t)$ is a time-average property. The number of samples for the time averaging in Equation (6.35) decreases when time increases. Owing to this, the data points collected near

the end of the MD simulation were excluded from the determination of D_{cm} .

Although we are only interested in the regime that $g_{cm} \sim t$, it is worthwhile to report the fact that two regimes were observed for both ring PEs with $N = 30$ and $N = 405$. For $N = 30$, the two regimes are $g_{cm}(t) \sim t^{0.69}$ and $g_{cm}(t) \sim t$, whereas for $N = 405$, they are $g_{cm}(t) \sim t^{0.42}$ and $g_{cm}(t) \sim t$. The exponent of 0.69 in ring PE $N = 30$, as observed in the first regime, is in good agreement with that reported by Brás *et al.* [94] and Halverson *et al.* [6], in which they observed an exponent of 0.79 and 0.75 in the first regime, respectively. The weaker time dependence in the first regime for larger N was also reported by Halverson *et al.*[6]. In addition, the relation of $g_{cm}(t) \sim t^{0.42}$ in the first regime, is in better agreement with Hur *et al.* [2].

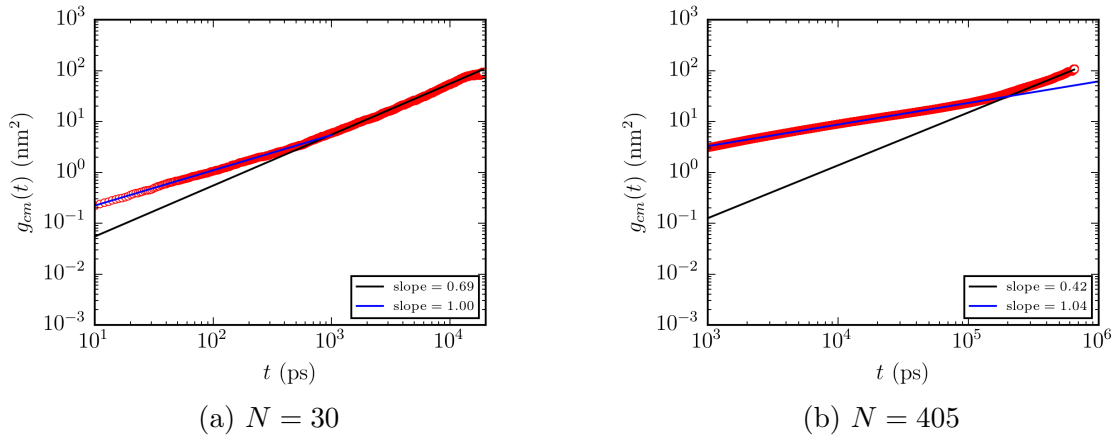


Figure 6.13: Log-log plots of $g_{cm}(t)$ of ring PEs with $N = 30$ and $N = 405$. The slopes and the y -intercepts of the black linear curves are 1.00 and $5.45 \times 10^{-3} \text{ nm}^2$, as well as 1.04 and $9.58 \times 10^{-5} \text{ nm}^2$, for $N = 30$ and $N = 405$, respectively, which were then used in the calculation of D_{cm} .

N Dependence

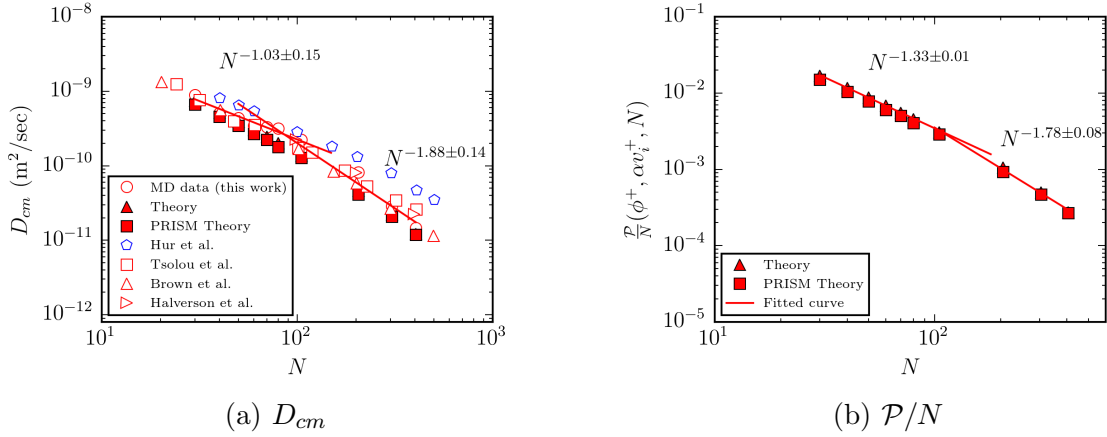


Figure 6.14: N dependence of (a) D_{cm} and (b) \mathcal{P}/N of ring PE melts. D_{cm} calculated from our MD simulation and theory are compared with Hur *et al.* [2, 3], Tsolou *et al.* [4], Brown *et al.* [5] and Halverson *et al.* [6].

D_{cm} s of ring PE melts that were determined from the MD simulation data are plotted as a function of ring size as shown in Figure 6.14(a). There is a clear crossover in D_{cm} from $D_{cm} \sim N^{-1.03 \pm 0.15}$ in the unentangled regime to $D_{cm} \sim N^{-1.88 \pm 0.14}$ in the entangled regime. The crossover ring size N_c is approximately $N_c \approx 100$. D_{cm} s at different ring sizes calculated using our theory are in good agreement with the MD simulation data, for $\phi^+ = 0.17$. Interestingly, compared with the MD simulation results of linear PE in our previous work, the exponent of the N dependence is slightly less negative in ring PE for both entangled and unentangled regimes. This indicates that the D_{cm} of rings is lower than the D_{cm} for their linear counterparts below N_c , but higher above N_c . This is well captured by our theory, and it is in good qualitative agreement with Robertson and Smith [80] as well as Chapman *et al.* [81]. They found that in the entangled regime, pure cyclic DNAs diffuse faster than their pure linear counterparts. We postulate that such good agreement is due to the following two reasons:

1. **Below N_c :** The N dependence of D_{cm} is not that sensitive to the values of ϕ^+ . It is worthwhile to note that below N_c , the probability of getting sufficient free volume for diffusion (F) in linear PE melts is higher than its ring counterparts. This leads to a higher mean value of $P_d(\phi)$ distribution in linear PE, which gives higher values of $\int_{\phi^+}^1 P_d(\phi) d\phi$ and

D_{cm} .

2. **Above N_c :** From the MD simulation results, the values of ϕ^+ are 0.22 and 0.17 for linear and ring PEs, respectively. One natural consequence of our free volume theory is that a stronger N dependence of D_{cm} in high- N region is resulted as we arbitrarily increase the value of ϕ^+ . The parameter ϕ^+ in our free volume theory is the fraction of beads of a ring PE having sufficient free volume for diffusion. This parameter is incorporated in our free volume theory because the diffusive movement of one bead can activate diffusion of its neighbours as they interact with one another through intramolecular potential. In other words, in a PE melt, the intermolecular force acting upon one of its carbon atoms can alter its intramolecular interaction with another bead of the same macromolecule. A smaller value of ϕ^+ in ring PE tells us that diffusive motion of beads can activate their neighbours much more readily than its linear counterpart.

The data in this work were compared with the data from Hur *et al.* [2, 3], Tsolou *et al.* [4], Brown and Szamel [5], and Halverson *et al.* [6] as shown in Figure 6.14(a). Since the data from Brown and Szamel [5] and Halverson *et al.* [6] were generated from Monte Carlo simulation and MD simulation in reduced units, respectively, their data were in reduced unit. Therefore, the center-of-mass diffusion coefficients from their work (D_{cm}^d) were firstly normalized by $D_{cm,max}^d$, where the subscript *max* indicates the largest D_{cm}^d in their data set, and it was then multiplied by a factor of $[D_{cm}(N = 30)] \times 30$ as obtained from our MD data. As Tsolou *et al.* [4] performed MD simulation also, their D_{cm} s were included directly for comparison with our data in Figure 6.14(a). As shown in Figure 6.14(a), our MD data agree well with the MD simulation by Tsolou *et al.* [4], Monte Carlo simulation by Brown and Szamel [5], as well as the MD simulation by Halverson *et al.* [6]. A significant discrepancy is only observed when our data are compared with that of Hur *et al.* [2, 3] as shown in Figure 6.14(a).

\mathcal{P}/N obtained from the theory ($\mathcal{P} = \int_{\phi^+}^1 P_d(\phi)d\phi$) is also plotted as a function of N in Figure 6.14(b). A clear crossover was also observed from $\mathcal{P}/N \sim N^{-1.33 \pm 0.01}$ to $\mathcal{P}/N \sim N^{-1.78 \pm 0.08}$. The exponent of N dependence of \mathcal{P}/N is slightly more negative and less negative in the unentangled and entangled regime, respectively, when compared with that of D_{cm} from MD simulation. Similarly, if the parameters obtained from the PRISM theory are plugged

into our free volume theory, the N dependence of D_{cm} and \mathcal{P}/N are also in good agreement with that obtained using the MD simulation data. Nonetheless, for the PRISM theory, ϕ^+ was found to be $\phi^+ = 0.47$, which is much higher than that from MD simulation. This is because the influence of angle bending and torsion potentials on the D_{cm} s is included explicitly in MD simulation, but not in the intramolecular radial distribution function in the PRISM theory. Therefore, for the PRISM theory to ‘capture’ the effect of these angle potentials in the calculation of D_{cm} , a higher value of ϕ^+ is resulted, indicating that the ideal chain used in the PRISM theory should have had more beads participating in the activation of diffusion due to the negligence of angle potentials.

Temperature Dependence

The temperature dependence of D_{cm} of n -alkane has been studied thoroughly by von Meerwall *et al.* [60, 1]. In their work [60, 1], it was argued that the apparent activation energy (E_a^{app}) derived from the experimental data can be divided into two contributions: 1. the energy required for the expansion of the free volume 2. the energy required for the activation of segmental jump. In our previous work of linear PE, the second contribution can be alternatively understood as the energy required to create the critical free volume for the activation of diffusion of $N\phi^+$ beads (this amount of energy is denoted as E_a). This amount of energy can be calculated as the value of ϕ^+ is known (cf., Figure 6.14). It has been proven both experimentally and numerically that E_a^{app} of linear PE ranges from 2.5 kcal · mole⁻¹ to 6 kcal · mole⁻¹.

Nonetheless, to our knowledge, there are only a very limited number of studies on temperature dependence of diffusion coefficients of ring PE. In the work by Alatas *et al.* [91] and von Meerwall *et al.* [90], they did not report the value of E_a for ring alkane because they only determined two D_{cm} s at 328 K and 338 K for $N = 5 - 16$ ($N = 80$ was chosen for temperature dependence investigate in this work), in which the calculation of apparent activation energy from only two data points is expected to be inaccurate. Also, von Meerwall *et al.* [90] did not extract E_a from their experimental data because of the failure of their empirical model in the absence of chain ends. (direct quotation: ‘In the absence of chain ends, this behavior cannot be explained by Eq. 6 with substitution of Eq. 2.’[90])

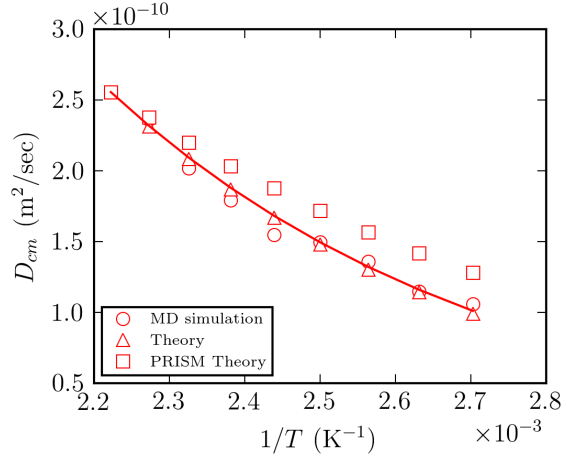


Figure 6.15: Temperature dependence of D_{cm} of ring PE with $N = 80$. $\phi^+ = 0.17$ for MD simulation and $\phi^+ = 0.47$ for the PRISM theory. The solid line is the fitting curve to the MD data, which has the form of $D_{cm}(T) = D_{cm}(T') \exp \left[-E_a^{app} \left(\frac{1}{RT} - \frac{1}{RT'} \right) \right]$, with $E_a^{app} = 3.84 \text{ kcal} \cdot \text{mole}^{-1}$.

Owing to the lack of literature data of the temperature dependence of ring PE, MD simulation of ring PE at different temperatures were performed, and it was found that by fitting the MD data to the Arrhenius formula, E_a^{app} of $N = 80$ ring PE has a value of $E_a^{app} \approx 3.84 \text{ kcal} \cdot \text{mole}^{-1}$ (cf., Figure 6.15). According to von Meerwall *et al.* [1], the temperature dependence of D_{cm} of linear alkanes can be described by the following:

$$D_{cm}(T) = D_{cm}(T') \exp \left(-\frac{1}{f} + \frac{1}{f'} \right) \exp \left[-E_a \left(\frac{1}{RT} - \frac{1}{RT'} \right) \right] \quad (6.36)$$

von Meerwall *et al.* [90] was unable to use Equation (6.36) to describe influence of temperature on the N dependence of D_{cm} of cyclic alkane at 328 K and 338 K. However, we found that Equation (6.36) is still applicable to account for the temperature dependence of D_{cm} of ring PE with a particular N . Note that the first term of Equation (6.36) can be found in the above free volume analysis in the integral equation and MD simulation. E_a can be then calculated by the following formula:

$$E_a = p_{eff} \left[\phi^+ \alpha v_i^+ + (1 - \phi^+) \langle v_{f,i} \rangle \right] \quad (6.37)$$

$p_{eff} = p + A\rho_b^2$ can be calculated with the knowledge of the GvdW parameter A based on the above free volume analysis. Equation (6.37) also implies E_a is dependent on ρ_b and T . We found that based on $g(r)$ and $g^{intra}(r)$ obtained from the MD simulation with ϕ^+ set to be

0.17, the temperature dependence of D_{cm} of ring PE $N = 80$ agrees well with that evaluated using Equation (6.36) and Equation (6.37) (cf., Figure 6.15). Nonetheless, the temperature dependence of D_{cm} predicted by using the parameters obtained from the PRISM theory does not agree well with the MD simulation data. This is because in the PRISM theory, f changes with temperature more dramatically than that observed in the MD simulation. This is supported by our free volume analysis in Section 4.1.2 and Section 4.2.3, in which we showed that the thermal expansion coefficient was higher in the PRISM theory. The effective pressure in an ideal PE melt is much lower than that in the MD simulation, in which intramolecular and intermolecular potentials were explicitly included, which gives a higher value of ϕ^+ in the PRISM theory.

The future plan of our research is as follows:

1. Even in the absence of chain ends, the exponent of the N dependence of D_{cm} for cyclic alkanes can be significantly influenced by temperature [90]. Our free volume theory should be able to account for this anomaly as it is expected that the mean value of $P_d(\phi)$ distribution should increase with increasing temperature.
2. The free volume theory that we proposed may be modified so as to predict the diffusivities of a blend of linear and ring PE, and PE in a dilute solution.
3. We also envisage that the free volume analysis presented in this work is useful in the derivation of a theory based on the distribution of free volume on viscoelastic properties and the relaxation dynamics of polymer melts and solution, which have been studied even more extensively than diffusivities [84, 79, 95].

6.5 Conclusion

In conclusion, our free volume theory describes the crossover in the ring size dependence of D_{cm} of ring PE melts from unentangled to entangled regimes without the concept of entanglements and obstacles as introduced in the reptation theory. The parameters in our free volume theory can be theoretically determined using either the PRISM theory, or more

accurately, MD simulation. In particular, in MD simulation, Voronoi tessellation analysis can be performed to obtain accurate values of the probability for a bead to find free volume. ϕ^+ , which is a parameter in our free volume theory, is related to the segmental E_a for activation of diffusion and it can also be used to predict the temperature dependence of D_{cm} of ring PE melts. It was found that although the PRISM theory is computationally less expensive than MD simulation, it is less accurate than that of MD simulation when it comes to predicting the temperature dependence of D_{cm} of ring PE melts due to the slightly higher thermal expansion coefficient obtained by calculation in the PRISM theory.

Chapter 7

A Theory for the Temperature Effect on the Chain Length Dependence of the Diffusivity of Oligomers¹

7.1 Introduction

The temperature dependence of the diffusion coefficient of monoatomic liquids is well described by the simple Cohen-Turnbull free volume theory [59]:

$$D = D_0 \exp\left(-\frac{\alpha v^+}{\langle v_f \rangle}\right) \quad (7.1)$$

v^+ is the critical free volume for the activation of diffusive motion, which is approximately the size of the particle. Here, $\langle v_f \rangle$ is the mean free volume and is temperature dependent, and α is the overlapping parameter. D_0 is the Chapman-Enskog diffusion coefficient of dilute gas, which has the following form [10]:

$$D_0 = \frac{3}{8\rho_1 r_c^2} \sqrt{\frac{1}{m\pi\beta}} \quad (7.2)$$

$\beta = \frac{1}{k_b T}$, where k_b is the Boltzmann constant and T is the temperature. ρ_1 is the extrapolated number density of the particle. r_c is the minimum incompressible diameter of the particle. m is the mass of the particle.

Nonetheless, the success of such theory has been undermined by the fact that it is empirical in nature that many parameters in the model can only be obtained by fitting it to

¹A version of this chapter has been published in *Soft Matter*, 2020, 16, 4283-4289.

the experimental data, instead of being derived from first principle. Owing to this, there has been impressive effort made in determining parameters, such as $\langle v_f \rangle$, α and v^+ , with the use of intermolecular radial distribution function $g(r)$ as well as the equation of state [64, 65, 62, 67, 66]. In this way, $g(r)$ can be easily obtained using integral equation method or more accurately derived from Monte Carlo and molecular dynamics (MD) simulations. The former method is more appealing that the calculation is not computationally expensive, whereas the latter gives more accurate results.

The conventional and famous Rouse model [20] predicts that D_{cm} of short polymers with any structures follows the relation $D_{cm} \sim N^{-1}$. However, it has been argued that the chain length dependence of the center-of-mass diffusion coefficient of n -alkane does not indeed agree with that of the Rouse model with the N dependence exponent being slightly more negative than -1 [60, 1]. In addition, in the Rouse model, $D_{cm} \sim N^{-1}$ and the exponent is not dependent on the temperature, but it was experimentally demonstrated that the exponent becomes less negative with increasing temperature. It is worth noting that the Rouse model was not originally derived for describing the diffusion of polymer melts. In fact, it is a model for a single chain (i.e., at infinite dilution) diffusing in a continuous medium of solvent based upon the concept of Brownian dynamics [20]. The chain is modeled by a series of beads connected by springs and the solvent medium exerts friction, which is quantified by a temperature independent friction coefficient, on the beads. In the Rouse model, the many-chain effect is not included. However, one could argue that the many-chain effect is implicitly included through the use of friction coefficient. Nonetheless, the Rouse model fails to predict the chain length dependence of the diffusion coefficient for dilute polymer solutions. Zimm [96] introduced the hydrodynamic interaction to the Rouse model and yielded the correct chain length dependence. Interestingly, the Rouse model predicts the chain length dependence correctly for unentangled polymer melts. Since the friction coefficient is temperature independent in the Rouse model, it is not able to predict the temperature effect on the chain length dependence of the diffusion coefficient. von Meerwall *et al.* [1] then attributed this observation to the chain end effect, and they determined empirically the fractional free volume in the melt at different temperatures. Nonetheless, their free volume model contains many adjustable parameters [1] and it is not applicable to cyclic alkane [90].

Recently, our group has developed a free volume theory for the diffusivity of linear polymer

[85], which is a consolidation of the proposition first demonstrated by Sabbagh and Eu [61]. In such model, the probability for one of the beads of the polymer chain to find sufficient volume for diffusion (F) is firstly calculated with the use of radial distribution functions and the generic van der Waals equation derived by Eu [64]. After that, the distribution of fraction of beads having that amount of volume ($v_i \geq \alpha v_i^+$, $v_i^+ = \frac{\pi r^+{}^3}{6}$ that r^+ is the effective diameter of the bead, α is the overlapping parameter) can be derived (P_d) and is found to follow a Poisson distribution. Since the total volume of a material is the sum of the van der Waals volume of the constituent molecules (temperature independent) and the free volume (temperature dependent), our free volume theory should capture the temperature effect on the scaling of the diffusion coefficient of unentangled polymer melts. Similar to the intuition of Cohen and Turnbull [59], diffusive motion of polymer is activated when the fraction of beads having $v_i \geq \alpha v_i^+$ (ϕ) greater than a certain value (ϕ^+ and it is related to the activation energy for segmental diffusion of polymers). Otherwise, there would have been no diffusive motion. Therefore, the diffusion coefficient of polymer (D_{cm}) averaged over all possible values of ϕ is:

$$D_{cm} = \frac{D}{N} \int_{\phi^+}^1 P_d(\phi) d\phi \quad (7.3)$$

The reader can find more details in the derivation of Equation (7.3) in our previous work [85]. This model was found to be successful in describing the crossover in the N dependence of diffusivity of polyethylene at $T = 450$ K, i.e., from $D_{cm} \sim N^{-1.5}$ in the unentangled regime to $D_{cm} \sim N^{-2.2}$ in the entangled regime. We argue that Equation (7.3) should also capture the temperature dependence of the exponent in the N dependence of D_{cm} of n -alkanes because F and P_d should alter accordingly as temperature changes, and thus influencing the exponent v in $D_{cm} \sim N^v$. In this work, the radial distribution functions were derived from the integral equations of polymers due to the simplicity of such model and the resultant pressure equation, compared with that in MD simulations. Equation (7.3) was then tested against the experimental results of von Meerwall *et al.* [1].

7.2 Integral Equation Theory of Polymers

The integral equation for polymers proposed by Schweizer and Curro [97] is as follows:

$$\mathbf{H}(r) = \int d\mathbf{r}_1 \int d\mathbf{r}_2 \Omega(|\mathbf{r} - \mathbf{r}_1|) \mathbf{C}(|\mathbf{r}_1 - \mathbf{r}_2|) [\Omega(r_2) + \rho \mathbf{H}(r_2)] \quad (7.4)$$

To use propane as an example, if we simply model the methylene and methyl groups as beads, then we have $N = 3$:

$$\mathbf{H} = \begin{bmatrix} h_{11} & h_{12} & h_{13} \\ h_{21} & h_{22} & h_{23} \\ h_{31} & h_{32} & h_{33} \end{bmatrix} \quad (7.5)$$

$$\mathbf{C} = \begin{bmatrix} c_{11} & c_{12} & c_{13} \\ c_{21} & c_{22} & c_{23} \\ c_{31} & c_{32} & c_{33} \end{bmatrix} \quad (7.6)$$

$$\mathbf{\Omega} = \begin{bmatrix} \omega_{11} & \omega_{12} & \omega_{13} \\ \omega_{21} & \omega_{22} & \omega_{23} \\ \omega_{31} & \omega_{32} & \omega_{33} \end{bmatrix} \quad (7.7)$$

$h_{\alpha\gamma} = g_{\alpha\gamma} - 1$, where $g_{\alpha\gamma}$ is the intermolecular radial distribution function between sites α and γ of two different molecules. $c_{\alpha\gamma}$ is the direct correlation function. $\omega_{\alpha\gamma}$ is the intramolecular radial distribution function between sites α and γ of the same molecule. ρ is the number density of the whole alkane molecule. Then, in Fourier space, the equation becomes:

$$\hat{\mathbf{H}}(k) = \hat{\mathbf{\Omega}} \hat{\mathbf{C}} \hat{\mathbf{\Omega}} + \hat{\mathbf{\Omega}} \hat{\mathbf{C}} \hat{\mathbf{H}} \rho \quad (7.8)$$

Then, algebraic rearrangement allows us to write:

$$\hat{\mathbf{H}} = (\mathbf{I} - \rho \hat{\mathbf{\Omega}} \hat{\mathbf{C}})^{-1} \hat{\mathbf{\Omega}} \hat{\mathbf{C}} \hat{\mathbf{\Omega}} \quad (7.9)$$

\mathbf{I} is a $N \times N$ identity matrix. The whole model is completed by the Percus-Yevick closure relation:

$$c_{\alpha\gamma}(r) = \left\{ \exp[-\beta u_{\alpha\gamma}(r)] - 1 \right\} [1 + h_{\alpha\gamma}(r) - c_{\alpha\gamma}(r)] \quad (7.10)$$

$u_{\alpha\gamma}$ is the intermolecular potential, for which we have used 6-12 Lennard Jones (LJ) potential in this work.

$$u_{\alpha\gamma}(r) = 4\varepsilon_{\alpha\gamma} \left[\frac{\sigma_{\alpha\gamma}^{12}}{r^{12}} - \frac{\sigma_{\alpha\gamma}^6}{r^6} \right] \quad (7.11)$$

$\varepsilon_{\alpha\gamma}$ and $\sigma_{\alpha\gamma}$ are the potential well and distance at $u_{\alpha\gamma} = 0$, respectively between sites α and γ . These interaction parameters are taken from Martin *et al.* [19]. With these, the final

average intermolecular radial distribution ($g(r)$) is as follows:

$$g(r) = \frac{1}{N^2} \sum_{\alpha} \sum_{\gamma} g_{\alpha\gamma}(r) \quad (7.12)$$

It is computationally expensive to solve the Equation (7.8) as N is large. Therefore, the following approximation may be applied, in which the chain ends are neglected.

$$\hat{h} = \frac{\hat{\omega}\hat{c}}{1 - \rho_b\hat{\omega}\hat{c}} \quad (7.13)$$

$\rho_b = \rho/N$. Such that:

$$h(r) = \frac{1}{N^2} \sum_{\alpha} \sum_{\gamma} h_{\alpha\gamma}(r) \quad (7.14)$$

$$\omega(r) = \frac{1}{N} \sum_{\alpha} \sum_{\gamma} \omega_{\alpha\gamma}(r) \quad (7.15)$$

Gaussian approximation gives:

$$\hat{\omega}_{\alpha\gamma}(k) = \exp(-nk^2d^2/6) \quad (7.16)$$

And:

$$\hat{\omega}(k) = \frac{1 - f^2 - 2N^{-1}f + 2N^{-1}f^{N+1}}{(1 - f)^2} \quad (7.17)$$

where n is the number of bonds in between site α and site γ . d is the statistical segmental length, for which we assume $d = \sigma_{\alpha\gamma}$, such that $f = \exp(-k^2d^2/6)$. Additionally, in our calculations, the ρ_b s of alkane at different chain length and temperature from von Meerwall *et al.* [1] were used, which were evaluated using Equation (7.18).

$$\rho_b = 43 \left[0.00076T + 0.93 + \frac{2(0.060T - 2.5)}{M} \right]^{-1} \quad (7.18)$$

M is the molecular weight of the alkane with the unit of $g \cdot \text{mole}^{-1}$ and T has the unit of K.

The discrete Fourier transform method and the corresponding inverse transform method are exactly the same as that were used by Martin *et al.* [88]. For example, the Fourier transformation of g can be determined as follows:

$$\hat{g}_j = 4 \sum_{i=0}^{N_s-1} \pi r_i \Delta r g_i \sin \left[\frac{\pi(j+1)(2i+1)}{2N_s} \right] \quad (7.19)$$

whereas, the corresponding inverse transformation is:

$$g_i = \frac{k_{N_s-1} \Delta k}{4\pi^2} (-1)^i \hat{g}_{N_s-1} + \frac{1}{2\pi^2} \sum_{j=0}^{N_s-2} k_j \Delta k \hat{g}_j \sin \left[\frac{\pi(2i+1)(j+1)}{2N_s} \right] \quad (7.20)$$

N_s is the size of the array.

7.2.1 Validity of Neglecting Chain Ends

As a test of the validity of neglecting the chain ends, by using $N = 3$ and $\rho_b = 30$, Equation (7.8) and Equation (7.13) were solved numerically using Picard method. In Equation (7.13), it is assumed that all the beads interact with one another via 6-12 LJ potential with the same parameters that all the beads were assumed to be methylene groups, whereas in Equation (7.8), the exact 6-12 LJ potential parameters for methyl-methyl, methylene-methylene and methyl-methylene intermolecular interactions were explicitly included. As shown in Figure 7.1, the solution to Equation (7.8) closely resembles to that to Equation (7.13). As it can be expected as $N \rightarrow \infty$, the chain end effect becomes even more trivial, Equation (7.13) is used in this work.

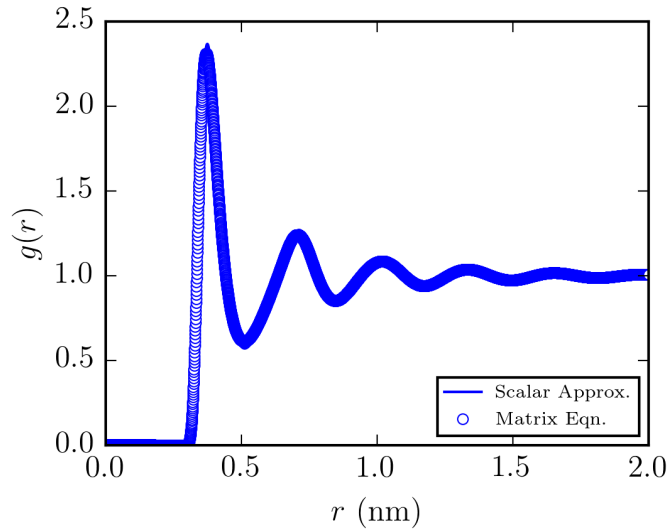


Figure 7.1: $g(r)$ derived from Equation (7.8) and Equation (7.13). The scalar approximation in Equation (7.13) is indeed accurate.

7.3 A Brief Introduction of Free Volume Theory

Consider a linear oligomer, each of its beads possesses certain amount of free volume. Due to many-chain effect, at a particular instant, some beads have free volume ($v_{f,i}$) greater than the activation volume (αv_i^+) for diffusion, some others do not. The probability for a bead to get $v_{f,i} \geq \alpha v_i^+$ is $F_{ct} = \exp(-\frac{\alpha v_i^+}{\langle v_{f,i} \rangle})$. Assuming that the chain ends always have enough

free volume for diffusion, we can calculate the fraction of beads of the chain, which have $v_{f,i} \geq \alpha v_i^+$, as $\phi = \frac{n_f}{N-2}$, where n_f is the number of beads having $v_{f,i} \geq \alpha v_i^+$. The number of ways arranging n_f beads of the chain molecule can be calculated as follows:

$$W = \frac{(N-2)!}{(N-n_f-2)!n_f!} \quad (7.21)$$

This is because the beads are distinguishable from one another. Then, the probability distribution of the chain having n_f , which is essentially P_d , is:

$$P_d = \frac{(N-2)!}{(N-n_f-2)!n_f!} F_{ct}^{n_f} (1-F_{ct})^{N-2-n_f} \quad (7.22)$$

We would like to rewrite Equation (7.22) in terms of ϕ and F_{ct} . This can be done using Stirling principle (i.e. $a! \approx \sqrt{2\pi a} [\frac{a^a}{\exp(a)}]$), which finally leads to:

$$\ln P_d = (N-2) \ln \left[\left(\frac{1-F_{ct}}{1-\phi+\varepsilon} \right)^{1-\phi} \left(\frac{F_{ct}}{\phi+\varepsilon} \right)^\phi \right] - \frac{1}{2} \ln \left[2\pi(N-2)\phi(1-\phi) + \exp\left(-\frac{\phi^2}{\varepsilon^2}\right) + \exp\left[-\frac{(\phi-1)^2}{\varepsilon^2}\right] \right] + \ln(c) \quad (7.23)$$

ε is a small number in the order of magnitude of 10^{-5} , which ensures numerical stability, whereas c is the normalization constant, such that $c = (\int_0^1 \tilde{P}_d d\phi)^{-1}$, where \tilde{P}_d is not normalized. There are three terms in Equation (7.23), the last term is for normalization, whereas the first two terms are consequences of the Stirling approximation. In the second term, $\exp(-\phi^2/\varepsilon^2) + \exp[-(\phi-1)^2/\varepsilon^2]$ are arbitrarily included as the Stirling principle is not accurate as $\phi = 0$ or $\phi = 1$. Hence, the first two terms capture the statistical arrangement and distribution of activation volume along the chain. The resultant $P_d(\phi)$ distribution in Equation (7.23) can be then input in the calculation of D_{cm} using Equation (3). More detailed derivation of $P_d(\phi)$ can be found in our previous work [85].

7.4 Calculation of Parameters and Comparison with Experimental Data

If we neglect the intramolecular contribution, the pressure equation for Gaussian polymer chains is as follows [73]:

$$\frac{p\beta}{\rho_b} = 1 - \frac{2\pi\beta\rho_b}{3} \int_0^\infty r^3 \frac{du}{dr} g(r) dr \quad (7.24)$$

A function $I(r)$ can be defined to extract important length scales, such as the hard-core diameter (r_c), cavity diameter (r^+). $I(r)$ is expressed in Equation (7.25). $g(r)$ and $I(r)$ at

different temperatures are plotted in Figure 7.2 and Figure 7.3, respectively, for oligomer with $N = 30$ as an example.

$$I(r) = -r^3 \frac{du}{dr} g(r) \quad (7.25)$$

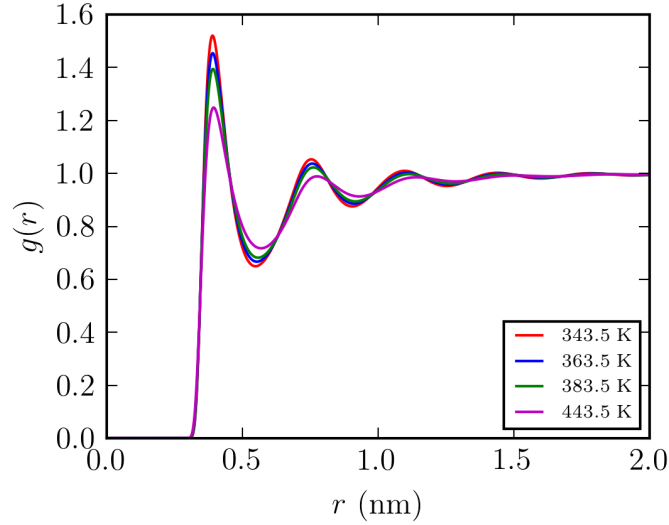


Figure 7.2: $g(r)$ at different temperatures for alkane with $N = 30$.

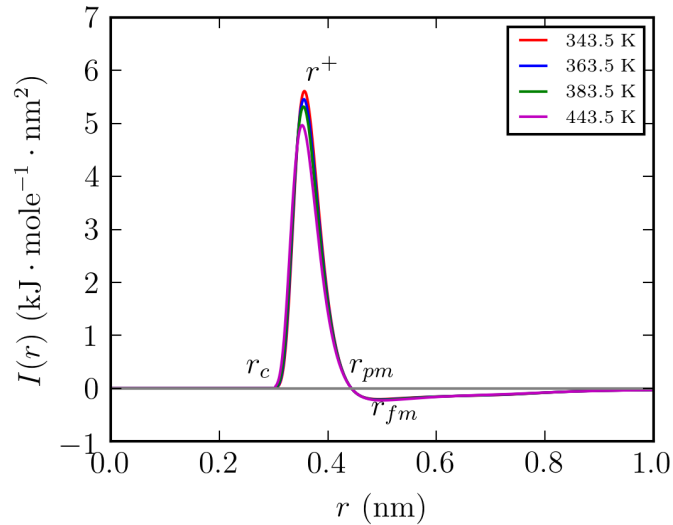


Figure 7.3: $I(r)$ at different temperatures for alkane with $N = 30$.

The physical meaning of the length scales as shown in Figure 7.3 have been discussed in our previous work and Laghaei *et al.* [65]. Briefly, the possibility of beads having en-

countered a large repulsive energy is the highest at r^+ , and thus it can be interpreted as the minimum size of cavity for accomodating a bead, whereas r_c corresponds to the minimum and incompressible diameter of the bead. r_{fm} and r_{pm} are the diameters at force and potential minima, respectively. These length scales do not vary much with temperature. It was found that $r_c \approx 0.305$ nm, $r^+ \approx 0.354$ nm, $r_{pm} \approx 0.444$ nm and $r_{fm} \approx 0.524$ nm. These length scales are important because they allow us to calculate the overlapping parameter $\alpha = (1 - \frac{|r_{pm} - r_{fm}|}{r^+})^3 \approx 0.464$ as well as the effective bead size $v_i^+ = \frac{\pi r^+{}^3}{6} \approx 0.0232$ nm³, and finally the probability for a bead to find sufficient activation volume (αv_i^+) for diffusion. Such probability is denoted as F_{ct} , which has an exponential form of $F_{ct} = \exp(-\alpha v_i^+ / \langle v_{f,i} \rangle)$ following the rationale of Cohen and Turnbull [59]. The calculated F_{ct} at different chain lengths of alkane and temperatures are plotted and fitted to an empirical form of $C_1/N + C_2$ in Figure 7.4. The fitting procedure allows us to extrapolate and obtain the value of $F_{ct}(N \rightarrow 1)$, which is necessary in the calculation of D using Equation (7.1). Another important feature is that F_{ct} decreases with increasing N and increases with increasing T . The former is attributed to chain end effect, whereas the latter is due to the expansion of free volume with temperature.

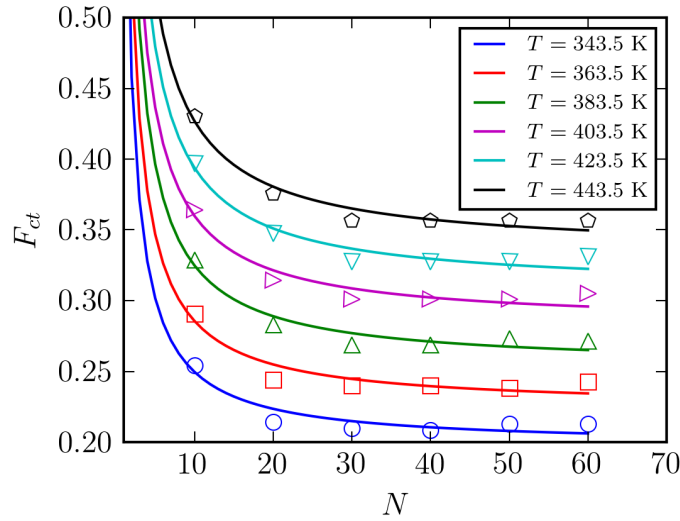


Figure 7.4: F_{ct} s at different chain lengths of alkane and temperatures, which were obtained from the free volume analysis. The markers are results from our calculations, and the solid lines are best fit to the data with the form: $C_1/N + C_2$. The values of C_1 and C_2 are: $C_1 = 0.52$, $C_2 = 0.2$ ($T = 343.5$ K); $C_1 = 0.61$, $C_2 = 0.22$ ($T = 363.5$ K); $C_1 = 0.72$, $C_2 = 0.25$ ($T = 383.5$ K); $C_1 = 0.77$, $C_2 = 0.28$ ($T = 403.5$ K); $C_1 = 0.86$, $C_2 = 0.31$ ($T = 423.5$ K); $C_1 = 0.93$, $C_2 = 0.33$ ($T = 443.5$ K).

To evaluate $\langle v_{f,i} \rangle$, the classic pressure equation can be recast in to the van der Waals equation of state, leading to a generic form, which was first demonstrated by Eu [64]:

$$(p + A\rho_b^2)(N - B\rho_b) = \rho_b\beta^{-1} \quad (7.26)$$

p is the pressure. The parameters A and B are expressed as follows:

$$A = -\frac{2\pi}{3} \int_{r^+}^{\infty} I(r)dr \quad (7.27)$$

$$B = \frac{1}{\rho_b} \left[N - \frac{1}{1 + \frac{2\pi\beta\rho_b}{3} \int_0^{r^+} I(r)dr} \right] \quad (7.28)$$

Such that:

$$\langle v_{f,i} \rangle = \frac{1}{\rho_b} (N - B\rho_b) \quad (7.29)$$

With F_{ct} obtained from the previous analysis, P_d distributions at different temperatures can be generated using the continuous approximation of P_d in Equation (7.23).

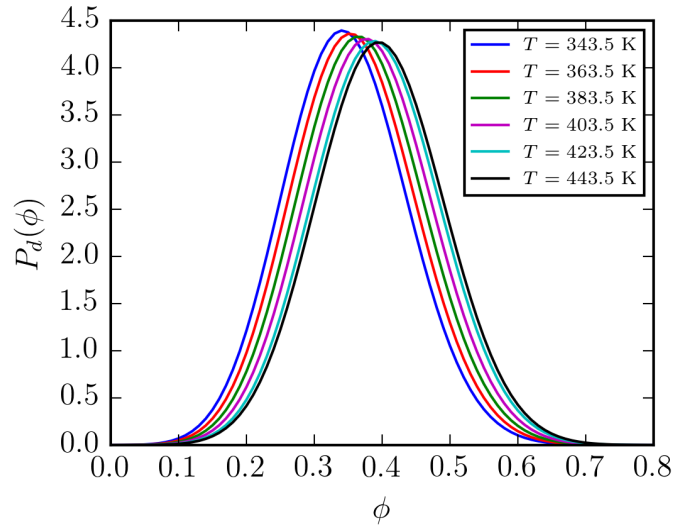


Figure 7.5: Effect of temperature on $P_d(\phi)$ distribution of oligomer with $N = 30$.

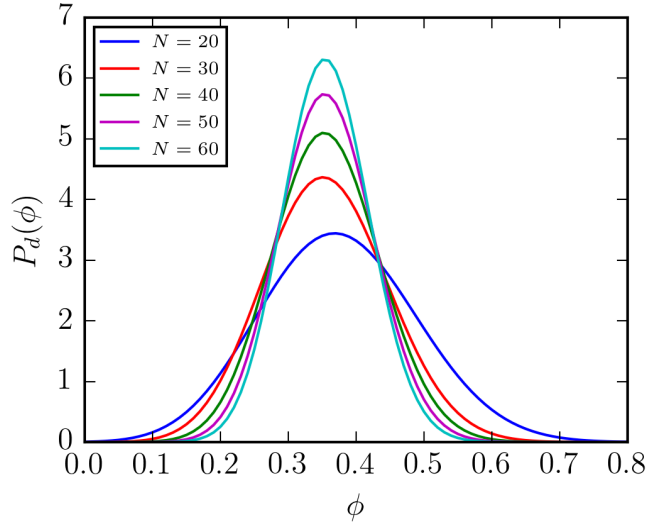


Figure 7.6: Effect of chain length on $P_d(\phi)$ distribution of oligomers at $T = 443.5$ K.

Figure 7.5 and Figure 7.6 show the effect of temperature and chain length on $P_d(\phi)$ distribution of oligomers with $N = 30$ and at $T = 443.5$ K, respectively. The P_d distribution shifts to a slightly higher average value of ϕ without any significant change in the peak width as temperature increases whereas at $T = 443.5$ K, as N increases, P_d distribution becomes narrower and moves to the left hand side of the plot. (cf., Figure 7.5 and Figure 7.6) This shows that as temperature increases, the average fraction of bead having sufficient activation free volume increases, which is in line with our intuition.

Our model is then tested against the N dependence of D_{cm} at different temperatures as observed by von Meerwall *et al.* [1]. As depicted in Figure 7.7, the linear curve was extracted directly from von Meerwall *et al.* [1], and the markers in the plot were generated from our free volume theory, whereas Figure 7.8 shows a plot of the magnitude of $\frac{1}{N} \int_{\phi^+}^1 P_d(\phi) d\phi$ computed using our free volume theory (markers) and fitted to the linear curves (solid lines) at different temperatures. ϕ^+ ranges from 0.33 at $T = 343.5$ K to 0.43 at $T = 443.5$ K. We are going to discuss the physical significance of these values of ϕ^+ s later in the next paragraph. In Figure 7.7 and Figure 7.8, we observed the exponent v is less negative with increasing temperature: $v = -2.53 \pm 0.06$, -2.32 ± 0.05 , -2.13 ± 0.05 , -1.94 ± 0.03 , -1.87 ± 0.04 , -1.78 ± 0.03 at $T = 343.5$ K, 363.5 K, 383.5 K, 403.5 K, 423.5 K, 443.5 K, respectively. This is similar to what has been reported by von Meerwall *et al.* [1] that $D_{cm} \sim N^{-1.85}$ at 443.5 K and

the exponent becomes more negative with decreasing temperature through $D_{cm} \sim N^{-2}$ at 403.5 K. With our obtained parameters, our model can describe the less negative exponent with increasing temperature in the N dependence of D_{cm} at different temperatures. Such behaviour is not captured by the Rouse model as it always gives the relation $D_{cm} \sim N^{-1}$ regardless of the temperature.

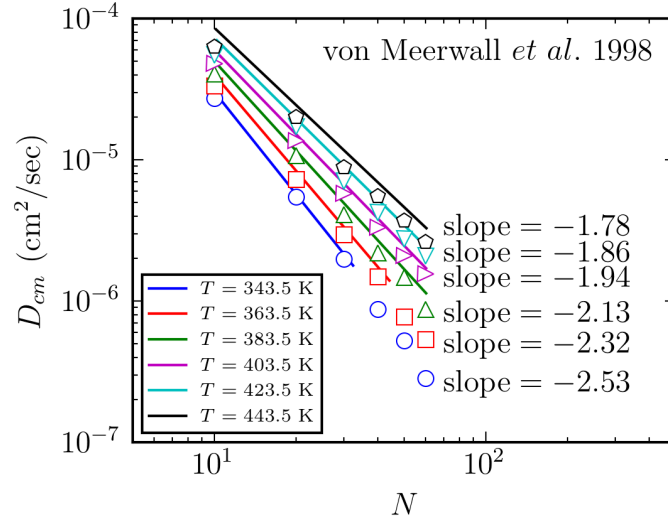


Figure 7.7: D_{cm} calculated using our free volume theory (markers) with that of the experimental data of von Meerwall *et al.* [1] (solid lines). The indicated slopes are the values calculated from our theory.

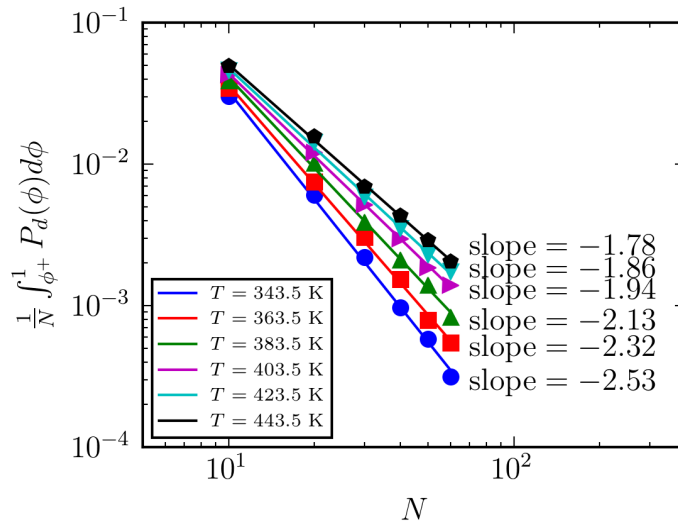


Figure 7.8: The magnitude of the integral $\frac{1}{N} \int_{\phi_+}^1 P_d(\phi) d\phi$ computed using our free volume theory at different temperatures (markers) fitted to the linear curves (solid lines).

As mentioned above, our theory (cf., Equation (7.3)) can capture both the N as well as temperature dependence of D_{cm} of alkane as measured by von Meerwall *et al.* [1], with ϕ^+ ranging from 0.33 at $T = 343.5$ K to 0.43 at $T = 443.5$ K. One may argue that ϕ^+ is an empirical parameter, but indeed it can be related to the activation energy of diffusion via the following formula [85]:

$$E_a = p_{eff} [\phi^+ \alpha v_i^+ + (1 - \phi^+) \langle v_{f,i} \rangle] \quad (7.30)$$

p_{eff} is the effective pressure, and it can be calculated using $p_{eff} = p + A\rho_b^2$. With Equation (7.30) as well as our calculated parameters, the E_a averaged over all chain lengths and temperatures ($\langle E_a \rangle$) was found to be $\langle E_a \rangle = 0.84 \pm 0.03$ kcal/mole, which is close to that empirically obtained by von Meerwall *et al.* [1] with $\langle E_a \rangle = 0.81 \pm 0.25$ kcal/mole. It is also pertinent to state that the higher value of ϕ^+ compared to that of the MD simulation results reported by Wong and Choi [85] is due to the fact that a Gaussian chain melt has a relatively lower p_{eff} than that of real chain melt. As a result, a higher value of ϕ^+ is expected from the Gaussian chain approximation so as to reflect the inflexibility of the chain in the reality. Interestingly, Bulacu and van der Giessen demonstrated that the flexibility of the chain can influence the exponent v [98, 27]. Such effect of flexibility is reflected in the ϕ^+ of our theory as this parameter defines the influence of a bead's diffusive motion on its neighbour. The change in flexibility of the molecule with temperature also implies that ϕ^+ is temperature dependent.

7.5 Conclusion

In summary, our free volume theory is successful in taking into account of the effect of temperature on the N dependence of D_{cm} of linear polymers, which is not captured by the classic Rouse model [20] and it is free of many adjustable parameters in the model proposed by von Meerwall *et al.* [1]. The reason for such robustness of our theory is that it has considered the change in the distribution of fraction of beads having sufficient activation volume for diffusion with temperature, i.e. such distribution slightly shifts to higher value as temperature increases, and thus this directly influences the final calculated values of D_{cm} . Most of the parameters in such theory can be easily obtained by the integral equation theory of polymer chains.

This work also gives insight to the dynamics of entangled polymers as it leads to questions, such as ‘Does the exponent also change with temperature in the entangled regime?’ One may argue that the temperature may have an effect on the density of the fixed obstacles in the surrounding of the chain, but the results of the reptation theory [50, 21] always give us an exponent of -2 regardless of the density of obstacles and the temperature. As it has been shown that our free volume theory can be applied to the entangled polymers at a particular temperature [85], it may not be surprising that it can also predict the change in the exponent with temperature for entangled polymers. However, without sufficient experimental data, this is merely our speculation. Owing to this, we decided to postpone such investigation in the future.

Chapter 8

Prediction of Crossover in the Molecular Weight Dependence of Polyethylene Viscosity Using a Polymer Free Volume Theory¹

8.1 Introduction

Transport phenomenon is a branch of physical science that deals with the rates of mass, momentum, and heat transfer. Conservation laws yield three separate transport equations in which transport coefficients, i.e., diffusivity, viscosity and thermal conductivity, determine the corresponding transport rates. There have been numerous attempts to determine these transport coefficients from first principle. The Boltzmann equation, an integrodifferential equation, is the central equation for describing the transport processes in dilute gases. Chapman and Enskog, as well as Cowling [10] were the first researchers who developed a method for solving the Boltzmann equation and derived the exact relations between all transport coefficients of dilute gases and their intermolecular potential. The concept of Brownian dynamics is also used and the diffusivity can be obtained by solving the corresponding equation of motion (i.e., Langevin equation) in which the position and velocity are the state variables.

Diffusivity (D_{cm}) and viscosity (η) are two transport coefficients being measured and used

¹A version of this chapter has been published in *Soft Matter*, 2020, 16, 7458-7469.

frequently in polymer science. They have been observed to change drastically with molecular weight and molecular structure. For example, in the case of linear polyethylene, the simplest polymer chemically, experimental and molecular simulation studies have revealed that at $T = 450$ K, D_{cm} and η exhibit a molecular weight dependence of $M^{-1.5}$ and $M^{1.8}$ [7, 1], respectively when M is below the so-called critical molecular weight (M_c), but when M is greater than M_c , the dependence switches to $M^{-2.3}$ and $M^{3.4}$ [7]. The crossover in the scaling also occurs to ring polymers but with the scaling being less negative and less positive for D_{cm} and η , respectively [4, 6, 99, 100]. To account for the crossovers, Rouse [20] applied the Brownian dynamics concept to describe the polymer motion below M_c . On the other hand, de Gennes [50], Doi and Edwards [21] developed the reptation theory based upon the concept of a chain moving in a tube with the curvilinear coordinate to describe its motion above M_c . These two impressive attempts serve to unravel the mystery behind the M dependence below and above M_c , respectively. Nonetheless, there are limitations associated with both approaches.

The Rouse model only gives us a weaker M dependence, i.e., $D_{cm} \sim M^{-1}$ and $\eta \sim M^1$ below M_c if we consider the whole M range below M_c . This has been attributed to the fact that in reality, the friction coefficient is slightly dependent on the chain length as the number density of chain ends is inversely proportional to the molecular weight of linear polymer. Therefore, this effect of free volume has to be removed when the data were compared with the Rouse model [7]. In this sense, we should expect such effect to be absent in the case of ring polymer, in which no such chain end effect has to be corrected. However, this is certainly not the case. The underestimation was also experimentally observed for cyclic polystyrene [84] and cyclic alkane [90] that the two cyclic polymers obviously do not contain chain ends. For instance, Mckenna *et al.* [84] demonstrated that without any so-called free volume correction, the M dependence of viscosity is more or less the same for both linear and ring polystyrene. One may still argue that this may be due to the fact that the ring polystyrene samples were not pure as the more recent findings by Doi *et al.* [100] and Tsalikis *et al.* [99] revealed that the M dependence of η of more pure cyclic polystyrene and ring PEO exhibits $\eta \sim M$. Nonetheless, if the effect of free volume is absent in ring polymer, we should not expect the M dependence of transport coefficient to change significantly as temperature changes, which was the case as demonstrated by von Meerwall *et al.* [90]. von Meerwall *et al.* even

demonstrated that D_{cm} of small cyclic alkane exhibit a scaling relation of $D_{cm} \sim M^{-2.5}$ at 328 K [90], which was later confirmed by MD simulation [91]. von Meerwall *et al.* [90] and Alatas *et al.* [91] then pointed out that the reasons for such deviation from Rouse model are high rigidity of small cyclic alkane, nonmonotonic change in density with M and topological constraints.

In the reptation theory, a chain made up of beads is postulated to wiggle in a confining tube surrounded by the neighboring chains. The tube diameter is significantly greater than the size of a bead. And the chain exhibits Rouse motion within the tube. Therefore, the center-of-mass diffusion coefficient of the Rouse chain is equal to its curvilinear diffusion coefficient. This leads to the M dependence of the center of mass diffusion coefficient (D_{cm}) and that of viscosity (η) being $D_{cm} \sim M^{-2}$ and $\eta \sim M^3$ above M_c . The M dependence is slightly weaker than what has been observed in many experiments and molecular simulation studies (i.e., -2.3 and 3.4). Such discrepancy has later been corrected by applying the concept of contour length fluctuation to the original reptation theory [101, 44]. However, it has also been argued that the angle bending and torsional potentials can also be responsible for the slightly stronger M dependence of diffusivity observed in the entangled regime [27]. Additionally, the identification of primitive path relies on a substantial perturbation of the system of polymer chains in molecular dynamics (MD) simulation [76, 102, 103, 77, 104]. In the approach proposed by Everaers *et al.* [102] as well as Rubinstein and Helfand [103], the polymer chain ends are fixed and certain intramolecular interaction potentials are switched off such that the chains only interact with one another via intermolecular potential as the temperature is gradually decreased to zero. The primitive path identification algorithms of Kröger [77], as well as Tsoumaneka and Theodorou [104] are athermal in nature, which rely on geometric operations of a polymer chain with two space-fixed ends. Kröger [77] pointed out that in the case of ring polymer, the algorithm is not applicable since the algorithm relies on two space-fixed ends. But if one artificially constructs a ring polymer by simply drawing a straight line from the head and tail of a linear polymer chain, then the algorithm can still approximate a primitive path in such case. Also, Robertson *et al.* [80] and Chapman *et al.* [81] argued that cyclic polymers are less ‘capable’ of forming the so-called entanglements than their linear counterpart as it was found that the diffusivity of cyclic polymer in a concentrated medium of linear polymers can be substantially reduced, but the reverse is

not true. In view of the difficulty of applying the entanglement concept to cyclic polymers, Rubinstein suggested that the motion of a cyclic polymer can be somehow mapped onto that of a randomly branched polymer to incorporate the entanglement effect [78].

In our free volume theory, which will be discussed in detail below, a chain can be thought of wiggling in a confining tube that is made up of the local free volume around the beads of the chain. The wiggling motion of the chain is a result of the free volume redistribution and it is due to the motion of the neighboring chains (i.e., topological constraints). However, unlike the tube model, the tube size in our free volume theory is on the same order of magnitude of the bead size. In addition, the angle bending and torsional potentials can be easily incorporated into the calculation if MD simulation is used to generate the radial distribution function, the key input for the theory. Also, there is no difficulty to apply the free volume concept to cyclic polymers.

The traditional free volume approach as proposed by Turnbull and Cohen [59] relates diffusivity and viscosity to the probability of finding free volume that is greater than a certain size around a molecule, the so-called critical free volume above which the molecule can move. The free volume is assumed to follow an exponential distribution function. At the outset of last decade, Sabbagh and Eu [61] extended the free volume theory of Turnbull and Cohen to calculate the diffusivity of polymer melts in both the unentangled and entangled regimes. In their free volume theory, the critical free volume of each bead in a polymer chain is assumed to be different and follows a stretched exponential distribution function. Even though the justification for the use of the stretched exponential distribution function is not clear, the theory provides the hope that the free volume concept can be used to describe the crossover in the M dependence of diffusivity observed experimentally. It should be pointed out that in the free volume theory of Sabbagh and Eu [61], free volume is rigorously defined by the generic van der Waals (GvdW) equation of state and the required parameters for the GvdW equation of state are obtained from the integral equations of polymer chains. Based on their work, our group has recently derived a polymer free volume theory that is able to account for the crossovers in the M dependence of diffusivity for both linear and cyclic polyethylene melts [85, 105]. The polymer free volume theory is also capable of describing the temperature dependence of the scaling for low molecular weight alkanes with M below M_c [106].

In our version of the free volume approach, no such stretched exponential distribution function is assumed that each bead shares the same value of critical free volume v_i^+ . The distribution of the fraction of beads of a polymer chain having free volume greater than or equal to αv_i^+ is the key in our free volume theory (α is the overlapping parameter), which is essentially a Poisson distribution. Armed with this knowledge, we only left with one empirical parameter, ϕ^+ , which is the fraction of beads having $v_{f,i} \geq \alpha v_i^+$ necessary for activation of momentum transfer or diffusive motion, and this one empirical parameter can be used to calculate the activation energy of the macromolecule. Similar to the free volume theory developed by Sabbagh and Eu [61], the calculation of transport coefficients in our free volume theory is based on statistical mechanics and kinetic theory. In our theory, the many-chain effect comes into play in terms of the intermolecular radial distribution function $g(r)$, which can be obtained by either MD simulation or more conveniently the Polymer Reference Interaction Site Model (PRISM) theory. Unlike the primitive path determination in the tube model as mentioned previously, the determination of free volume within the polymer melts is free of any perturbation and the same calculation can be straightforwardly achieved regardless of the polymer architecture. Since each methylene group and methyl group of a polyethylene molecule can be regarded as a bead with a certain interaction potential and the electrostatic interaction is negligible, theoretical and molecular simulation studies on such material are simplified to a large extent. As the potential well of the Lennard-Jones 6-12 potential of the beads is not deep, this will ensure the convergence in the PRISM [86] when it is used along with the GvdW equation of state for the determination of the free volume parameters. It is worth noting that the PRISM has been extensively used to obtain the radial distribution function of polyethylene due to its simplicity and elegance. Hence, we are going to use PRISM theory in this work along with the generic van der Waals equation developed by Eu and Rah [64] so as to approximate the free volume in polyethylene melt. Our free volume approach can be summarized in a mind map as illustrated in Figure 8.1. As shown in Figure 8.1, the boxes in blue are the steps involved in obtaining F , p_{eff} as well as $\langle v_{f,i} \rangle$ from inputting $g(r)$ to GvdW Equation of State. $g(r)$, which is the intermolecular radial distribution function, was obtained numerically from the PRISM theory. The obtained values of F , p_{eff} as well as $\langle v_{f,i} \rangle$ are then input into the free volume theory along with the η_0 and D , which are the viscosity and diffusivity of a bead of dilute polymer medium and they are equal to that of a dilute ideal gas particle, calculated by solving the Boltzmann equation

using the Chapman-Enskog method (The boxes that are highlighted in green). This finally gives us values of η as well as D_{cm} . The inputs of PRISM theory are number density of bead ρ_b , as well as parameters of the Lennard-Jones 6-12 potential.

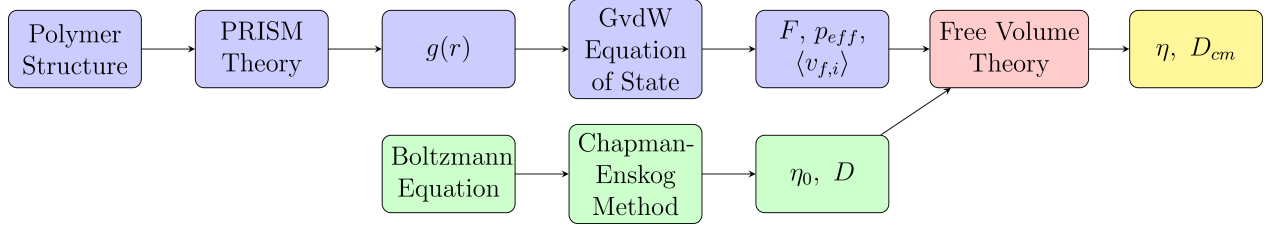


Figure 8.1: A summary of a free volume approach for calculating η and D_{cm} .

8.2 Theoretical Background

8.2.1 Viscosity of a Dilute Polymer Medium

Before any calculation of free volume, it is important to understand momentum transfer in a dilute polyethylene medium. As mentioned in the Introduction, it is possible to evaluate the viscosity with the knowledge of velocity distribution function from the Boltzmann equation, it is therefore pertinent to discuss the Boltzmann equation in this context. For a polyethylene chain in a dilute medium, the normal solution to Boltzmann equation should have the following form:

$$\Psi^{(0)}(\mathbf{r}, \mathbf{c}, t) = \rho_b(\mathbf{r}, t) \left(\frac{m}{2\pi k_b T(\mathbf{r}, t)} \right)^{1.5} \exp \left[- \frac{m(\mathbf{c} - \mathbf{c}_0(\mathbf{r}, t))^2}{2k_b T(\mathbf{r}, t)} \right] \quad (8.1)$$

Equation (8.1) is essentially the Maxwell-Boltzmann distribution, with m as the mass of the bead, \mathbf{c}_0 as the flow velocity, ρ_b as the number density of the bead, k_b is the Boltzmann constant. However, $\Psi^{(0)}$ is not that interesting as the evaluation of pressure tensor from such distribution does not allow us to get the viscosity. We are interested in the first approximation $\Psi^{(1)}(\mathbf{r}, \mathbf{c}, t)$, which can be calculated from $\Psi^{(0)}$.

$$\frac{\partial \Psi^{(0)}}{\partial \rho_b} \frac{\partial \rho_b}{\partial t} + \frac{\partial \Psi^{(0)}}{\partial T} \frac{\partial T}{\partial t} + \frac{\partial \Psi^{(0)}}{\partial \mathbf{c}_0} \frac{\partial \mathbf{c}_0}{\partial t} + \mathbf{c} \cdot \nabla_{\mathbf{r}} \Psi^{(0)} = - \frac{\Psi^{(1)} - \Psi^{(0)}}{\tau} \quad (8.2)$$

The equations of changes of ρ_b , T as well as \mathbf{c}_0 with respect to time are essentially derived from the macroscopic mass, energy and momentum conservation laws. A single bead has a

mean free path of $\frac{1}{\rho_b \pi \sigma^2}$. For a polyethylene molecule with N beads, the mean free path for the whole molecule is therefore $\frac{N}{\rho_b \pi \sigma^2}$. Therefore, τ , which is the time scale for momentum transfer in polyethylene, can be calculated as:

$$\tau = \frac{N}{\rho_b \pi \sigma^2 \langle C \rangle} \quad (8.3)$$

$\langle C \rangle = \sqrt{\frac{8k_b T}{\pi m}}$, where $\mathbf{C} = \mathbf{c} - \mathbf{c}_0$, and C is the magnitude of \mathbf{C} . The velocity distribution function of the bead of both a dilute polymer medium and ideal gas must be a Maxwell-Boltzmann distribution function, as the kinetic energy of each particle or bead in both cases must be $\frac{mC^2}{2}$. Then, in this sense, $\langle C \rangle$ should be the same in both cases as the velocity distribution functions are the same. Following the derivation in the Supporting Information (SI) Section 1, the result is obtained as:

$$\Psi^{(1)}(\mathbf{r}, \mathbf{c}, t) = \Psi^{(0)} \left[1 - \tau \left[\left(-\frac{5}{2} \mathbf{C} \cdot \nabla_{\mathbf{r}} \ln T + W^2 \mathbf{C} \cdot \nabla_{\mathbf{r}} \ln T \right) + 2(\mathbf{W}\mathbf{W} : \nabla_{\mathbf{r}} \mathbf{c}_0 - \frac{1}{3} W^2 \mathbf{I} : \nabla_{\mathbf{r}} \mathbf{c}_0) + \mathbf{C} \cdot \sum_j \frac{\rho_j \mathbf{F}_j}{\rho_b k_b T} \right] \right] \quad (8.4)$$

With $\mathbf{W} = \sqrt{\frac{m}{2k_b T}} \mathbf{C}$. ρ_j is the number density of the j th bead such that $\rho_b = \sum_j \rho_j$ and \mathbf{F}_j is the intramolecular force acting upon j th bead. In this case, in a dilute medium of Gaussian chains without any intermolecular interaction, there exists an additional summation term of all intramolecular forces among the beads in Equation (8.4). Note that such term, which is independent of \mathbf{C} , has no effect on the shear stress. The pressure tensor \mathbf{P} is defined as:

$$\mathbf{P} = m \int_{-\infty}^{\infty} \mathbf{C} \mathbf{C} \Psi^{(1)} d\mathbf{C} \quad (8.5)$$

For shear stress, we are interested in the p_{xy} component of \mathbf{P} .

$$p_{xy} = \left[-2m \int_{-\infty}^{\infty} \tau C_x C_y (W_x W_y) \Psi^{(0)} d\mathbf{C} \right] \left(\frac{\partial c_{0,y}}{\partial x} + \frac{\partial c_{0,x}}{\partial y} \right) \quad (8.6)$$

because:

$$\int_{-\infty}^{\infty} C_x C_y \Psi^{(0)} d\mathbf{C} = 0 \quad (8.7)$$

and

$$-\tau \left[\int_{-\infty}^{\infty} C_x C_y \left(-\frac{5}{2} \mathbf{C} + W^2 \mathbf{C} \right) \Psi^{(0)} d\mathbf{C} \cdot \nabla_{\mathbf{r}} \ln T + \int_{-\infty}^{\infty} C_x C_y \mathbf{C} \Psi^{(0)} d\mathbf{C} \cdot \sum_j \frac{\rho_j \mathbf{F}_j}{\rho_b k_b T} \right] = 0 \quad (8.8)$$

The proof of this is shown in SI Section 2. Then, the viscosity is:

$$\eta_d = 2m\tau \int_{-\infty}^{\infty} C_x C_y W_x W_y \Psi^{(0)} d\mathbf{C} = \frac{m^2 \tau}{k_b T} \int_{-\infty}^{\infty} C_x C_y C_x C_y \Psi^{(0)} d\mathbf{C} \quad (8.9)$$

This integral is solved as demonstrated in the SI Section 3. It was found that

$$\eta_d = \rho_b k_b T \tau \quad (8.10)$$

With:

$$\eta_d = N \eta_0 \quad (8.11)$$

We have the following:

$$\eta_0 = \frac{1}{\sigma^2} \sqrt{\frac{m k_b T}{8\pi}} \quad (8.12)$$

This form of η_0 is also the viscosity of a bead in a dilute polymer medium, which is equal to that of a monoatomic ideal gas particle.

8.2.2 Free Volume Theory for Polyethylene with Different Structures

For a polymer with N beads, we can count the number of beads (n_f) having free volume greater than that of the activation volume, i.e. $v_{f,i} \geq \alpha v_i^+$, where α is the overlapping parameter and v_i^+ is the effective volume of bead i . Assuming that the bead of the chain end always possesses enough volume for diffusive motion, the number of ways to arrange n_f beads for a polymer with N is as follows:

$$W = \frac{(N-x)!}{(N-x-n_f)! n_f!} \quad (8.13)$$

x is the number of chain ends of the polymers, such that $x = 2$, $x = 0$ and $x = 4$ for linear, ring and four-arm symmetric polymers, respectively. Therefore, the probability for a polymer having n_f beads can be calculated as follows:

$$P_d(\phi) = \frac{(N-x)!}{(N-x-n_f)! n_f!} F^{n_f} (1-F)^{N-x-n_f} \quad (8.14)$$

F is the probability for a bead having $v_{f,i} \geq \alpha v_i^+$. Usually, for the sake of simplicity, following the rationale of Turnbull and Cohen [59], $F = \exp(-\alpha v_i^+ / \langle v_{f,i} \rangle)$, where $\langle v_{f,i} \rangle$ is the mean free volume per bead. And the argument of this distribution $P_d(\phi)$ is $\phi = \frac{n_f}{N-x}$. Equation (8.14) can be further simplified as a normal distribution with F and $F/(N-x)$ as mean value and covariance, respectively, (this normal distribution approximation is justified as shown in SI Section 4) such that we obtain:

$$P_d(\phi) \approx \sqrt{\frac{N-x}{2\pi F}} \exp \left[-\frac{(N-x)(\phi - F)^2}{2F} \right] \quad (8.15)$$

The integral of $P_d(\phi)$ from ϕ^+ to 1 is of our particular interest as this is important in the calculation of the viscosity and diffusivity. ϕ^+ is the fraction of beads that is necessary for activation of motion and as $\phi < \phi^+$, no motion of polymer is activated. The upper limit of such integral can be assumed to be ∞ as $P_d(\phi)$ vanishes when $\phi \rightarrow 1$. In this sense, such integral tells us the probability of motion of polymer being activated. (cf., Equation (8.16))

$$\int_{\phi^+}^{\infty} P_d(\phi) d\phi \approx \frac{1}{2} - \frac{1}{2} \operatorname{erf}\left[\sqrt{\frac{N-x}{2F}}(\phi^+ - F)\right] \quad (8.16)$$

The error function $\operatorname{erf}\left[\sqrt{\frac{N-x}{2F}}(\phi^+ - F)\right]$ can be approximated by polynomial:

$$\operatorname{erf}\left[\sqrt{\frac{N-x}{2F}}(\phi^+ - F)\right] \approx 1 - 2\left\{1 + \left[a_1 + a_2\sqrt{\frac{N-x}{2F}}(\phi^+ - F)\right]^{a_3}\right\}^{a_4} \quad (8.17)$$

where $a_1 = 0.6446930$, $a_2 = 0.22908$, $a_3 = 4.874$, $a_4 = -6.158$ according to the approximation formula developed by Burr [107]. Equation (8.16) can be rewritten as:

$$\int_{\phi^+}^{\infty} P_d(\phi) d\phi \approx \left\{1 + \left[a_1 + a_2\sqrt{\frac{N-x}{2F}}(\phi^+ - F)\right]^{a_3}\right\}^{a_4} \quad (8.18)$$

In Doolittle equation, it was proposed that viscosity is inversely proportional to the Turnbull and Cohen probability of finding activation free volume [108]. In this sense, based upon our polymer free volume theory, the zero-shear viscosity should be inversely related to Equation (8.18), such that:

$$\boxed{\eta = \eta_0 N \left\{1 + \left[a_1 + a_2\sqrt{\frac{N-x}{2F}}(\phi^+ - F)\right]^{a_3}\right\}^{-a_4}} \quad (8.19)$$

By inspection of Equation (8.19), parameters, such as F , can be determined by PRISM theory along with generic van der Waals (GvdW) equation. ϕ^+ can be related to the activation energy and the effective pressure of the polymer melt. η_0 is the viscosity of dilute gas determined using Boltzmann Equation as shown in the previous section.

To account for the temperature dependence of η of polyethylene, Equation (8.19) has to be modified as follows:

$$\boxed{\eta(T) = \eta_{\infty} \exp\left[\frac{1}{\rho_b \langle v_{f,i} \rangle} + \frac{p_{eff}(\phi^+ \alpha v_i^+ + (1 - \phi^+) \langle v_{f,i} \rangle)}{RT}\right] N \left\{1 + \left[a_1 + a_2\sqrt{\frac{N-x}{2F}}(\phi^+ - F)\right]^{a_3}\right\}^{-a_4}} \quad (8.20)$$

p_{eff} is the effective pressure, which can be obtained from first principle that is going to be discussed in the forthcoming section. η_∞ is the viscosity of a single bead as temperature is infinitely high. η_0 is not used in Equation (8.20) as it does not capture the change of viscosity with temperature and density accurately, which is critical when we attempt to predict T dependence of η for linear polyethylene with different M . In Equation (8.20), the term $\frac{1}{\rho_b \langle v_{f,i} \rangle}$ accounts for the expansion of free volume with temperature and the term $p_{eff}(\phi^+ \alpha v_i^+ + (1 - \phi^+) \langle v_{f,i} \rangle)$ is the energy associated with creation of activation volume and free volume to accomodate the beads in the melt. As shown in the Result and Discussion Section, the same value of $\phi^+ - F$ in Equation (8.19) and Equation (8.20) can describe both M dependence and T dependence of linear polyethylene chain reasonably well.

8.2.3 PRISM Theory

The integral equation theory developed by Schweizer and Curro [86] in Fourier space is as follows:

$$\hat{\mathbf{H}} = (\mathbf{I} - \rho \hat{\mathbf{\Omega}} \hat{\mathbf{Y}})^{-1} \hat{\mathbf{\Omega}} \hat{\mathbf{Y}} \hat{\mathbf{\Omega}} \quad (8.21)$$

\mathbf{I} is a $N \times N$ identity matrix. $\hat{\mathbf{H}}$ is a matrix with components $\hat{h}_{\alpha,\gamma}(k)$, such that $h_{\alpha,\gamma}(r) = g_{\alpha,\gamma}(r) - 1$ where $g_{\alpha,\gamma}(r)$ is the intermolecular radial distribution function between sites α and γ of two different polymers in real space. $\hat{\mathbf{Y}}$ is a matrix with components $\hat{y}_{\alpha,\gamma}(k)$, which is the direct correlation function between sites α and γ in Fourier space. $\hat{\mathbf{\Omega}}$ is a matrix with components $\hat{\omega}_{\alpha,\gamma}(k)$, where $\omega_{\alpha,\gamma}(r)$ is the intramolecular radial distribution function between sites α and γ of the same polymer. ρ is the number density of the whole polymer such that $\rho = \rho_b/N$. Equation (8.21) can be simplified into a scalar equation with the following:

$$\hat{h}(k) = \frac{\hat{\omega}^2 \hat{y}}{1 - \rho_b \hat{\omega} \hat{y}} \quad (8.22)$$

In the calculation, ρ_b was always fixed at $\rho_b = 32 \text{ nm}^{-3}$ at $T = 450 \text{ K}$ for M dependence calculation, and for calculations at different T , $\rho_b(T) = 43(0.00076T + 0.93)^{-1}$ [1]. There are no subscripts in any of these functions $\hat{h}(k)$, $\hat{y}(k)$ and $\hat{\omega}(k)$ as they are average quantity over all the sites:

$$\hat{h}(k) = \frac{1}{N^2} \sum_{\alpha=1}^N \sum_{\gamma=1}^N \hat{h}_{\alpha,\gamma}(k) \quad (8.23)$$

$$\hat{\omega}(k) = \frac{1}{N} \sum_{\alpha=1}^N \sum_{\gamma=1}^N \hat{\omega}_{\alpha,\gamma}(k) \quad (8.24)$$

There are two unknowns in Equation (8.22), which are $\hat{h}(k)$ and $\hat{y}(k)$, and thus we need one more equation relating $y(r)$ to $h(r)$. In this work, $y(r)$ is related to $h(r)$ through the hypernetted chain closure relation [88], which is a slightly more complicated closure relation compared to Percus-Yevick closure relation that was used in our previous work on n -alkane [106].

$$y^{(k+1)}(r) = e^{-\beta u(r) + h^{(k)}(r) - y^{(k)}(r)} - 1 - h^{(k)}(r) + y^{(k)}(r) \quad (8.25)$$

The superscript (k) indicates that these quantities are evaluated at the k th iteration. $u(r)$ is the 6-12 Lennard-Jones potential.

$$u(r) = 4\varepsilon \left[\left(\frac{\sigma}{r} \right)^{12} - \left(\frac{\sigma}{r} \right)^6 \right] \quad (8.26)$$

$\varepsilon = 0.380 \text{ kJ} \cdot \text{mole}^{-1}$ and $\sigma = 0.395 \text{ nm}$ based on the forcefield developed by Martin *et al.* [19]. For the sake of simplicity, all the beads of linear, ring and four-arm symmetrical star polyethylene are assumed to be methylene groups, such that their corresponding 6-12 Lennard-Jones potential parameters are identical. For a Gaussian chain, $\hat{\omega}_{\alpha,\gamma} = \exp(-nk^2 \langle r^2 \rangle / 6)$, for which $\langle r^2 \rangle = \sigma^2$. n is the number of bonds separating site α and site γ of the same chain. For a linear chain, we have:

$$\hat{\omega}(k) = \frac{1 - f^2 - 2\frac{f}{N} + 2\frac{f^{N+1}}{N}}{(1 - f)^2} \quad (8.27)$$

For a ring polymer, we have [109, 97]:

$$\hat{\omega}(k) = 1 + \frac{2}{N} \sum_{p=1}^{N-1} (N - p) f^{\frac{p(N-p)}{N}} \quad (8.28)$$

For a four-arm symmetric star polyethylene, we have:

$$\hat{\omega}(k) = \frac{1}{N} \left[2N_a + 4 \sum_{p=1}^{N_a-1} (N_a - p) f^p + 8 \sum_{p=2}^{(N_a+1)/2} (p-1) f^p + 8 \sum_{p=1}^{(N_a-3)/2} \left(\frac{N_a-1}{2} - p \right) f^p f^{(N_a+1)/2 - 1} \right] \quad (8.29)$$

where $f = \exp(-k^2 \sigma^2 / 6)$ and N_a is the number of beads of two arms including the central bead. For example, when $N = 33$, $N_a = (N - 1) / 2 + 1 = 17$. More detailed explanation on $\hat{\omega}(k)$ of different structures can be found in SI Section 5.

8.2.4 Pressure Equation, Intramolecular Term and GvdW Equation of State

The contribution to pressure from intramolecular interaction in Gaussian chain molecule, which does not have any intermolecular interaction, (P_1) is as follows:

$$P_1 = -\frac{\rho_b}{3} \int_0^\infty 4\pi r^3 \frac{du_{bond}}{dr} P(r) dr \quad (8.30)$$

With:

$$P(r) = \left(\frac{3}{2\pi \langle r^2 \rangle} \right)^{3/2} \exp \left(-\frac{3r^2}{2\langle r^2 \rangle} \right) \quad (8.31)$$

$P(r)$ is the probability distribution function of the distance r between two beads interacting with one another through a harmonic bond stretching potential $u_{bond}(r)$. $\langle r^2 \rangle$ is the mean-square value of the distance r . The derivation of Equation (8.30) is shown in SI Section 6 and $\beta = \frac{1}{k_b T}$. Without intermolecular potential, we have:

$$p\beta = N\rho - P_1\beta \quad (8.32)$$

N is the number of beads of a Gaussian chain.

$$\frac{p\beta}{N\rho} = 1 - \frac{4\pi\beta}{3} \int_0^\infty r^3 \frac{du_{bond}}{dr} P(r) dr \quad (8.33)$$

If we assume that, $du_{bond}/dr = k_{bond}r$ and $k_{bond} = 3\beta^{-1}\langle r^2 \rangle^{-1}$. We found that without any intermolecular interaction:

$$\frac{p\beta}{N\rho} = 1 - \frac{4\pi\beta k_{bond}}{3} \int_0^\infty r^4 P(r) dr = 1 - \frac{\beta 3\beta^{-1} \langle r^2 \rangle \langle r^2 \rangle^{-1}}{3} = 0 \quad (8.34)$$

Additional potentials, such as bending and torsional potentials, can be ignored in the pressure equation as the change in the bond angle and torsional angle with respect to volume are zeros, which were previously shown by Honnell *et al.* [73]. However, effect of these angle potentials can be reflected in the intermolecular radial distribution function $g(r)$, which can eventually affect the results derived from the equation of state. In this study, for the sake of simplicity, we did not incorporate such angle potentials in the calculation using PRISM theory as we assumed all the polyethylene molecules follow Gaussian statistics. One may derive $g(r)$ from MD simulations of polyethylene, in which all the bonded potentials, such as bond stretching, angle bending and torsion potentials, and non-bonded potential are explicitly included. This may affect values of p_{eff} , $\langle v_{f,i} \rangle$ and F . However, we found that the resultant value of $(\phi^+ - F)$

in our free volume theory is always within the range of 0.02 to 0.06 in our forthcoming analysis in the Results and Discussion.

This shows that the compressibility factor of Gaussian chains without intermolecular interaction is 0. For Gaussian chains with both intermolecular and intramolecular interactions, we then have:

$$\frac{p\beta}{N\rho} = 1 - \frac{2\pi\beta\rho_b}{3} \int_0^\infty g(r)r^3 \frac{du}{dr} dr - \frac{4\pi\beta k_{bond}}{3} \int_0^\infty r^4 P(r) dr \quad (8.35)$$

And if the intramolecular interaction is neglected, we have:

$$\frac{p\beta}{N\rho} = 1 - \frac{2\pi\beta\rho_b}{3} \int_0^\infty g(r)r^3 \frac{du}{dr} dr \quad (8.36)$$

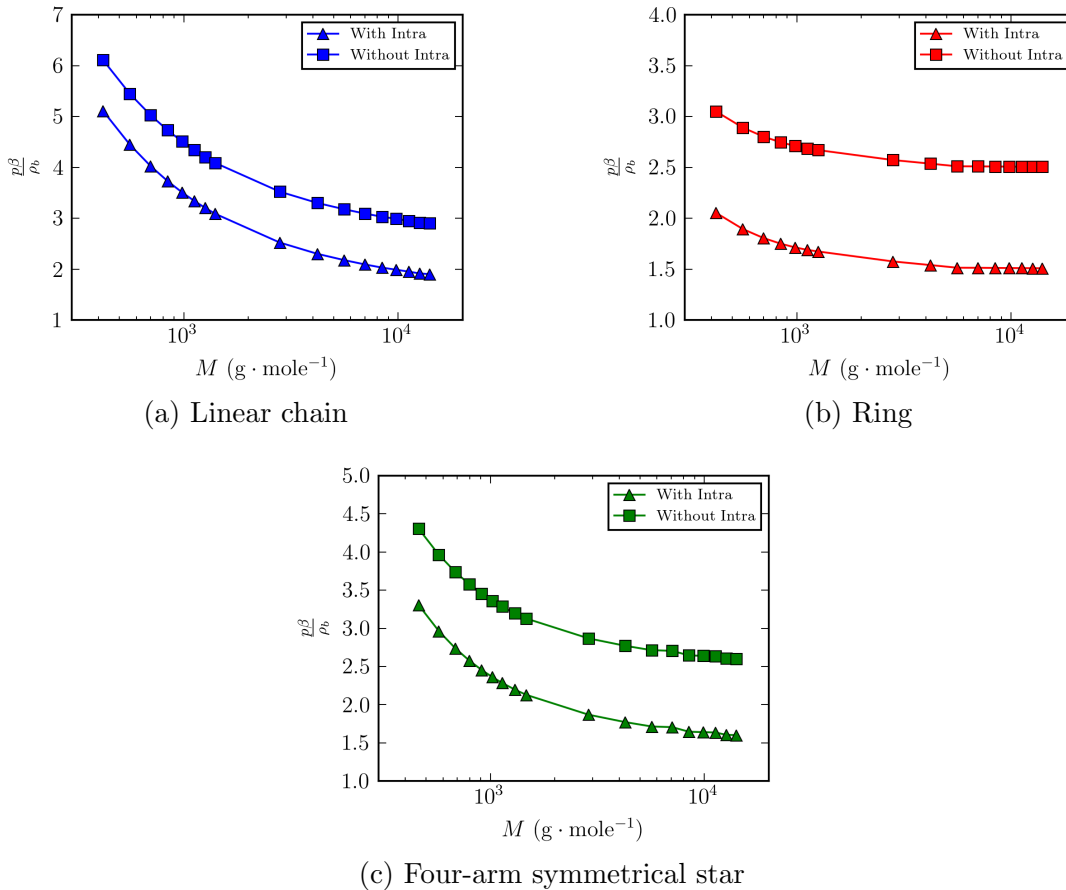


Figure 8.2: Compressibility factor with and without incorporation of intramolecular term in the pressure equation as a function of M for linear chain, ring as well as four-arm symmetrical star at $T = 450$ K.

Figure 8.2 shows plots of the compressibility factor with and without the intramolecular term for polyethylene with different structures and molecular weight at $T = 450$ K. As expected, for all the structures, the compressibility factor is reduced by one when the intramolecular term is included. Interestingly, among all these structures, the linear chain has the highest compressibility factor and it changes with M to the largest extent. This is because even without the intramolecular term in the pressure equation (cf., Equation (8.35)), the intramolecular effect is still captured in the resultant $g(r)$. Equation (8.35) can be rewritten as:

$$\frac{p\beta}{N\rho} = 1 + \frac{2\pi\beta\rho_b}{3} \int_0^\infty I(r)dr \quad (8.37)$$

We have let the function $I(r)$ have the following form:

$$I(r) = -r^3 \frac{du}{dr} g(r) - \frac{2k_{bond}r^4 P(r)}{\rho_b} \quad (8.38)$$

This function $I(r)$ was originally developed by Laghaei *et al.*[65] in their work on Monte Carlo Simulation of Lennard-Jones monoatomic particle. This function $I(r)$ is related to the required work done to move the beads in dense polymer melt for a particular distance R per $2\pi/3$.

$$\mathcal{W}(R) = -\rho_b \int_0^R \left[r^3 \frac{du}{dr} g(r) + 2k_{bond}r^4 P(r)/\rho_b \right] dr \quad (8.39)$$

Then, $I(r)$ is the integrand in Equation (8.39), which has a unit of $\text{kJ} \cdot \text{mole}^{-1} \cdot \text{nm}^2$. The amplitude of $I(r)$ reflects the possibility that the bead is going to experience a repulsive or attractive force as a function of r due to the many-chain effect and the harmonic bond stretching potential, and this allows us to approximate the amount of excluded volume in a polymer melt. The repulsive force within the range of 0 to r^+ is responsible for the excluded volume of the bead, as r^+ is the cavity diameter of the bead and thus its effective diameter (cf., Results and Discussion). And unlike our previous work on n -alkane [106], we have included the intramolecular interaction in Equation (8.38), even though the contribution is not that significant. It can be expected that the intramolecular term is going to lead to a slightly larger free volume due to its attractive nature that the intramolecular force $-du_{bond}/dr$ is always negative. As shown in our previous work [85], Equation (8.37) can be recast to a van der Waals equation, which then enables us to quantify effective pressure and free volume in the melt. This GvdW equation was originally developed by Eu and Rah [64].

$$(p + A\rho_b^2)(N - B\rho_b) = \beta^{-1}\rho_b \quad (8.40)$$

With the GvdW parameters A and B defined as:

$$A = -\frac{2\pi}{3} \int_{r^+}^{\infty} I(r) dr \quad (8.41)$$

$$B = \frac{1}{\rho_b} \left[N - \frac{1}{1 + \frac{2\pi\beta\rho_b}{3} \int_0^{r^+} I(r) dr} \right] \quad (8.42)$$

The mean free volume per bead and the effective pressure are then defined as $\langle v_{f,i} \rangle = \frac{1}{\rho_b} (N - B\rho_b)$ and $p_{eff} = p + A\rho_b^2$, respectively. The lower and upper limit of the integrals in Equation (8.41) and Equation (8.42), which are r^+ , is the cavity diameter of the bead obtained from the plot of $I(r)$ as a function r (cf., Results and Discussion).

8.3 Results and Discussion

8.3.1 Length Scales and GvdW Parameters

Table 8.1: r_c , r^+ and α for polyethylene with different structures at $T = 450$ K. These quantities are not dependent significantly on M .

Structures	r_c (nm)	r^+ (nm)	α
Linear chain	0.305	0.354	0.578
Ring	0.307	0.354	0.578
Four-arm symmetrical star	0.306	0.354	0.578

Figure 8.3 shows a plot of $I(r)$ as a function of r for polyethylene with different structures and $M = 14000 \text{ g} \cdot \text{mole}^{-1}$ at $T = 450$ K. From such plot, four different length scales can be extracted straightforwardly. In Figure 8.3, these four different lengths are r_c , r^+ , r_{pm} and r_{fm} , which correspond to the hard-core diameter, cavity diameter, distances at potential minimum and force minimum, respectively. The overlapping parameter α is related to the r^+ , r_{pm} as well as r_{fm} that $\alpha = \left[1 - \left(\frac{r_{fm} - r_{pm}}{r^+} \right) \right]^3$. The corresponding values of these length scales and α , as well as the activation volume $v_i^+ = \frac{\pi}{6} r^+{}^3$ for polyethylene with all different structures are summarized in Table 8.1. Polyethylene with different structures share the same values of r^+ , α and v_i^+ , which are 0.354 nm, 0.578 and 0.0232 nm^3 .

The effect of temperature on these length scales were also investigated as a function of temperature. Table 8.2 shows the values of these length scales and α at different temperatures

for linear polyethylene chain with $M = 2128 \text{ g} \cdot \text{mole}^{-1}$. It was found that again these parameters were not strongly dependent on temperature.

Table 8.2: T dependence of different r_c , r^+ and α of linear polyethylene chain with $M = 2128 \text{ g} \cdot \text{mole}^{-1}$.

Temperature (K)	r_c (nm)	r^+ (nm)	α
400	0.305	0.352	0.576
416	0.304	0.352	0.575
476	0.302	0.350	0.574
500	0.301	0.349	0.573

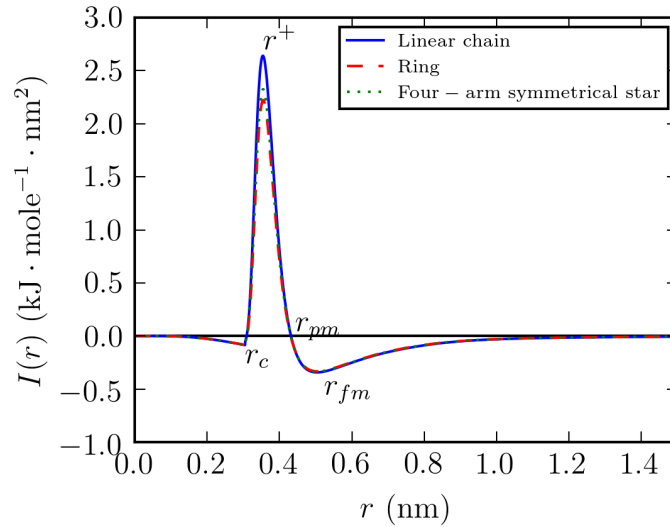


Figure 8.3: A plot of $I(r)$ as a function of r for polyethylene with different structures. Four length scales r_c , r^+ , r_{pm} and r_{fm} are extracted from this plot at $T = 450 \text{ K}$.

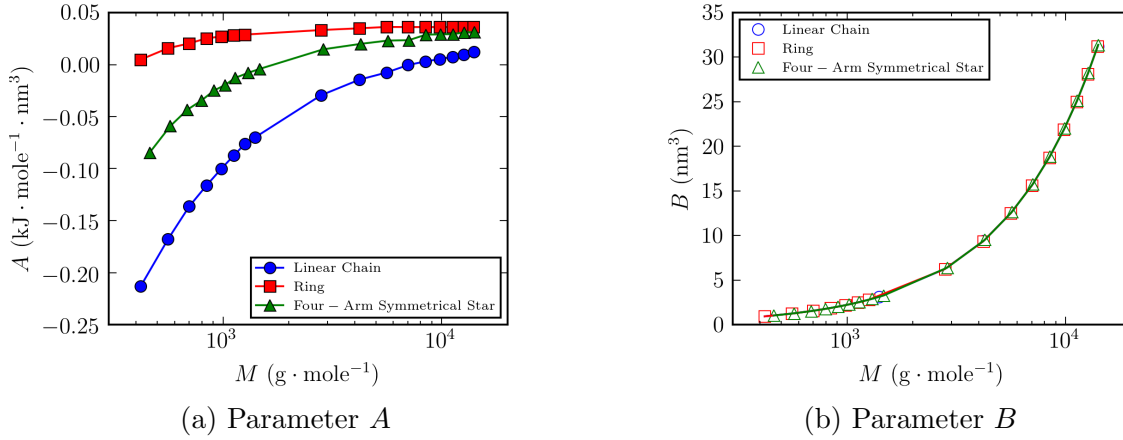


Figure 8.4: GvdW parameters A and B as a function of M for polyethylene with different structures at $T = 450$ K. A and B are calculated using Equation (8.41) and Equation (8.42). The solid lines are guides only.

Table 8.3: Parameter B of polyethylene with three different structures and M . These values are listed in this Table as the difference is not obvious as depicted in Figure 8.4b at $T = 450$ K. Yet, we found that a small difference in B can lead to a significant disparity in free volume calculation.

M (Linear) ($\text{g} \cdot \text{mole}^{-1}$)	B (nm^3)	M (Ring) ($\text{g} \cdot \text{mole}^{-1}$)	B (nm^3)	M (Star) ($\text{g} \cdot \text{mole}^{-1}$)	B (nm^3)
420	0.928	420	0.923	462	1.019
560	1.240	560	1.235	574	1.269
700	1.552	700	1.547	686	1.518
840	1.864	840	1.859	798	1.768
980	2.176	980	2.171	910	2.017
1120	2.488	1120	2.484	1022	2.267
1260	2.800	1260	2.796	1134	2.517
1400	3.112	2800	6.233	1302	2.892
2800	6.236	4200	9.358	1470	3.266
4200	9.361	5600	12.483	2870	6.391
5600	12.485	7000	15.608	4270	9.515
7000	15.610	8400	18.733	5670	12.640
8400	18.735	9800	21.858	7070	15.765
9800	21.860	11200	24.983	8470	18.890
11200	24.984	12600	28.108	9870	22.015
12600	28.109	13986	31.202	11270	25.140

Armed with the knowledge of r^+ , the parameters A and B are calculated using Equation (8.41) and Equation (8.42) for all structures with different M as shown in Figure 8.4a and

b, respectively. As mentioned above, they are useful in quantifying the mean free volume as well as the effective pressure. The magnitude of A can be negative as demonstrated in simulation of Lennard-Jones particle by Laghaei *et al.* [65]. Similar to the compressibility factor, A changes most dramatically with M in linear chain and it remains more or less at a constant positive value for ring polymer. As for the parameter B , M dependence of this parameter is more or less the same for polyethylene with different structures. The fact that B increases with M is expected as B is related to the excluded volume of the whole polyethylene molecule, of which the molecular size increases with M . The difference in the parameter B is not obvious as depicted in Figure 8.4. But a small difference in parameter B can lead to a huge disparity in the calculated mean free volume per bead $\langle v_{f,i} \rangle$. Such difference in parameter B is much better appreciated in Table 8.3.

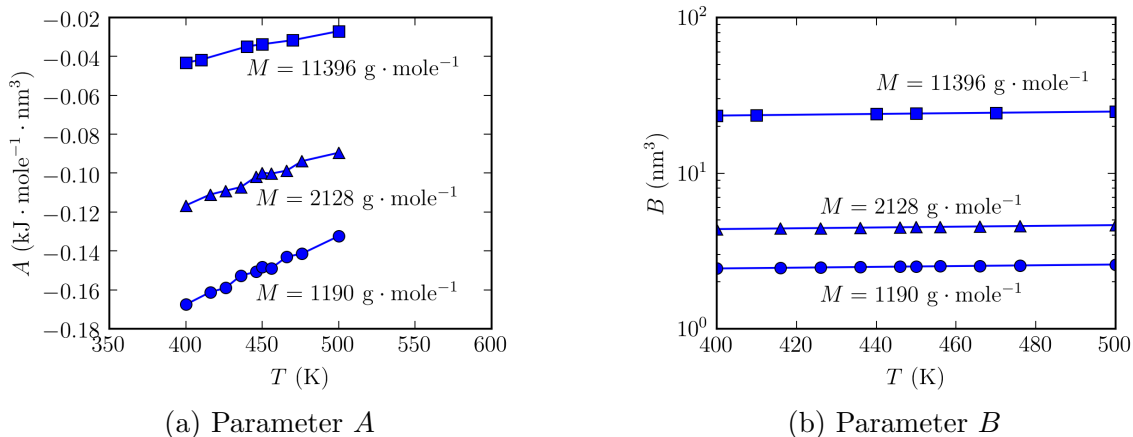


Figure 8.5: GvdW parameters A and B as a function of T for linear polyethylene chain with different M . A and B are calculated using Equation (8.41) and Equation (8.42). The solid lines are guides only.

The influence of temperature on A and B for linear polyethylene chain with $M = 1190 \text{ g} \cdot \text{mole}^{-1}$, $M = 2128 \text{ g} \cdot \text{mole}^{-1}$ and $M = 11396 \text{ g} \cdot \text{mole}^{-1}$ is illustrated in Figure 8.5. For A , A becomes less negative as temperature increases; Similarly, the difference in B seems not to change much with temperature as shown in Figure 8.5. However, a small change in B with temperature can significantly influence the calculated value of $\langle v_{f,i} \rangle$ at different temperatures. Such difference in parameter B at different temperatures for linear polyethylene is much better observed in Table 8.4.

Table 8.4: Parameter B as a function of temperature for linear polyethylene with $M = 1190 \text{ g} \cdot \text{mole}^{-1}$, $M = 2128 \text{ g} \cdot \text{mole}^{-1}$ and $M = 11306 \text{ g} \cdot \text{mole}^{-1}$. The change in these values of parameters B with temperature are listed in this Table as it is not obvious as shown in Figure 8.5b.

$M = 1190 \text{ g} \cdot \text{mole}^{-1}$		$M = 2128 \text{ g} \cdot \text{mole}^{-1}$		$M = 11306 \text{ g} \cdot \text{mole}^{-1}$	
T (K)	B (nm ³)	T (K)	B (nm ³)	T (K)	B (nm ³)
400	2.440	400	4.369	400	23.434
416	2.464	416	4.411	410	23.578
426	2.478	426	4.438	440	24.009
436	2.493	436	4.464	450	24.152
446	2.508	446	4.491	470	24.439
450	2.514	450	4.502	500	24.870

8.3.2 Molecular Weight Dependence of Zero-Shear Viscosity

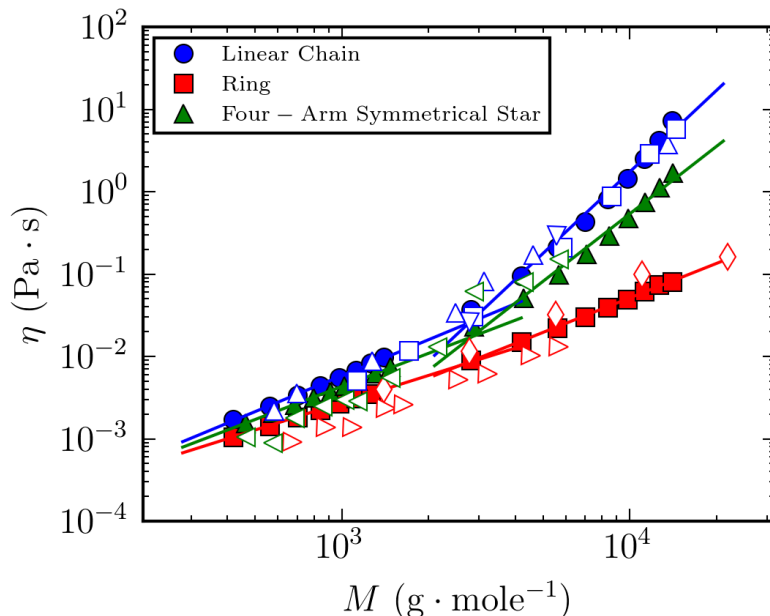


Figure 8.6: Zero-shear viscosity as a function of M for polyethylene with different structures at $T = 450$ K calculated using Equation (8.19) and the parameters obtained from the free volume analysis (filled markers). Our calculation results of linear polyethylene were compared with experimental data by Pearson *et al.* (\square) [7] as well as simulation data of Padding and Briels (\triangle) [8], as well as Halverson *et al.* (∇) [6]. Results for ring polyethylene were compared with simulation data by Halverson *et al.* (\diamond) [6] as well as Tsolou *et al.* (\triangleright) [4]. Results for four-arm symmetrical star polyethylene are compared with our MD simulation data (\triangleleft) [9]. It should be noted that the data from Halverson *et al.* [6] have been shifted accordingly to compare with our theory as in their work, the viscosity are in reduced unit. Note that the blue, red and green colours as depicted in the plots correspond to linear, ring and four-arm symmetrical polyethylene, respectively. Slopes of these linear curves below and above M_c are listed in Table 8.5.

Using Equation (8.19) along with the free volume parameters determined from last section, viscosity of polyethylene with different structures over the molecular weight range of 420 – 14,000 $\text{g} \cdot \text{mole}^{-1}$ at 450 K were calculated and the results are shown in Figure 8.6. The data show a positive non-linear dependence on molecular weight. For each structure, linear lines were fitted to the low and high molecular weight regimes. The resultant slopes are indicated in Table 8.5 with $M_c \approx 3,000 \text{ g} \cdot \text{mole}^{-1}$. As mentioned in the Introduction, for linear polyethylene, the slopes below and above M_c are always stronger than 1 and 3 than that predicted in the Rouse model and reptation model, respectively. Comparison among

different structures reveals that the slope is slightly less positive both below and above M_c for ring and four-arm symmetrical star polyethylene. This is in good agreement with the simulation data of Xu *et al.* [110], which shows that the exponent in the M dependence is slightly weaker in branched polymers compared to that of linear chain. Due to the absence of experimental and simulation viscosity of four-arm symmetrical star polymer, η of the four-arm symmetrical star polyethylene is compared with our own MD simulation data, which was evaluated using the method as described in one of our previous work [9] and these data are not yet published.² We found good agreement between simulation and our free volume theory that the slopes below and above M_c are similar. For linear and ring polyethylene, within a range of $M = 420 - 14000 \text{ g} \cdot \text{mole}^{-1}$, the calculated viscosity agrees well with the experimental data of Pearson *et al.* [7] as well as the simulation data of Halverson *et al.* [6], and Padding and Briels [8]. For ring polyethylene melts, our data were compared with Tsolou *et al.* [4] as well as Halverson *et al.* [6]. The slope below M_c for ring polyethylene is 1.1, which is very close to 1, and that this scaling for rings below M_c at $T = 450 \text{ K}$ agrees well with that of the Rouse model. The slope above M_c for ring polyethylene is significantly lower than that of its linear counterpart (cf., Table 8.5). Mckenna *et al.* [84] found that both M dependence and T dependence of η is not much different in linear and cyclic polystyrene. However, a weaker M dependence of cyclic polystyrene compared to its linear counterpart for $M < 10^5 \text{ g} \cdot \text{mole}^{-1}$ above M_c was observed in a more recent experimental measurement of high-purity cyclic polystyrene by Doi *et al.* [100]. Tsalikis *et al.* [99] also demonstrated a scaling of $\eta \sim M^{1.7}$ above M_c for ring PEO, which is much weaker than its linear counterpart. It has to be noted that the slightly higher calculated value of η of ring polyethylene compared with the MD simulation data of Tsolou *et al.* [4] observed below M_c is due to the fact that in our calculation using PRISM theory, the number density of bead ρ_b is always fixed at $\rho_b = 32 \text{ nm}^{-3}$ (cf., Section 8.2.3) and that the viscosity obtained from the solution to Boltzmann equation is not dependent on ρ_b , whereas in the MD simulation done by Tsolou *et al.* [4], the calculated value of ρ_b is a result from numerical solution to the equation of motion of bead, which can change with N , leading to different values of η .

²The data as depicted in Figure 8.6 were extracted using the POD method (as described in ref. [9]) on NPT MD simulation, whereas the data as published in ref. [9] were obtained from NVT MD simulation. In addition, in the latter case, the data are for unentangled polyethylene only. This is why we claimed that these data are not yet published.

Table 8.5: Slopes of the linear curves as shown in Figure 8.6 for polyethylene with different structures, as well as the corresponding values of $\phi^+ - F$.

Structures	Below M_c	Above M_c	$\phi^+ - F$
Linear chain	1.45	3.28	0.06
Ring	1.10	1.40	0.02
Four-Arm Symmetrical Star	1.33	2.72	0.05

One noteworthy point is that the accuracy of the viscosity calculated using Equation (8.19) is very sensitive to the difference between the two free volume parameters in the equation (i.e., $(\phi^+ - F)$). In other words, values other than those shown in Table 8.5 (0.06, 0.02 and 0.05 for the linear, ring and four-arm symmetrical star polyethylene, respectively) would yield incorrect viscosity prediction. It is also interesting to note that the values of ϕ^+ and F are sensitive to the simulation method or model used but their difference $(\phi^+ - F)$ is not. For example, in our previous work, when the PRISM theory along with the Percus-Yevick closure was used for linear polyethylene oligomer, a ϕ^+ value of 0.43 was obtained at 443.5 K [106]. However, MD simulation yielded a ϕ^+ value of 0.22 at 450 K [85]. This is because ϕ^+ is related to the activation energy of the macromolecule, which in turn relies on the effective pressure. Since the effective pressure of a real polymer chain in MD simulation is higher than that of a Gaussian chain used in the PRISM theory, ϕ^+ determined from the PRISM theory must be higher than that of the MD simulation as both methods should give the same activation energy. The PRISM theory also gives higher F value than the MD simulation. This leads to the situation that $(\phi^+ - F)$ is insensitive to the simulation method used and was observed in our previous work [85, 105, 106].

8.3.3 Temperature Dependence of Zero-Shear Viscosity

With GvdW parameters at different temperatures as well as the values of $\phi^+ - F$ obtained in the previous section (cf., Table 8.5), it is possible to calculate η as a function of temperature using Equation (8.20). It is well-known that the temperature dependence of η also follows an Arrhenius relation in the high temperature region:

$$\eta \sim \exp\left(\frac{E_a^{app}}{RT}\right) \quad (8.43)$$

where E_a^{app} is the apparent activation energy and R is the ideal gas constant. This relation is going to be used as a means to extract E_a^{app} from the experimental data of Pearson *et al.* [7] and our calculated data from Equation (8.20) so as to evaluate the quality of agreement between our free volume theory and the experimental measurements. As shown in Figure 8.7, the calculated results (filled markers) agree well with that of the experimental results (unfilled markers) for polyethylene chains with all three different M s ($M = 1190 \text{ g} \cdot \text{mole}^{-1}$, $M = 2128 \text{ g} \cdot \text{mole}^{-1}$, $M = 11396 \text{ g} \cdot \text{mole}^{-1}$). The data were then fitted to the Arrhenius relation with the solid and dashed lines being fits to the calculated data and experimental data in Figure 8.7, respectively. The fitting results were also listed in Table 8.6. Our free volume theory predicts $E_a^{app} \approx 5.30 - 7.70 \text{ kcal} \cdot \text{mole}^{-1}$, whereas experimental values are $E_a^{app} \approx 5.50 - 6.75 \text{ kcal} \cdot \text{mole}^{-1}$.³

Table 8.6: GvdW parameters obtained at different temperatures and the very same value of ϕ^+ evaluated from above results were input in Equation (8.20) to calculate $\eta(T)$ for polyethylene with different M and structures. The apparent activation energy E_a^{app} is derived from fitting of both the calculated and experimental data to an Arrhenius form.

$M \text{ (g} \cdot \text{mole}^{-1}\text{)}$	Calc. $E_a^{app} \text{ (kcal} \cdot \text{mole}^{-1}\text{)}$	Expt. $E_a^{app} \text{ (kcal} \cdot \text{mole}^{-1}\text{)}$
1190 (Linear chain)	5.29	5.49
2128 (Linear chain)	5.46	6.36
11396 (Linear chain)	7.66	6.74

³The deviation in E_a^{app} between prediction and experiment changes with M because in the polymer free volume theory, the integral $\int_{\phi^+}^{\infty} P_d d\phi$ becomes a much stronger function of temperature as M increases, which then affects the calculated value of viscosity (cf., Equation (8.20)).

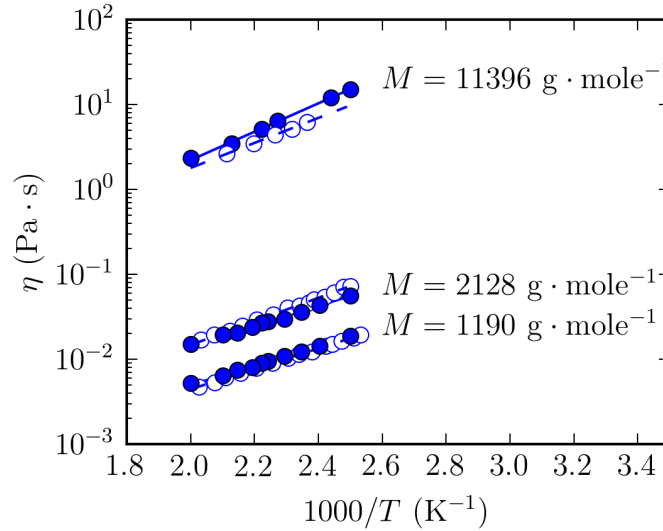


Figure 8.7: Temperature dependence of η for linear polyethylene chain with $M = 1190 \text{ g} \cdot \text{mole}^{-1}$, $M = 2128 \text{ g} \cdot \text{mole}^{-1}$ and $M = 11396 \text{ g} \cdot \text{mole}^{-1}$. The filled markers are data calculated using Equation (8.20) and the unfilled markers are experimental data of Pearson *et al.* [7]. The solid and dashed linear curves are fitting of the calculated and the experimental to the Arrhenius relation, which gives us the apparent activation energy in Table 8.6.

Finally, in the future, the temperature dependence of the viscosity of ring and four-arm symmetrical star polyethylene shall be investigated either experimentally or by MD simulation, so as to verify the validity of the associated values of $\phi^+ - F$. We are also aware of the exponential behavior in the M dependence of viscosity of highly entangled branched polymers, which is as follows:

$$\eta \sim \sqrt{M_a/M_e} \exp\left(\nu \frac{M_a}{M_e}\right) \quad (8.44)$$

M_a and M_e are the molecular weight of arm and entanglement molecular weight, respectively [111]. However, this exponential behaviour is observed in highly entangled star polystyrene with $M \gg 10^{5.5} \text{ g} \cdot \text{mole}^{-1}$, which corresponds to around 3000 repeat units [112], whereas in this work, we only consider star polyethylene with a molecular weight range of $M = 420 \text{ g} \cdot \text{mole}^{-1}$ to $M = 14000 \text{ g} \cdot \text{mole}^{-1}$, which corresponds to 15 to 500 repeat units. The tube model predicts that the exponent ν in Equation (8.44) has a value of 15/8; however experiment showed a value of 0.6 for polyisoprene [111]. As for whether the present free volume approach could predict such exponential behavior or not, we would like to postpone

this as a future research plan, which will focus only on branched polymers. The main focus of the present study is to demonstrate the capability of our free volume theory in predicting the crossovers in the M dependence of viscosity of polyethylene with different structures.

In addition, owing to the fact that the potential well in the Lennard-Jones potential for a coarse-grained polystyrene is too deep as the potential well is around $3 \text{ kJ} \cdot \text{mole}^{-1}$ to $4 \text{ kJ} \cdot \text{mole}^{-1}$ [113], which leads to a difficulty in the convergence of PRISM theory calculation, our plan in the calculation of free volume and viscosity of polystyrene was thwarted. Our next plan also includes troubleshooting this issue.

8.4 Conclusion

Based upon the Doolittle concept that viscosity and free volume are inversely related, we applied the Boltzmann equation and the polymer free volume theory of Wong and Choi to describe the crossovers in the M dependence of viscosity for polyethylene with linear, ring and four-arm symmetrical star structures over a M range of $420 - 14,000 \text{ g} \cdot \text{mole}^{-1}$. In particular, the predicted scaling of M below (1.5) and above (3.3) the crossover for linear polyethylene and the crossover value ($3,000 \text{ g} \cdot \text{mole}^{-1}$) agrees well with experiment. A weaker M dependence of η was observed in ring and four-arm symmetrical star polyethylene. In this work, we demonstrated that the accuracy of the viscosity prediction was sensitive to the difference between two free volume parameters (i.e., $(\phi^+ - F)$) and that such differences are 0.06, 0.02 and 0.05 for the linear, ring and four-arm symmetrical star polyethylene, respectively. Here, F signifies the probability of a bead finding free volume greater than the critical free volume while the fraction of such beads (ϕ^+) is related to the activation energy. The corresponding $(\phi^+ - F)$ value of the linear structure was then used to determine the T dependence of η at three different M , giving apparent activation energy E_a^{app} values in the range of $5.30 - 7.70 \text{ kcal} \cdot \text{mole}^{-1}$ that are in good agreement with experimental values of $5.50 - 6.75 \text{ kcal} \cdot \text{mole}^{-1}$.

Chapter 9

Conclusion

9.1 Main Findings and Contributions

All in all, this thesis can be divided into two main parts: Rouse model and relaxation dynamics of polyethylene melts with different structures (Chapter 3 and Chapter 4), and a free volume theory for the diffusivity and viscosity of linear, ring and four-arm symmetrical star polyethylene melts (Chapters 5–8).

In the first part of the thesis, we have demonstrated that an inertia term can be incorporated into a linear equation of motion of Rouse's chain so as to extract the velocity time correlation function, which relies on the eigenvalue and eigenfunction method. When the equation of motion becomes nonlinear, in which the eigenfunction cannot be analytically obtained, the POD method can be applied. Based on the numerical solution to the nonlinear equation of motion, eigenmodes can be determined using the POD method. The eigenmodes allow us to easily calculate the zero-shear viscosity of the polymer melts.

In the second part of the thesis, a free volume theory, which can account for the crossover in the size dependence of the diffusivity and viscosity of polymers with different structures, was presented. Such theory was derived based on the probability for the polymer molecules having sufficient free volume for activation of diffusive motion or momentum transfer, and the probability can be theoretically calculated utilizing the radial distribution functions of the polymer melts, which can be obtained from either MD simulation or PRISM theory. The

free volume theory is also capable of describing the temperature effect on the size dependence of the diffusivity of oligomers as reported by von Meerwall *et al.* [1]. It was found that our free volume theory is more powerful in prediction of viscosity compared to that of diffusivity of polymer melts that it covers a wider range of M in the former case.

9.2 Future Work

9.2.1 Nonlinear BD model and POD method

To the best of our knowledge, most theoretical studies on the dynamic properties in the literature focus on the polyethylene due to its simple structure, whereas studies on other polymers, such as polystyrene, polybutadiene and polyethylene glycol, seem to be lacking. As the POD method does not require the knowledge of the analytical solution of equation of motion, it can be readily applied to these aforementioned polymers even if they are not coarse-grained. Additionally, the nonlinear BD model presented is only restricted to unentangled polymers, but not entangled polymers. Future investigation is directed towards the possibility of incorporating extra terms in the BD equation of motion to account for the entanglement effect.

In addition, experimental data and simulation data of entangled symmetrical star polyethylene are also lacking in the literature, which makes comparison with our free volume theory impossible. As mentioned in Chapter 8, preliminary POD analysis was performed for the MD data of four-arm symmetrical star polyethylene with $N > N_c$, and these data will be more thoroughly studied in the future.

9.2.2 Free Volume Theory

Calculation of Shear Relaxation Modulus

Furthermore, it is possible that the analysis of free volume may be incorporated into the analysis of relaxation times of the macromolecules, such that it can generate shear relaxation modulus of polymer with different structures. This is an interesting question to think about

as a plateau modulus is absent in ring polymer with $M > M_c$, whereas the reverse is true in linear polymer. We envisage that with the same value of $\phi^+ - F$ in our free volume theory along with the Verdier-Stockmayer theory [114, 115], one may be able to predict the shear relaxation modulus as a function of time for polymer melts with different structures in addition to their corresponding N dependence of η .

Limitation and Possible Improvement of the Free Volume Theory

Despite the success of our free volume theory in describing the crossover in the size dependence of the diffusivity of linear and ring polymers, there exists a two limitations in our theory:

1. Our free volume theory can only describe the crossover in diffusivity within a particular range of N (i.e., $N < 500$) and that in viscosity with $N < 1000$. As $N \rightarrow \infty$, our theory gives a much more negative and more positive exponent than -2.4 and 3.4 , respectively. As shown in Chapter 7, as $N \rightarrow \infty$, the $P_d(\phi)$ becomes narrower as determined by our theoretical approximation. This theoretical approximation of $P_d(\phi)$ may not be valid anymore as $N \rightarrow \infty$, and it may be tested by MD simulation in the future. This is because in MD simulation, one can count the number of beads of the macromolecule having sufficient free volume directly, and thus to get the exact $P_d(\phi)$ distribution.
2. As shown in Chapter 5 and Chapter 6, the justification of ϕ^+ still relies on the experimental data of D_{cm} and η as a function of temperature due to the absence of a theoretical method for determining the activation energy of a macromolecule. It is postulated that such activation energy should be related to the flexibility of the chain molecule. In other words, the angle bending potential as well as torsion potential may influence how high the activation energy is. Another way to justify the value of ϕ^+ is perhaps the application of the same value of $(\phi^+ - F)$ in the reproduction of the experimental value of shear relaxation modulus of the polymer.
3. The theory in the present form depends on free volume analysis of polymer melts, which is a numerical procedure. This makes our free volume theory less easily accessible. Hence, another future plan is that we should attempt to simplify the free volume

analysis such that it is analytical (or at least any numerical calculations are further minimized) and can be done even without any computer.

Branched Polymer Melts, Blend of Linear and Ring Polymers, as well as Polymer Solutions

It is envisaged that the existing free volume theory at this stage can be readily applied to the calculation of diffusivity in other cases, such as a star polymer, a polydisperse polymer melt, a blend of linear and ring polymers, as well as polymer solutions. The intermolecular and intramolecular radial distribution functions of these systems can be straightforwardly calculated using either PRISM or MD simulation for obtaining the probability for the macromolecule finding sufficient free volume.

9.2.3 Relation among the Velocity Time Correlation Function, the POD Method and the Free Volume Theory

The procedures and results as demonstrated in Chapter 3 are useful in the evaluation of diffusivity and viscosity of dilute polymer medium. The more precise form of the stress tensor is:

$$\sigma = \sum_j \frac{m\mathbf{v}_j\mathbf{v}_j}{V} + \frac{1}{2V} \sum_i \sum_j \mathbf{r}_{ij}\mathbf{F}_{ij} \quad (9.1)$$

In Chapter 1, we have shown that armed with the understanding of binary collision between two particles, the diffusivity and viscosity of dilute gases can be derived from the velocity time correlation function and the time correlation function of stress, respectively. In the Rouse model, the kinetic term in the stress tensor of Equation (9.1) is neglected. In Chapter 4, we have used such assumption in the Rouse model to derive the zero-shear viscosity of unentangled polyethylene melt. On the contrary, in Chapter 8, we have only considered the kinetic contribution to the stress tensor, as mathematically it can be shown that the potential term from intramolecular interaction has no effect on the shear stress. Nonetheless, armed with the knowledge of velocity time correlation function of polymers in Chapter 3 and the kinetic theory of gases in Chapter 1, we should also be able to evaluate the viscosity of dilute polymer medium by integrating the stress correlation function over time instead of using

Boltzmann equation. This is another possible direction of our future plan. The validity of neglecting the kinetic contribution to the stress tensor in the Rouse model will also be tested in the future.

Finally, as demonstrated in Chapter 4 and Chapter 8, the POD analysis and the free volume theory both give us the zero-shear viscosity of the polyethylene melts, which is reasonably comparable to the experimental values. The zero-shear viscosity calculated by these two methods will be more thoroughly compared in the future.

References

- [1] E. Von Meerwall, S. Beckman, J. Jang and W. Mattice, *J. Chem. Phys.*, 1998, **108**, 4299–4304.
- [2] K. Hur, R. G. Winkler and D. Y. Yoon, *Macromolecules*, 2006, **39**, 3975–3977.
- [3] K. Hur, C. Jeong, R. G. Winkler, N. Lacevic, R. H. Gee and D. Y. Yoon, *Macromolecules*, 2011, **44**, 2311–2315.
- [4] G. Tsolou, N. Stratikis, C. Baig, P. S. Stephanou and V. G. Mavrantzas, *Macromolecules*, 2010, **43**, 10692–10713.
- [5] S. Brown and G. Szamel, *J. Chem. Phys.*, 1998, **108**, 4705–4708.
- [6] J. D. Halverson, W. B. Lee, G. S. Grest, A. Y. Grosberg and K. Kremer, *The Journal of chemical physics*, 2011, **134**, 204905.
- [7] D. Pearson, G. Ver Strate, E. Von Meerwall and F. Schilling, *Macromolecules*, 1987, **20**, 1133–1141.
- [8] J. Padding and W. J. Briels, *J. Chem. Phys.*, 2002, **117**, 925–943.
- [9] C. P. J. Wong and P. Choi, *Macromol. Theory Simul.*, 2019, 1800072.
- [10] S. Chapman, T. G. Cowling and D. Burnett, *The mathematical theory of non-uniform gases: an account of the kinetic theory of viscosity, thermal conduction and diffusion in gases*, Cambridge university press, 1990.
- [11] P. Flory and M. Volkenstein, *Statistical mechanics of chain molecules*, 1969.
- [12] W. L. Mattice and U. W. Suter, *Conformational theory of large molecules: the rotational isomeric state model in macromolecular systems*, Wiley-Interscience, 1994.
- [13] P. C. Hiemenz and T. P. Lodge, *Polymer chemistry*, CRC press, 2007.
- [14] M. Rubinstein and R. H. Colby, *NEW YORK: Oxford University*.
- [15] A. Rudin and P. Choi, *The elements of polymer science and engineering*, Academic press, 2012.
- [16] P. J. Flory, *Statistical Mechanics of Chain Molecules*, Interscience, New York, 1969.
- [17] D. J. Evans and G. Morriss, *Statistical mechanics of nonequilibrium liquids*, Cambridge University Press, 2008.
- [18] M. G. Martin and J. I. Siepmann, *J. Phys. Chem. B*, 1999, **103**, 4508–4517.

- [19] M. G. Martin and J. I. Siepmann, *J. Phys. Chem. B*, 1998, **102**, 2569–2577.
- [20] P. E. Rouse Jr, *J. Chem. Phys.*, 1953, **21**, 1272–1280.
- [21] M. Doi and S. F. Edwards, *The theory of polymer dynamics*, oxford university press, 1988, vol. 73.
- [22] J. T. Kalathi, S. K. Kumar, M. Rubinstein and G. S. Grest, *Macromolecules*, 2014, **47**, 6925–6931.
- [23] J. T. Kalathi, S. K. Kumar, M. Rubinstein and G. S. Grest, *Soft Matter*, 2015, **11**, 4123–4132.
- [24] A. Ghosh, *Relaxation dynamics of branched polymers*, The Pennsylvania State University, 2007.
- [25] K. Kremer and G. S. Grest, *J. Chem. Phys.*, 1990, **92**, 5057–5086.
- [26] J. S. Shaffer, *J. Chem. Phys.*, 1995, **103**, 761–772.
- [27] M. Bulacu and E. van der Giessen, *J. Chem. Phys.*, 2005, **123**, 114901.
- [28] M. Vladkov and J.-L. Barrat, *Macromol. Theory Simul.*, 2006, **15**, 252–262.
- [29] A. Chatterjee, *Curr. Sci.*, 2000, 808–817.
- [30] P. Holmes, J. L. Lumley, G. Berkooz and C. W. Rowley, *Turbulence, coherent structures, dynamical systems and symmetry*, Cambridge university press, 2012.
- [31] H. T. Banks, *Control and estimation in distributed parameter systems*, SIAM, 1992.
- [32] K. Foteinopoulou, N. C. Karayiannis, M. Laso and M. Kröger, *J. Phys. Chem. B*, 2008, **113**, 442–455.
- [33] J. Chang, J. Han, L. Yang, R. L. Jaffe and D. Y. Yoon, *J. Chem. Phys.*, 2001, **115**, 2831–2840.
- [34] M. Fixman, *Macromolecules*, 1986, **19**, 1195–1204.
- [35] L. Martínez, R. Andrade, E. G. Birgin and J. M. Martínez, *J. Comput. Chem.*, 2009, **30**, 2157–2164.
- [36] M. J. Abraham, T. Murtola, R. Schulz, S. Páll, J. C. Smith, B. Hess and E. Lindahl, *SoftwareX*, 2015, **1**, 19–25.
- [37] S. Sen, S. K. Kumar and P. Keblinski, *Macromolecules*, 2005, **38**, 650–653.
- [38] R. Faller and F. Müller-Plathe, *ChemPhysChem*, 2001, **2**, 180–184.
- [39] K. Kremer, G. S. Grest and I. Carmesin, *Phys. Rev. Lett.*, 1988, **61**, 566.
- [40] L. Harnau, R. G. Winkler and P. Reineker, *J. Chem. Phys.*, 1995, **102**, 7750–7757.
- [41] T. A. Kavassalis and J. Noolandi, *Macromolecules*, 1988, **21**, 2869–2879.
- [42] M. Mondello, G. S. Grest, E. B. Webb III and P. Peczak, *J. Chem. Phys.*, 1998, **109**, 798–805.

- [43] D. W. McCall, D. C. Douglass and E. W. Anderson, *J. Chem. Phys.*, 1959, **30**, 771–773.
- [44] T. P. Lodge, *Phys. Rev. Lett.*, 1999, **83**, 3218.
- [45] P. Schleger, B. Farago, C. Lartigue, A. Kollmar and D. Richter, *Phys. Rev. Lett.*, 1998, **81**, 124.
- [46] A. Wischnewski, M. Monkenbusch, L. Willner, D. Richter, A. Likhtman, T. McLeish and B. Farago, *Phys. Rev. Lett.*, 2002, **88**, 058301.
- [47] W. Paul, G. Smith, D. Y. Yoon, B. Farago, S. Rathgeber, A. Zirkel, L. Willner and D. Richter, *Phys. Rev. Lett.*, 1998, **80**, 2346.
- [48] M. Kröger and S. Hess, *Phys. Rev. Lett.*, 2000, **85**, 1128.
- [49] K. Evans and S. F. Edwards, *J. Chem. Soc., Faraday Trans. 2*, 1981, **77**, 1891–1912.
- [50] P.-G. de Gennes, *J. Chem. Phys.*, 1971, **55**, 572–579.
- [51] A. L. Frischknecht and S. T. Milner, *Macromolecules*, 2000, **33**, 5273–5277.
- [52] M. Doi, *J. Polym. Sci. Polym. Phys. Ed.*, 1983, **21**, 667–684.
- [53] M. Rubinstein, *Phys. Rev. Lett.*, 1987, **59**, 1946.
- [54] J. Qin and S. T. Milner, *Soft Matter*, 2011, **7**, 10676–10693.
- [55] M. Kröger and H. Voigt, *Macromol. Theory Simul.*, 1994, **3**, 639–647.
- [56] K. Foteinopoulou, N. C. Karayiannis, V. G. Mavrantzas and M. Kröger, *Macromolecules*, 2006, **39**, 4207–4216.
- [57] J. Vrentas and J. Duda, *J. Appl. Polym. Sci.*, 1978, **22**, 2325–2339.
- [58] J. Vrentas, J. Duda, H.-C. Ling and A.-C. Hou, *J. Polym. Sci. Polym. Phys. Ed.*, 1985, **23**, 289–304.
- [59] D. Turnbull and M. H. Cohen, *J. Chem. Phys.*, 1970, **52**, 3038–3041.
- [60] E. Von Meerwall, J. Grigsby, D. Tomich and R. Van Antwerp, *J. Polym. Sci. Polym. Phys. Ed.*, 1982, **20**, 1037–1053.
- [61] H. Sabbagh and B. C. Eu, *Physica A: Statistical Mechanics and its Applications*, 2010, **389**, 2325–2338.
- [62] B. C. Eu, *Phys. Chem. Chem. Phys.*, 2007, **9**, 6171–6186.
- [63] B. C. Eu, *Transport Coefficients of Fluids*, Springer Science & Business Media, 2006, vol. 82.
- [64] B. C. Eu and K. Rah, *Phys. Rev. E*, 2001, **63**, 031203.
- [65] R. Laghaei, A. Eskandari Nasrabad and B. C. Eu, *J. Chem. Phys.*, 2006, **124**, 154502.
- [66] R. Laghaei, A. Eskandari Nasrabad and B. C. Eu, *J. Phys. Chem. B*, 2005, **109**, 21375–21379.
- [67] K. Rah and B. C. Eu, *J. Chem. Phys.*, 2001, **115**, 2634–2640.

- [68] Y.-L. Zhu, H. Liu and Z.-Y. Lu, *J. Chem. Phys.*, 2012, **136**, 144903.
- [69] V. Harmandaris, V. Mavrantzas, D. Theodorou, M. Kröger, J. Ramirez, H. Öttinger and D. Vlassopoulos, *Macromolecules*, 2003, **36**, 1376–1387.
- [70] G. Tsolou, V. G. Mavrantzas and D. N. Theodorou, *Macromolecules*, 2005, **38**, 1478–1492.
- [71] J. Liu, Q. Deng and Y. Jean, *Macromolecules*, 1993, **26**, 7149–7155.
- [72] P. Macedo and T. Litovitz, *J. Chem. Phys.*, 1965, **42**, 245–256.
- [73] K. Honnell, C. Hall and R. Dickman, *J. Chem. Phys.*, 1987, **87**, 664–674.
- [74] R. P. White and J. E. Lipson, *ACS Macro Letters*, 2015, **4**, 588–592.
- [75] C. Rycroft, *Lawrence Berkeley National Laboratory*, 2009.
- [76] S. Shanbhag and M. Kröger, *Macromolecules*, 2007, **40**, 2897–2903.
- [77] M. Kröger, *Computer physics communications*, 2005, **168**, 209–232.
- [78] M. Rubinstein, *Phys. Rev. Lett.*, 1986, **57**, 3023.
- [79] M. Kapnistos, M. Lang, D. Vlassopoulos, W. Pyckhout-Hintzen, D. Richter, D. Cho, T. Chang and M. Rubinstein, *Nat. Mater.*, 2008, **7**, 997.
- [80] R. M. Robertson and D. E. Smith, *Proc. Natl. Acad. Sci. U.S.A.*, 2007, **104**, 4824–4827.
- [81] C. D. Chapman, S. Shanbhag, D. E. Smith and R. M. Robertson-Anderson, *Soft Matter*, 2012, **8**, 9177–9182.
- [82] M. H. Cohen and D. Turnbull, *J. Chem. Phys.*, 1959, **31**, 1164–1169.
- [83] M. L. Williams, R. F. Landel and J. D. Ferry, *Journal of the American Chemical society*, 1955, **77**, 3701–3707.
- [84] G. McKenna, G. Hadziioannou, P. Lutz, G. Hild, C. Strazielle, C. Straupe, P. Rempp and A. Kovacs, *Macromolecules*, 1987, **20**, 498–512.
- [85] C. P. J. Wong and P. Choi, *Soft matter*, 2019, **15**, 9300–9309.
- [86] K. S. Schweizer and J. Curro, in *Atomistic Modeling of Physical Properties*, Springer, 1994, pp. 319–377.
- [87] R. M. Dammert, S. L. Maunu, F. H. Maurer, I. M. Neelov, S. Niemelä, F. Sundholm and C. Wästlund, *Macromolecules*, 1999, **32**, 1930–1938.
- [88] T. B. Martin, T. E. Gartner III, R. L. Jones, C. R. Snyder and A. Jayaraman, *Macromolecules*, 2018, **51**, 2906–2922.
- [89] M. D. Hanwell, D. E. Curtis, D. C. Lonie, T. Vandermeersch, E. Zurek and G. R. Hutchison, *J. Cheminf.*, 2012, **4**, 17.
- [90] E. Von Meerwall, R. Ozisik, W. Mattice and P. Pfister, *J. Chem. Phys.*, 2003, **118**, 3867–3873.

- [91] P. V. Alatas, D. G. Tsalikis and V. G. Mavrantzas, *Macromol. Theory Simul.*, 2017, **26**, 1600049.
- [92] H. H. Gan and B. C. Eu, *J. Chem. Phys.*, 1995, **103**, 2140–2156.
- [93] D. Huang, S. L. Simon and G. B. McKenna, *J. Chem. Phys.*, 2005, **122**, 084907.
- [94] A. R. Brás, S. Gooßen, M. Krutyeva, A. Radulescu, B. Farago, J. Allgaier, W. Pyckhout-Hintzen, A. Wischnewski and D. Richter, *Soft Matter*, 2014, **10**, 3649–3655.
- [95] K. R. Peddireddy, M. Lee, Y. Zhou, S. Adalbert, S. Anderson, C. M. Schroeder and R. M. Robertson-Anderson, *Soft matter*, 2020, **16**, 152–161.
- [96] B. H. Zimm, *J. Chem. Phys.*, 1956, **24**, 269–278.
- [97] K. S. Schweizer and J. G. Curro, *Macromolecules*, 1988, **21**, 3070–3081.
- [98] M. I. Bulacu, *Ph.D. thesis*, 2008.
- [99] D. G. Tsalikis, P. V. Alatas, L. D. Peristeras and V. G. Mavrantzas, *ACS Macro Letters*, 2018, **7**, 916–920.
- [100] Y. Doi, K. Matsubara, Y. Ohta, T. Nakano, D. Kawaguchi, Y. Takahashi, A. Takano and Y. Matsushita, *Macromolecules*, 2015, **48**, 3140–3147.
- [101] S. T. Milner and T. McLeish, *Phys. Rev. Lett.*, 1998, **81**, 725.
- [102] R. Everaers, S. K. Sukumaran, G. S. Grest, C. Svaneborg, A. Sivasubramanian and K. Kremer, *Science*, 2004, **303**, 823–826.
- [103] M. Rubinstein and E. Helfand, *J. Chem. Phys.*, 1985, **82**, 2477–2483.
- [104] C. Tzoumanekas and D. N. Theodorou, *Macromolecules*, 2006, **39**, 4592–4604.
- [105] C. P. J. Wong and P. Choi, *Soft Matter*, 2020, **16**, 2350–2362.
- [106] C. P. J. Wong and P. Choi, *Soft Matter*, 2020, **16**, 4283–4289.
- [107] I. W. Burr, *Technometrics*, 1967, **9**, 647–651.
- [108] A. K. Doolittle and D. B. Doolittle, *J. Appl. Phys.*, 1957, **28**, 901–905.
- [109] K. S. Schweizer and J. G. Curro, *Phys. Rev. Lett.*, 1987, **58**, 246.
- [110] X. Xu, J. Chen and L. An, *J. Chem. Phys.*, 2015, **142**, 074903.
- [111] D. S. Pearson and E. Helfand, *Macromolecules*, 1984, **17**, 888–895.
- [112] W. Graessley and J. Roovers, *Macromolecules*, 1979, **12**, 959–965.
- [113] Q. Xiao and H. Guo, *Phys. Chem. Chem. Phys.*, 2016, **18**, 29808–29824.
- [114] P. H. Verdier and W. Stockmayer, *J. Chem. Phys.*, 1962, **36**, 227–235.
- [115] P. H. Verdier, *J. Chem. Phys.*, 1970, **52**, 5512–5517.

- [116] P.-G. De Gennes and P.-G. Gennes, *Scaling concepts in polymer physics*, Cornell university press, 1979.
- [117] S. Brown and G. Szamel, *J. Chem. Phys.*, 1998, **109**, 6184–6192.
- [118] G. S. Grest, L. J. Fetters, J. S. Huang and D. Richter, *Adv. Chem. Phys.*, 2007, **94**, 67.
- [119] S. Brown and G. Szamel, *Macromol. Theory Simul.*, 2000, **9**, 14–19.
- [120] C. P. J. Wong and P. Choi, *Comput. Mater. Sci*, 2018, **155**, 320–324.
- [121] Y. Masubuchi, H. Takata, Y. Amamoto and T. Yamamoto, *Nihon Reoroji Gakkaishi*, 2018, **46**, 171–178.
- [122] H. Watanabe, *Polymer journal*, 2009, **41**, 929–950.
- [123] A. Mitsutake, H. Iijima and H. Takano, *J. Chem. Phys.*, 2011, **135**, 10B623.
- [124] A. Mitsutake and H. Takano, *Biophys. Rev. Lett.*, 2018, **10**, 375–389.
- [125] K. Hagita and H. Takano, *J. Phys. Soc. Jpn.*, 2002, **71**, 673–676.
- [126] T. Nagai, A. Mitsutake and H. Takano, *J. Phys. Soc. Jpn*, 2013, **82**, 023803.
- [127] W. B. Lee and K. Kremer, *Macromolecules*, 2009, **42**, 6270–6276.
- [128] A. R. Khokhlov, *Statistical physics of macromolecules*, Amer Inst of Physics, 1994.
- [129] M. Dettenmaier, *J. Chem. Phys.*, 1978, **68**, 2319–2322.

Appendix A

A Review on the Relaxation Dynamics Analysis of Unentangled Polymers with Different Structures¹

A.1 Introduction

Polyethylene melts exhibit interesting dynamic behavior as a function of the chain length. Due to the simplicity of its structure, its dynamic properties, such as diffusivity (D_{cm}) and viscosity (η), have been studied both experimentally and theoretically [21, 116, 50, 7, 1, 20, 43]. In particular, its dynamic properties as a function of its size has drawn a lot of attentions from both theorists and experimentalists. Generally, it was experimentally observed that for linear polymers, at a temperature of 175 °C, $D_{cm} \sim N^{-1.5}$ and $D_{cm} \sim N^{-2.2}$ in unentangled and entangled regimes, respectively [1, 85, 44, 3] and N is the chain length. Two classic theoretical models, which are the Rouse model [20] and reptation model [21, 116, 50], were developed to aid interpretation of experimental data in the unentangled and entangled regimes, respectively. The studies on the dynamics of polyethylene melts are not only restricted to the classic linear structure, but also ring [117, 5, 79, 6, 3, 4] and branched polymers [110, 118, 119], due to their peculiar dynamic behavior and topological properties. Understanding of the dynamic behavior of ring polymers is also important in the area of molecular biology due to the fact that DNA exhibits circular structure [80].

¹A version of this chapter has been published in *Mol Simul*, 2020, 1-12.

It is pertinent to point out that the scaling relation $D_{cm} \sim N^{-1}$ and $D_{cm} \sim N^{-2}$ derived from the Rouse model and reptation model, respectively, are not perfectly in line with the experimental and simulation results. For the classic linear structure, the Rouse model can only account for the scaling relation within a very narrow range of M below the crossover molecular weight (M_c). Harmadaris *et al.* [69] showed that $D_{cm} \sim N^{-1}$ only within the range of $60 < N < N_c$, whereas for $N < 60$, the scaling relation is much stronger as demonstrated by von Meerwall *et al.* [1]. The reptation model is only capable for accounting the scaling relation in the entangled regime only after consideration of contour length fluctuation. [101, 44] In addition, the reptation model cannot be directly applied to polymers with different architectures. For instance, it was proposed that the motion of branched polymer adopts an arm retraction mechanism, which should be incorporated in the reptation model [21, 116, 50] and that the motion of ring polymer has to be mapped to that of branched polymer so as to elucidate its peculiar dynamic behavior [78, 79]. In spite of these limitations, these models still give us insight into the motion of a linear chain. In particular, multiple researchers still applied the eigenfunctions derived from the Rouse model, also known as the Rouse modes, to the numerical solution of the nonlinear equation of motion and entangled polymer melts for the determination of different relaxation times (τ_p), even though the Rouse mode may not be valid in the case of entangled polymer melts [22, 8, 27].

In this paper, we would like to focus on the relaxation dynamic and the viscosity of polymers with different structures in the unentangled regime. The Rouse model [20] is useful in such analysis. Nonetheless, it is limited to the case of unentangled linear polyethylene (i.e. for short polyethylene), and neglects the inertia term in the equation of motion. This would make the calculation of velocity time correlation functions impossible. Such inertia term can be incorporated to the equation of motion and an analytical solution can then be derived as demonstrated previously by our group [120]. Briefly, such derivation relies on the eigenvalue and eigenfunction method. In the forthcoming section, we will show that similar analysis can be applied to ring and four-arm symmetrical star polymers. However, such eigenvalues and eigenfunctions can only be obtained when the equation of motion is linear. This shows that the Rouse model can be improved by incorporation of inertia term and it can also be changed to apply to polymers with different structures, such as ring and four-arm symmetrical star.

As mentioned above, another limitation of the Rouse model is that the harmonic bond

stretching potential has an equilibrium length of zero, which means that the beads are allowed to overlap with one another. Nonetheless, if a finite value of equilibrium length was to be used in the harmonic bond stretching potential, the equation of motion is nonlinear, which makes the analytical derivation of eigenfunctions impossible [9]. This is also true in MD simulation, in which angle bending and torsion potentials, as well as 6-12 Lennard-Jones potential are included, making the equations of motion highly nonlinear. We are going to discuss Rouse mode analysis and other available relaxation mode analysis methods, such as proper orthogonal decomposition (POD) method, which offers a way to reduce the order of the model and allows us to calculate such ‘eigenfunctions’ (also known as eigenmodes) from the numerical solutions to the nonlinear equations of motion. The eigenmodes can be applied for obtaining different relaxation times. This method can then be readily applied to polymers with different structures to obtain dynamic properties, such as the zero-shear viscosities. Below is an overview of this paper:

- Analytical solutions to the Rouse model with inertia effect for polymers with different structures.
- Review of the Rouse mode analysis and other available relaxation mode analysis method.
- Time correlation functions of eigenmodes from the POD method and zero-shear viscosity.

A.2 Preliminaries

Consider the simplest case that a single classical particle in one dimensional space is subjected to a harmonic potential. The Langevin dynamics equation of motion for a single particle under such potential can be written as follows:

$$m \frac{d^2x}{dt^2} + \zeta \frac{dx}{dt} = -kx + f(t) \quad (\text{A.1})$$

ζ is the friction coefficient, m is the mass of that single classical particle, k is the spring constant and x is the position of the particle. $f(t)$ is the stochastic force. Alternatively,

Equation (A.1) can be rewritten in a system of two ordinary differential equations.

$$m \frac{dv}{dt} + \zeta v = -kx + f(t) \quad (\text{A.2})$$

$$v = \frac{dx}{dt} \quad (\text{A.3})$$

This system of differential equations can be easily solved by rewriting in the state-space representation.

$$\frac{d}{dt} \begin{bmatrix} x \\ v \end{bmatrix} = \begin{bmatrix} 0 & 1 \\ -\frac{k}{m} & -\frac{\zeta}{m} \end{bmatrix} \begin{bmatrix} x \\ v \end{bmatrix} + \begin{bmatrix} 0 \\ \frac{f(t)}{m} \end{bmatrix} \quad (\text{A.4})$$

The solution is as follows:

$$\begin{bmatrix} x \\ v \end{bmatrix} = e^{\mathbf{A}t} \begin{bmatrix} x \\ v \end{bmatrix}_0 + e^{\mathbf{A}t} \int_0^t e^{-\mathbf{A}\tau} \begin{bmatrix} 0 \\ \frac{f(\tau)}{m} \end{bmatrix} d\tau \quad (\text{A.5})$$

Laplace transformation of the above solution gives us:

$$\begin{bmatrix} X(s) \\ V(s) \end{bmatrix} = (s\mathbf{I} - \mathbf{A})^{-1} \begin{bmatrix} x \\ v \end{bmatrix}_0 + (s\mathbf{I} - \mathbf{A})^{-1} \begin{bmatrix} 0 \\ \frac{F(s)}{m} \end{bmatrix} \quad (\text{A.6})$$

The task has become evaluating $(s\mathbf{I} - \mathbf{A})^{-1}$, which has the following form:

$$(s\mathbf{I} - \mathbf{A})^{-1} = \begin{bmatrix} \frac{s + \frac{\zeta}{m}}{s(s + \frac{\zeta}{m}) + \frac{k}{m}} & \frac{1}{s(s + \frac{\zeta}{m}) + \frac{k}{m}} \\ \frac{-\frac{k}{m}}{s(s + \frac{\zeta}{m}) + \frac{k}{m}} & \frac{s}{s(s + \frac{\zeta}{m}) + \frac{k}{m}} \end{bmatrix} \quad (\text{A.7})$$

A.2.1 Case 1: $\frac{k}{m} > \frac{\zeta^2}{4m^2}$

This can be transformed back to the time domain. If $\frac{k}{m} \gg \frac{\zeta^2}{4m^2}$:

$$e^{\mathbf{A}t} = e^{-\frac{\zeta t}{2m}} \begin{bmatrix} \cos\left(\sqrt{\frac{k}{m} - \frac{\zeta^2}{4m^2}}t\right) + \frac{\zeta \sin\left(\sqrt{\frac{k}{m} - \frac{\zeta^2}{4m^2}}t\right)}{2m\left(\sqrt{\frac{k}{m} - \frac{\zeta^2}{4m^2}}\right)} & \frac{\sin\left(\sqrt{\frac{k}{m} - \frac{\zeta^2}{4m^2}}t\right)}{\sqrt{\frac{k}{m} - \frac{\zeta^2}{4m^2}}} \\ -\frac{k \sin\left(\sqrt{\frac{k}{m} - \frac{\zeta^2}{4m^2}}t\right)}{m\sqrt{\frac{k}{m} - \frac{\zeta^2}{4m^2}}} & \cos\left(\sqrt{\frac{k}{m} - \frac{\zeta^2}{4m^2}}t\right) - \frac{\zeta \sin\left(\sqrt{\frac{k}{m} - \frac{\zeta^2}{4m^2}}t\right)}{2m\sqrt{\frac{k}{m} - \frac{\zeta^2}{4m^2}}} \end{bmatrix} \quad (\text{A.8})$$

Leading to the following solutions:

$$x(t) = x(0)e^{-\frac{\zeta t}{2m}} \left[\cos\left(\sqrt{\frac{k}{m} - \frac{\zeta^2}{4m^2}}t\right) + \frac{\zeta \sin\left(\sqrt{\frac{k}{m} - \frac{\zeta^2}{4m^2}}t\right)}{2m\left(\sqrt{\frac{k}{m} - \frac{\zeta^2}{4m^2}}\right)} \right] + v(0) \frac{e^{-\frac{\zeta}{2m}t} \sin\left(\sqrt{\frac{k}{m} - \frac{\zeta^2}{4m^2}}t\right)}{\sqrt{\frac{k}{m} - \frac{\zeta^2}{4m^2}}} + h(t) \quad (\text{A.9})$$

$$v(t) = -x(0)e^{-\frac{\zeta t}{2m}} \frac{k \sin(\sqrt{\frac{k}{m} - \frac{\zeta^2}{4m^2}} t)}{m\sqrt{\frac{k}{m} - \frac{\zeta^2}{4m^2}}} + v(0)e^{-\frac{\zeta t}{2m}} \left[\cos(\sqrt{\frac{k}{m} - \frac{\zeta^2}{4m^2}} t) - \frac{\zeta \sin(\sqrt{\frac{k}{m} - \frac{\zeta^2}{4m^2}} t)}{2m\sqrt{\frac{k}{m} - \frac{\zeta^2}{4m^2}}} \right] + g(t) \quad (\text{A.10})$$

where,

$$h(t) = e^{-\frac{\zeta t}{2m}} \int_0^t e^{\frac{\zeta}{2m}\tau} \frac{\sin(\sqrt{\frac{k}{m} - \frac{\zeta^2}{4m^2}}(t - \tau))}{\sqrt{\frac{k}{m} - \frac{\zeta^2}{4m^2}}} f(\tau) d\tau \quad (\text{A.11})$$

$$g(t) = e^{-\frac{\zeta t}{2m}} \int_0^t e^{\frac{\zeta}{2m}\tau} \left[\cos(\sqrt{\frac{k}{m} - \frac{\zeta^2}{4m^2}}(t - \tau)) + \frac{\zeta \sin(\sqrt{\frac{k}{m} - \frac{\zeta^2}{4m^2}}(t - \tau))}{2m\sqrt{\frac{k}{m} - \frac{\zeta^2}{4m^2}}} \right] f(\tau) d\tau \quad (\text{A.12})$$

We can then obtain different time correlation functions of the position and velocity:

$$\langle x(t)x(0) \rangle = \langle x^2 \rangle e^{-\frac{\zeta t}{2m}} \left[\cos(\sqrt{\frac{k}{m} - \frac{\zeta^2}{4m^2}} t) + \frac{\zeta \sin(\sqrt{\frac{k}{m} - \frac{\zeta^2}{4m^2}} t)}{2m(\sqrt{\frac{k}{m} - \frac{\zeta^2}{4m^2}})} \right] \quad (\text{A.13})$$

$$\langle v(t)v(0) \rangle = \langle v^2 \rangle e^{-\frac{\zeta t}{2m}} \left[\cos(\sqrt{\frac{k}{m} - \frac{\zeta^2}{4m^2}} t) - \frac{\zeta \sin(\sqrt{\frac{k}{m} - \frac{\zeta^2}{4m^2}} t)}{2m\sqrt{\frac{k}{m} - \frac{\zeta^2}{4m^2}}} \right] \quad (\text{A.14})$$

A.2.2 Case 2: $\frac{\zeta^2}{4m^2} > \frac{k}{m}$

If $\frac{\zeta^2}{4m^2} \gg \frac{k}{m}$, then the matrix exponential $e^{\mathbf{A}t}$ has the following form:

$$e^{\mathbf{A}t} = e^{-\frac{\zeta t}{2m}} \begin{bmatrix} \cosh(\sqrt{\frac{\zeta^2}{4m^2} - \frac{k}{m}} t) + \frac{\zeta \sinh(\sqrt{\frac{\zeta^2}{4m^2} - \frac{k}{m}} t)}{2m(\sqrt{\frac{\zeta^2}{4m^2} - \frac{k}{m}})} & \frac{\sinh(\sqrt{\frac{\zeta^2}{4m^2} - \frac{k}{m}} t)}{\sqrt{\frac{\zeta^2}{4m^2} - \frac{k}{m}}} \\ -\frac{k \sinh(\sqrt{\frac{\zeta^2}{4m^2} - \frac{k}{m}} t)}{m\sqrt{\frac{\zeta^2}{4m^2} - \frac{k}{m}}} & \cosh(\sqrt{\frac{\zeta^2}{4m^2} - \frac{k}{m}} t) - \frac{\zeta \sinh(\sqrt{\frac{\zeta^2}{4m^2} - \frac{k}{m}} t)}{2m\sqrt{\frac{\zeta^2}{4m^2} - \frac{k}{m}}} \end{bmatrix} \quad (\text{A.15})$$

Such that, the solution now becomes:

$$x(t) = x(0)e^{-\frac{\zeta t}{2m}} \left[\cosh(\sqrt{\frac{\zeta^2}{4m^2} - \frac{k}{m}} t) + \frac{\zeta \sinh(\sqrt{\frac{\zeta^2}{4m^2} - \frac{k}{m}} t)}{2m(\sqrt{\frac{\zeta^2}{4m^2} - \frac{k}{m}})} \right] + v(0) \frac{e^{-\frac{\zeta t}{2m}} \sinh(\sqrt{\frac{\zeta^2}{4m^2} - \frac{k}{m}} t)}{\sqrt{\frac{\zeta^2}{4m^2} - \frac{k}{m}}} + h(t) \quad (\text{A.16})$$

$$v(t) = -x(0)e^{-\frac{\zeta t}{2m}} \frac{k \sinh(\sqrt{\frac{\zeta^2}{4m^2} - \frac{k}{m}} t)}{m\sqrt{\frac{\zeta^2}{4m^2} - \frac{k}{m}}} + v(0)e^{-\frac{\zeta t}{2m}} \left[\cosh(\sqrt{\frac{k}{m} - \frac{\zeta^2}{4m^2}} t) - \frac{\zeta \sinh(\sqrt{\frac{\zeta^2}{4m^2} - \frac{k}{m}} t)}{2m\sqrt{\frac{\zeta^2}{4m^2} - \frac{k}{m}}} \right] + g(t) \quad (\text{A.17})$$

where,

$$h(t) = e^{-\frac{\zeta}{2m}t} \int_0^t e^{\frac{\zeta}{2m}\tau} \frac{\sinh(\sqrt{\frac{\zeta^2}{4m^2} - \frac{k}{m}}(t - \tau))}{\sqrt{\frac{\zeta^2}{4m^2} - \frac{k}{m}}} f(\tau) d\tau \quad (\text{A.18})$$

$$g(t) = e^{-\frac{\zeta}{2m}t} \int_0^t e^{\frac{\zeta}{2m}\tau} \left[\cosh(\sqrt{\frac{\zeta^2}{4m^2} - \frac{k}{m}}(t - \tau)) + \frac{\zeta \sinh(\sqrt{\frac{\zeta^2}{4m^2} - \frac{k}{m}}(t - \tau))}{2m\sqrt{\frac{\zeta^2}{4m^2} - \frac{k}{m}}} \right] f(\tau) d\tau \quad (\text{A.19})$$

The time correlation functions now become:

$$\langle x(t)x(0) \rangle = \langle x^2 \rangle e^{-\frac{\zeta t}{2m}} \left[\cosh(\sqrt{\frac{\zeta^2}{4m^2} - \frac{k}{m}}t) + \frac{\zeta \sinh(\sqrt{\frac{\zeta^2}{4m^2} - \frac{k}{m}}t)}{2m(\sqrt{\frac{\zeta^2}{4m^2} - \frac{k}{m}})} \right] \quad (\text{A.20})$$

$$\langle v(t)v(0) \rangle = \langle v^2 \rangle e^{-\frac{\zeta t}{2m}} \left[\cosh(\sqrt{\frac{k}{m} - \frac{\zeta^2}{4m}}t) - \frac{\zeta \sinh(\sqrt{\frac{\zeta^2}{4m^2} - \frac{k}{m}}t)}{2m\sqrt{\frac{\zeta^2}{4m^2} - \frac{k}{m}}} \right] \quad (\text{A.21})$$

In this case, we can extract the diffusivity easily by assuming that $\frac{\zeta^2}{4m^2} \gg \frac{k}{m}$ such that the evaluation of the mean square displacement $\langle (x(t) - x_0)^2 \rangle$ can be simplified.

$$\langle (x(t) - x_0)^2 \rangle = \langle h(t)^2 \rangle \quad (\text{A.22})$$

With:

$$\langle h(t)^2 \rangle = \frac{m^2}{\zeta^2} \int_0^t \int_0^t \left(1 - e^{-\frac{\zeta}{m}(t-\tau_1)}\right) \left(1 - e^{-\frac{\zeta}{m}(t-\tau_2)}\right) \langle f(\tau_1)f(\tau_2) \rangle d\tau_1 d\tau_2 \quad (\text{A.23})$$

$\langle f(\tau_1)f(\tau_2) \rangle = 2k_b T \frac{\zeta}{m^2} \delta(\tau_1 - \tau_2)$. This is going to give us:

$$\langle h^2(t) \rangle = \frac{2k_b T}{\zeta} t - \frac{3k_b T m}{\zeta^2} + \frac{4k_b T m}{\zeta^2} e^{-\frac{\zeta}{m}t} - \frac{k_b T m}{\zeta^2} e^{-\frac{2\zeta}{m}t} \quad (\text{A.24})$$

As time approaches to infinity, we then have:

$$\lim_{t \rightarrow \infty} \langle (r - r_0)^2 \rangle = \frac{2k_b T t}{\zeta} \quad (\text{A.25})$$

Therefore, $D = \frac{k_b T}{\zeta}$.

A.3 Analytical Solution of Linear Dynamics: Time Correlation Functions and Velocity Correlation Functions of Linear, Ring, and Star Polymers

In this sense, we can also write a Langevin dynamics equation of motion for polymers with different structures by assuming that beads are collected to one another by a harmonic bond

stretching potential. By obtaining the solutions to these equations of motion, different time correlation functions can then be derived.

A.3.1 Linear Polymer

For linear polymer, the Langevin dynamics equation of motion is written as follows:

$$\frac{d}{dt} \begin{bmatrix} \mathbf{x}_n \\ \mathbf{y}_n \\ \mathbf{z}_n \\ \mathbf{v}_{x,n} \\ \mathbf{v}_{y,n} \\ \mathbf{v}_{z,n} \end{bmatrix} = \begin{bmatrix} \mathbf{0} & \mathbf{0} & \mathbf{0} & \mathbf{I} & \mathbf{0} & \mathbf{0} \\ \mathbf{0} & \mathbf{0} & \mathbf{0} & \mathbf{0} & \mathbf{I} & \mathbf{0} \\ \mathbf{0} & \mathbf{0} & \mathbf{0} & \mathbf{0} & \mathbf{0} & \mathbf{I} \\ \frac{k}{m}\mathbf{A} & \mathbf{0} & \mathbf{0} & \xi\mathbf{I} & \mathbf{0} & \mathbf{0} \\ \mathbf{0} & \frac{k}{m}\mathbf{A} & \mathbf{0} & \mathbf{0} & \xi\mathbf{I} & \mathbf{0} \\ \mathbf{0} & \mathbf{0} & \frac{k}{m}\mathbf{A} & \mathbf{0} & \mathbf{0} & \xi\mathbf{I} \end{bmatrix} \begin{bmatrix} \mathbf{x}_n \\ \mathbf{y}_n \\ \mathbf{z}_n \\ \mathbf{v}_{x,n} \\ \mathbf{v}_{y,n} \\ \mathbf{v}_{z,n} \end{bmatrix} + \frac{1}{m} \begin{bmatrix} \mathbf{0} \\ \mathbf{0} \\ \mathbf{0} \\ \mathbf{f}_{x,n} \\ \mathbf{f}_{y,n} \\ \mathbf{f}_{z,n} \end{bmatrix} \quad (\text{A.26})$$

Such that $\xi = \frac{\zeta}{m}$ and \mathbf{A} contains the information of how the beads are connected to one another. For linear polymer, \mathbf{A} has the following form:

$$\mathbf{A} = \begin{bmatrix} -1 & 1 & 0 & 0 & \dots & 0 & 0 \\ 1 & -2 & 1 & 0 & \dots & 0 & 0 \\ 0 & 1 & -2 & 1 & \dots & 0 & 0 \\ 0 & \vdots & \ddots & \ddots & \ddots & 0 & 0 \\ 0 & \dots & \dots & 1 & -2 & 1 & 0 \\ 0 & \dots & \dots & 0 & 1 & -2 & 1 \\ 0 & \dots & \dots & 0 & 0 & 1 & -1 \end{bmatrix} \quad (\text{A.27})$$

\mathbf{I} is $N \times N$ identity matrix and \mathbf{A} is $N \times N$ matrix. \mathbf{x}_n , \mathbf{y}_n and \mathbf{z}_n contains Cartesian coordinates of the N beads in x , y and z directions, respectively; $\mathbf{v}_{x,n}$, $\mathbf{v}_{y,n}$ and $\mathbf{v}_{z,n}$ contain velocities of N beads in three different directions; $\mathbf{f}_{x,n}$, $\mathbf{f}_{y,n}$ and $\mathbf{f}_{z,n}$ contains the stochastic force component acting upon the N beads in three directions. These position, velocity and force vectors in a particular direction have a dimension of $N \times 1$. It is a daunting task to solve matrix Equation (A.26), but the matrix Equation (A.26) can be rewritten into a partial differential equation with boundary conditions.

$$\frac{\partial^2 \mathbf{r}_n}{\partial t^2} + \xi \frac{\partial \mathbf{r}_n}{\partial t} = \frac{k}{m} \frac{\partial^2 \mathbf{r}_n}{\partial n^2} + \frac{\mathbf{f}_n}{m} \quad (\text{A.28})$$

where \mathbf{r}_n and \mathbf{f}_n are vectors containing the positions of and stochastic force acting upon n th beads. Thus, these two vectors have N components. Note that the mean $\langle f_n \rangle$ and mean-sqaure $\langle f_n(t)f_n(t') \rangle$ values of stochastic force \mathbf{f}_n are 0 and $6k_b T \zeta \delta(t - t')$. The partial

differential equation (cf., Equation (A.28)) is subjected to the following boundary conditions:

$$\left. \frac{\partial \mathbf{r}_n}{\partial n} \right|_{n=0} = 0, \quad \left. \frac{\partial \mathbf{r}_n}{\partial n} \right|_{n=N-1} = 0 \quad (\text{A.29})$$

Eigenvalues of $\lambda_p^2 = \frac{p^2 \pi^2}{N^2}$ and eigenfunctions of $\cos(p\pi \frac{n}{N})$ for $p = 0, 1, 2, \dots, N-1$ are obtained. It is convenient to define normal coordinates for reconstruction of different time correlation functions:

$$\mathbf{X}_p(t) = \frac{1}{N} \int_0^N \mathbf{r}_n(t) \cos(p\pi \frac{n}{N}) dn \quad (\text{A.30})$$

$$\mathbf{V}_p(t) = \frac{1}{N} \int_0^N \mathbf{v}_n(t) \cos(p\pi \frac{n}{N}) dn \quad (\text{A.31})$$

\mathbf{v}_n is the velocity vector. Based on this, different time correlation functions can be derived easily. More details on the derivation of the analytical forms of $\mathbf{X}_p(t)$ and $\mathbf{V}_p(t)$ for the linear polymer are available in our previous work [120], but we are going to show such procedures in the case of ring polymer in the forthcoming section, which was not demonstrated in our previous work [120].

A.3.2 Ring Polymer

As mentioned above, \mathbf{A} contains information of the structure of polymer. Therefore, in the case of ring polymers, we have:

$$\mathbf{A} = \begin{bmatrix} -2 & 1 & 0 & 0 & \dots & 0 & 1 \\ 1 & -2 & 1 & 0 & \dots & 0 & 0 \\ 0 & 1 & -2 & 1 & \dots & 0 & 0 \\ 0 & \vdots & \ddots & \ddots & \ddots & 0 & 0 \\ 0 & \dots & \dots & 1 & -2 & 1 & 0 \\ 0 & \dots & \dots & 0 & 1 & -2 & 1 \\ 1 & \dots & \dots & 0 & 0 & 1 & -2 \end{bmatrix} \quad (\text{A.32})$$

The partial differential equation (cf., Equation (A.28)) is now subjected to a slight different set of boundary conditions:

$$\left. \frac{\partial \mathbf{r}_n}{\partial n} \right|_{n=0} = \left. \frac{\partial \mathbf{r}_n}{\partial n} \right|_{n=N-1} = 0 \quad (\text{A.33})$$

Interestingly, the eigenvalues of this problem are $\lambda_p^2 = \frac{4p^2 \pi^2}{N^2}$ and there are two sets of eigenfunctions: $\psi_p(n) = \cos(2p\pi \frac{n}{N})$ as well as $\psi_p(n) = \sin(2p\pi \frac{n}{N})$, for $p = 0, 1, 2, \dots, \frac{N-1}{2}$ assuming

that N is an odd number. This leads to two different sets of normal coordinates for positions and velocities. \mathbf{X}_p and \mathbf{V}_p now become:

$$\mathbf{X}_p(t) = \frac{1}{N} \int_0^N \mathbf{r}_n(t) \cos(2p\pi \frac{n}{N}) dn \quad (\text{A.34})$$

$$\mathbf{V}_p(t) = \frac{1}{N} \int_0^N \mathbf{v}_n(t) \cos(2p\pi \frac{n}{N}) dn \quad (\text{A.35})$$

With an additional set of normal coordinates defined as:

$$\mathbf{Y}_p(t) = \frac{1}{N} \int_0^N \mathbf{r}_n(t) \sin(2p\pi \frac{n}{N}) dn \quad (\text{A.36})$$

$$\mathbf{W}_p(t) = \frac{1}{N} \int_0^N \mathbf{v}_n(t) \sin(2p\pi \frac{n}{N}) dn \quad (\text{A.37})$$

For instance, considering \mathbf{X}_p and \mathbf{V}_p , this allows us to write ordinary differential equations for each value of p :

$$\frac{d}{dt} \mathbf{X}_p(t) = \mathbf{V}_p(t) \quad (\text{A.38})$$

$$\frac{d}{dt} \mathbf{V}_p(t) + \xi \mathbf{V}_p(t) = -\frac{\lambda_p^2 k}{m} \mathbf{X}_p(t) + \frac{1}{Nm} \int_0^N \mathbf{f}_n \cos(2p\pi \frac{n}{N}) dn \quad (\text{A.39})$$

In state-space representation, we obtain:

$$\frac{d}{dt} \begin{bmatrix} \mathbf{X}_p(t) \\ \mathbf{V}_p(t) \end{bmatrix} = \begin{bmatrix} 0 & 1 \\ -\frac{\lambda_p^2 k}{m} & -\xi \end{bmatrix} \begin{bmatrix} \mathbf{X}_p(t) \\ \mathbf{V}_p(t) \end{bmatrix} + \begin{bmatrix} 0 \\ \frac{1}{Nm} \int_0^N \mathbf{f}_n \cos(2p\pi \frac{n}{N}) dn \end{bmatrix} \quad (\text{A.40})$$

We can then obtain the exact solution easily:

$$\begin{bmatrix} \mathbf{X}_p(t) \\ \mathbf{V}_p(t) \end{bmatrix} = e^{\mathcal{A}t} \begin{bmatrix} \mathbf{X}_p(0) \\ \mathbf{V}_p(0) \end{bmatrix} + \frac{1}{Nm} \int_0^t e^{\mathcal{A}(t-\tau)} \begin{bmatrix} 0 \\ \int_0^N \mathbf{f}_n \cos(2p\pi \frac{n}{N}) dn \end{bmatrix} d\tau \quad (\text{A.41})$$

where the matrix \mathcal{A} has the following form:

$$\mathcal{A} = \begin{bmatrix} 0 & 1 \\ -\frac{\lambda_p^2 k}{m} & -\xi \end{bmatrix} \quad (\text{A.42})$$

Laplace transformation then gives us:

$$\begin{bmatrix} \tilde{\mathbf{X}}_p(s) \\ \tilde{\mathbf{V}}_p(s) \end{bmatrix} = (s\mathbf{I} - \mathcal{A})^{-1} \begin{bmatrix} \mathbf{X}_p(0) \\ \mathbf{V}_p(0) \end{bmatrix} + (s\mathbf{I} - \mathcal{A})^{-1} \begin{bmatrix} 0 \\ \frac{1}{Nm} \int_0^N \tilde{\mathbf{f}}_n(s) \cos(2p\pi \frac{n}{N}) dn \end{bmatrix} \quad (\text{A.43})$$

which can be written more explicitly as:

$$\begin{bmatrix} \tilde{\mathbf{X}}_p(s) \\ \tilde{\mathbf{V}}_p(s) \end{bmatrix} = \frac{1}{s(s + \xi) + \frac{\lambda_p^2 k}{m}} \begin{bmatrix} s + \xi & 1 \\ -\frac{\lambda_p^2 k}{m} & s \end{bmatrix} \begin{bmatrix} \mathbf{X}_p(0) \\ \mathbf{V}_p(0) + \frac{1}{Nm} \int_0^N \tilde{\mathbf{f}}_n(s) \cos(2p\pi \frac{n}{N}) dn \end{bmatrix} \quad (\text{A.44})$$

Inverse laplace transformation can then give us the solution in the time domain:

$$\mathbf{X}_{\mathbf{p}}(t) = e^{-\frac{\xi t}{2}} \left\{ \mathbf{X}_{\mathbf{p}}(0) \left[\cosh(\omega t) + \frac{\xi \sinh(\omega t)}{2\omega} \right] + \frac{\mathbf{V}_{\mathbf{p}}(0) \sinh(\omega t)}{\omega} \right\} + \mathbf{H}_{\mathbf{p}}(t) \quad (\text{A.45})$$

$$\mathbf{V}_{\mathbf{p}}(t) = e^{-\frac{\xi t}{2}} \left\{ -\frac{\mathbf{X}_{\mathbf{p}}(0) \lambda_p^2 k}{m\omega} \sinh(\omega t) + \mathbf{V}_{\mathbf{p}}(0) \left[\cosh(\omega t) - \frac{\xi}{2\omega} \sinh(\omega t) \right] \right\} + \mathbf{G}_{\mathbf{p}}(t) \quad (\text{A.46})$$

Note that:

$$\omega = \sqrt{\frac{\xi^2}{4} - \frac{\lambda_p^2 k}{m}} \quad (\text{A.47})$$

In this case, ω is a real number, if $\frac{\xi^2}{4}$ is greater than $\frac{\lambda_p^2 k}{m}$, whereas ω is an imaginary number if the reverse is true. And:

$$\mathbf{H}_{\mathbf{p}}(t) = \frac{1}{Nm} \int_0^t e^{-\frac{\xi}{2}(t-\tau)} \frac{\sinh(\omega(t-\tau))}{\omega} \int_0^N \mathbf{f}_{\mathbf{n}}(\tau) \cos(2p\pi \frac{n}{N}) dnd\tau \quad (\text{A.48})$$

$$\mathbf{G}_{\mathbf{p}}(t) = \frac{1}{Nm} \int_0^t e^{-\frac{\xi}{2}(t-\tau)} \left[\cosh(\omega(t-\tau)) - \frac{\xi}{2\omega} \sinh(\omega(t-\tau)) \right] \int_0^N \mathbf{f}_{\mathbf{n}}(\tau) \cos(2p\pi \frac{n}{N}) dnd\tau \quad (\text{A.49})$$

The time correlation functions (TCFs) of $\mathbf{X}_{\mathbf{p}}$ and the VCFs of $\mathbf{V}_{\mathbf{p}}$ can be easily obtained by multiplying Equation (A.45) and Equation (A.46) with $\mathbf{X}_{\mathbf{p}}(0)$ and $\mathbf{V}_{\mathbf{p}}(0)$, respectively, followed by taking average. Using the fact that $\langle \mathbf{X}_{\mathbf{p}} \cdot \mathbf{G}_{\mathbf{p}} \rangle = 0$, $\langle \mathbf{X}_{\mathbf{p}} \cdot \mathbf{H}_{\mathbf{p}} \rangle = 0$, $\langle \mathbf{V}_{\mathbf{p}} \cdot \mathbf{G}_{\mathbf{p}} \rangle = 0$, $\langle \mathbf{V}_{\mathbf{p}} \cdot \mathbf{H}_{\mathbf{p}} \rangle = 0$, $\langle \mathbf{X}_{\mathbf{p}} \cdot \mathbf{V}_{\mathbf{p}} \rangle = 0$ as they are not correlated to one another, except themselves, we can write:

$$\langle \mathbf{X}_{\mathbf{p}}(t) \cdot \mathbf{X}_{\mathbf{p}}(0) \rangle = e^{-\frac{\xi t}{2}} \langle X_p^2 \rangle \left[\cosh(\omega t) + \frac{\xi \sinh(\omega t)}{2\omega} \right] \quad (\text{A.50})$$

$$\langle \mathbf{V}_{\mathbf{p}}(t) \cdot \mathbf{V}_{\mathbf{p}}(0) \rangle = e^{-\frac{\xi t}{2}} \langle V_p^2 \rangle \left[\cosh(\omega t) - \frac{\xi}{2\omega} \sinh(\omega t) \right] \quad (\text{A.51})$$

Following these procedures, one should obtain very similar expressions for $\langle \mathbf{Y}_{\mathbf{p}}(t) \cdot \mathbf{Y}_{\mathbf{p}}(0) \rangle$ and $\langle \mathbf{W}_{\mathbf{p}}(t) \cdot \mathbf{W}_{\mathbf{p}}(0) \rangle$.

$$\langle \mathbf{Y}_{\mathbf{p}}(t) \cdot \mathbf{Y}_{\mathbf{p}}(0) \rangle = e^{-\frac{\xi t}{2}} \langle Y_p^2 \rangle \left[\cosh(\omega t) + \frac{\xi \sinh(\omega t)}{2\omega} \right] \quad (\text{A.52})$$

$$\langle \mathbf{W}_{\mathbf{p}}(t) \cdot \mathbf{W}_{\mathbf{p}}(0) \rangle = e^{-\frac{\xi t}{2}} \langle W_p^2 \rangle \left[\cosh(\omega t) - \frac{\xi}{2\omega} \sinh(\omega t) \right] \quad (\text{A.53})$$

Assuming that N is an odd number. The exact solution $\mathbf{r}_{\mathbf{n}}(t)$ and $\mathbf{v}_{\mathbf{n}}(t)$ can be written as:

$$\mathbf{r}_{\mathbf{n}}(t) = \mathbf{X}_{\mathbf{0}}(t) + \sum_{p=1}^{(N-1)/2} 2\mathbf{X}_{\mathbf{p}}(t) \cos(2p\pi \frac{n}{N}) + 2\mathbf{Y}_{\mathbf{p}}(t) \sin(2p\pi \frac{n}{N}) \quad (\text{A.54})$$

$$\mathbf{v}_n(t) = \mathbf{V}_0(t) + \sum_{p=1}^{(N-1)/2} 2\mathbf{V}_p(t) \cos(2p\pi \frac{n}{N}) + 2\mathbf{W}_p(t) \sin(2p\pi \frac{n}{N}) \quad (\text{A.55})$$

With these solutions, the TCF of 0-to- $(N-1)/2$ vector of the ring polymer as well as the VCF of the n th bead can be easily obtained as:

$$\langle \mathbf{R}(t) \cdot \mathbf{R}(0) \rangle = 16 \sum_{p=1, \text{odd}}^{(N-1)/2} \langle \mathbf{X}_p(t) \cdot \mathbf{X}_p(0) \rangle \quad (\text{A.56})$$

$$\langle \mathbf{v}_n(t) \cdot \mathbf{v}_n(0) \rangle = \langle \mathbf{V}_0(t) \cdot \mathbf{V}_0(0) \rangle + \sum_{p=1}^{(N-1)/2} 4\langle \mathbf{V}_p(t) \cdot \mathbf{V}_p(0) \rangle \cos(2p\pi \frac{n}{N})^2 + 4\langle \mathbf{W}_p(t) \cdot \mathbf{W}_p(0) \rangle \sin(2p\pi \frac{n}{N})^2 \quad (\text{A.57})$$

A.3.3 Four-Arm Symmetrical Star Polymer

Matrix \mathbf{A} for the star structure with four arms was derived using a similar approach as demonstrated by Ghosh [24]. In such case, the eigenvalues and eigenfunctions (ψ_p) of \mathbf{A} were obtained numerically.

$$\mathbf{A} = \begin{bmatrix} \mathbf{A}_1 & \mathbf{0} & \mathbf{V} & \mathbf{0} & \mathbf{0} \\ \mathbf{0} & \mathbf{A}_1 & \mathbf{V} & \mathbf{0} & \mathbf{0} \\ \mathbf{V}^T & \mathbf{V}^T & -4 & \mathbf{U}^T & \mathbf{U}^T \\ \mathbf{0} & \mathbf{0} & \mathbf{U} & \mathbf{A}_2 & \mathbf{0} \\ \mathbf{0} & \mathbf{0} & \mathbf{U} & \mathbf{0} & \mathbf{A}_2 \end{bmatrix} \quad (\text{A.58})$$

For which, we let the followings:

$$\mathbf{A}_1 = \begin{bmatrix} -1 & 1 & 0 & \dots & 0 \\ 1 & -2 & 1 & \dots & 0 \\ 0 & \ddots & \ddots & \ddots & 0 \\ 0 & \dots & 1 & -2 & 1 \\ 0 & \dots & 0 & 1 & -2 \end{bmatrix} \quad (\text{A.59})$$

$$\mathbf{A}_2 = \begin{bmatrix} -2 & 1 & 0 & \dots & 0 \\ 1 & -2 & 1 & \dots & 0 \\ 0 & \ddots & \ddots & \ddots & 0 \\ 0 & \dots & 1 & -2 & 1 \\ 0 & \dots & 0 & 1 & -1 \end{bmatrix} \quad (\text{A.60})$$

The dimensions of \mathbf{A}_1 and \mathbf{A}_2 are both $N_f \times N_f$, where N_f is the number of beads per arm, excluding the central bead.

$$\mathbf{V} = [0 \ 0 \ \dots \ 1]^T \quad (\text{A.61})$$

$$\mathbf{U} = [1 \quad 0 \quad \dots \quad 0]^T \quad (\text{A.62})$$

The eigenvalues and eigenvectors can be computed numerically. We found that three eigenvectors can share the same magnitude of eigenvalue and the eigenvectors are not monotonic functions of n [9]. In the next section, we will demonstrate that this remains true even if the equation of motion becomes more non-linear and complicated, such as the case in MD simulations.

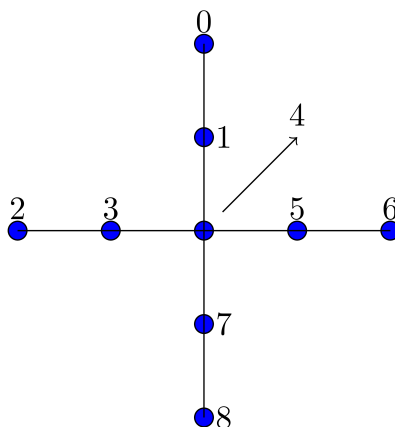


Figure A.1: Indices of beads in four-arm star polyethylene $N = 9$. This figure is reproduced with permission from [9].

A.4 Application of Rouse Mode, Extraction of Relaxation Times from Simulation Data using Rouse Modes as well as other Available Methods

Based upon the classic Rouse model as well as the analysis in Section A.3, one can see that by analytically obtaining the eigenfunction, different relaxation times of a polymer chain can thus be obtained. This allows us to derive different time correlation functions of different vectors straightforwardly. Such mathematical concept is important in the development of the tube model by Doi and Edwards [21]. By following the same logic in the Rouse model, the probability of the polymer chain staying in the tube can also be expressed in terms of different modes, which have the very same form as that of the Rouse mode, except the independent variable is the curvilinear variable. This eventually allows them to qualitatively estimate the shear relaxation modulus of an entangled polymer chain.

Nonetheless, derivation of such eigenfunctions is only feasible in linear system of equations of motion, which can be solved analytically. Most equations of motion that can describe the reality are highly nonlinear, in which the extraction of eigenvalues and eigenfunctions is impossible. Even though this is the case, other research groups also applied the Rouse modes directly to their MD data of linear polyethylene.

Padding and Briels [8], Tsolou *et al.* [4], Kalathi *et al.* [22, 23] as well as Masubuchi *et al.* [121] used such approach to obtain different relaxation times, so as to identify the scaling behavior of τ_p with N/p . For instance, Kalathi *et al.* [22, 23] demonstrated that a plot of β_p , which is the kinetic constraint, derived from the Rouse mode analysis, with N/p allows one to identify the entanglement chain length. With such analysis, they were also able to show that the presence of small nanoparticles in the polymer melt serve to reduce the number of entanglements [23]. Shaffer [26] as well as Bulac and van der Giessen [27] applied the Rouse mode analysis so as to investigate the effect of angle bending and torsion potential on the relaxation of polymer. Masubuchi *et al.* [121] showed that in the Kremer-Grest simulations, the time correlation function of the shorter wavelength motion (namely $p = 2$ and $p = 3$) of the chain deviates from that of the prediction of Rouse model, whereas such deviation is absent in dissipative particle dynamics simulations. Padding and Briels [8] found that by analyzing these Rouse mode relaxations, a dependence of $\tau \sim N^{2.8}$ and $\tau \sim N^{3.5}$ was obtained, which eventually lead to the results of $\eta \sim N^{1.8}$ and $\eta \sim N^{3.6}$ in the unentangled and entangled regimes, respectively. A more recent studies by Kalathi *et al.* [22] reveals a similar trend, but they found a dependence of $\tau \sim N^2$ and $\tau \sim N^{3.4}$ below and above $N = 100$. Even though direct application of Rouse mode seems to work in these studies, Padding and Briels [8], as well as Kalathi *et al.* [22, 23] stated that such Rouse mode may not be true, as it is not directly derived from the available trajectory data, especially in the entangled regime. In addition, its limitation is that it may not be easily applied to polymer systems with a much more sophisticated chemical structures, such as randomly branched and dendrimer polymers. Furthermore, the effect of many-chain and other bonded potentials, such as bond angle and torsion angle, have not been taken into account in the derivation of the Rouse mode. Such Rouse mode also may not be applicable in lattice bond fluctuation model and Monte Carlo simulation.

Intriguingly, there also exists other methods to extract these relaxation times without

any assumption of the Rouse mode and it can be literally applied in Monte Carlo simulation as well as MD simulations, which fully relies on the knowledge of the trajectory only. In the relaxation mode analysis developed by Watanabe [122] and Mitsutake *et al.* [123, 124], without the knowledge of Rouse mode, one can construct a so-called equilibrium time correlation matrix (with components $C_{i,j}$) based upon the fluctuation in the position of the i th and j th beads of the polymer chain and obtain the corresponding relaxation rates by solving the generalized eigenvalues problem (cf., Equation (A.63) and Equation (A.64)), which was derived from a master equation and variational problem.

$$\sum_{j=1}^{3N} C_{i,j}(t_0 + \tau) f_{p,j} = \exp(-\lambda_p \tau) \sum_{j=1}^{3N} C_{i,j}(t_0) f_{p,j} \quad (\text{A.63})$$

t_0 is the starting time that one arbitrarily picked for the calculation.

$$\sum_{i=1}^{3N} \sum_{j=1}^{3N} f_{p,i} C_{i,j}(t_0) f_{q,j} = \delta_{p,q} \quad (\text{A.64})$$

$f_{p,i}$ is the relaxation mode in their relaxation mode analysis and λ_p in this context is similar to that we have derived previously. Hagita *et al.* [125] applied such method on data from the Monte Carlo simulation of bond fluctuation lattice model and found that the longest relaxation time exhibits $\tau \sim N^{3.5}$ based on the data collected for $N = 256, 384, 512$ in the entangled regime and that $\lambda_p \sim p^2$. The degree of freedom associated with this relaxation mode analysis can be further reduced with the aid of principal component analysis, which was demonstrated by Mitsutake *et al.* [123] as well as Nagai *et al.* [126].

A.4.1 Eigenmodes from POD

The proper orthogonal decomposition (POD) analysis in our case generates a reduced order model of the numerical solutions to these non-linear equations of motion. The rationale is very similar to that of the previously mentioned relaxation mode analysis, but it is less complicated. The procedures in POD analysis is summarized in the flow chart as shown in Figure A.2.



Figure A.2: Flow chart showing the procedure of POD analysis.

It basically generates different eigenmodes based on the numerical solution to the highly nonlinear equation of motion in the MD simulation, which may not be obtained analytically. The eigenmodes can then be used in the analysis of different relaxation of the polymer chains in MD simulation. Cartesian coordinates of different beads were subtracted from the center-of-mass of the polymer, followed by averaging over time. A correlation matrix \mathbf{C} is then constructed, with the eigenvectors of \mathbf{C} being the eigenmodes, which can be used as alternative to the Rouse mode. Contrary to the relaxation mode analysis, our goal in using POD is to directly extract eigenmodes from MD data, which can then be used to evaluate relaxation times and viscosity. The normalized eigenmodes $\tilde{\psi}_p^q$ can be used for coordinate transformation. The normal coordinate in a particular direction q can be obtained:

$$X'_{p,q}(t) = \sum_{n=0}^{N-1} q_n(t) \tilde{\psi}_p^q(n) \quad (\text{A.65})$$

With these normal coordinates, it is possible to know the relaxation times of different eigenmodes. Different time correlation functions can be also derived thence.

In MD simulation, as there are many polymer molecules in the box, the POD analysis was performed for each molecule. After that, the result was then averaged over all the molecules. Interestingly, given the fact that the angle bending and torsion potentials, as well as the many chain effect were explicitly included in the equation of motion, the eigenmodes derived from the MD simulation are very similar to that of the simpler Brownian Dynamics (BD) model. This means that in the unentangled regime, the harmonic bond stretching potential plays the most dominant role in the relaxation dynamics of the polymers. Intuitively, this is not surprising because the force constant is the largest in the harmonic bond stretching potential in the forcefield of the MD simulation [19]. For example, in our case of MD simulation, the force constant in the harmonic bond stretching potential is approximately 100 times greater than that of the angle bending potential [9, 19]. Therefore, to certain extent, the similarity of the eigenmodes in nonlinear BD and MD simulations, as demonstrated in our previous

work [9], is expected even if the former only includes harmonic bond stretching potential.

With the extracted eigenmodes, the corresponding normal coordinates in a particular direction can be computed using Equation (A.65). The time correlation function of the p th eigenmode ($\mu_p(t)$) can be evaluated using Equation (A.66).

$$\mu_p(t) = \frac{\langle X'_{p,x}(t)X'_{p,x}(0) + X'_{p,y}(t)X'_{p,y}(0) + X'_{p,z}(t)X'_{p,z}(0) \rangle}{\langle X'^2_{p,x} + X'^2_{p,y} + X'^2_{p,z} \rangle} \approx \exp \left[- (t/\tau_p^*)^{\beta_p} \right] \quad (\text{A.66})$$

It was found that $\mu_p(t)$ can be well described by a stretched exponential function of time with β_p always smaller than unity due to the kinetic constraint imposed on the bead from the harmonic bond stretching potential [9]. Note that there is no kinetic constraint on the bead motion if $\beta_p = 1$, which gives a pure exponential function of time. Distinct τ_p s were obtained for linear polymers, whereas two and three eigenmodes can share the same value of τ_p in ring and star polymers, respectively [9].

A.4.2 Zero-Shear Viscosity: Rouse model and POD method

The Green-Kubo relation tells us that the zero-shear viscosity is related to the the integral of the stress correlation function. Therefore, the strategy to compute the viscosity is to know the time correlation function of stress from MD simulation data. Halverson *et al.* [6] computed directly the shear stress time correlation function of linear and ring polymer.

$$\eta_0 = \frac{V}{3k_bT} \int_0^\infty \left[\langle \sigma_{xy}(\tau)\sigma_{xy}(0) \rangle + \langle \sigma_{xz}(\tau)\sigma_{xz}(0) \rangle + \langle \sigma_{zy}(\tau)\sigma_{zy}(0) \rangle \right] d\tau \quad (\text{A.67})$$

V is the volume and $\sigma_{xy}(\tau)$ is the shear stress acting on the x -plane in the y direction. The shear stress is pre-averaged stress, which can be computed by considering the velocities of the bead as well as the separation between the beads and the corresponding force acting upon them, followed by a time-averaging procedure as demonstrated by Lee and Kremer [127]. Integration of such shear stress time correlation function allowed them to obtain the zero-shear viscosity of both linear and ring polymers [6]. Nonetheless, it is not an easy task to compute the stress as proposed by Lee and Kremer [127] in the case of many-chain system as one has to know the separation distances among all the beads and the corresponding forces acting upon them. In such case, the stress tensor is expressed as follows:

$$\sigma(t) = \sum_j \frac{m}{V} \mathbf{v}_j \mathbf{v}_j + \frac{1}{2V} \sum_i \sum_j \mathbf{r}_{ij} \mathbf{F}_{ij} \quad (\text{A.68})$$

\mathbf{F}_{ij} is the total force between the i th and j th beads. Consider such stress tensor (cf., Equation (A.68)), if the velocity tensor term is ignored and with the assumption of the Gaussian statistics and Rouse dynamics of linear polymer chain without many-chain effect, the stress tensor can be simplified to a large extent as:

$$\sigma(t) = \frac{1}{V} \sum_j \mathbf{r}_j \mathbf{F}_j \quad (\text{A.69})$$

\mathbf{F}_j is the total force acting upon the j th bead. The stress tensor according to Equation (A.69) can be simplified as:

$$\sigma(t) = \frac{1}{V} \left[\mathbf{r}_0 k (\mathbf{r}_1 - \mathbf{r}_0) + \mathbf{r}_{N-1} k (\mathbf{r}_{N-2} - \mathbf{r}_{N-1}) + \sum_{n=1}^{N-2} \mathbf{r}_n k (\mathbf{r}_{n+1} - 2\mathbf{r}_n + \mathbf{r}_{n-1}) \right] \quad (\text{A.70})$$

$k = \frac{3k_b T}{b^2}$. This then gives us:

$$\sigma(t) = -\frac{k}{V} \sum_{n=0}^{N-2} \left[\mathbf{r}_{n+1}(t) - \mathbf{r}_n(t) \right]^2 \quad (\text{A.71})$$

In Rouse model, $\mathbf{r}_{n+1}(t) - \mathbf{r}_n(t) \approx \frac{\partial \mathbf{r}_n(t)}{\partial n}$ and that $\mathbf{r}_n = \mathbf{X}_0 + 2 \sum_{p=1}^{N-1} \mathbf{X}_p \cos(p\pi \frac{n}{N})$. We can then easily find that:

$$\frac{\partial \mathbf{r}_n}{\partial n} = -2 \sum_{p=1}^{N-1} \mathbf{X}_p \sin(p\pi \frac{n}{N}) \frac{p\pi}{N} \quad (\text{A.72})$$

And thus:

$$\sum_{n=0}^{N-2} \left[\mathbf{r}_{n+1} - \mathbf{r}_n \right]^2 \approx \sum_{n=0}^{N-2} \sum_{p=1}^{N-1} \mathbf{X}_p \mathbf{X}_p \frac{4p^2 \pi^2}{N^2} \sin^2(p\pi \frac{n}{N}) = \sum_{p=1}^{N-1} \mathbf{X}_p \mathbf{X}_p \frac{2p^2 \pi^2}{N} \quad (\text{A.73})$$

This is because:

$$\sum_{n=0}^{N-2} \sin^2(p\pi \frac{n}{N}) \approx \int_0^N \sin^2(p\pi \frac{n}{N}) dn = \frac{N}{2} \quad (\text{A.74})$$

Putting this back to Equation (A.71):

$$\sigma(t) \approx -\frac{3k_b T}{V} \sum_{p=1}^{N-1} \frac{\mathbf{X}_p(t) \mathbf{X}_p(t) 2p^2 \pi^2}{Nb^2} \quad (\text{A.75})$$

Now, in order to further simplify Equation (A.75), we have to know the probability distribution of a Gaussian chain based on our knowledge of statistical mechanics. Consider the potential energy (U_N) of a Gaussian chain:

$$U_N = \frac{3k_b T}{2b^2} \sum_{n=0}^{N-2} (\mathbf{r}_{n+1} - \mathbf{r}_n) \cdot (\mathbf{r}_{n+1} - \mathbf{r}_n) \quad (\text{A.76})$$

Using the result of Equation (A.73), we can express U_N in terms of \mathbf{X}_p . Note that the only difference between the summation term in Equation (A.76) and Equation (A.73) is that we have a dot product of $(\mathbf{r}_{n+1} - \mathbf{r}_n) \cdot (\mathbf{r}_{n+1} - \mathbf{r}_n)$ in Equation (A.76) instead of a tensor $(\mathbf{r}_{n+1} - \mathbf{r}_n)^2$ in Equation (A.73).

$$U_N = \frac{3k_b T}{b^2} \sum_{p=1}^{N-1} \mathbf{X}_p \cdot \mathbf{X}_p \frac{p^2 \pi^2}{N} \quad (\text{A.77})$$

The probability distribution (P) with \mathbf{X}_p as argument is thus:

$$P = C \exp\left(-\frac{U_N}{k_b T}\right) = C \exp\left[-\frac{3}{b^2} \sum_{p=1}^{N-1} \frac{p^2 \pi^2}{N} X_p^2\right] \quad (\text{A.78})$$

C is the normalization constant. This kind of distribution is exactly the form of Maxwell-Boltzmann distribution. It can be shown that using spherical coordinates, the mean-square value of \mathbf{X}_p ($\langle X_p^2 \rangle$) from such distribution similar to that demonstrated by Chapman and Cowling [10] when they derived the mean-square peculiar velocity of ideal gas in different directions. Consider the p th Rouse mode, the Gaussian distribution has this form:

$$\left(\frac{3p^2 \pi}{Nb^2}\right)^{1.5} X_p^2 \exp\left[-\frac{3p^2 \pi^2 X_p^2}{Nb^2}\right] dX_p d\phi \sin \theta d\theta \quad (\text{A.79})$$

The spherical coordinates are defined as:

$$\begin{bmatrix} X_{p,x} \\ X_{p,y} \\ X_{p,z} \end{bmatrix} = X_p \begin{bmatrix} \sin \theta \cos \phi \\ \sin \theta \sin \phi \\ \cos \theta \end{bmatrix} \quad (\text{A.80})$$

Thus, we have:

$$\langle X_p^2 \rangle = \left(\frac{3p^2 \pi}{Nb^2}\right)^{1.5} \int_0^{2\pi} d\phi \int_0^\pi \sin \theta d\theta \int_0^\infty X_p^4 \exp\left[-\frac{3p^2 \pi^2 X_p^2}{Nb^2}\right] dX_p = \frac{Nb^2}{2p^2 \pi^2} \quad (\text{A.81})$$

And that:

$$\frac{\langle X_p^2 \rangle}{3} = \langle X_{p,x}^2 \rangle = \langle X_{p,y}^2 \rangle = \langle X_{p,z}^2 \rangle \quad (\text{A.82})$$

This is because:

$$\int_0^{2\pi} \cos^2 \phi d\phi \int_0^\pi \sin^3 \theta d\theta = \int_0^{2\pi} \sin^2 \phi d\phi \int_0^\pi \sin^3 \theta d\theta = \int_0^{2\pi} d\phi \int_0^\pi \cos^2 \theta \sin \theta d\theta = \frac{4\pi}{3} \quad (\text{A.83})$$

Hence, the time correlation function of shear stress $\langle \sigma_{xy}(t) \sigma_{xy}(0) \rangle$:

$$\langle \sigma_{xy}(t) \sigma_{xy}(0) \rangle \approx \frac{9k_b^2 T^2}{V^2} \sum_{p=1}^{N-1} \frac{\langle X_{p,x}(t) X_{p,x}(0) \rangle \langle X_{p,y}(t) X_{p,y}(0) \rangle}{\langle X_{p,x}^2 \rangle \langle X_{p,y}^2 \rangle} = \frac{k_b^2 T^2}{V^2} \sum_{p=1}^{N-1} \left[\frac{\langle \mathbf{X}_p(t) \cdot \mathbf{X}_p(0) \rangle}{\langle X_p^2 \rangle} \right]^2 \quad (\text{A.84})$$

The shear relaxation modulus $G(t)$ can be expressed as follows:

$$G(t) = \frac{\rho RT}{M} \sum_{p=1}^{N-1} \left[\frac{\langle \mathbf{X}_p(t) \cdot \mathbf{X}_p(0) \rangle}{\langle X_p^2 \rangle} \right]^2 \quad (\text{A.85})$$

With the chain literally following Gaussian statistics, Watanabe [122] also showed that shear relaxation modulus of polymers can be approximated using different time correlation functions of bond vectors. The result in Equation (A.85) is for a **single** Rouse chain, which has the harmonic bond stretching potential as the only bonded potential. However, in reality, even in unentangled regime, a single polymer chain is surrounded by multiple polymer chains in the melt. In addition to such many-chain effect, angle bending and torsion potentials also play roles in the chain relaxation. Such effect is taken into account by rewriting Equation (A.85) as Equation (A.86) using the results of $\mu_p(t)$ from the POD method as indicated in Equation (A.66), which is a stretched exponential function of time due to the highly nonlinear bonded and non-bonded potentials.

$$G(t) = \frac{\rho RT}{M} \sum_{p=1}^{N-1} \exp \left[-2(t/\tau_p^*)^{\beta_p} \right] \quad (\text{A.86})$$

Furthermore, in Equation (A.86), we argue that in spite of the high nonlinearity of the equation of motion in MD simulation due to the presence of angle bending and torsion potentials as well as nonbonded potential, the bond stretching force always dominates the relaxation dynamics of the polymers. The shear stress should be therefore dominated by the bond stretching force between beads. This is supported by the fact that the eigenmodes in nonlinear BD simulation are very similar to that in MD simulation [9]. With Equation (A.86), it is then possible to approximate the zero-shear viscosity using the time correlation functions of different eigenmodes or Rouse modes. The shear stress time correlation function can be approximated using the time correlation functions of the eigenmodes. ρ is the mass density of the bead. The zero-shear viscosity (η_0) can then be obtained by integrating $G(t)$.

$$\eta_0 = \int_0^{\infty} G(\tau) d\tau \quad (\text{A.87})$$

As shown in Figure A.3, with such approximation of the stress correlation function and the values of β_p and τ_p^* from POD method, our results agree with the experimental and simulation results of other groups satisfactorily for linear and ring polymers [7, 4, 42]. For star polymer, it is worthwhile to note that the agreement in η_0 between the BD and MD simulations is

excellent. This again proves that relaxation dynamics in polymer melt is mainly stifled by the bond stretching force. Our results qualitatively agree well with the experimental result of Pearson *et al.* [7] that in the MD simulation of linear polymers, $\eta_0 \sim N^{1.8}$. The stronger N dependence of η_0 for all structures in MD simulation compared to that of BD simulation is again attributed to the higher nonlinearity of the equation in the latter case.

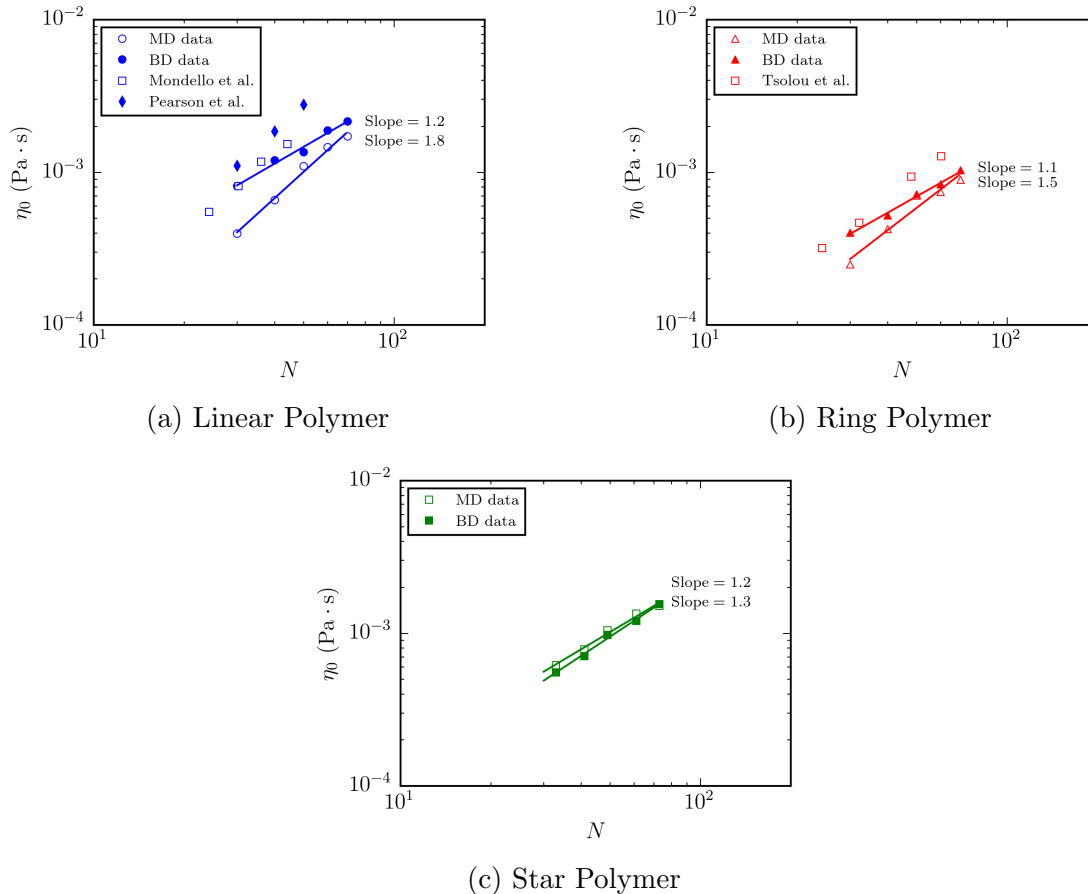


Figure A.3: Dependence of zero-shear viscosities on size of polymer in the unentangled regime of our nonlinear Brownian dynamic and MD simulation data compared with other simulation and experimental data from other research groups. These figures are reproduced with permission from [9].

A.5 Conclusion

We have reviewed analytical and numerical methods for analyzing linear and non-linear dynamics of polymers with different molecular structures. The equation of motion in the

Rouse model, essentially a BD model, is linear. With the addition of an inertia term, the equation of motion is still linear. Such linear equations of motion of polymers with linear and ring structures can be solved analytically using the method of eigenvalue and eigenfunction to yield relaxation times and velocity correlation functions. Since harmonic bond stretching, bond bending and torsion potentials, as well as nonbonded potential are included in the MD simulation, the corresponding equation of motion is nonlinear. Analytical solutions for such nonlinear systems are impossible. Instead, the POD analysis of the numerical solutions is used to derive eigenmodes so that relaxation times and time correlation functions can be determined. The POD analysis not only elucidates the nonlinearity of the relaxation dynamics of polymers but also allows the estimation of the zero-shear viscosities of the polymer melts.

It is believed that the POD analysis can be readily applied to polymers with more complicated molecular structures than those of polyethylene that was used in this work, as the POD analysis only requires the knowledge of the positions of the constituent atoms as a function of time.

Appendix B

Supporting Information for Chapter 3

B.1 C++ program for numerical simulation

```
#include <iostream>
#include <istream>
#include <fstream>
#include <iomanip>
#include <cstdio>
#include <sstream>
#include <eigen/Eigen/Dense>
#include <vector>
#include <stdlib.h>
#include <stdio.h>
#include <random>
#include <chrono>
#include <string>
#include <omp.h>
using namespace std;
using namespace Eigen;
using namespace std::chrono;
//compile with g++ -std=c++11 -Ofast main2.cpp -o ld4

VectorXd TDMA2(const MatrixXd& A,const VectorXd& b)
{
    int row=A.rows();
    int col=A.cols();
    VectorXd x=VectorXd::Zero(row);
    VectorXd b2=b;
    VectorXd c(row);
    VectorXd a(row);
    for(int i=0;i<row;i++)
    {
```

```

    if(i==0)
    {
        c(i)=A(i,i+1);
        a(i)=0;
    }
    else if(i==row-1)
    {
        a(i)=A(i,i-1);
        c(i)=0;
    }
    else
    {
        a(i)=A(i,i-1);
        c(i)=A(i,i+1);
    }
}
double err=1;
double sum1;
VectorXd d1p(row);
VectorXd c1p(row);
VectorXd err1(row);
int count=0;
for(int i=0;i<row;i++)
{
    if(i==0)
    {
        c1p(i)=c(i)/A(i,i);
    }
    else
    {
        c1p(i)=c(i)/(A(i,i)-a(i)*c1p(i-1));
    }
}
while(abs(err)>pow(10,-6))
{

    for(int i=0;i<row;i++)
    {
        if(i==0)
        {
            d1p(i)=b2(i)/A(i,i);
        }
        else
        {
            d1p(i)=(b2(i)-a(i)*d1p(i-1))/(A(i,i)-a(i)*c1p(i-1));
        }
    }
}
x(row-1)=d1p(row-1);

```

```

for(int i=row-2;i>=0;--i)
{
    x(i)=d1p(i)-c1p(i)*x(i+1);
}
for(int i=0;i<row;i++)
{
    sum1=0;
    for(int j=0;j<col;j++)
    {
        if(j==i || j==i+1 || j==i-1)
        {
            ;
        }
        else
        {
            sum1=sum1+A(i,j)*x(j);
        }
    }
    b2(i)=b(i)-sum1;
}
err1=A*x-b;
err=0;
for(int i=0;i<row;i++)
{
    err=err+pow(err1(i),2)/row;
}
err=pow(err,0.5);
count=count+1;
if(count>1000)
{
    break;
}
}
return x;
}

int main(int argc, char** argv){
    default_random_engine generator;
    char* filename;
    int N,t_step,count,n_save,f_save,count2;
    double dt;
    for(int i=1;i<argc;i++){
        if(strcmp(argv[i], "-n") == 0){
            N=stoi(argv[i+1],NULL);//length of polymer
        }
        else if(strcmp(argv[i], "-t") == 0){
            t_step=stoi(argv[i+1],NULL);//t_step
        }
    }
}

```

```

else if(strcmp(argv[i], "-dt") == 0){
    dt=stod(argv[i+1],NULL);//size of time step dt=0.001 ps
}
else if(strcmp(argv[i], "-f")==0){
    filename=argv[i+1];//initial configuration file
}
else if(strcmp(argv[i], "-s")==0){
    f_save=stoi(argv[i+1],NULL);//number of steps to be saved
}
else{
    ;
}
}
n_save=t_step/f_save;
ifstream infile(filename);
VectorXd x(N),y(N),z(N),bx(2*N),by(2*N),bz(2*N),rx(2*N),ry(2*N),rz(2*N);
MatrixXd x1(N,n_save),y1(N,n_save),z1(N,n_save),vx1(N,n_save),vy1(N,n_save),vz1(N,n_save);
MatrixXd A=MatrixXd::Zero(N,N);
MatrixXd I=MatrixXd::Identity(N,N);
MatrixXd I2=MatrixXd::Identity(N,N);
MatrixXd E=MatrixXd::Identity(N,N);
MatrixXd Z=MatrixXd::Zero(N,N);
I2=dt*I2;
for(int i=0;i<N;i++){
    infile>>rx(i);
    infile>>ry(i);
    infile>>rz(i);
}
for(int i=0;i<N;i++){
    rx(i)=0.01*rx(i);
    ry(i)=0.01*ry(i);
    rz(i)=0.01*rz(i);
}
double lam,err,rcmx,rcmy,rcmz;
double k_b=1.38065*pow(10,-27);//A^2 kg ps^-2K^-1
double T=450;//K
double xi=5;//ps^-1
double m=2.327*pow(10,-26);//kg
double k=1.8*pow(10,-23);//kg ps^-2
double c2=900;// k/(m)
double sigma=pow(2*k_b*T*xi*m,0.5);//normal distribution force
double sigma2=pow(k_b*T/m,0.5);
E=-(xi*dt)*E;
normal_distribution<double> distribution(0,sigma);
normal_distribution<double> distribution2(0,sigma2);
for(int i=0;i<N;i++){

```

```

    rx(i+N)=distribution2(generator);
    ry(i+N)=distribution2(generator);
    rz(i+N)=distribution2(generator);
}
high_resolution_clock::time_point t1 = high_resolution_clock::now
();
count=0;
for(int i=0;i<N;i++){
    if(i==0){
        A(i,i)=-c2*dt;
        A(i,i+1)=c2*dt;
    }
    else if(i==N-1){
        A(i,i)=-c2*dt;
        A(i,i-1)=c2*dt;
    }
    else{
        A(i,i)=-2*c2*dt;
        A(i,i-1)=c2*dt;
        A(i,i+1)=c2*dt;
    }
}
MatrixXd A1(A.rows()+A.rows(), A.cols()+A.cols());
A1 << Z, I2,
    A, E;
MatrixXd I1=MatrixXd::Identity(2*N,2*N);
A1=A1-I1;
for(int it=0;it<t_step;it++){
    if(it==0){
        for(int i=0;i<N;i++){
            x1(i,count)=rx(i);
            y1(i,count)=ry(i);
            z1(i,count)=rz(i);
            vx1(i,count)=rx(i+N);
            vy1(i,count)=ry(i+N);
            vz1(i,count)=rz(i+N);
        }
        count=count+1;
        //cout << "nothing wrong with initialization" << endl;
    }
    else{
        //VectorXd Fr=VectorXd::Zero(3*N);
        for(int i=0;i<N;i++){
            bx(i)=-rx(i);
            by(i)=-ry(i);
            bz(i)=-rz(i);
            bx(i+N)=-rx(i+N)-distribution(generator)*dt/m;
            by(i+N)=-ry(i+N)-distribution(generator)*dt/m;

```

```

    bz(i+N)=-rz(i+N)-distribution(generator)*dt/m;
}
rx=TDMA2(A1,bx);
ry=TDMA2(A1,by);
rz=TDMA2(A1,bz);
if(remainder(it,f_save)==0){
    for(int i=0;i<N;i++){
        x1(i,count)=rx(i);
        y1(i,count)=ry(i);
        z1(i,count)=rz(i);
        vx1(i,count)=rx(i+N);
        vy1(i,count)=ry(i+N);
        vz1(i,count)=rz(i+N);
    }
    count=count+1;
    cout << "Saved_time_step=" << count << endl;
}
}
}
ofstream myfile;
myfile.open("trj_x.dat", ios::binary);
myfile.write((char *) x1.data(), x1.rows() * x1.cols() * sizeof(
double));
myfile.close();
myfile.open("trj_y.dat", ios::binary);
myfile.write((char *) y1.data(), y1.rows() * y1.cols() * sizeof(
double));
myfile.close();
myfile.open("trj_z.dat", ios::binary);
myfile.write((char *) z1.data(), z1.rows() * z1.cols() * sizeof(
double));
myfile.close();
myfile.open("trj_vx.dat", ios::binary);
myfile.write((char *) vx1.data(), vx1.rows() * vx1.cols() * sizeof(
double));
myfile.close();
myfile.open("trj_vy.dat", ios::binary);
myfile.write((char *) vy1.data(), vy1.rows() * vy1.cols() * sizeof(
double));
myfile.close();
myfile.open("trj_vz.dat", ios::binary);
myfile.write((char *) vz1.data(), vz1.rows() * vz1.cols() * sizeof(
double));
myfile.close();
high_resolution_clock::time_point t2 = high_resolution_clock::now
();
auto duration = duration_cast<seconds>( t2 - t1 ).count();
cout << "run_time=" << duration << "seconds" << endl;

```

```
    return 0;
}
```

B.2 Python 3.5 program for initial conformation construction using rotational isomeric state model

```
#!/usr/bin/env python3

import numpy as np
import matplotlib.pyplot as plt
from numpy import linalg
from mpl_toolkits.mplot3d import Axes3D
from random import randint
import warnings
warnings.filterwarnings("ignore")
def cos(x):
    x = x*np.pi/180
    f = np.cos(x)
    return f
def sin(x):
    x = x*np.pi/180
    f = np.sin(x)
    return f
def lamb1(sigma,omega):
    a = 0.5*(sigma*(1+omega)+1+np.sqrt((-sigma*(1+omega)+1)**2+8*sigma
))
    return a
def lamb2(sigma,omega):
    a = 0.5*(sigma*(1+omega)+1-np.sqrt((-sigma*(1+omega)+1)**2+8*sigma
))
    return a
def Z(n,lamb1,lamb2):
    f=(lamb1**(n-1)*(lamb2-1))/(lamb2-lamb1)+(lamb2**(n-1)*(1-lamb1))
    /(lamb2-lamb1)
    return f

#Evaluation of partition function Z and probability
sigma = 0.54
omega=0.088
l = 1.54
theta= 180-112
l1 = lamb1(sigma,omega)
l2 = lamb2(sigma,omega)
U = np.zeros((2,2))
```

```

U[0][0] = 1
U[1][0] = 1
U[0][1] = 2*sigma
U[1][1] = sigma*(1+omega)
v,w = linalg.eig(U)
w_in = linalg.inv(w)
n=50#input the N, which is the number of beads of a chain
n1 = np.arange(2,n,1)
count = 0
bond_i_a = np.arange(2,n,1)
p_i = []
for i in range(len(bond_i_a)):
    bond_i = bond_i_a[i]
    xl = bond_i-2
    xr = n-1-bond_i
    U_prim = np.zeros((2,2))
    U_prim[0][1] = 2*sigma
    U_prim[1][1] = sigma*(1+omega)
    vd = np.zeros((2,2))
    if xl == 0:
        vd[0][0] = v[0]**xr
        vd[1][1] = v[1]**xr
        Tr = np.mat(w)*np.mat(vd)
        Tr = np.mat(Tr)*np.mat(w_in)
        T = np.mat(U_prim)*np.mat(Tr)
    elif xr == 0:
        vd[0][0] = v[0]**xl
        vd[1][1] = v[1]**xl
        Tl = np.mat(w)*np.mat(vd)
        Tl = np.mat(Tl)*np.mat(w_in)
        T = np.mat(Tl)*np.mat(U_prim)
    else:
        vd[0][0] = v[0]**xr
        vd[1][1] = v[1]**xr
        Tr = np.mat(w)*np.mat(vd)
        Tr = np.mat(Tr)*np.mat(w_in)
        vd[0][0] = v[0]**xl
        vd[1][1] = v[1]**xl
        Tl = np.mat(w)*np.mat(vd)
        Tl = np.mat(Tl)*np.mat(w_in)
        T = np.mat(Tl)*np.mat(U_prim)
        T = np.mat(T)*np.mat(Tr)
    if xl == 0 and xr == 0:
        T = U_prim
    Zt = Z(n,l1,l2)
    row = T[0,:].reshape(1,2).T
    p = float(0.5*(row[0]+row[1]))
    p_i.append(p/Zt)

```

```

n1 = np.arange(2,n,1)
count = 0
bond_i_a = np.arange(3,n,1)
p_i_tg = []
for i in range(len(bond_i_a)):
    bond_i = bond_i_a[i]
    xl = bond_i-2
    xr = n-1-bond_i
    U_prim = np.zeros((2,2))
    U_prim[0][1] = 2*sigma
    vd = np.zeros((2,2))
    if xl == 0:
        vd[0][0] = v[0]**xr
        vd[1][1] = v[1]**xr
        Tr = np.mat(w)*np.mat(vd)
        Tr = np.mat(Tr)*np.mat(w_in)
        T = np.mat(U_prim)*np.mat(Tr)
    elif xr == 0:
        vd[0][0] = v[0]**xl
        vd[1][1] = v[1]**xl
        Tl = np.mat(w)*np.mat(vd)
        Tl = np.mat(Tl)*np.mat(w_in)
        T = np.mat(Tl)*np.mat(U_prim)
    else:
        vd[0][0] = v[0]**xr
        vd[1][1] = v[1]**xr
        Tr = np.mat(w)*np.mat(vd)
        Tr = np.mat(Tr)*np.mat(w_in)
        vd[0][0] = v[0]**xl
        vd[1][1] = v[1]**xl
        Tl = np.mat(w)*np.mat(vd)
        Tl = np.mat(Tl)*np.mat(w_in)
        T = np.mat(Tl)*np.mat(U_prim)
        T = np.mat(T)*np.mat(Tr)
    if xl == 0 and xr == 0:
        T = U_prim
    Zt = Z(n,l1,l2)
    row = T[0,:].reshape(1,2).T
    p = float(0.5*(row[0]+row[1]))
    p_i_tg.append(p/Zt)

n1 = np.arange(2,n,1)
count = 0
bond_i_a = np.arange(3,n,1)
p_i_gt = []
for i in range(len(bond_i_a)):
    bond_i = bond_i_a[i]

```

```

xl = bond_i-2
xr = n-1-bond_i
U_prim = np.zeros((2,2))
U_prim[1][0] = 1
vd = np.zeros((2,2))
if xl == 0:
    vd[0][0] = v[0]**xr
    vd[1][1] = v[1]**xr
    Tr = np.mat(w)*np.mat(vd)
    Tr = np.mat(Tr)*np.mat(w_in)
    T = np.mat(U_prim)*np.mat(Tr)
elif xr == 0:
    vd[0][0] = v[0]**xl
    vd[1][1] = v[1]**xl
    Tl = np.mat(w)*np.mat(vd)
    Tl = np.mat(Tl)*np.mat(w_in)
    T = np.mat(Tl)*np.mat(U_prim)
else:
    vd[0][0] = v[0]**xr
    vd[1][1] = v[1]**xr
    Tr = np.mat(w)*np.mat(vd)
    Tr = np.mat(Tr)*np.mat(w_in)
    vd[0][0] = v[0]**xl
    vd[1][1] = v[1]**xl
    Tl = np.mat(w)*np.mat(vd)
    Tl = np.mat(Tl)*np.mat(w_in)
    T = np.mat(Tl)*np.mat(U_prim)
    T = np.mat(T)*np.mat(Tr)
if xl == 0 and xr == 0:
    T = U_prim
Zt = Z(n,l1,l2)
row = T[0,:].reshape(1,2).T
p = float(0.5*(row[0]+row[1]))
p_i_gt.append(p/Zt)

n1 = np.arange(2,n,1)
count = 0
bond_i_a = np.arange(3,n,1)
p_i_gg = []
for i in range(len(bond_i_a)):
    bond_i = bond_i_a[i]
    xl = bond_i-2
    xr = n-1-bond_i
    U_prim = np.zeros((2,2))
    U_prim[1][1] = sigma*(1+omega)
    vd = np.zeros((2,2))
    if xl == 0:
        vd[0][0] = v[0]**xr

```

```

    vd[1][1] = v[1]**xr
    Tr = np.mat(w)*np.mat(vd)
    Tr = np.mat(Tr)*np.mat(w_in)
    T= np.mat(U_prim)*np.mat(Tr)
elif xr == 0:
    vd[0][0] = v[0]**x1
    vd[1][1] = v[1]**x1
    Tl = np.mat(w)*np.mat(vd)
    Tl = np.mat(Tl)*np.mat(w_in)
    T = np.mat(Tl)*np.mat(U_prim)
else:
    vd[0][0] = v[0]**xr
    vd[1][1] = v[1]**xr
    Tr = np.mat(w)*np.mat(vd)
    Tr = np.mat(Tr)*np.mat(w_in)
    vd[0][0] = v[0]**x1
    vd[1][1] = v[1]**x1
    Tl = np.mat(w)*np.mat(vd)
    Tl = np.mat(Tl)*np.mat(w_in)
    T = np.mat(Tl)*np.mat(U_prim)
    T = np.mat(T)*np.mat(Tr)
if x1 == 0 and xr == 0:
    T = U_prim
Zt = Z(n,l1,l2)
row = T[0,:].reshape(1,2).T
p = float(0.5*(row[0]+row[1]))
p_i_gg.append(p/Zt)

n1 = np.arange(2,n,1)
count = 0
bond_i_a = np.arange(3,n,1)
p_i_tt = []
for i in range(len(bond_i_a)):
    bond_i = bond_i_a[i]
    x1 = bond_i-2
    xr = n-1-bond_i
    U_prim = np.zeros((2,2))
    U_prim[0][0] = 1
    vd = np.zeros((2,2))
    if x1 == 0:
        vd[0][0] = v[0]**xr
        vd[1][1] = v[1]**xr
        Tr = np.mat(w)*np.mat(vd)
        Tr = np.mat(Tr)*np.mat(w_in)
        T= np.mat(U_prim)*np.mat(Tr)
    elif xr == 0:
        vd[0][0] = v[0]**x1

```

```

    vd[1][1] = v[1]**xl
    Tl = np.mat(w)*np.mat(vd)
    Tl = np.mat(Tl)*np.mat(w_in)
    T = np.mat(Tl)*np.mat(U_prim)
else:
    vd[0][0] = v[0]**xr
    vd[1][1] = v[1]**xr
    Tr = np.mat(w)*np.mat(vd)
    Tr = np.mat(Tr)*np.mat(w_in)
    vd[0][0] = v[0]**xl
    vd[1][1] = v[1]**xl
    Tl = np.mat(w)*np.mat(vd)
    Tl = np.mat(Tl)*np.mat(w_in)
    T = np.mat(Tl)*np.mat(U_prim)
    T = np.mat(T)*np.mat(Tr)
if xl == 0 and xr == 0:
    T = U_prim
Zt = Z(n,l1,l2)
row = T[0,:].reshape(1,2).T
p = float(0.5*(row[0]+row[1]))
p_i_tt.append(p/Zt)

qs_gt=np.zeros(len(bond_i_a))
qs_gg=np.zeros(len(bond_i_a))
qs_tt=np.zeros(len(bond_i_a))
qs_tg=np.zeros(len(bond_i_a))
for i in range(len(bond_i_a)):
    qs_gt[i]=p_i_gt[i]/(2*p_i[i])
    qs_gg[i]=p_i_gg[i]/(2*p_i[i])
    qs_tt[i]=p_i_tt[i]/(1-2*p_i[i])
    qs_tg[i]=p_i_tg[i]/(1-2*p_i[i])

fig=plt.figure()
plt.rc('font', **{'family': 'serif', 'serif': ['Computer_Modern']})
plt.rc('text', usetex=True)
plt.gcf().set_size_inches(3,3,forward=True)
plt.gcf().set_size_inches(3,3,forward=True)
plt.subplots_adjust(left=0.12,bottom=0.15)
ax = fig.add_subplot(111, projection='3d')

xf=[]
yf=[]
zf=[]

n1 = np.arange(2,n,1)
lv = [1,0,0]
lo = [0,0,0]

```

```

xf.append(lo[0])
yf.append(lo[1])
zf.append(lo[2])

xf.append(lv[0])
yf.append(lv[1])
zf.append(lv[2])

T1 = np.zeros((3,3))
T1[0][0] = cos(theta)
T1[0][1] = sin(theta)
T1[1][0] = sin(theta)
T1[1][1] = -cos(theta)
T1[2][2] = -1
phi = 180
Tt = np.zeros((3,3))
Tt[0][0] = cos(theta)
Tt[0][1] = sin(theta)
Tt[1][0] = -sin(theta)*cos(phi)
Tt[1][1] = cos(theta)*cos(phi)
Tt[1][2] = -sin(phi)
Tt[2][0] = -sin(theta)*sin(phi)
Tt[2][1] = cos(theta)*sin(phi)
Tt[2][2] = cos(phi)
phi = 60
Tg = np.zeros((3,3))
Tg[0][0] = cos(theta)
Tg[0][1] = sin(theta)
Tg[1][0] = -sin(theta)*cos(phi)
Tg[1][1] = cos(theta)*cos(phi)
Tg[1][2] = -sin(phi)
Tg[2][0] = -sin(theta)*sin(phi)
Tg[2][1] = cos(theta)*sin(phi)
Tg[2][2] = cos(phi)
phi = 300
Tgm = np.zeros((3,3))
Tgm[0][0] = cos(theta)
Tgm[0][1] = sin(theta)
Tgm[1][0] = -sin(theta)*cos(phi)
Tgm[1][1] = cos(theta)*cos(phi)
Tgm[1][2] = -sin(phi)
Tgm[2][0] = -sin(theta)*sin(phi)
Tgm[2][1] = cos(theta)*sin(phi)
Tgm[2][2] = cos(phi)
p_sw=np.zeros(len(n1))
for i in range(len(n1)):
    if i == 0 or i == len(n1)-1:
        pn=randint(0,100)

```

```

pg=randint(1,2)
if pn <= 23 and pg == 1:
    p_sw[i]=1
elif pn <= 23 and pg == 2:
    p_sw[i]=2
elif pn > 23:
    p_sw[i]=0
else:
    pn=randint(0,100)
    pn = pn/100
    pg=randint(1,2)
    if (p_sw[i-1]==1 or p_sw[i-1]==2) and pn>qs_gt[i] and pn<=qs_gt[
        i]+qs_gg[i] and pg==1:
        p_sw[i]=1
    elif (p_sw[i-1]==1 or p_sw[i-1]==2) and pn>qs_gt[i] and pn<=
        qs_gt[i]+qs_gg[i] and pg==2:
        p_sw[i]=2
    elif (p_sw[i-1]==1 or p_sw[i-1]==2) and pn<=qs_gt[i]:
        p_sw[i]=0
    elif (p_sw[i-1]==0) and pn>qs_gt[i]+qs_gg[i] and pn<=qs_gt[i]+
        qs_gg[i]+qs_tt[i]:
        p_sw[i]=0
    elif (p_sw[i-1]==0) and pn>qs_gt[i]+qs_gg[i]+qs_tt[i] and pn<=
        qs_gt[i]+qs_gg[i]+qs_tt[i]+qs_tg[i] and pg==1:
        p_sw[i]=1
    elif (p_sw[i-1]==0) and pn>qs_gt[i]+qs_gg[i]+qs_tt[i] and pn<=
        qs_gt[i]+qs_gg[i]+qs_tt[i]+qs_tg[i] and pg==2:
        p_sw[i]=2

l2=np.zeros(3)
l1=np.mat(T1).dot(lv)
l1 = l1[0,:].reshape(1,3).T
l1 = [float(ii) for ii in l1]
xf.append(l1[0]+1)
yf.append(l1[1])
zf.append(l1[2])
l2[0]=l1[0]+1
l2[1]=l1[1]
l2[2]=l1[2]
for i in range(len(p_sw)):
    if i == 0:
        if p_sw[i]==0:
            l1=np.mat(Tt).dot(lv)
        elif p_sw[i]==1:
            l1=np.mat(Tg).dot(lv)
        elif p_sw[i]==2:
            l1=np.mat(Tgm).dot(lv)
    l1 = l1[0,:].reshape(1,3).T

```

```

l1 = [float(ii) for ii in l1]
l1=np.mat(T1).dot(l1)
l1 = l1[0,:].reshape(1,3).T
l1 = [float(ii) for ii in l1]
xf.append(l1[0]+l2[0])
yf.append(l1[1]+l2[1])
zf.append(l1[2]+l2[2])
l2[0]=l1[0]+l2[0]
l2[1]=l1[1]+l2[1]
l2[2]=l1[2]+l2[2]
else:
    if p_sw[i]==0:
        l1=np.mat(Tt).dot(lv)
    elif p_sw[i]==1:
        l1=np.mat(Tg).dot(lv)
    elif p_sw[i]==2:
        l1=np.mat(Tgm).dot(lv)
l1 = l1[0,:].reshape(1,3).T
l1 = [float(ii) for ii in l1]
for j in range(i):
    if p_sw[i-1-j]==0:
        l1=np.mat(Tt).dot(l1)
    elif p_sw[i-1-j]==1:
        l1=np.mat(Tg).dot(l1)
    elif p_sw[i-1-j]==2:
        l1=np.mat(Tgm).dot(l1)
l1 = l1[0,:].reshape(1,3).T
l1 = [float(ii) for ii in l1]
l1=np.mat(T1).dot(l1)
l1 = l1[0,:].reshape(1,3).T
l1 = [float(ii) for ii in l1]
xf.append(l1[0]+l2[0])
yf.append(l1[1]+l2[1])
zf.append(l1[2]+l2[2])
l2[0]=l1[0]+l2[0]
l2[1]=l1[1]+l2[1]
l2[2]=l1[2]+l2[2]
xcm=sum(xf)/len(xf)
ycm=sum(yf)/len(yf)
zcm=sum(zf)/len(zf)

rgx=0
rgy=0
rgz=0
for i in range(len(xf)):
    rgx=rgx+(xf[i]-xcm)**2
    rgy=rgy+(yf[i]-ycm)**2
    rgz=rgz+(zf[i]-zcm)**2

```

```

rgx=np.sqrt(rgx/len(xf))
rgy=np.sqrt(rgy/len(yf))
rgz=np.sqrt(rgz/len(zf))

rg_magn=np.sqrt(rgx**2+rgy**2+rgz**2)
a=-rg_magn
b=rg_magn
plt.xlim((a+xcm)*0.1,(b+xcm)*0.1)#in nm
plt.ylim((a+ycm)*0.1,(b+ycm)*0.1)#in nm
ax.set_zlim((a+zcm)*0.1,(b+zcm)*0.1)#in nm
xf2=[ii*0.1 for ii in xf]
yf2=[ii*0.1 for ii in yf]
zf2=[ii*0.1 for ii in zf]
ax.plot_wireframe(xf2,yf2,zf2)#in nm
ax.scatter(xf2,yf2,zf2,'o',c='b')#in nm
plt.xlabel("$x~(\mathrm{nm})$")
plt.ylabel("$y~(\mathrm{nm})$")
ax.set_zlabel("$z~(\mathrm{nm})$")
plt.savefig("3d-plot.png",dpi=300)

filename2="initial3.txt"
writefile = open(filename2,'w')
for j in range(n):
    writefile.write(str(xf[j]))#in anstrogm
    writefile.write("\t")
    writefile.write(str(yf[j]))#in anstrogm
    writefile.write("\t")
    writefile.write(str(zf[j]))#in anstrogm
    writefile.write("\n")

```

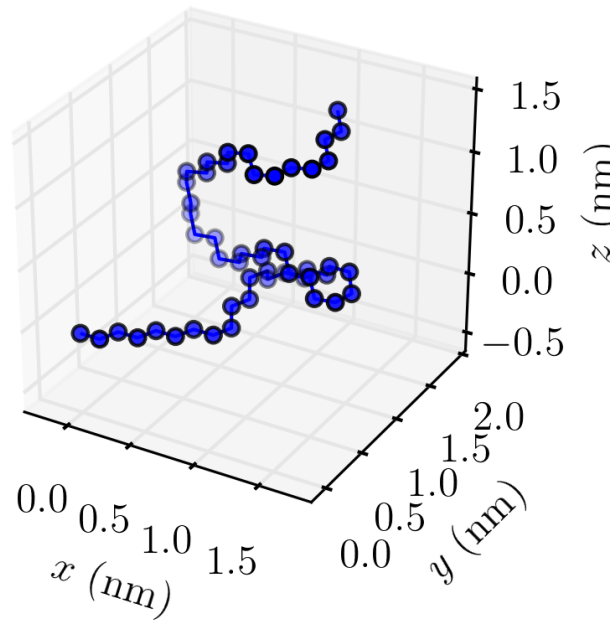


Figure B.1: Initial conformation of chain with $N = 50$ in the numerical simulation described in the letter, which is generated using the Python 3.5 program above.

Appendix C

Supporting Information for Chapter 4

C.1 Harmonic Potential with $b = 0$

Let us first consider the case of linear polyethylene, the equations of motion of N beads without the inertia term and hydrodynamic interaction is given as follows:

$$\frac{d\mathbf{q}}{dt} = \frac{k}{\zeta} \mathcal{A}\mathbf{q} + \frac{\mathbf{g}}{\zeta} \quad (\text{C.1})$$

In this simple case, the change in the position \mathbf{q} with time is equal to sum of the matrix \mathcal{A} operates on itself and the random force \mathbf{g} (cf., Equation (C.2)), which has a normal distribution with $\langle g_{n,q} \rangle = 0$ and $\langle g_{n,q}(t)g_{n,q}(t') \rangle = 2k_b T \zeta \delta(t - t')$.

$$\mathbf{g} = [g_{0,x} \ \cdots \ g_{N-1,x} \ g_{0,y} \ \cdots \ g_{N-1,y} \ g_{0,z} \ \cdots \ g_{N-1,z}]^T \quad (\text{C.2})$$

It is important to know the form of \mathcal{A} , which are formed by blocks of \mathbf{A} ($N \times N$ matrix).

$$\mathcal{A} = \begin{bmatrix} \mathbf{A} & \mathbf{0} & \mathbf{0} \\ \mathbf{0} & \mathbf{A} & \mathbf{0} \\ \mathbf{0} & \mathbf{0} & \mathbf{A} \end{bmatrix} \quad (\text{C.3})$$

The eigenvalues of \mathbf{A} is related to the relaxation time of different modes of the linear chain, which is critical in the evaluation of different time correlation functions. As pointed out by Rouse [20], \mathbf{A} is a tridiagonal matrix, which has the following form:

$$\mathbf{A} = \begin{bmatrix} -1 & 1 & 0 & 0 & \cdots & 0 \\ 1 & -2 & 1 & 0 & \cdots & 0 \\ 0 & 1 & -2 & 1 & \cdots & 0 \\ 0 & 0 & \ddots & \ddots & \ddots & 0 \\ 0 & 0 & \cdots & 1 & -2 & 1 \\ 0 & 0 & \cdots & 0 & 1 & -1 \end{bmatrix} \quad (\text{C.4})$$

Equation (C.1) can be solved numerically using the implicit Euler method:

$$\left[\Delta t \frac{k}{\zeta} \mathcal{A} - \mathbf{I}\right] \mathbf{q}_{j+1} = -\frac{\Delta t}{\zeta} \mathbf{g}_{j+1} - \mathbf{q}_j \quad (\text{C.5})$$

\mathbf{I} is a $3N \times 3N$ identity matrix. At each time step j , a system of linear equations can be solved numerically using algorithm, such as tridiagonal matrix algorithm, to obtain \mathbf{q}_{j+1} . This method was implemented in a C++ program.

C.2 Preliminaries: Linear Brownian Dynamics of Polymer with $b = 0$

In this section, we would like to demonstrate the eigenfunctions in the Rouse model of polyethylene with different structures and their applications in obtaining the time correlation functions of different vectors.

C.2.1 Linear Structure

Interestingly, the operator \mathbf{A} can be replaced by the operator $\partial^2/\partial n^2$ if we are interested in the long time scale motion of the linear chain [21]. And Equation (C.1) will become a second order parabolic partial differential equation subjected to the boundary conditions $\frac{\partial \mathbf{R}_0}{\partial n} = 0$ and $\frac{\partial \mathbf{R}_N}{\partial n} = 0$:

$$\frac{\partial \mathbf{R}_n}{\partial t} = \frac{k}{\zeta} \frac{\partial^2 \mathbf{R}_n}{\partial n^2} + \frac{\mathbf{f}_n}{\zeta} \quad (\text{C.6})$$

In which $\mathbf{R}_n = [R_{n,x} \ R_{n,y} \ R_{n,z}]^T$ and $\mathbf{f}_n = [g_{n,x} \ g_{n,y} \ g_{n,z}]^T$. Subjected to the following boundary conditions:

$$\frac{\partial \mathbf{R}_0}{\partial n} = 0, \quad \frac{\partial \mathbf{R}_N}{\partial n} = 0$$

With these boundary conditions, $\psi_p = \cos(p\pi \frac{n}{N})$ for $p = 0, 1, 2, 3 \dots N - 1$. The solution is therefore:

$$\mathbf{R}_n = \mathbf{X}_0 + 2 \sum_{p=1}^{N-1} \mathbf{X}_p \cos(p\pi \frac{n}{N})$$

With the following:

$$\mathbf{X}_0(t) = \frac{1}{N} \left[\mathbf{A}_0 + \int_0^t \int_0^N \frac{\mathbf{f}_n}{\zeta} dnd\tau \right] \quad (\text{C.7})$$

$$\mathbf{X}_p(t) = \frac{1}{N} e^{-\lambda_p^2 t} \left[\mathbf{A}_p + \int_0^t e^{\lambda_p^2 \tau} \int_0^N \frac{\mathbf{f}_n}{\zeta} \cos(p\pi \frac{n}{N}) dnd\tau \right] \quad (\text{C.8})$$

We can now study the longest relaxation time, which is the relaxation time of the end-to-end vector,

$$\mathbf{R} = \mathbf{R}_{N-1} - \mathbf{R}_0 = 2 \sum_{p=1}^{N-1} \mathbf{X}_p \left[\cos(p\pi) - 1 \right] = -4 \sum_{p=1, \text{odd}}^{N-1} \mathbf{X}_p \quad (\text{C.9})$$

Therefore, the correlation function for the end-to-end vector is:

$$\langle \mathbf{R}(t) \cdot \mathbf{R}(0) \rangle = 16 \sum_{p=1, \text{odd}}^{N-1} \langle \mathbf{X}_p(t) \cdot \mathbf{X}_p(0) \rangle = 8 \sum_{p=1, \text{odd}}^{N-1} \frac{Nb^2}{p^2 \pi^2} e^{-t/\tau_p} \quad (\text{C.10})$$

The random force term in Equations (C.7) and (C.8) disappears when we multiply these expression by $\mathbf{X}_p(0)$ and $\mathbf{X}_0(0)$, as \mathbf{f}_n is not correlated with \mathbf{A}_p and \mathbf{A}_0 , respectively. Equation (C.10) is therefore verified numerically (cf., Figure C.1(a)).

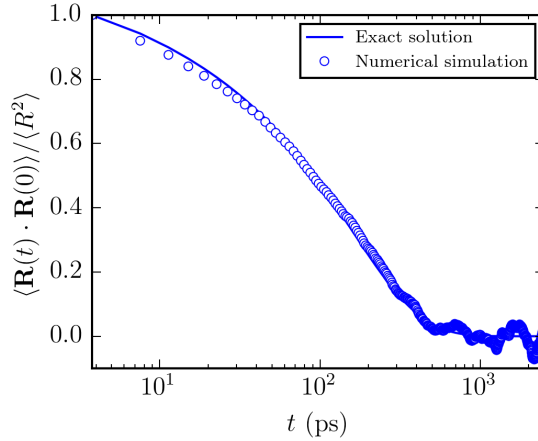


Figure C.1: Time correlation function of the end-to-end vector of a linear polyethylene compared with the exact solution.

Armed with this knowledge, we can envisage that once we know the eigenvalues and eigenfunctions of the operator \mathbf{A} for the ring and star structures, we can directly use this information to construct the corresponding time correlation functions of the particular vectors.

C.2.2 Ring Structure

The matrix \mathbf{A} for the ring structure is as follows:

$$\mathbf{A} = \begin{bmatrix} -2 & 1 & 0 & 0 & \dots & 1 \\ 1 & -2 & 1 & 0 & \dots & 0 \\ 0 & 1 & -2 & 1 & \dots & 0 \\ 0 & 0 & \ddots & \ddots & \ddots & 0 \\ 0 & 0 & \dots & 1 & -2 & 1 \\ 1 & 0 & \dots & 0 & 1 & -2 \end{bmatrix} \quad (\text{C.11})$$

We can also make use of the continuous approach for the ring structure and the partial differential equation is in the same form as that of the linear chain, but with slightly different boundary condition:

$$\mathbf{R}_0 = \mathbf{R}_N, \quad \frac{\partial \mathbf{R}_0}{\partial n} = \frac{\partial \mathbf{R}_{N-1}}{\partial n}$$

We notice that both eigenfunctions $\sin(2p\pi \frac{n}{N})$ as well as $\cos(2p\pi \frac{n}{N})$ satisfy the boundary conditions, and eigenvalues $\lambda_p^2 = \frac{4p^2\pi^2k}{N^2\zeta}$. Therefore, for the ring structure with size N , there are $\frac{N}{2}$ eigenmodes with $\sin(2p\pi \frac{n}{N})$ and other $\frac{N}{2}$ eigenmodes with $\cos(2p\pi \frac{n}{N})$ as eigenfunctions.

The solution now becomes:

$$\mathbf{R}_n = \mathbf{X}_0 + 2 \sum_{p=1}^{N/2-1} \mathbf{X}_p(t) \cos(2p\pi \frac{n}{N}) + 2 \sum_{p=1}^{N/2-1} \mathbf{Y}_p(t) \sin(2p\pi \frac{n}{N}) \quad (\text{C.12})$$

As it is known that relaxation times for different normal modes are $\tau_p = 1/\lambda_p^2$. From this result, we immediately know that relaxation times of different modes of the ring structure are faster by a factor of 4 compared to its linear counterpart.

Similar to the formulation presented in the previous section of this paper, in the case of the ring structure, we are interested in the time correlation function of a vector \mathbf{R} , which connects the n th bead to the m th bead. The equation now becomes:

$$\mathbf{R}(t) = \mathbf{R}_m(t) - \mathbf{R}_n(t) = 2 \left(\sum_{p=1}^{N/2-1} \mathbf{X}_p(t) \left[\cos(2p\pi \frac{m}{N}) - \cos(2p\pi \frac{n}{N}) \right] + \mathbf{Y}_p(t) \left[\sin(2p\pi \frac{m}{N}) - \sin(2p\pi \frac{n}{N}) \right] \right) \quad (\text{C.13})$$

The time correlation function of \mathbf{R} is therefore:

$$\langle \mathbf{R}(t) \cdot \mathbf{R}(0) \rangle = 4 \left(\sum_{p=1}^{N/2-1} \langle Y_p^2 \rangle e^{-\lambda_p^2 t} \left[\sin(2p\pi \frac{m}{N}) - \sin(2p\pi \frac{n}{N}) \right]^2 + \langle X_p^2 \rangle e^{-\lambda_p^2 t} \left[\cos(2p\pi \frac{m}{N}) - \cos(2p\pi \frac{n}{N}) \right]^2 \right) \quad (\text{C.14})$$

To construct $\langle \mathbf{R}(t) \cdot \mathbf{R}(0) \rangle$, we need to know $\langle X_p^2 \rangle$ and $\langle Y_p^2 \rangle$. Consider a three dimensional Gaussian distribution Ψ with a normalization constant C in the case of an ideal ring structure (Details of derivation of Ψ can be found in the book written by Khokhlov [128]):

$$\begin{aligned} \Psi(\mathbf{R}_0 \dots \mathbf{R}_N) &= C \exp \left(-\frac{3}{2b^2/2} \sum_{i=n}^{m-1} (\mathbf{R}_{i+1} - \mathbf{R}_i)^2 \right) \\ &= C \exp \left(-\frac{3}{2b^2/2} \int_n^m \left(\frac{\partial \mathbf{R}_n}{\partial n} \right)^2 dn \right) \\ &= C \exp \left(-\sum_{p=1}^{N/2-1} \frac{3 \cdot 2p^2 \pi^2}{2Nb^2/2} [\mathbf{X}_p \mathbf{X}_p + \mathbf{Y}_p \mathbf{Y}_p] \right) \end{aligned}$$

For the simple case that $n = 0$ and $m = N/2$, we have:

$$\langle X_p^2 \rangle = \frac{Nb^2}{4p^2\pi^2} \quad (\text{C.15})$$

And:

$$\langle Y_p^2 \rangle = \frac{Nb^2}{4p^2\pi^2} \quad (\text{C.16})$$

For $p = 1, 2, 3 \dots N/2 - 1$. This leads to:

$$\langle \mathbf{R}(t) \cdot \mathbf{R}(0) \rangle = \frac{Nb^2}{2} \sum_{p=1}^{N/2-1} \frac{8}{p^2\pi^2} e^{-\lambda_p^2 t} \quad (\text{C.17})$$

This exact solution is confirmed by numerical simulation results as shown in Figure C.2(a).

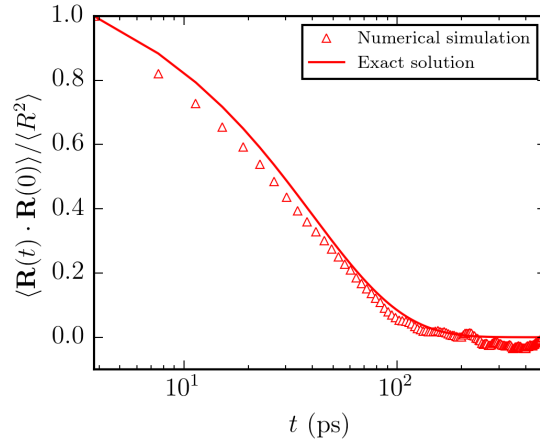


Figure C.2: Time correlation function of the m -to- n vector of the ring structure compared with the exact solution.

C.2.3 Star Structure

Matrix \mathbf{A} for the star structure with four arms was derived using a similar approach of Ghosh [24]. In such a case, the eigenvalues and eigenfunctions (ψ_p) of \mathbf{A} were obtained numerically.

$$\mathbf{A} = \begin{bmatrix} \mathbf{A}_1 & \mathbf{0} & \mathbf{V} & \mathbf{0} & \mathbf{0} \\ \mathbf{0} & \mathbf{A}_1 & \mathbf{V} & \mathbf{0} & \mathbf{0} \\ \mathbf{V}^T & \mathbf{V}^T & -4 & \mathbf{U}^T & \mathbf{U}^T \\ \mathbf{0} & \mathbf{0} & \mathbf{U} & \mathbf{A}_2 & \mathbf{0} \\ \mathbf{0} & \mathbf{0} & \mathbf{U} & \mathbf{0} & \mathbf{A}_2 \end{bmatrix} \quad (\text{C.18})$$

For which, we let the followings:

$$\mathbf{A}_1 = \begin{bmatrix} -1 & 1 & 0 & \dots & 0 \\ 1 & -2 & 1 & \dots & 0 \\ 0 & \ddots & \ddots & \ddots & 0 \\ 0 & \dots & 1 & -2 & 1 \\ 0 & \dots & 0 & 1 & -2 \end{bmatrix} \quad (\text{C.19})$$

$$\mathbf{A}_2 = \begin{bmatrix} -2 & 1 & 0 & \dots & 0 \\ 1 & -2 & 1 & \dots & 0 \\ 0 & \ddots & \ddots & \ddots & 0 \\ 0 & \dots & 1 & -2 & 1 \\ 0 & \dots & 0 & 1 & -1 \end{bmatrix} \quad (\text{C.20})$$

The dimensions of \mathbf{A}_1 and \mathbf{A}_2 are both $N_f \times N_f$, where N_f is the number of beads per arm.

$$\mathbf{V} = [0 \ 0 \ \dots \ 1]^T \quad (\text{C.21})$$

$$\mathbf{U} = [1 \ 0 \ \dots \ 0]^T \quad (\text{C.22})$$

Figure C.3 shows the plots of the first three most dominant eigenfunctions of \mathbf{A} (ψ_p) for the star structure. Eigenvalues of \mathbf{A} can be used to obtain the relaxation time τ_p . Interestingly, as shown in Figure C.4, three normal modes can share the same value τ_p in star polymer.

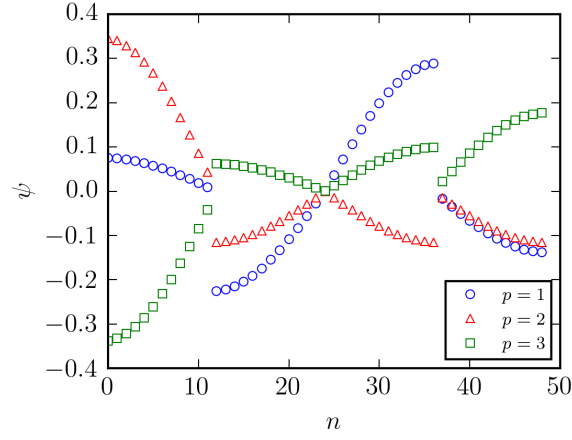


Figure C.3: Eigenfunctions for the three most dominant normal modes of the star structure with $N = 49$.

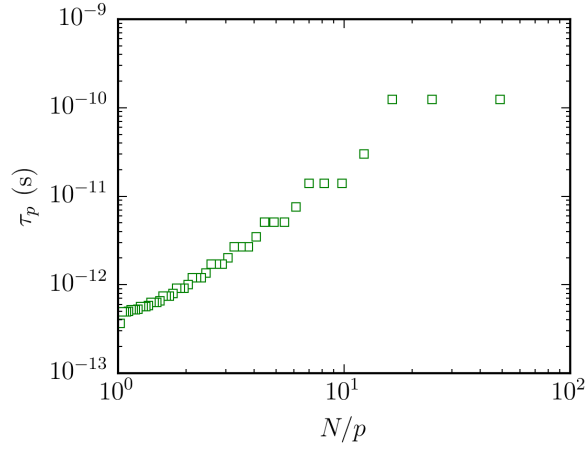


Figure C.4: τ_p in star polymer with $N = 49$.

With the numerically determined eigenfunctions and eigenvalues, we can easily calculate the time correlation function for the arms of the star polymers:

$$\langle \mathbf{R}(t) \cdot \mathbf{R}(0) \rangle = \sum_{p=1}^{N-1} \langle X_p^2 \rangle e^{-t/\tau_p} \left[\psi_p(0) - \psi_p\left(\frac{N-1}{2}\right) \right]^2 \quad (\text{C.23})$$

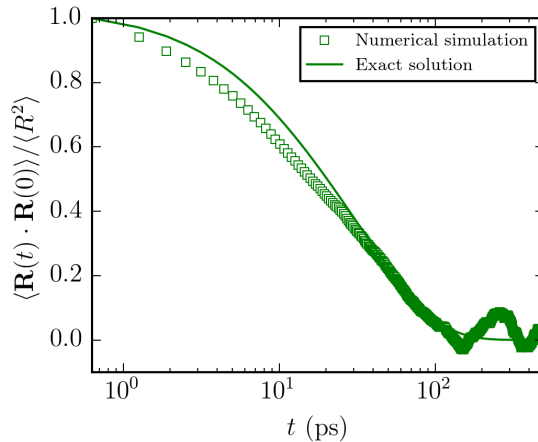


Figure C.5: Time correlation function of the arm vector compared with the exact solution.

C.3 $\sqrt{\langle R_g^2 \rangle}$ of Polyethylene with Different Structures in BD and MD Simulations

Figure C.6 shows plots of $\sqrt{\langle R_g^2 \rangle}$ with N derived from the BD and MD simulations for the three different structures. In BD simulation, a Gaussian statistics was observed as indicated by $\sqrt{\langle R_g^2 \rangle} \sim N^{0.5}$, whereas in MD simulation, N dependence of $\sqrt{\langle R_g^2 \rangle}$ with an exponent slightly greater than 0.5, ranging from 0.66 to 0.70, was observed. Nonetheless, we found that our MD data of linear and ring structures are in excellent agreement with Hur *et al.* [2] as well as Tsolou *et al.* [4], and the experimental data of Dettenmaier [129]. In addition, the magnitude of the $\sqrt{\langle R_g^2 \rangle}$ is always slightly higher in BD simulation. We speculate that this may be due to the lack of many-chain effect in BD simulation, as the magnitude of the characteristic ratio (C_∞) can be influenced by the density of the polymer melt.

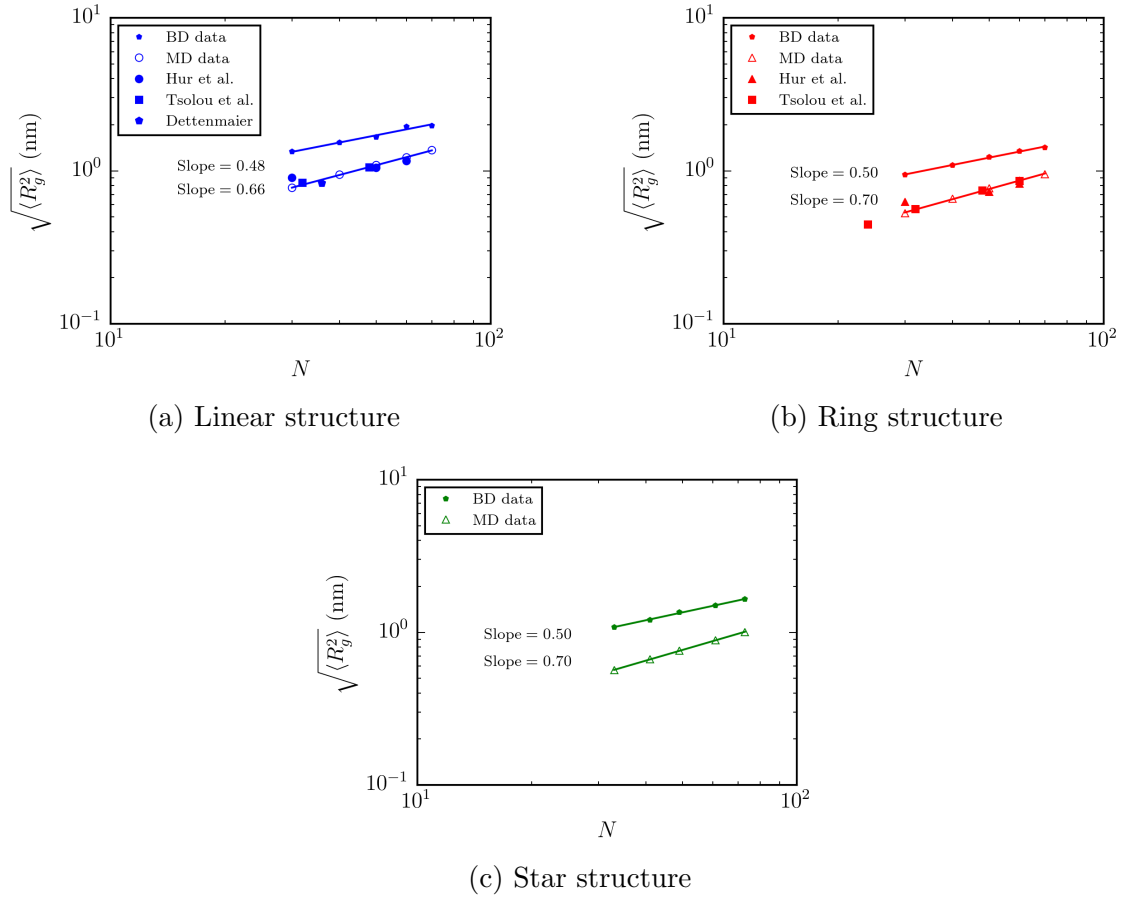


Figure C.6: $\sqrt{\langle R_g^2 \rangle}$ of polyethylene with linear, ring and star structures in BD and MD simulations as well as the literature data.

C.4 D_{cm} of Polyethylene with Different Structures in BD and MD Simulations

Figure C.7 shows a plot of D_{cm} with N for polyethylene with different structures. For all structures, we observed that the N dependence of D_{cm} is slightly stronger in MD simulation for linear and star structures, in which the exponents are -1.8 and -1.5 , respectively, than that in BD simulation with the exponents of -1.3 and -1.1 , respectively. The reverse is true for ring structure that the exponents of -1.3 and -0.9 were observed in BD and MD simulations, respectively. Our MD simulation data are in good agreement with that of Hur *et al.* [2] and Tsolou *et al.* [4]. For linear structure, our observation that a stronger N

dependence of D_{cm} in MD simulation with an exponent greater than unity was also evident in the experimental data of von Meerwall *et al.* [1] (cf., Figure C.7(a)). For ring structure, a smaller exponent of -0.9 in the N dependence of D_{cm} was obtained (cf., Figure C.7(b)). This may be due to the fact that there are no chain ends in ring structure, and therefore the effect of density on the self-diffusion of ring polyethylene is weaker in the MD simulation.

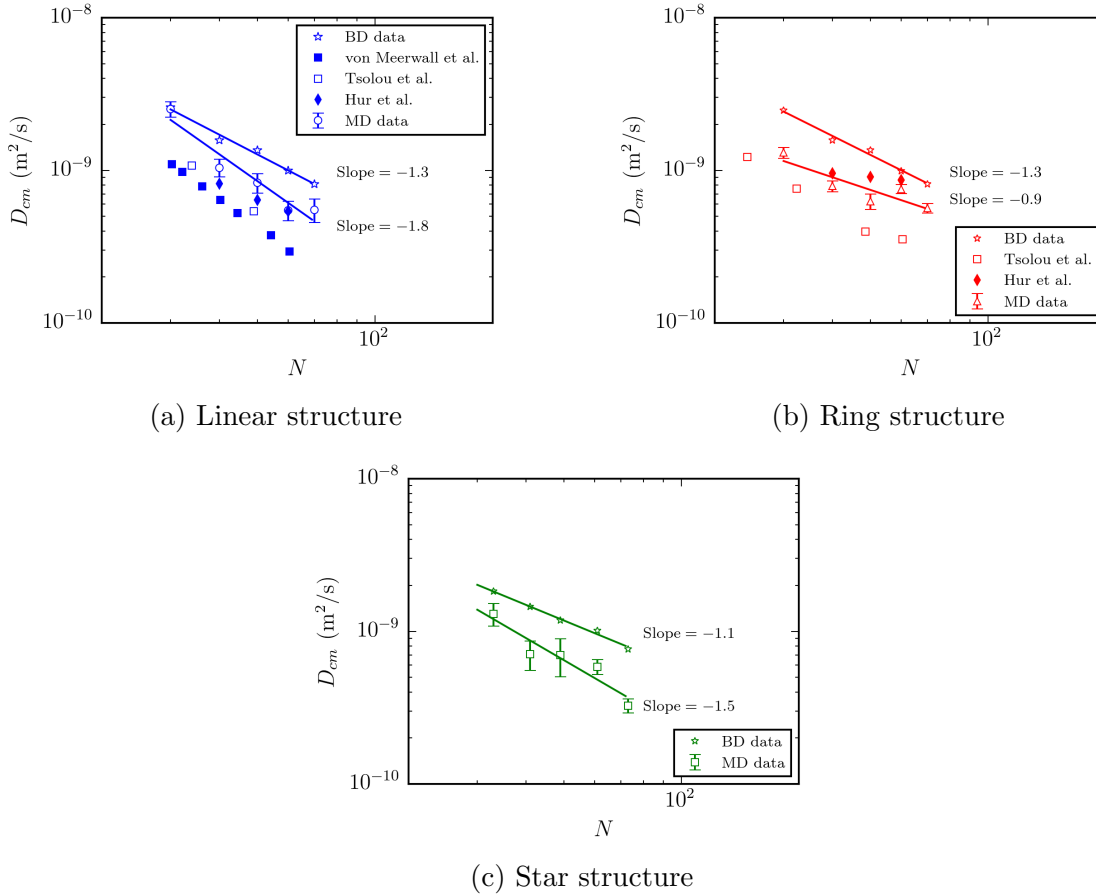


Figure C.7: Comparison of D_{cm} derived from MD simulation with different references in the literature.

C.5 $\sqrt{\langle R^2 \rangle}$ of Polyethylene with Different Structures in BD Simulation Compared with $\sqrt{NC_\infty b_0}$

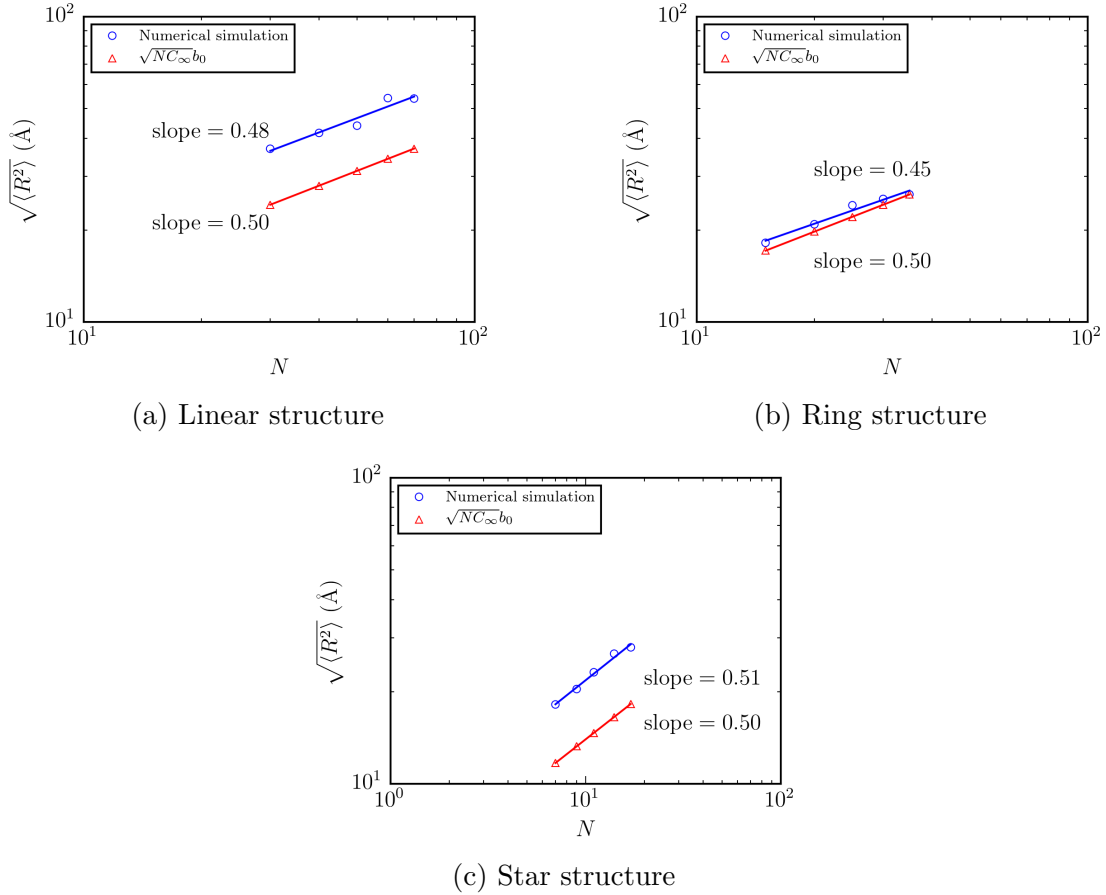


Figure C.8: $\sqrt{\langle R^2 \rangle}$ of polyethylene with linear, ring and star structures in BD as well as that calculated by $\sqrt{NC_\infty b_0}$.

As shown in Figure C.8, the expected $\sqrt{\langle R^2 \rangle} \sim N^{0.5}$ is reproduced in the BD simulation. In addition, this also proves that the harmonic bond stretching potential can avoid the overlapping of beads as the computed values of $\sqrt{\langle R^2 \rangle}$ in BD simulation are always slightly higher than $\sqrt{NC_\infty b_0}$.

C.6 C++ Program for Numerical Simulation of Star Polymer with $b = 0$

```

#include <iostream>
#include <istream>
#include <fstream>
#include <iomanip>
#include <cstdio>
#include <sstream>
#include <eigen/Eigen/Core>
#include <vector>
#include <stdlib.h>
#include <stdio.h>
#include <random>
#include <chrono>
#include <string>
#include <omp.h>
using namespace std;
using namespace Eigen;
using namespace std::chrono;
//compile with g++ -std=c++11 -Ofast main2.cpp -o ld4

VectorXd TDMA2(const MatrixXd& A,const VectorXd& b)
{
    int row=A.rows();
    int col=A.cols();
    VectorXd x=VectorXd::Zero(row);
    VectorXd b2=b;
    VectorXd c(row);
    VectorXd a(row);
    for(int i=0;i<row;i++)
    {
        if(i==0)
        {
            c(i)=A(i,i+1);
            a(i)=0;
        }
        else if(i==row-1)
        {
            a(i)=A(i,i-1);
            c(i)=0;
        }
        else
        {
            a(i)=A(i,i-1);
            c(i)=A(i,i+1);
        }
    }
    double err=1;
    double sum1;

```

```

VectorXd d1p(row);
VectorXd c1p(row);
VectorXd err1(row);
int count=0;
for(int i=0;i<row;i++)
{
    if(i==0)
    {
        c1p(i)=c(i)/A(i,i);
    }
    else
    {
        c1p(i)=c(i)/(A(i,i)-a(i)*c1p(i-1));
    }
}
while(abs(err)>pow(10,-6))
{
    for(int i=0;i<row;i++)
    {
        if(i==0)
        {
            d1p(i)=b2(i)/A(i,i);
        }
        else
        {
            d1p(i)=(b2(i)-a(i)*d1p(i-1))/(A(i,i)-a(i)*c1p(i-1));
        }
    }
    x(row-1)=d1p(row-1);
    for(int i=row-2;i>=0;--i)
    {
        x(i)=d1p(i)-c1p(i)*x(i+1);
    }
    for(int i=0;i<row;i++)
    {
        sum1=0;
        for(int j=0;j<col;j++)
        {
            if(j==i || j==i+1 || j==i-1)
            {
                ;
            }
            else
            {
                sum1=sum1+A(i,j)*x(j);
            }
        }
    }
}

```

```

        b2(i)=b(i)-sum1;
    }
    err1=A*x-b;
    err=0;
    for(int i=0;i<row;i++)
    {
        err=err+pow(err1(i),2)/row;
    }
    err=pow(err,0.5);
    count=count+1;
    if(count>1000)
    {
        break;
    }
}
return x;
}

int main(int argc, char** argv){
    default_random_engine generator;
    char* filename;
    int N,t_step,count,n_save,f_save,mid_point,count_a;
    double dt;
    for(int i=1;i<argc;i++){
        if(strcmp(argv[i], "-n") == 0){
            N=stoi(argv[i+1],NULL);//length of polymer
        }
        else if(strcmp(argv[i], "-t") == 0){
            t_step=stoi(argv[i+1],NULL);//t_step
        }
        else if(strcmp(argv[i], "-dt") == 0){
            dt=stod(argv[i+1],NULL);//size of time step dt=0.001 ps
        }
        else if(strcmp(argv[i], "-f")==0){
            filename=argv[i+1];//initial configuration file
        }
        else if(strcmp(argv[i], "-s")==0){
            f_save=stoi(argv[i+1],NULL);//number of steps to be saved
        }
        else{
            ;
        }
    }
    n_save=t_step/f_save;
    ifstream infile(filename);
    VectorXd x(N),y(N),z(N),bx(N),by(N),bz(N);
    MatrixXd x1(N,n_save),y1(N,n_save),z1(N,n_save);
    MatrixXd A1=MatrixXd::Zero(N,N);

```

```

MatrixXd I=MatrixXd::Identity(N,N);
mid_point=(N-1)/2;
int f=((N-1)/4)+1);
count_a=0;
for(int i=0;i<mid_point+1;i++){
    if(i==mid_point){
        A1(i,i)=-4;
        A1(i,i-1)=1;
        A1(i,i+1)=1;
        A1(i,i-f)=1;
        A1(i,i+f)=1;
    }
    else{
        if(i%(f-1)==0){
            for(int j=0;j<(f-1);j++){
                if(j==0){
                    A1(j+count_a,j+count_a)=-1;
                    A1(j+count_a,j+count_a+1)=1;
                }
                else if(j==(f-2)){
                    A1(j+count_a,j+count_a)=-2;
                    A1(j+count_a,j-1+count_a)=1;
                    A1(j+count_a,mid_point)=1;
                }
                else{
                    A1(j+count_a,j+count_a)=-2;
                    A1(j+count_a,j-1+count_a)=1;
                    A1(j+count_a,j+1+count_a)=1;
                }
            }
            count_a=count_a+(f-1);
        }
        else{
            ;
        }
    }
}
int a11=mid_point+1;
count_a=0;
for(int i2=0;i2<mid_point;i2++){
    int i=i2+a11;
    if((i-1)%(f-1)==0){
        for(int j=0;j<f-1;j++){
            if(j==0){
                A1(j+a11+count_a,j+a11+count_a)=-2;
                A1(j+a11+count_a,j+a11+1+count_a)=1;
                A1(j+a11+count_a,mid_point)=1;
            }
        }
    }
}

```

```

        else if(j==f-2){
            A1(j+a11+count_a , j+a11+count_a)=-1;
            A1(j+a11+count_a , j+a11-1+count_a)=1;
        }
        else{
            A1(j+count_a+a11 , a11+j+count_a)=-2;
            A1(j+count_a+a11 , j-1+a11+count_a)=1;
            A1(j+count_a+a11 , a11+j+1+count_a)=1;
        }
    }
    count_a=count_a+(f-1);
}
else{
    ;
}
}
for(int i=0;i<N;i++){
    infile>>x(i);
    infile>>y(i);
    infile>>z(i);
}
double c1,lam;
double k_b=1.38065*pow(10,-27); //A^2 kg ps^-2K^-1
double T=450; //K
double xi=8; //ps^-1
double b=4.42; //A
double m=2.32664*pow(10,-26); //kg
double k=(3*k_b*T)/(pow(b,2)); //kg ps^-2
double sigma=pow(2*k_b*T*xi*m,0.5); //normal distribution force
c1=(k/(m*xi))*dt;
A1=A1*c1-I;
normal_distribution<double> distribution(0,sigma);
high_resolution_clock::time_point t1 = high_resolution_clock::now
();
count=0;
for(int it=0;it<t_step;it++){
    if(it==0){
        for(int i=0;i<N;i++){
            x1(i,count)=x(i);
            y1(i,count)=y(i);
            z1(i,count)=z(i);
        }
        count=count+1;
    }
}
else{
    VectorXd Fx=VectorXd::Zero(N);
    VectorXd Fy=VectorXd::Zero(N);
    VectorXd Fz=VectorXd::Zero(N);
}

```

```

    for(int i=0;i<N;i++){
        Fx(i)=distribution(generator);
        Fy(i)=distribution(generator);
        Fz(i)=distribution(generator);
        bx(i)=-x(i)-Fx(i)*dt/(m*xi);
        by(i)=-y(i)-Fy(i)*dt/(m*xi);
        bz(i)=-z(i)-Fz(i)*dt/(m*xi);
    }
    x=TDMA2(A1,bx);
    y=TDMA2(A1,by);
    z=TDMA2(A1,bz);
    if(remainder(it,f_save)==0){
        for(int i=0;i<N;i++){
            x1(i,count)=x(i);
            y1(i,count)=y(i);
            z1(i,count)=z(i);
        }
        count=count+1;
        cout << "Saved_time_step=" << count << endl;
    }
}
}
ofstream myfile;
myfile.open("x.dat", ios::binary);
myfile.write((char *) x1.data(), x1.rows() * x1.cols() * sizeof(
double));
myfile.close();
myfile.open("y.dat", ios::binary);
myfile.write((char *) y1.data(), y1.rows() * y1.cols() * sizeof(
double));
myfile.close();
myfile.open("z.dat", ios::binary);
myfile.write((char *) z1.data(), z1.rows() * z1.cols() * sizeof(
double));
myfile.close();
high_resolution_clock::time_point t2 = high_resolution_clock::now
();
auto duration = duration_cast<seconds>( t2 - t1 ).count();
cout << "run_time=" << duration << "seconds" << endl;
return 0;
}

```

C.7 C++ Program for Numerical Simulation of Star Polymer with $b = 4.42 \text{ \AA}$

```
#include <iostream>
#include <istream>
#include <fstream>
#include <iomanip>
#include <cstdio>
#include <sstream>
#include </home/chipuije/eigen/Eigen/Dense>
#include <vector>
#include <stdlib.h>
#include <stdio.h>
#include <random>
#include <chrono>
#include <string>
#include <omp.h>
using namespace std;
using namespace Eigen;
using namespace std::chrono;
//compile with g++ -std=c++11 -Ofast main2.cpp -o ld4

double dFb_dx(double x1,double x2,double y1,double y2,double z1,
double z2,int p1,double k){
//tridiagonal elements of Jacobian matrix
double R12=pow((x2-x1)*(x2-x1)+(y2-y1)*(y2-y1)+(z2-z1)*(z2-z1)
,0.5),l=4.42;
if(p1==0){
return -k*(R12-1)/R12+k*(x2-x1)*(x2-x1)*(R12-1)/pow(R12,3)-k*(x2
-x1)*(x2-x1)/(R12*R12);
}
else if(p1==1){
return -k*(R12-1)/R12+k*(y2-y1)*(y2-y1)*(R12-1)/pow(R12,3)-k*(y2
-y1)*(y2-y1)/(R12*R12);
}
else if(p1==2){
return -k*(R12-1)/R12+k*(z2-z1)*(z2-z1)*(R12-1)/pow(R12,3)-k*(z2
-z1)*(z2-z1)/(R12*R12);
}
}

double dFxdy1(double x1,double x2,double y1,double y2,double z1,
double z2,int p1,int p2,double k){
//off-tridiagonal elements of Jacobian matrix
double R12=pow((x2-x1)*(x2-x1)+(y2-y1)*(y2-y1)+(z2-z1)*(z2-z1)
,0.5),l=4.42;
if((p1==0 && p2==1) || (p1==1 && p2==0)){
```

```

    return k*(x2-x1)*(y2-y1)*(R12-1)/pow(R12,3)-k*(x2-x1)*(y2-y1)/(
        R12*R12);
}
else if((p1==0 && p2==2) || (p1==2 && p2==0)){
    return k*(x2-x1)*(z2-z1)*(R12-1)/pow(R12,3)-k*(x2-x1)*(z2-z1)/(
        R12*R12);
}
else if((p1==1 && p2==2) || (p1==2 && p2==1)){
    return k*(y2-y1)*(z2-z1)*(R12-1)/pow(R12,3)-k*(y2-y1)*(z2-z1)/(
        R12*R12);
}
}
}

double Fb(double x1,double x2,double y1,double y2,double z1,double
    z2,int p1,double k){
    double R12=pow((x2-x1)*(x2-x1)+(y2-y1)*(y2-y1)+(z2-z1)*(z2-z1)
        ,0.5),l=4.42;
    if(p1==0){
        return k*(R12-1)*(x2-x1)/R12;
    }
    else if(p1==1){
        return k*(R12-1)*(y2-y1)/R12;
    }
    else if(p1==2){
        return k*(R12-1)*(z2-z1)/R12;
    }
}

int main(int argc, char** argv){
    default_random_engine generator;
    char* filename;
    int N,t_step,count,n_save,f_save,count2,mid_point,f,count_a;
    double dt;
    for(int i=1;i<argc;i++){
        if(strcmp(argv[i], "-n") == 0){
            N=stoi(argv[i+1],NULL);//length of polymer
        }
        else if(strcmp(argv[i], "-t") == 0){
            t_step=stoi(argv[i+1],NULL);//t_step
        }
        else if(strcmp(argv[i], "-dt") == 0){
            dt=stod(argv[i+1],NULL);//size of time step dt=0.001 ps
        }
        else if(strcmp(argv[i], "-f")==0){
            filename=argv[i+1];//initial configuration file
        }
        else if(strcmp(argv[i], "-s")==0){
            f_save=stoi(argv[i+1],NULL);//number of steps to be saved

```

```

    }
    else{
        ;
    }
}
n_save=t_step/f_save;
ifstream infile(filename);
VectorXd x(N),y(N),z(N),bx(N),by(N),bz(N),res(3*N),delr(3*N),
product1(3*N),err_v(n_save),count_it(n_save);
MatrixXd x1(N,n_save),y1(N,n_save),z1(N,n_save),r(N,3),r2(N,3);
MatrixXd J=MatrixXd::Zero(3*N,3*N),JTJ(3*N,3*N),JT(3*N,3*N);
for(int i=0;i<N;i++){
    infile>>x(i);
    infile>>y(i);
    infile>>z(i);
    x(i)=x(i)*4.42/1.54;
    y(i)=y(i)*4.42/1.54;
    z(i)=z(i)*4.42/1.54;
}
double lam,err,rcmx,rcmy,rcmz;
double k_b=1.38065*pow(10,-27);//A^2 kg ps^-2K^-1
double T=450;//K
double xi=2.58;//ps^-1
double b=4.42;//A
double m=2.32664*pow(10,-26);//kg
double k=(3*k_b*T)/(pow(b,2));//kg ps^-2
double c2=k/(m*xi);
dt=m*xi/k;
double sigma=pow(2*k_b*T*xi*m,0.5);//normal distribution force
normal_distribution<double> distribution(0,sigma);
high_resolution_clock::time_point t1 = high_resolution_clock::now
();
count=0;
for(int i=0;i<N;i++){
    r(i,0)=x(i);
    r(i,1)=y(i);
    r(i,2)=z(i);
}
r2=r;
mid_point=(N-1)/2;
f=((N-1)/4)+1);

for(int it=0;it<t_step;it++){
    if(it==0){
        for(int i=0;i<N;i++){
            x1(i,count)=r(i,0);
            y1(i,count)=r(i,1);
            z1(i,count)=r(i,2);

```

```

}
err_v(count)=0;
count_it(count)=0;
count=count+1;
}
else{
VectorXd Fr=VectorXd::Zero(3*N);
for(int i=0;i<3*N;i++){
    Fr(i)=distribution(generator)*dt/(m*xi);
}
err=1;
count2=0;
while(abs(err)>pow(10,-10)){
    for(int i=0;i<3;i++){
        count_a=0;
        for(int i2=0;i2<mid_point+1;i2++){
            if(i2==mid_point){
                res(i2+i*N)=Fb(r2(i2,0),r2(i2+1,0),r2(i2,1),r2(i2+1,1),
                    r2(i2,2),r2(i2+1,2),i,c2*dt)+Fb(r2(i2,0),r2(i2-1,0),r2(i2,1),r2(i2-1,1),r2(i2,2),r2(i2-1,2),i,c2*dt)+r(i2,i)-r2(i2,i)+Fr(i2+i*N)+Fb(r2(i2,0),r2(i2+f,0),r2(i2,1),r2(i2+f,1),r2(i2,2),r2(i2+f,2),i,c2*dt)+Fb(r2(i2,0),r2(i2-f,0),r2(i2,1),r2(i2-f,1),r2(i2,2),r2(i2-f,2),i,c2*dt));
                J(i2+i*N,i2+i*N)=dFb_dx(r2(i2,0),r2(i2+1,0),r2(i2,1),r2(i2+1,1),r2(i2,2),r2(i2+1,2),i,c2*dt)+dFb_dx(r2(i2,0),r2(i2-1,0),r2(i2,1),r2(i2-1,1),r2(i2,2),r2(i2-1,2),i,c2*dt)+dFb_dx(r2(i2,0),r2(i2+f,0),r2(i2,1),r2(i2+f,1),r2(i2,2),r2(i2+f,2),i,c2*dt)+dFb_dx(r2(i2,0),r2(i2-f,0),r2(i2,1),r2(i2-f,1),r2(i2,2),r2(i2-f,2),i,c2*dt))-1;
                J(i2+i*N,i2+i*N+1)=-dFb_dx(r2(i2,0),r2(i2+1,0),r2(i2,1),r2(i2+1,1),r2(i2,2),r2(i2+1,2),i,c2*dt);
                J(i2+i*N,i2+i*N-1)=-dFb_dx(r2(i2,0),r2(i2-1,0),r2(i2,1),r2(i2-1,1),r2(i2,2),r2(i2-1,2),i,c2*dt);
                J(i2+i*N,i2+i*N+f)=-dFb_dx(r2(i2,0),r2(i2+f,0),r2(i2,1),r2(i2+f,1),r2(i2,2),r2(i2+f,2),i,c2*dt);
                J(i2+i*N,i2+i*N-f)=-dFb_dx(r2(i2,0),r2(i2-f,0),r2(i2,1),r2(i2-f,1),r2(i2,2),r2(i2-f,2),i,c2*dt);
            if(i==0){
                //x direction
                J(i2,i2+N)=dFxdy1(r2(i2,0),r2(i2+1,0),r2(i2,1),r2(i2+1,1),r2(i2,2),r2(i2+1,2),0,1,c2*dt)+dFxdy1(r2(i2,0),r2(i2-1,0),r2(i2,1),r2(i2-1,1),r2(i2,2),r2(i2-1,2),0,1,c2*dt)+dFxdy1(r2(i2,0),r2(i2-f,0),r2(i2,1),r2(i2-f,1),r2(i2,2),r2(i2-f,2),0,1,c2*dt)+dFxdy1(r2(i2,0),r2(i2+f,0),r2(i2,1),r2(i2+f,1),r2(i2,2),r2(i2+f,2),0,1,c2*dt);
            }
        }
    }
}
}

```

```

J(i2,i2+N+1)=-dFxdy1(r2(i2,0),r2(i2+1,0),r2(i2,1),r2
(i2+1,1),r2(i2,2),r2(i2+1,2),0,1,c2*dt);
J(i2,i2+N-1)=-dFxdy1(r2(i2,0),r2(i2-1,0),r2(i2,1),r2
(i2-1,1),r2(i2,2),r2(i2-1,2),0,1,c2*dt);
J(i2,i2+N+f)=-dFxdy1(r2(i2,0),r2(i2+f,0),r2(i2,1),r2
(i2+f,1),r2(i2,2),r2(i2+f,2),0,1,c2*dt);
J(i2,i2+N-f)=-dFxdy1(r2(i2,0),r2(i2-f,0),r2(i2,1),r2
(i2-f,1),r2(i2,2),r2(i2-f,2),0,1,c2*dt);
J(i2,i2+2*N)=dFxdy1(r2(i2,0),r2(i2+1,0),r2(i2,1),r2(
i2+1,1),r2(i2,2),r2(i2+1,2),0,2,c2*dt)+dFxdy1(r2(
i2,0),r2(i2-1,0),r2(i2,1),r2(i2-1,1),r2(i2,2),r2(
i2-1,2),0,2,c2*dt)+dFxdy1(r2(i2,0),r2(i2-f,0),r2(
i2,1),r2(i2-f,1),r2(i2,2),r2(i2-f,2),0,2,c2*dt)+
dFxdy1(r2(i2,0),r2(i2+f,0),r2(i2,1),r2(i2+f,1),r2
(i2,2),r2(i2+f,2),0,2,c2*dt);
J(i2,i2+2*N+1)=-dFxdy1(r2(i2,0),r2(i2+1,0),r2(i2,1),
r2(i2+1,1),r2(i2,2),r2(i2+1,2),0,2,c2*dt);
J(i2,i2+2*N-1)=-dFxdy1(r2(i2,0),r2(i2-1,0),r2(i2,1),
r2(i2-1,1),r2(i2,2),r2(i2-1,2),0,2,c2*dt);
J(i2,i2+2*N+f)=-dFxdy1(r2(i2,0),r2(i2+f,0),r2(i2,1),
r2(i2+f,1),r2(i2,2),r2(i2+f,2),0,2,c2*dt);
J(i2,i2+2*N-f)=-dFxdy1(r2(i2,0),r2(i2-f,0),r2(i2,1),
r2(i2-f,1),r2(i2,2),r2(i2-f,2),0,2,c2*dt);
}
else if(i==1){
//y direction
J(i2+i*N,i2)=dFxdy1(r2(i2,0),r2(i2+1,0),r2(i2,1),r2(
i2+1,1),r2(i2,2),r2(i2+1,2),1,0,c2*dt)+dFxdy1(r2(
i2,0),r2(i2-1,0),r2(i2,1),r2(i2-1,1),r2(i2,2),r2(
i2-1,2),1,0,c2*dt)+dFxdy1(r2(i2,0),r2(i2-f,0),r2(
i2,1),r2(i2-f,1),r2(i2,2),r2(i2-f,2),1,0,c2*dt)+
dFxdy1(r2(i2,0),r2(i2+f,0),r2(i2,1),r2(i2+f,1),r2
(i2,2),r2(i2+f,2),1,0,c2*dt);
J(i2+i*N,i2+1)=-dFxdy1(r2(i2,0),r2(i2+1,0),r2(i2,1),
r2(i2+1,1),r2(i2,2),r2(i2+1,2),1,0,c2*dt);
J(i2+i*N,i2-1)=-dFxdy1(r2(i2,0),r2(i2-1,0),r2(i2,1),
r2(i2-1,1),r2(i2,2),r2(i2-1,2),1,0,c2*dt);
J(i2+i*N,i2+f)=-dFxdy1(r2(i2,0),r2(i2+f,0),r2(i2,1),
r2(i2+f,1),r2(i2,2),r2(i2+f,2),1,0,c2*dt);
J(i2+i*N,i2-f)=-dFxdy1(r2(i2,0),r2(i2-f,0),r2(i2,1),
r2(i2-f,1),r2(i2,2),r2(i2-f,2),1,0,c2*dt);
J(i2+i*N,i2+2*N)=dFxdy1(r2(i2,0),r2(i2+1,0),r2(i2,1),
r2(i2+1,1),r2(i2,2),r2(i2+1,2),1,2,c2*dt)+dFxdy1
(r2(i2,0),r2(i2-1,0),r2(i2,1),r2(i2-1,1),r2(i2,2),
r2(i2-1,2),1,2,c2*dt)+dFxdy1(r2(i2,0),r2(i2-f,0),
r2(i2,1),r2(i2-f,1),r2(i2,2),r2(i2-f,2),1,2,c2*
dt)+dFxdy1(r2(i2,0),r2(i2+f,0),r2(i2,1),r2(i2+f
,1),r2(i2,2),r2(i2+f,2),1,2,c2*dt);

```

```

J(i2+i*N,i2+2*N+1)=-dFxdy1(r2(i2,0),r2(i2+1,0),r2(i2
,1),r2(i2+1,1),r2(i2,2),r2(i2+1,2),1,2,c2*dt);
J(i2+i*N,i2+2*N-1)=-dFxdy1(r2(i2,0),r2(i2-1,0),r2(i2
,1),r2(i2-1,1),r2(i2,2),r2(i2-1,2),1,2,c2*dt);
J(i2+i*N,i2+2*N+f)=-dFxdy1(r2(i2,0),r2(i2+f,0),r2(i2
,1),r2(i2+f,1),r2(i2,2),r2(i2+f,2),1,2,c2*dt);
J(i2+i*N,i2+2*N-f)=-dFxdy1(r2(i2,0),r2(i2-f,0),r2(i2
,1),r2(i2-f,1),r2(i2,2),r2(i2-f,2),1,2,c2*dt);
}
else if(i==2){
//z direction
J(i2+i*N,i2)=dFxdy1(r2(i2,0),r2(i2+1,0),r2(i2,1),r2(
i2+1,1),r2(i2,2),r2(i2+1,2),2,0,c2*dt)+dFxdy1(r2(
i2,0),r2(i2-1,0),r2(i2,1),r2(i2-1,1),r2(i2,2),r2(
i2-1,2),2,0,c2*dt)+dFxdy1(r2(i2,0),r2(i2-f,0),r2(
i2,1),r2(i2-f,1),r2(i2,2),r2(i2-f,2),2,0,c2*dt)+
dFxdy1(r2(i2,0),r2(i2+f,0),r2(i2,1),r2(i2+f,1),r2
(i2,2),r2(i2+f,2),2,0,c2*dt);
J(i2+i*N,i2+1)=-dFxdy1(r2(i2,0),r2(i2+1,0),r2(i2,1),
r2(i2+1,1),r2(i2,2),r2(i2+1,2),2,0,c2*dt);
J(i2+i*N,i2-1)=-dFxdy1(r2(i2,0),r2(i2-1,0),r2(i2,1),
r2(i2-1,1),r2(i2,2),r2(i2-1,2),2,0,c2*dt);
J(i2+i*N,i2+f)=-dFxdy1(r2(i2,0),r2(i2+f,0),r2(i2,1),
r2(i2+f,1),r2(i2,2),r2(i2+f,2),2,0,c2*dt);
J(i2+i*N,i2-f)=-dFxdy1(r2(i2,0),r2(i2-f,0),r2(i2,1),
r2(i2-f,1),r2(i2,2),r2(i2-f,2),2,0,c2*dt);
J(i2+i*N,i2+N)=dFxdy1(r2(i2,0),r2(i2+1,0),r2(i2,1),
r2(i2+1,1),r2(i2,2),r2(i2+1,2),1,2,c2*dt)+dFxdy1(
r2(i2,0),r2(i2-1,0),r2(i2,1),r2(i2-1,1),r2(i2,2),
r2(i2-1,2),1,2,c2*dt)+dFxdy1(r2(i2,0),r2(i2-f,0),
r2(i2,1),r2(i2-f,1),r2(i2,2),r2(i2-f,2),1,2,c2*dt
)+dFxdy1(r2(i2,0),r2(i2+f,0),r2(i2,1),r2(i2+f,1),
r2(i2,2),r2(i2+f,2),1,2,c2*dt);
J(i2+i*N,i2+N+1)=-dFxdy1(r2(i2,0),r2(i2+1,0),r2(i2
,1),r2(i2+1,1),r2(i2,2),r2(i2+1,2),1,2,c2*dt);
J(i2+i*N,i2+N-1)=-dFxdy1(r2(i2,0),r2(i2-1,0),r2(i2
,1),r2(i2-1,1),r2(i2,2),r2(i2-1,2),1,2,c2*dt);
J(i2+i*N,i2+N+f)=-dFxdy1(r2(i2,0),r2(i2+f,0),r2(i2
,1),r2(i2+f,1),r2(i2,2),r2(i2+f,2),1,2,c2*dt);
J(i2+i*N,i2+N-f)=-dFxdy1(r2(i2,0),r2(i2-f,0),r2(i2
,1),r2(i2-f,1),r2(i2,2),r2(i2-f,2),1,2,c2*dt);
}
}
else{
if(i2%(f-1)==0){
for(int i3=0;i3<(f-1);i3++){
int j2=i3+count_a;
if(i3==0){

```

```

res(j2+i*N)=Fb(r2(j2,0),r2(j2+1,0),r2(j2,1),r2(
    j2+1,1),r2(j2,2),r2(j2+1,2),i,c2*dt)+r(j2,i)-
    r2(j2,i)+Fr(j2+i*N);
J(j2+i*N,j2+i*N)=dFb_dx(r2(j2,0),r2(j2+1,0),r2(
    j2,1),r2(j2+1,1),r2(j2,2),r2(j2+1,2),i,c2*dt)
    -1;
J(j2+i*N,j2+i*N+1)=-dFb_dx(r2(j2,0),r2(j2+1,0),
    r2(j2,1),r2(j2+1,1),r2(j2,2),r2(j2+1,2),i,c2*
    dt);
if(i==0){
    //x direction
    J(j2+i*N,j2+N)=dFxdy1(r2(j2,0),r2(j2+1,0),r2(
        j2,1),r2(j2+1,1),r2(j2,2),r2(j2+1,2),0,1,c2
        *dt);
    J(j2+i*N,j2+N+1)=-dFxdy1(r2(j2,0),r2(j2+1,0),
        r2(j2,1),r2(j2+1,1),r2(j2,2),r2(j2+1,2)
        ,0,1,c2*dt);
    J(j2+i*N,j2+2*N)=dFxdy1(r2(j2,0),r2(j2+1,0),r2
        (j2,1),r2(j2+1,1),r2(j2,2),r2(j2+1,2),0,2,
        c2*dt);
    J(j2+i*N,j2+2*N+1)=-dFxdy1(r2(j2,0),r2(j2+1,0)
        ,r2(j2,1),r2(j2+1,1),r2(j2,2),r2(j2+1,2)
        ,0,2,c2*dt);
}
else if(i==1){
    //y direction
    J(j2+i*N,j2)=dFxdy1(r2(j2,0),r2(j2+1,0),r2(j2
        ,1),r2(j2+1,1),r2(j2,2),r2(j2+1,2),1,0,c2*
        dt);
    J(j2+i*N,j2+1)=-dFxdy1(r2(j2,0),r2(j2+1,0),r2(
        j2,1),r2(j2+1,1),r2(j2,2),r2(j2+1,2),1,0,c2
        *dt);
    J(j2+i*N,j2+2*N)=dFxdy1(r2(j2,0),r2(j2+1,0),r2
        (j2,1),r2(j2+1,1),r2(j2,2),r2(j2+1,2),1,2,
        c2*dt);
    J(j2+i*N,j2+2*N+1)=-dFxdy1(r2(j2,0),r2(j2+1,0)
        ,r2(j2,1),r2(j2+1,1),r2(j2,2),r2(j2+1,2)
        ,1,2,c2*dt);
}
else if(i==2){
    //z direction
    J(j2+i*N,j2)=dFxdy1(r2(j2,0),r2(j2+1,0),r2(j2
        ,1),r2(j2+1,1),r2(j2,2),r2(j2+1,2),2,0,c2*
        dt);
    J(j2+i*N,j2+1)=-dFxdy1(r2(j2,0),r2(j2+1,0),r2(
        j2,1),r2(j2+1,1),r2(j2,2),r2(j2+1,2),2,0,c2
        *dt);

```

```

        J(j2+i*N, j2+N)=dFxdy1(r2(j2,0), r2(j2+1,0), r2(
            j2,1), r2(j2+1,1), r2(j2,2), r2(j2+1,2), 2,1, c2
            *dt);
        J(j2+i*N, j2+N+1)=-dFxdy1(r2(j2,0), r2(j2+1,0),
            r2(j2,1), r2(j2+1,1), r2(j2,2), r2(j2+1,2)
            , 2,1, c2*dt);
    }
}
else if(i3==(f-2)){
    res(j2+i*N)=Fb(r2(j2,0), r2(mid_point,0), r2(j2,1)
        , r2(mid_point,1), r2(j2,2), r2(mid_point,2), i,
        c2*dt)+Fb(r2(j2,0), r2(j2-1,0), r2(j2,1), r2(j2
        -1,1), r2(j2,2), r2(j2-1,2), i, c2*dt)+r(j2,i)-r2
        (j2,i)+Fr(j2+i*N);
    J(j2+i*N, j2+i*N)=dFb_dx(r2(j2,0), r2(mid_point,0)
        , r2(j2,1), r2(mid_point,1), r2(j2,2), r2(
        mid_point,2), i, c2*dt)+dFb_dx(r2(j2,0), r2(j2
        -1,0), r2(j2,1), r2(j2-1,1), r2(j2,2), r2(j2-1,2)
        , i, c2*dt)-1;
    J(j2+i*N, j2+i*N-1)=-dFb_dx(r2(j2,0), r2(j2-1,0),
        r2(j2,1), r2(j2-1,1), r2(j2,2), r2(j2-1,2), i, c2*
        dt);
    J(j2+i*N, mid_point+i*N)=-dFb_dx(r2(j2,0), r2(
        mid_point,0), r2(j2,1), r2(mid_point,1), r2(j2
        ,2), r2(mid_point,2), i, c2*dt);
    if(i==0){
        //x direction
        J(j2+i*N, j2+N)=dFxdy1(r2(j2,0), r2(mid_point,0)
            , r2(j2,1), r2(mid_point,1), r2(j2,2), r2(
            mid_point,2), 0,1, c2*dt)+dFxdy1(r2(j2,0), r2(
            j2-1,0), r2(j2,1), r2(j2-1,1), r2(j2,2), r2(j2
            -1,2), 0,1, c2*dt);
        J(j2+i*N, j2+N-1)=-dFxdy1(r2(j2,0), r2(j2-1,0),
            r2(j2,1), r2(j2-1,1), r2(j2,2), r2(j2-1,2)
            , 0,1, c2*dt);
        J(j2+i*N, mid_point+N)=-dFxdy1(r2(j2,0), r2(
            mid_point,0), r2(j2,1), r2(mid_point,1), r2(j2
            ,2), r2(mid_point,2), 0,1, c2*dt);
        J(j2+i*N, j2+2*N)=dFxdy1(r2(j2,0), r2(mid_point
            ,0), r2(j2,1), r2(mid_point,1), r2(j2,2), r2(
            mid_point,2), 0,2, c2*dt)+dFxdy1(r2(j2,0), r2(
            j2-1,0), r2(j2,1), r2(j2-1,1), r2(j2,2), r2(j2
            -1,2), 0,2, c2*dt);
        J(j2+i*N, j2+2*N-1)=-dFxdy1(r2(j2,0), r2(j2-1,0)
            , r2(j2,1), r2(j2-1,1), r2(j2,2), r2(j2-1,2)
            , 0,2, c2*dt);
        J(j2+i*N, mid_point+2*N)=-dFxdy1(r2(j2,0), r2(
            mid_point,0), r2(j2,1), r2(mid_point,1), r2(j2

```

```

        ,2),r2(mid_point ,2) ,0,2,c2*dt);
}
else if(i==1){
    //y direction
    J(j2+i*N,j2)=dFxdy1(r2(j2,0),r2(mid_point ,0) ,
        r2(j2,1),r2(mid_point ,1),r2(j2,2),r2(
            mid_point ,2) ,0,1,c2*dt)+dFxdy1(r2(j2,0),r2(
                j2-1,0),r2(j2,1),r2(j2-1,1),r2(j2,2),r2(j2
                    -1,2) ,0,1,c2*dt);
    J(j2+i*N,j2-1)=-dFxdy1(r2(j2,0),r2(j2-1,0),r2(
        j2,1),r2(j2-1,1),r2(j2,2),r2(j2-1,2) ,0,1,c2
            *dt);
    J(j2+i*N,mid_point)=-dFxdy1(r2(j2,0),r2(
        mid_point ,0),r2(j2,1),r2(mid_point ,1),r2(j2
            ,2),r2(mid_point ,2) ,0,1,c2*dt);
    J(j2+i*N,j2+2*N)=dFxdy1(r2(j2,0),r2(mid_point
        ,0),r2(j2,1),r2(mid_point ,1),r2(j2,2),r2(
            mid_point ,2) ,1,2,c2*dt)+dFxdy1(r2(j2,0),r2(
                j2-1,0),r2(j2,1),r2(j2-1,1),r2(j2,2),r2(j2
                    -1,2) ,1,2,c2*dt);
    J(j2+i*N,j2+2*N-1)=-dFxdy1(r2(j2,0),r2(j2-1,0)
        ,r2(j2,1),r2(j2-1,1),r2(j2,2),r2(j2-1,2)
            ,1,2,c2*dt);
    J(j2+i*N,mid_point+2*N)=-dFxdy1(r2(j2,0),r2(
        mid_point ,0),r2(j2,1),r2(mid_point ,1),r2(j2
            ,2),r2(mid_point ,2) ,1,2,c2*dt);
}
else if(i==2){
    //z direction
    J(j2+i*N,j2)=dFxdy1(r2(j2,0),r2(mid_point ,0) ,
        r2(j2,1),r2(mid_point ,1),r2(j2,2),r2(
            mid_point ,2) ,0,2,c2*dt)+dFxdy1(r2(j2,0),r2(
                j2-1,0),r2(j2,1),r2(j2-1,1),r2(j2,2),r2(j2
                    -1,2) ,0,2,c2*dt);
    J(j2+i*N,j2-1)=-dFxdy1(r2(j2,0),r2(j2-1,0),r2(
        j2,1),r2(j2-1,1),r2(j2,2),r2(j2-1,2) ,0,2,c2
            *dt);
    J(j2+i*N,mid_point)=-dFxdy1(r2(j2,0),r2(
        mid_point ,0),r2(j2,1),r2(mid_point ,1),r2(j2
            ,2),r2(mid_point ,2) ,0,2,c2*dt);
    J(j2+i*N,j2+N)=dFxdy1(r2(j2,0),r2(mid_point ,0)
        ,r2(j2,1),r2(mid_point ,1),r2(j2,2),r2(
            mid_point ,2) ,1,2,c2*dt)+dFxdy1(r2(j2,0),r2(
                j2-1,0),r2(j2,1),r2(j2-1,1),r2(j2,2),r2(j2
                    -1,2) ,1,2,c2*dt);
    J(j2+i*N,j2+N-1)=-dFxdy1(r2(j2,0),r2(j2-1,0) ,
        r2(j2,1),r2(j2-1,1),r2(j2,2),r2(j2-1,2)

```

```

        ,1,2,c2*dt);
    J(j2+i*N,mid_point+N)=-dFxdy1(r2(j2,0),r2(
        mid_point,0),r2(j2,1),r2(mid_point,1),r2(j2
        ,2),r2(mid_point,2),1,2,c2*dt);
    }
}
else{
    res(j2+i*N)=Fb(r2(j2,0),r2(j2+1,0),r2(j2,1),r2(
        j2+1,1),r2(j2,2),r2(j2+1,2),i,c2*dt)+Fb(r2(j2
        ,0),r2(j2-1,0),r2(j2,1),r2(j2-1,1),r2(j2,2),
        r2(j2-1,2),i,c2*dt)+r(j2,i)-r2(j2,i)+Fr(j2+i*
        N);
    J(j2+i*N,j2+i*N)=dFb_dx(r2(j2,0),r2(j2+1,0),r2(
        j2,1),r2(j2+1,1),r2(j2,2),r2(j2+1,2),i,c2*dt)
        +dFb_dx(r2(j2,0),r2(j2-1,0),r2(j2,1),r2(j2
        -1,1),r2(j2,2),r2(j2-1,2),i,c2*dt)-1;
    J(j2+i*N,j2+i*N-1)=-dFb_dx(r2(j2,0),r2(j2-1,0),
        r2(j2,1),r2(j2-1,1),r2(j2,2),r2(j2-1,2),i,c2*
        dt);
    J(j2+i*N,j2+i*N+1)=-dFb_dx(r2(j2,0),r2(j2+1,0),
        r2(j2,1),r2(j2+1,1),r2(j2,2),r2(j2+1,2),i,c2*
        dt);
    if(i==0){
        //x direction
        J(j2+i*N,j2+N)=dFxdy1(r2(j2,0),r2(j2+1,0),r2(
            j2,1),r2(j2+1,1),r2(j2,2),r2(j2+1,2),0,1,c2
            *dt)+dFxdy1(r2(j2,0),r2(j2-1,0),r2(j2,1),r2
            (j2-1,1),r2(j2,2),r2(j2-1,2),0,1,c2*dt);
        J(j2+i*N,j2+N+1)=-dFxdy1(r2(j2,0),r2(j2+1,0),
            r2(j2,1),r2(j2+1,1),r2(j2,2),r2(j2+1,2)
            ,0,1,c2*dt);
        J(j2+i*N,j2+N-1)=-dFxdy1(r2(j2,0),r2(j2-1,0),
            r2(j2,1),r2(j2-1,1),r2(j2,2),r2(j2-1,2)
            ,0,1,c2*dt);
        J(j2+i*N,j2+2*N)=dFxdy1(r2(j2,0),r2(j2+1,0),r2
            (j2,1),r2(j2+1,1),r2(j2,2),r2(j2+1,2),0,2,
            c2*dt)+dFxdy1(r2(j2,0),r2(j2-1,0),r2(j2,1),
            r2(j2-1,1),r2(j2,2),r2(j2-1,2),0,2,c2*dt);
        J(j2+i*N,j2+2*N+1)=-dFxdy1(r2(j2,0),r2(j2+1,0)
            ,r2(j2,1),r2(j2+1,1),r2(j2,2),r2(j2+1,2)
            ,0,2,c2*dt);
        J(j2+i*N,j2+2*N-1)=-dFxdy1(r2(j2,0),r2(j2-1,0)
            ,r2(j2,1),r2(j2-1,1),r2(j2,2),r2(j2-1,2)
            ,0,2,c2*dt);
    }
    else if(i==1){
        //y direction

```

```

J(j2+i*N, j2)=dFxdy1(r2(j2,0),r2(j2+1,0),r2(j2
,1),r2(j2+1,1),r2(j2,2),r2(j2+1,2),0,1,c2*
dt)+dFxdy1(r2(j2,0),r2(j2-1,0),r2(j2,1),r2(
j2-1,1),r2(j2,2),r2(j2-1,2),0,1,c2*dt);
J(j2+i*N, j2+1)=-dFxdy1(r2(j2,0),r2(j2+1,0),r2(
j2,1),r2(j2+1,1),r2(j2,2),r2(j2+1,2),0,1,c2
*dt);
J(j2+i*N, j2-1)=-dFxdy1(r2(j2,0),r2(j2-1,0),r2(
j2,1),r2(j2-1,1),r2(j2,2),r2(j2-1,2),0,1,c2
*dt);
J(j2+i*N, j2+2*N)=dFxdy1(r2(j2,0),r2(j2+1,0),r2
(j2,1),r2(j2+1,1),r2(j2,2),r2(j2+1,2),1,2,
c2*dt)+dFxdy1(r2(j2,0),r2(j2-1,0),r2(j2,1),
r2(j2-1,1),r2(j2,2),r2(j2-1,2),1,2,c2*dt);
J(j2+i*N, j2+2*N+1)=-dFxdy1(r2(j2,0),r2(j2+1,0)
,r2(j2,1),r2(j2+1,1),r2(j2,2),r2(j2+1,2)
,1,2,c2*dt);
J(j2+i*N, j2+2*N-1)=-dFxdy1(r2(j2,0),r2(j2-1,0)
,r2(j2,1),r2(j2-1,1),r2(j2,2),r2(j2-1,2)
,1,2,c2*dt);
}
else if(i==2){
//z direction
J(j2+i*N, j2)=dFxdy1(r2(j2,0),r2(j2+1,0),r2(j2
,1),r2(j2+1,1),r2(j2,2),r2(j2+1,2),0,2,c2*
dt)+dFxdy1(r2(j2,0),r2(j2-1,0),r2(j2,1),r2(
j2-1,1),r2(j2,2),r2(j2-1,2),0,2,c2*dt);
J(j2+i*N, j2+1)=-dFxdy1(r2(j2,0),r2(j2+1,0),r2(
j2,1),r2(j2+1,1),r2(j2,2),r2(j2+1,2),0,2,c2
*dt);
J(j2+i*N, j2-1)=-dFxdy1(r2(j2,0),r2(j2-1,0),r2(
j2,1),r2(j2-1,1),r2(j2,2),r2(j2-1,2),0,2,c2
*dt);
J(j2+i*N, j2+N)=dFxdy1(r2(j2,0),r2(j2+1,0),r2(
j2,1),r2(j2+1,1),r2(j2,2),r2(j2+1,2),1,2,c2
*dt)+dFxdy1(r2(j2,0),r2(j2-1,0),r2(j2,1),r2
(j2-1,1),r2(j2,2),r2(j2-1,2),1,2,c2*dt);
J(j2+i*N, j2+N+1)=-dFxdy1(r2(j2,0),r2(j2+1,0),
r2(j2,1),r2(j2+1,1),r2(j2,2),r2(j2+1,2)
,1,2,c2*dt);
J(j2+i*N, j2+N-1)=-dFxdy1(r2(j2,0),r2(j2-1,0),
r2(j2,1),r2(j2-1,1),r2(j2,2),r2(j2-1,2)
,1,2,c2*dt);
}
}
count_a=count_a+f-1;
}

```

```

    }
}
int a11=mid_point+1;
count_a=0;
for(int i2=0;i2<mid_point;i2++){
    int i3=i2+a11;
    if((i3-1)%(f-1)==0){
        for(int j=0;j<f-1;j++){
            int j2=j+a11+count_a;
            if(j==0){
                res(j2+i*N)=Fb(r2(j2,0),r2(j2+1,0),r2(j2,1),r2(j2
                    +1,1),r2(j2,2),r2(j2+1,2),i,c2*dt)+Fb(r2(j2,0),
                    r2(mid_point,0),r2(j2,1),r2(mid_point,1),r2(j2
                    ,2),r2(mid_point,2),i,c2*dt)+r(j2,i)-r2(j2,i)+
                    Fr(j2+i*N);
                J(j2+i*N,j2+i*N)=dFb_dx(r2(j2,0),r2(j2+1,0),r2(j2
                    ,1),r2(j2+1,1),r2(j2,2),r2(j2+1,2),i,c2*dt)+
                    dFb_dx(r2(j2,0),r2(mid_point,0),r2(j2,1),r2(
                    mid_point,1),r2(j2,2),r2(mid_point,2),i,c2*dt)
                    -1;
                J(j2+i*N,j2+i*N+1)=-dFb_dx(r2(j2,0),r2(j2+1,0),r2(
                    j2,1),r2(j2+1,1),r2(j2,2),r2(j2+1,2),i,c2*dt);
                J(j2+i*N,i*N+mid_point)=-dFb_dx(r2(j2,0),r2(
                    mid_point,0),r2(j2,1),r2(mid_point,1),r2(j2,2),
                    r2(mid_point,2),i,c2*dt);
            if(i==0){
                //x direction
                J(j2+i*N,j2+N)=dFxdy1(r2(j2,0),r2(j2+1,0),r2(j2
                    ,1),r2(j2+1,1),r2(j2,2),r2(j2+1,2),0,1,c2*dt)
                    +dFxdy1(r2(j2,0),r2(mid_point,0),r2(j2,1),r2(
                    mid_point,1),r2(j2,2),r2(mid_point,2),0,1,c2*
                    dt);
                J(j2+i*N,j2+N+1)=-dFxdy1(r2(j2,0),r2(j2+1,0),r2(
                    j2,1),r2(j2+1,1),r2(j2,2),r2(j2+1,2),0,1,c2*
                    dt);
                J(j2+i*N,N+mid_point)=-dFxdy1(r2(j2,0),r2(
                    mid_point,0),r2(j2,1),r2(mid_point,1),r2(j2
                    ,2),r2(mid_point,2),0,1,c2*dt);
                J(j2+i*N,j2+2*N)=dFxdy1(r2(j2,0),r2(j2+1,0),r2(
                    j2,1),r2(j2+1,1),r2(j2,2),r2(j2+1,2),0,2,c2*
                    dt)+dFxdy1(r2(j2,0),r2(mid_point,0),r2(j2,1),
                    r2(mid_point,1),r2(j2,2),r2(mid_point,2),0,2,
                    c2*dt);
                J(j2+i*N,j2+2*N+1)=-dFxdy1(r2(j2,0),r2(j2+1,0),
                    r2(j2,1),r2(j2+1,1),r2(j2,2),r2(j2+1,2),0,2,
                    c2*dt);
                J(j2+i*N,2*N+mid_point)=-dFxdy1(r2(j2,0),r2(
                    mid_point,0),r2(j2,1),r2(mid_point,1),r2(j2

```

```

        ,2),r2(mid_point,2),0,2,c2*dt);
}
else if(i==1){
    //y direction
    J(j2+i*N,j2)=dFxdy1(r2(j2,0),r2(j2+1,0),r2(j2,1)
        ,r2(j2+1,1),r2(j2,2),r2(j2+1,2),0,1,c2*dt)+
        dFxdy1(r2(j2,0),r2(mid_point,0),r2(j2,1),r2(
            mid_point,1),r2(j2,2),r2(mid_point,2),0,1,c2*
            dt);
    J(j2+i*N,j2+1)=-dFxdy1(r2(j2,0),r2(j2+1,0),r2(j2
        ,1),r2(j2+1,1),r2(j2,2),r2(j2+1,2),0,1,c2*dt)
        ;
    J(j2+i*N,mid_point)=-dFxdy1(r2(j2,0),r2(
        mid_point,0),r2(j2,1),r2(mid_point,1),r2(j2
        ,2),r2(mid_point,2),0,1,c2*dt);
    J(j2+i*N,j2+2*N)=dFxdy1(r2(j2,0),r2(j2+1,0),r2(
        j2,1),r2(j2+1,1),r2(j2,2),r2(j2+1,2),1,2,c2*
        dt)+dFxdy1(r2(j2,0),r2(mid_point,0),r2(j2,1),
        r2(mid_point,1),r2(j2,2),r2(mid_point,2),1,2,
        c2*dt);
    J(j2+i*N,j2+2*N+1)=-dFxdy1(r2(j2,0),r2(j2+1,0),
        r2(j2,1),r2(j2+1,1),r2(j2,2),r2(j2+1,2),1,2,
        c2*dt);
    J(j2+i*N,2*N+mid_point)=-dFxdy1(r2(j2,0),r2(
        mid_point,0),r2(j2,1),r2(mid_point,1),r2(j2
        ,2),r2(mid_point,2),1,2,c2*dt);
}
else if(i==2){
    //z direction
    J(j2+i*N,j2)=dFxdy1(r2(j2,0),r2(j2+1,0),r2(j2,1)
        ,r2(j2+1,1),r2(j2,2),r2(j2+1,2),0,2,c2*dt)+
        dFxdy1(r2(j2,0),r2(mid_point,0),r2(j2,1),r2(
            mid_point,1),r2(j2,2),r2(mid_point,2),0,2,c2*
            dt);
    J(j2+i*N,j2+1)=-dFxdy1(r2(j2,0),r2(j2+1,0),r2(j2
        ,1),r2(j2+1,1),r2(j2,2),r2(j2+1,2),0,2,c2*dt)
        ;
    J(j2+i*N,mid_point)=-dFxdy1(r2(j2,0),r2(
        mid_point,0),r2(j2,1),r2(mid_point,1),r2(j2
        ,2),r2(mid_point,2),0,2,c2*dt);
    J(j2+i*N,j2+N)=dFxdy1(r2(j2,0),r2(j2+1,0),r2(j2
        ,1),r2(j2+1,1),r2(j2,2),r2(j2+1,2),1,2,c2*dt)
        +dFxdy1(r2(j2,0),r2(mid_point,0),r2(j2,1),r2(
            mid_point,1),r2(j2,2),r2(mid_point,2),1,2,c2*
            dt);
    J(j2+i*N,j2+N+1)=-dFxdy1(r2(j2,0),r2(j2+1,0),r2(
        j2,1),r2(j2+1,1),r2(j2,2),r2(j2+1,2),1,2,c2*
        dt);
}

```

```

        J(j2+i*N,N+mid_point)=-dFxdy1(r2(j2,0),r2(
            mid_point,0),r2(j2,1),r2(mid_point,1),r2(j2
            ,2),r2(mid_point,2),1,2,c2*dt);
    }
}
else if(j==f-2){
    res(j2+i*N)=Fb(r2(j2,0),r2(j2-1,0),r2(j2,1),r2(j2
        -1,1),r2(j2,2),r2(j2-1,2),i,c2*dt)+r(j2,i)-r2(
        j2,i)+Fr(j2+i*N);
    J(j2+i*N,j2+i*N)=dFb_dx(r2(j2,0),r2(j2-1,0),r2(j2
        ,1),r2(j2-1,1),r2(j2,2),r2(j2-1,2),i,c2*dt)-1;
    J(j2+i*N,j2+i*N-1)=-dFb_dx(r2(j2,0),r2(j2-1,0),r2(
        j2,1),r2(j2-1,1),r2(j2,2),r2(j2-1,2),i,c2*dt);
    if(i==0){
        //x direction
        J(j2+i*N,j2+N)=dFxdy1(r2(j2,0),r2(j2-1,0),r2(j2
            ,1),r2(j2-1,1),r2(j2,2),r2(j2-1,2),0,1,c2*dt)
            ;
        J(j2+i*N,j2+N-1)=-dFxdy1(r2(j2,0),r2(j2-1,0),r2(
            j2,1),r2(j2-1,1),r2(j2,2),r2(j2-1,2),0,1,c2*
            dt);
        J(j2+i*N,j2+2*N)=dFxdy1(r2(j2,0),r2(j2-1,0),r2(
            j2,1),r2(j2-1,1),r2(j2,2),r2(j2-1,2),0,2,c2*
            dt);
        J(j2+i*N,j2+2*N-1)=-dFxdy1(r2(j2,0),r2(j2-1,0),
            r2(j2,1),r2(j2-1,1),r2(j2,2),r2(j2-1,2),0,2,
            c2*dt);
    }
    else if(i==1){
        //y direction
        J(j2+i*N,j2)=dFxdy1(r2(j2,0),r2(j2-1,0),r2(j2,1)
            ,r2(j2-1,1),r2(j2,2),r2(j2-1,2),0,1,c2*dt);
        J(j2+i*N,j2-1)=-dFxdy1(r2(j2,0),r2(j2-1,0),r2(j2
            ,1),r2(j2-1,1),r2(j2,2),r2(j2-1,2),0,1,c2*dt)
            ;
        J(j2+i*N,j2+2*N)=dFxdy1(r2(j2,0),r2(j2-1,0),r2(
            j2,1),r2(j2-1,1),r2(j2,2),r2(j2-1,2),1,2,c2*
            dt);
        J(j2+i*N,j2+2*N-1)=-dFxdy1(r2(j2,0),r2(j2-1,0),
            r2(j2,1),r2(j2-1,1),r2(j2,2),r2(j2-1,2),1,2,
            c2*dt);
    }
    else if(i==2){
        //z direction
        J(j2+i*N,j2)=dFxdy1(r2(j2,0),r2(j2-1,0),r2(j2,1)
            ,r2(j2-1,1),r2(j2,2),r2(j2-1,2),0,2,c2*dt);
        J(j2+i*N,j2-1)=-dFxdy1(r2(j2,0),r2(j2-1,0),r2(j2
            ,1),r2(j2-1,1),r2(j2,2),r2(j2-1,2),0,2,c2*dt)

```

```

        ;
        J(j2+i*N,j2+N)=dFxdy1(r2(j2,0),r2(j2-1,0),r2(j2
            ,1),r2(j2-1,1),r2(j2,2),r2(j2-1,2),1,2,c2*dt)
        ;
        J(j2+i*N,j2+N-1)=-dFxdy1(r2(j2,0),r2(j2-1,0),r2(
            j2,1),r2(j2-1,1),r2(j2,2),r2(j2-1,2),1,2,c2*
            dt);
    }
}
else{
    res(j2+i*N)=Fb(r2(j2,0),r2(j2-1,0),r2(j2,1),r2(j2
        -1,1),r2(j2,2),r2(j2-1,2),i,c2*dt)+Fb(r2(j2,0),
        r2(j2+1,0),r2(j2,1),r2(j2+1,1),r2(j2,2),r2(j2
        +1,2),i,c2*dt)+r(j2,i)-r2(j2,i)+Fr(j2+i*N);
    J(j2+i*N,j2+i*N)=dFb_dx(r2(j2,0),r2(j2-1,0),r2(j2
        ,1),r2(j2-1,1),r2(j2,2),r2(j2-1,2),i,c2*dt)+
        dFb_dx(r2(j2,0),r2(j2+1,0),r2(j2,1),r2(j2+1,1),
        r2(j2,2),r2(j2+1,2),i,c2*dt)-1;
    J(j2+i*N,j2+i*N-1)=-dFb_dx(r2(j2,0),r2(j2-1,0),r2(
        j2,1),r2(j2-1,1),r2(j2,2),r2(j2-1,2),i,c2*dt);
    J(j2+i*N,j2+i*N+1)=-dFb_dx(r2(j2,0),r2(j2+1,0),r2(
        j2,1),r2(j2+1,1),r2(j2,2),r2(j2+1,2),i,c2*dt);
    if(i==0){
        //x direction
        J(j2+i*N,j2+N)=dFxdy1(r2(j2,0),r2(j2-1,0),r2(j2
            ,1),r2(j2-1,1),r2(j2,2),r2(j2-1,2),0,1,c2*dt)
            +dFxdy1(r2(j2,0),r2(j2+1,0),r2(j2,1),r2(j2
            +1,1),r2(j2,2),r2(j2+1,2),0,1,c2*dt);
        J(j2+i*N,j2+N-1)=-dFxdy1(r2(j2,0),r2(j2-1,0),r2(
            j2,1),r2(j2-1,1),r2(j2,2),r2(j2-1,2),0,1,c2*
            dt);
        J(j2+i*N,j2+N+1)=-dFxdy1(r2(j2,0),r2(j2+1,0),r2(
            j2,1),r2(j2+1,1),r2(j2,2),r2(j2+1,2),0,1,c2*
            dt);
        J(j2+i*N,j2+2*N)=dFxdy1(r2(j2,0),r2(j2-1,0),r2(
            j2,1),r2(j2-1,1),r2(j2,2),r2(j2-1,2),1,2,c2*
            dt)+dFxdy1(r2(j2,0),r2(j2+1,0),r2(j2,1),r2(j2
            +1,1),r2(j2,2),r2(j2+1,2),1,2,c2*dt);
        J(j2+i*N,j2+2*N-1)=-dFxdy1(r2(j2,0),r2(j2-1,0),
            r2(j2,1),r2(j2-1,1),r2(j2,2),r2(j2-1,2),1,2,
            c2*dt);
        J(j2+i*N,j2+2*N+1)=-dFxdy1(r2(j2,0),r2(j2+1,0),
            r2(j2,1),r2(j2+1,1),r2(j2,2),r2(j2+1,2),1,2,
            c2*dt);
    }
}
else if(i==1){
    //y direction

```

```

J(j2+i*N, j2)=dFxdy1(r2(j2,0),r2(j2-1,0),r2(j2,1)
,r2(j2-1,1),r2(j2,2),r2(j2-1,2),0,1,c2*dt)+
dFxdy1(r2(j2,0),r2(j2+1,0),r2(j2,1),r2(j2
+1,1),r2(j2,2),r2(j2+1,2),0,1,c2*dt);
J(j2+i*N, j2-1)=-dFxdy1(r2(j2,0),r2(j2-1,0),r2(j2
,1),r2(j2-1,1),r2(j2,2),r2(j2-1,2),0,1,c2*dt)
;
J(j2+i*N, j2+1)=-dFxdy1(r2(j2,0),r2(j2+1,0),r2(j2
,1),r2(j2+1,1),r2(j2,2),r2(j2+1,2),0,1,c2*dt)
;
J(j2+i*N, j2+2*N)=dFxdy1(r2(j2,0),r2(j2-1,0),r2(
j2,1),r2(j2-1,1),r2(j2,2),r2(j2-1,2),0,2,c2*
dt)+dFxdy1(r2(j2,0),r2(j2+1,0),r2(j2,1),r2(j2
+1,1),r2(j2,2),r2(j2+1,2),0,2,c2*dt);
J(j2+i*N, j2+2*N-1)=-dFxdy1(r2(j2,0),r2(j2-1,0),
r2(j2,1),r2(j2-1,1),r2(j2,2),r2(j2-1,2),0,2,
c2*dt);
J(j2+i*N, j2+2*N+1)=-dFxdy1(r2(j2,0),r2(j2+1,0),
r2(j2,1),r2(j2+1,1),r2(j2,2),r2(j2+1,2),0,2,
c2*dt);
}
else if(i==2){
//z direction
J(j2+i*N, j2)=dFxdy1(r2(j2,0),r2(j2-1,0),r2(j2,1)
,r2(j2-1,1),r2(j2,2),r2(j2-1,2),0,2,c2*dt)+
dFxdy1(r2(j2,0),r2(j2+1,0),r2(j2,1),r2(j2
+1,1),r2(j2,2),r2(j2+1,2),0,2,c2*dt);
J(j2+i*N, j2-1)=-dFxdy1(r2(j2,0),r2(j2-1,0),r2(j2
,1),r2(j2-1,1),r2(j2,2),r2(j2-1,2),0,2,c2*dt)
;
J(j2+i*N, j2+1)=-dFxdy1(r2(j2,0),r2(j2+1,0),r2(j2
,1),r2(j2+1,1),r2(j2,2),r2(j2+1,2),0,2,c2*dt)
;
J(j2+i*N, j2+N)=dFxdy1(r2(j2,0),r2(j2-1,0),r2(j2
,1),r2(j2-1,1),r2(j2,2),r2(j2-1,2),1,2,c2*dt)
+dFxdy1(r2(j2,0),r2(j2+1,0),r2(j2,1),r2(j2
+1,1),r2(j2,2),r2(j2+1,2),1,2,c2*dt);
J(j2+i*N, j2+N-1)=-dFxdy1(r2(j2,0),r2(j2-1,0),r2(
j2,1),r2(j2-1,1),r2(j2,2),r2(j2-1,2),1,2,c2*
dt);
J(j2+i*N, j2+N+1)=-dFxdy1(r2(j2,0),r2(j2+1,0),r2(
j2,1),r2(j2+1,1),r2(j2,2),r2(j2+1,2),1,2,c2*
dt);
}
}
count_a=count_a+(f-1);
}

```

```

    }
}
//delr=TDMA2(J,res);
JT=J.transpose();
product1=JT*res;
JTJ=JT*J;
JTJ=JTJ.inverse();
delr=JTJ*product1;
for(int i=0;i<N;i++){
    r2(i,0)=r2(i,0)-delr(i);
    r2(i,1)=r2(i,1)-delr(i+N);
    r2(i,2)=r2(i,2)-delr(i+2*N);
}
err=0;
for(int i=0;i<3*N;i++){
    err=err+res(i)*res(i)/(3*N);
}
err=pow(err,0.5);
if(count2>1000){
    break;
}
count2=count2+1;
}
//cout << (J(mid_point,mid_point)+1)/(c2*dt) << "\t" << (J(
    mid_point+N,mid_point+N)+1)/(c2*dt) << endl;
r=r2;
if(remainder(it,f_save)==0){
    for(int i=0;i<N;i++){
        x1(i,count)=r(i,0);
        y1(i,count)=r(i,1);
        z1(i,count)=r(i,2);
    }
    err_v(count)=err;
    count_it(count)=count2;
    count=count+1;
    cout << "Saved\ttime\tstep=\t" << count << "; \tErr=" << err << " ";
        \tcount2=" << count2 << endl;
}
}
}
ofstream myfile;
myfile.open("trj_x.dat", ios::binary);
myfile.write((char *) x1.data(), x1.rows() * x1.cols() * sizeof(
    double));
myfile.close();
myfile.open("trj_y.dat", ios::binary);
myfile.write((char *) y1.data(), y1.rows() * y1.cols() * sizeof(
    double));

```

```

myfile.close();
myfile.open("trj_z.dat", ios::binary);
myfile.write((char *) z1.data(), z1.rows() * z1.cols() * sizeof(
    double));
myfile.close();
myfile.open("err.dat", ios::binary);
myfile.write((char *) err_v.data(), err_v.rows() * err_v.cols() *
    sizeof(double));
myfile.close();
myfile.open("count_it.dat", ios::binary);
myfile.write((char *) count_it.data(), count_it.rows() * count_it.
    cols() * sizeof(double));
myfile.close();
high_resolution_clock::time_point t2 = high_resolution_clock::now
    ();
auto duration = duration_cast<seconds>( t2 - t1 ).count();
cout << "run_time=" << duration << "seconds" << endl;
return 0;
}

```

C.8 Proper Orthogonal Decomposition Analysis

```
import scipy.io
import numpy as np
import matplotlib.pyplot as plt
import warnings
warnings.filterwarnings("ignore")
import scipy
import sys

for i2 in range(len(sys.argv)):
    if sys.argv[i2]=="-ns":
        ns=int(sys.argv[i2+1])
    elif sys.argv[i2]=="-nx":
        nx=int(sys.argv[i2+1])
    elif sys.argv[i2]=="-cm":
        cm=int(sys.argv[i2+1])
    else:
        pass

print("y⊥ direction")
u=np.fromfile("y.dat", dtype=float)
#u=data["xt"]
#u=np.transpose(u)
#ns=4000
ms=1
#nx=30
dx1=1
u_mean=np.zeros(ns)
x=np.arange(1,nx+dx1,dx1)
cn=1
us=np.zeros((nx,ns))
for ti in range(ns):
    for j in range(nx):
        us[j][ti]=u[j+(ti*ms)*nx]
#com=np.zeros(ns)
#for i in range(ns):
# for j in range(nx):
#     com[i]=com[i]+us[j][i]/30
for i in range(ns):
    for j in range(nx):
        u_mean[i]=u_mean[i]+(us[j][i])/nx
up=np.zeros((nx,ns))
for i in range(ns):
    for j in range(nx):
        up[j][i]=(us[j][i])-u_mean[i]
```

```

C=np.zeros((nx,nx))
for i in range(nx):
    for j in range(nx):
        if i<j:
            pass
        else:
            inner_p=np.zeros(ns)
            for k in range(ns):
                inner_p[k]=up[i][k]*up[j][k]
            C[i][j]=np.trapz(inner_p,dx=dx1)/ns
            if i==j:
                pass
            else:
                C[j][i]=C[i][j]

lam,v=scipy.linalg.eig(C)
np.savetxt("lamy.txt",lam)
idx = lam.argsort()[::-1]#sort eigenvalues
lam = lam[idx]
v=v[:,idx]#sort eigenvectors
phi=np.zeros((nx,nx))
for i in range(nx):
    for k in range(nx):
        phi[k][i]=v[k][i]#phi[k][i]+up[k][j]*
norm=np.zeros(nx)
inner_p=np.zeros(nx)
for p in range(nx):
    for j in range(nx):
        inner_p[j]=phi[j][p]*phi[j][p]
    norm[p]=np.sqrt(np.trapz(inner_p,dx=dx1))
    for j in range(nx):
        phi[j][p]=phi[j][p]/norm[p]
for p in range(4):
    for j in range(nx):
        inner_p[j]=phi[j][0]*phi[j][p+1]
    print(np.trapz(inner_p,dx=dx1))

for p in range(6):
    plt.figure()
    plt.rc('font', **{'family': 'serif', 'serif': ['ComputerUModern',
        ]})
    plt.rc('text', usetex=True)
    plt.gcf().set_size_inches(4,3,forward=True)
    plt.subplots_adjust(left=0.18,bottom=0.15)
    filename="phi_"+str(p+1)+"y.png"
    for j in range(nx):

```

```

plt.plot(x[j],phi[j][p],'^',markerfacecolor='w',markeredgecolor=
'r',markersize=4)
plt.savefig(filename,dpi=300)
str_emode="phiy"+str(cm)+".mat"
scipy.io.savemat(str_emode,{'phi':phi})

filename2="phiy.txt"
writefile = open(filename2,'w')
for i in range(nx):
    for j in range(nx):
        writefile.write(str(phi[i][j]))
        writefile.write("\t")
        writefile.write("\n")

print("x_direction")
u=np.fromfile("x.dat", dtype=float)
#u=data["xt"]
#u=np.transpose(u)
#ns=4000
ms=1
#nx=30
dx1=1
u_mean=np.zeros(ns)
x=np.arange(1,nx+dx1,dx1)
cn=1
us=np.zeros((nx,ns))
for ti in range(ns):
    for j in range(nx):
        us[j][ti]=u[j+(ti*ms)*nx]
#com=np.zeros(ns)
#for i in range(ns):
# for j in range(nx):
# com[i]=com[i]+us[j][i]/30
for i in range(ns):
    for j in range(nx):
        u_mean[i]=u_mean[i]+(us[j][i])/nx
up=np.zeros((nx,ns))
for i in range(ns):
    for j in range(nx):
        up[j][i]=(us[j][i])-u_mean[i]

C=np.zeros((nx,nx))
for i in range(nx):
    for j in range(nx):
        if i<j:
            pass
        else:
            inner_p=np.zeros(ns)

```

```

    for k in range(ns):
        inner_p[k]=up[i][k]*up[j][k]
    C[i][j]=np.trapz(inner_p,dx=dx1)/ns
    if i==j:
        pass
    else:
        C[j][i]=C[i][j]

lam,v=scipy.linalg.eig(C)
np.savetxt("lamx.txt",lam)
idx = lam.argsort()[::-1]#sort eigenvalues
lam = lam[idx]
v=v[:,idx]#sort eigenvectors
phi=np.zeros((nx,nx))
for i in range(nx):
    for k in range(nx):
        phi[k][i]=v[k][i]#phi[k][i]+up[k][j]*
norm=np.zeros(nx)
inner_p=np.zeros(nx)
for p in range(nx):
    for j in range(nx):
        inner_p[j]=phi[j][p]*phi[j][p]
    norm[p]=np.sqrt(np.trapz(inner_p,dx=dx1))
    for j in range(nx):
        phi[j][p]=phi[j][p]/norm[p]
for p in range(4):
    for j in range(nx):
        inner_p[j]=phi[j][0]*phi[j][p+1]
    print(np.trapz(inner_p,dx=dx1))

for p in range(6):
    plt.figure()
    plt.rc('font', **{'family': 'serif', 'serif': ['ComputerUModern',
    ]})
    plt.rc('text', usetex=True)
    plt.gcf().set_size_inches(4,3,forward=True)
    plt.subplots_adjust(left=0.18,bottom=0.15)
    filename="phi_"+str(p+1)+"x.png"
    for j in range(nx):
        plt.plot(x[j],phi[j][p],'^',markerfacecolor='w',markeredgecolor=
        'r',markersize=4)
    plt.savefig(filename,dpi=300)
str_emode="phix"+str(cm)+".mat"
scipy.io.savemat(str_emode,{'phi':phi})
filename2="phix.txt"
writefile = open(filename2,'w')
for i in range(nx):
    for j in range(nx):

```

```

        writefile.write(str(phi[i][j]))
        writefile.write("\t")
        writefile.write("\n")
print("z-direction")
u=np.fromfile("z.dat", dtype=float)
#u=data["xt"]
#u=np.transpose(u)
#ns=4000
ms=1
#nx=30
dx1=1
u_mean=np.zeros(ns)
x=np.arange(1,nx+dx1,dx1)
cn=1
us=np.zeros((nx,ns))
for ti in range(ns):
    for j in range(nx):
        us[j][ti]=u[j+(ti*ms)*nx]
#com=np.zeros(ns)
#for i in range(ns):
# for j in range(nx):
#     com[i]=com[i]+us[j][i]/30
for i in range(ns):
    for j in range(nx):
        u_mean[i]=u_mean[i]+(us[j][i])/nx
up=np.zeros((nx,ns))
for i in range(ns):
    for j in range(nx):
        up[j][i]=(us[j][i])-u_mean[i]

C=np.zeros((nx,nx))
for i in range(nx):
    for j in range(nx):
        if i<j:
            pass
        else:
            inner_p=np.zeros(ns)
            for k in range(ns):
                inner_p[k]=up[i][k]*up[j][k]
            C[i][j]=np.trapz(inner_p,dx=dx1)/ns
            if i==j:
                pass
            else:
                C[j][i]=C[i][j]

lam,v=scipy.linalg.eig(C)
np.savetxt("lamz.txt",lam)
idx = lam.argsort()[::-1]#sort eigenvalues

```

```

lam = lam[idx]
v=v[:,idx]#sort eigenvectors
phi=np.zeros((nx,nx))
for i in range(nx):
    for k in range(nx):
        phi[k][i]=v[k][i]#phi[k][i]+up[k][j]*
norm=np.zeros(nx)
inner_p=np.zeros(nx)
for p in range(nx):
    for j in range(nx):
        inner_p[j]=phi[j][p]*phi[j][p]
    norm[p]=np.sqrt(np.trapz(inner_p,dx=dx1))
    for j in range(nx):
        phi[j][p]=phi[j][p]/norm[p]
for p in range(4):
    for j in range(nx):
        inner_p[j]=phi[j][0]*phi[j][p+1]
    print(np.trapz(inner_p,dx=dx1))

for p in range(6):
    plt.figure()
    plt.rc('font', **{'family': 'serif', 'serif': ['Computer_Modern',
        ]})
    plt.rc('text', usetex=True)
    plt.gcf().set_size_inches(4,3,forward=True)
    plt.subplots_adjust(left=0.18,bottom=0.15)
    filename="phi_"+str(p+1)+"z.png"
    for j in range(nx):
        plt.plot(x[j],phi[j][p],'^',markerfacecolor='w',markeredgecolor=
            'r',markersize=4)
    plt.savefig(filename,dpi=300)
str_emode="phiz"+str(cm)+".mat"
scipy.io.savemat(str_emode,{'phi':phi})
filename2="phiz.txt"
writefile = open(filename2,'w')
for i in range(nx):
    for j in range(nx):
        writefile.write(str(phi[i][j]))
        writefile.write("\t")
    writefile.write("\n")

```

Appendix D

Supporting Information for Chapter 6

D.1 PRISM Theory Calculation Program

Python 3.6 source code for PRISM theory calculation of a polymer ring with different N at $T = 450$ K.

```
import numpy as np
import matplotlib as mpl
import matplotlib.pyplot as plt
from scipy.optimize import curve_fit
import warnings
warnings.filterwarnings("ignore")
plt.style.use("classic")
from scipy.fftpack import dst
def lj_f(e,sigma,r):
    f=4*e*(-12*(sigma**12/r**10)+6*(sigma**6/r**4))
    return f

def lj_p(r):
    f=4*(1)*((1/(r)**12)-(1/(r)**6))
    return f

def omega(k,N):
    d=1
    sum1=0
    for i in range(N):
        if i==0:
            pass
        else:
            sum1=sum1+(N-i)*np.exp(-k**2*d**2*i*(N-i)/(6*N))
    return 1+(2/N)*sum1
```

```

sigma=1
beta=0.101

dr=0.001
r=np.arange(dr,100,dr)
dk=np.pi/(dr*(len(r)+1))
k=np.linspace(dk,dk*len(r),len(r))
g=np.zeros(len(r))
h=np.zeros(len(r))
y=np.zeros(len(r))
y_o=np.zeros(len(r))
err=10
count=0
alpha=0.2
d=0
c=np.zeros(len(r))
for i in range(len(r)):
    if r[i]<=d:
        pass
    else:
        g[i]=np.exp(-beta*lj_p(r[i]))
        h[i]=g[i]-1
        c[i]=h[i]
coeff_to_fourier=2.0*np.pi*r*dr
coeff_to_real=k*dk/(4*np.pi**2)

hk=np.zeros(len(r))
ck=np.zeros(len(r))
ci=np.zeros(len(r))
wk=np.zeros(len(r))
err=1
count=0
#gk=dst(coeff_to_fourier*g,type=2)/k
#gr=dst(coeff_to_real*gk,type=3)/r
N=input("number of beads: ")
N=int(N)
rho=32.73318525-23.78266866/float(N)
rho=float(rho)*0.395**3
frac=1
while(err>10**(-6)):
    #get direct correlation function to approximate c according to
    #closure
    for i in range(len(r)):
        c[i]=(np.exp(-beta*lj_p(r[i]))-1)*(1+h[i]-c[i]))
    #Fourier Transform 1D
    ck=dst(coeff_to_fourier*c,type=2)/k
    for i in range(len(h)):

```

```

    hk[i]=omega(k[i],N)**2*ck[i]/(1-rho*omega(k[i],N)*ck[i])#omega12
        [i]**2*ck[i]/(1-rho*omega12[i]*ck[i])
#Inverse Fourier Transform 1D
h2=dst(coeff_to_real*hk,type=3)/r
err=0
for i in range(len(h)):
    err=err+(h[i]-h2[i])**2/len(h)
    h[i]=frac*(h2[i])+(1-frac)*h[i]
err=np.sqrt(err)
if count>=2000:
    break
count=count+1
if count%1==0:
    print(count,err)

plt.figure()
plt.rc('font', **{'family': 'serif', 'serif': ['Computer_Modern']})
plt.rc('text', usetex=True)
plt.gcf().set_size_inches(4,3,forward=True)
plt.subplots_adjust(left=0.18,bottom=0.15)
g=[ii+1 for ii in h]
plt.plot(r,g,'-r')
plt.plot(r,g,'o',markerfacecolor='w',markeredgecolor='r',markersize
    =4)
plt.xlim(0,4)
plt.xlabel("$r$")
plt.ylabel("$g(r)$")
plt.savefig("g-"+str(N)+".png",dpi=300)

filename2 = "g-"+str(N)+"-py.txt"
writefile = open(filename2,'w')
for i in range(len(r)):
    writefile.write(str(r[i]))
    writefile.write("\t")
    writefile.write(str(g[i]))
    writefile.write("\n")

```

Appendix E

Supporting Information for Chapter 8

E.1 First Approximation

First term:

$$\frac{\partial \Psi^{(0)}}{\partial \rho_b} \frac{\partial \rho_b}{\partial t} = -\Psi^{(0)} \nabla_{\mathbf{r}} \cdot \mathbf{c}_0 - \frac{\Psi^{(0)} \mathbf{c}_0}{\rho_b} \cdot \nabla_{\mathbf{r}} \rho_b \quad (\text{E.1})$$

Second term:

$$\frac{\partial \Psi^{(0)}}{\partial \mathbf{c}_0} \frac{\partial \mathbf{c}_0}{\partial t} = \Psi^{(0)} \frac{m}{k_b T} (\mathbf{c} - \mathbf{c}_0) \cdot \left(-\frac{k_b}{m} \nabla_{\mathbf{r}} T - \mathbf{c}_0 \nabla_{\mathbf{r}} \cdot \mathbf{c}_0 - \frac{k_b T}{m \rho_b} \nabla_{\mathbf{r}} \rho_b + \sum_j \frac{\rho_j \mathbf{F}_j}{m \rho_b} \right) \quad (\text{E.2})$$

$$= -\Psi^{(0)} \mathbf{C} \cdot \nabla_{\mathbf{r}} \ln T - \Psi^{(0)} \frac{m}{k_b T} \mathbf{C} \cdot (\mathbf{c}_0 \nabla_{\mathbf{r}} \cdot \mathbf{c}_0) - \frac{\Psi^{(0)}}{\rho_b} \mathbf{C} \cdot \nabla_{\mathbf{r}} \rho_b + \Psi^{(0)} \mathbf{C} \cdot \sum_j \frac{\rho_j \mathbf{F}_j}{\rho_b k_b T} \quad (\text{E.3})$$

Third term:

$$\frac{\partial \Psi^{(0)}}{\partial T} \frac{\partial T}{\partial t} = \frac{3}{2} \Psi^{(0)} \mathbf{c}_0 \cdot \nabla_{\mathbf{r}} \ln T + \Psi^{(0)} \nabla_{\mathbf{r}} \cdot \mathbf{c}_0 - \Psi^{(0)} W^2 \mathbf{c}_0 \cdot \nabla_{\mathbf{r}} \ln T - \Psi^{(0)} \frac{2}{3} W^2 \nabla_{\mathbf{r}} \cdot \mathbf{c}_0 \quad (\text{E.4})$$

We have used $W^2 = \frac{m}{2k_b T}(\mathbf{c} - \mathbf{c}_0)^2$ and the conservation laws of mass, momentum and energy.

¹ Eventually, the last term:

$$\mathbf{c} \cdot \nabla_{\mathbf{r}} \Psi^{(0)} = \frac{\mathbf{c} \Psi^{(0)}}{\rho_b} \cdot \nabla_{\mathbf{r}} \rho_b - \frac{3}{2} \Psi^{(0)} \mathbf{c} \cdot \nabla_{\mathbf{r}} \ln T + \Psi^{(0)} W^2 \mathbf{c} \cdot \nabla_{\mathbf{r}} \ln T + 2 \Psi^{(0)} \sqrt{\frac{m}{2k_b T}} \mathbf{W} \cdot (\mathbf{c} \nabla_{\mathbf{r}} \cdot \mathbf{c}_0) \quad (\text{E.5})$$

To reiterate, we have let $\mathbf{C} = \mathbf{c} - \mathbf{c}_0$, this leads to:

$$\Psi^{(0)} \left(\left[-\frac{5}{2} \mathbf{C} \cdot \nabla_{\mathbf{r}} \ln T + W^2 \mathbf{C} \cdot \nabla_{\mathbf{r}} \ln T \right] + 2[\mathbf{W}\mathbf{W} : \nabla_{\mathbf{r}} \mathbf{c}_0 - \frac{1}{3} W^2 \mathbf{I} : \nabla_{\mathbf{r}} \mathbf{c}_0] + \mathbf{C} \cdot \sum_j \frac{\rho_j \mathbf{F}_j}{\rho_b k_b T} \right) = -\frac{\Psi^{(1)} - \Psi^{(0)}}{\tau} \quad (\text{E.6})$$

$$\Psi^{(1)} = \Psi^{(0)} \left[1 - \tau \left[\left(-\frac{5}{2} \mathbf{C} \cdot \nabla_{\mathbf{r}} \ln T + W^2 \mathbf{C} \cdot \nabla_{\mathbf{r}} \ln T \right) + 2(\mathbf{W}\mathbf{W} : \nabla_{\mathbf{r}} \mathbf{c}_0 - \frac{1}{3} W^2 \mathbf{I} : \nabla_{\mathbf{r}} \mathbf{c}_0) + \mathbf{C} \cdot \sum_j \frac{\rho_j \mathbf{F}_j}{\rho_b k_b T} \right] \right] \quad (\text{E.7})$$

\mathbf{I} is a 3×3 identity matrix. ρ_j is the number density of the j th bead such that $\rho_b = \sum_j \rho_j$ and \mathbf{F}_j is the intramolecular force acting upon the j th bead.

E.2 Evaluation of the Component p_{xy}

C is the magnitude of the vector \mathbf{C} , C_x and C_y are the x and y components of the vector \mathbf{C} .

To be more explicit,

$$\mathbf{C} = \begin{bmatrix} C_x \\ C_y \\ C_z \end{bmatrix} \quad (\text{E.8})$$

$$C = \sqrt{C_x^2 + C_y^2 + C_z^2} \quad (\text{E.9})$$

¹To reiterate, the terms $\frac{\partial \rho_b}{\partial t}$, $\frac{\partial \mathbf{c}_0}{\partial t}$ and $\frac{\partial T}{\partial t}$ can be known by conservation laws along with the normal solution $\Psi^{(0)}$, which gives us $\mathbf{P}^{(0)} = \rho_b k_b T \mathbf{I}$ and $\mathbf{q}^{(0)} = \mathbf{0}$. To be explicit:

$$\begin{aligned} \frac{\partial \rho_b}{\partial t} &= -\nabla_{\mathbf{r}} \cdot (\rho_b \mathbf{c}_0) \\ \frac{\partial \mathbf{c}_0}{\partial t} &= -\mathbf{c}_0 \nabla_{\mathbf{r}} \cdot \mathbf{c}_0 - \frac{1}{m \rho_b} \nabla_{\mathbf{r}} \cdot \mathbf{P}^{(0)} + \sum_j \frac{\rho_j \mathbf{F}_j}{m \rho_b} \\ \frac{\partial T}{\partial t} &= -\mathbf{c}_0 \cdot \nabla_{\mathbf{r}} T - \frac{2}{3k_b \rho_b} (\mathbf{P}^{(0)} : \nabla_{\mathbf{r}} \mathbf{c}_0) \end{aligned}$$

These equations of conservation are exactly the same as that in continuum mechanics.

In spherical coordinates, we have:

$$\mathbf{C} = \begin{bmatrix} C \sin \theta \cos \psi \\ C \sin \theta \sin \psi \\ C \cos \theta \end{bmatrix} \quad (\text{E.10})$$

Then:

$$\int_{-\infty}^{\infty} C_x C_y \Psi^{(0)} d\mathbf{C} = \int_0^{2\pi} \sin \psi \cos \psi d\psi \int_0^{\pi} \sin^3 \theta d\theta \int_0^{\infty} C^4 \Psi^{(0)} dC \quad (\text{E.11})$$

The integral $\int_0^{2\pi} \sin \psi \cos \psi d\psi = 0$, therefore:

$$\int_{-\infty}^{\infty} C_x C_y \Psi^{(0)} d\mathbf{C} = 0 \quad (\text{E.12})$$

Now, consider the terms:

$$\int_{-\infty}^{\infty} C_x C_y \left(-\frac{5}{2}\mathbf{C} + W^2\mathbf{C}\right) \Psi^{(0)} d\mathbf{C} \cdot \nabla_{\mathbf{r}} \ln T \quad (\text{E.13})$$

And:

$$\int_{-\infty}^{\infty} C_x C_y \mathbf{C} \Psi^{(0)} d\mathbf{C} \cdot \sum_j \frac{\rho_j \mathbf{F}_j}{\rho_b k_b T} \quad (\text{E.14})$$

By considering terms in three different directions:

$$\left(W^2 - \frac{5}{2}\right) \frac{\partial \ln T}{\partial l} \int_0^{2\pi} \int_0^{\pi} \int_0^{\infty} C_x C_y C_l \Psi^{(0)} C^2 dC \sin \theta d\theta d\psi \quad (\text{E.15})$$

$$\left(\sum_j \frac{\rho_j F_{j,l}}{\rho_b k_b T}\right) \int_0^{2\pi} \int_0^{\pi} \int_0^{\infty} C_x C_y C_l \Psi^{(0)} C^2 dC \sin \theta d\theta d\psi \quad (\text{E.16})$$

where l can be x , y or z . $F_{j,l}$ is the intramolecular force acting upon j th bead in the l direction. Consider the integral over ψ , by the fact that $C_x = C \sin \theta \cos \psi$, $C_y = C \sin \theta \sin \psi$, and $C_z = C \cos \theta$, we only have to confirm that the followings are zeros:

$$\int_0^{2\pi} \cos^2 \psi \sin \psi d\psi = -\frac{1}{3} \left[\cos^3 \psi \right]_0^{2\pi} = 0 \quad (\text{for, } l = x) \quad (\text{E.17})$$

$$\int_0^{2\pi} \cos \psi \sin^2 \psi d\psi = \frac{1}{3} \left[\sin^3 \psi \right]_0^{2\pi} = 0 \quad (\text{for, } l = y) \quad (\text{E.18})$$

$$\int_0^{2\pi} \cos \psi \sin \psi d\psi = -\frac{1}{2} \left[\cos^2 \psi \right]_0^{2\pi} = 0 \quad (\text{for, } l = z) \quad (\text{E.19})$$

We then come to the conclusion that:

$$\int_{-\infty}^{\infty} C_x C_y \left(-\frac{5}{2} \mathbf{C} + W^2 \mathbf{C}\right) \Psi^{(0)} d\mathbf{C} \cdot \nabla_{\mathbf{r}} \ln T = 0 \quad (\text{E.20})$$

$$\int_{-\infty}^{\infty} C_x C_y \mathbf{C} \Psi^{(0)} d\mathbf{C} \cdot \sum_j \frac{\rho_j \mathbf{F}_j}{\rho_b k_b T} = 0 \quad (\text{E.21})$$

Hence, combining Equation (E.20) and Equation (E.21) together and multiply it by $-\tau$, we then get Equation (8).

E.3 Integration in Evaluation of η_d

Consider the integral in Equation (9),

$$\int_{-\infty}^{\infty} C_x C_y C_x C_y \Psi^{(0)} d\mathbf{C} \quad (\text{E.22})$$

In spherical coordinate, this gives us:

$$\int_0^{2\pi} \int_0^{\pi} \int_0^{\infty} C_x C_y C_x C_y C^2 \Psi^{(0)} \sin \theta dC d\theta d\psi \quad (\text{E.23})$$

It is known that $C_x = C \sin \theta \cos \psi$ and $C_y = C \sin \theta \sin \psi$. Then, we have:

$$\int_0^{2\pi} \cos^2 \psi \sin^2 \psi d\psi \int_0^{\pi} \sin^5 \theta d\theta \int_0^{\infty} C^6 \Psi^{(0)} dC \quad (\text{E.24})$$

Firstly, we consider the integration over ψ :

$$\cos^2 \psi \sin^2 \psi = \left(\frac{e^{i\psi} + e^{-i\psi}}{2}\right)^2 \left(\frac{e^{i\psi} - e^{-i\psi}}{2i}\right)^2 \quad (\text{E.25})$$

$$\int_0^{2\pi} \cos^2 \psi \sin^2 \psi d\psi = -\frac{1}{16} \int_0^{2\pi} [(e^{4i\psi} + e^{-4i\psi}) - 2] d\psi \quad (\text{E.26})$$

$$= -\frac{1}{16} \left[\frac{e^{4i\psi}}{4i} - \frac{e^{-4i\psi}}{4i} - 2\psi \right]_0^{2\pi} \quad (\text{E.27})$$

$$= -\frac{1}{16} \left(\frac{2i \sin 4\psi}{2} \right)_0^{2\pi} = \frac{\pi}{4} \quad (\text{E.28})$$

where $i = \sqrt{-1}$. Secondly, the integration over θ is considered:

$$\int_0^\pi \sin^5 \theta d\theta = - \int_0^\pi (1 - \cos^2 \theta)^2 d \cos \theta \quad (\text{E.29})$$

$$= - \int_0^\pi (1 - 2 \cos^2 \theta + \cos^4 \theta) d \cos \theta \quad (\text{E.30})$$

$$= - \left(\cos \theta \right)_0^\pi + \frac{2}{3} \left(\cos^3 \theta \right)_0^\pi - \frac{1}{5} \left(\cos^5 \theta \right)_0^\pi \quad (\text{E.31})$$

$$= -(-1 - 1) + \frac{2}{3}(-1 - 1) - \frac{1}{5}(-1 - 1) = 2 - \frac{4}{3} + \frac{2}{5} \quad (\text{E.32})$$

$$= \frac{16}{15} \quad (\text{E.33})$$

The integration over C is evaluated:

$$\rho_b \left(\frac{b}{\pi} \right)^{1.5} \int_0^\infty e^{-bC^2} C^6 dC \quad (\text{E.34})$$

$$\int_0^\infty C^6 e^{-bC^2} dC = \int_0^\infty \frac{e^{-br^2}}{2b} 5C^4 dC \quad (\text{E.35})$$

$$= \frac{5}{2b} \int_0^\infty \frac{e^{-bC^2}}{2b} 3C^2 dC \quad (\text{E.36})$$

$$= \frac{15}{4b^2} \int_0^\infty e^{-bC^2} C^2 dC \quad (\text{E.37})$$

$$= \frac{15}{4b^2} \int_0^\infty \frac{e^{-bC^2}}{2b} dC \quad (\text{E.38})$$

$$= \frac{15}{8b^3} \cdot \frac{1}{2} \sqrt{\frac{\pi}{b}} = \frac{15}{16b^3} \sqrt{\frac{\pi}{b}} \quad (\text{E.39})$$

where $b = \frac{m}{2k_b T}$. Finally, we have:

$$\int_{-\infty}^\infty C_x C_y C_x C_y \Psi^{(0)} d\mathbf{C} = \rho_b \frac{4\pi}{15} \left(\frac{b}{\pi} \right)^{1.5} \frac{15}{16b^3} \sqrt{\frac{\pi}{b}} = \frac{\rho_b}{4b^2} = \frac{\rho_b k_b^2 T^2}{m^2} \quad (\text{E.40})$$

E.4 Normal Distribution Approximation of $\int_{\phi^+}^\infty P_d(\phi) d\phi$

In our previous work [85, 105, 106], the following form of $P_d(\phi)$ distribution was used:

$$\ln P_d = (N-x) \ln \left[\left(\frac{1-F}{1-\phi+\lambda} \right)^{1-\phi} \left(\frac{F}{\phi+\lambda} \right)^\phi \right] - \frac{1}{2} \ln \left[2\pi(N-x)\phi(1-\phi) + \exp\left(-\frac{\phi^2}{\lambda^2}\right) + \exp\left[-\frac{(\phi-1)^2}{\lambda^2}\right] \right] + \ln(\mu) \quad (\text{E.41})$$

where λ is a small number of order of magnitude of 10^{-5} , and μ is the normalization constant. Equation (E.41) is a result of Stirling approximation. Consider the integral:

$$\int_{\phi^+}^{\infty} P_d(\phi) d\phi \quad (\text{E.42})$$

It can be either approximated as a normal distribution with mean value and covariance being F and $F/(N-x)$, respectively, (cf., Equation (18)) or evaluated numerically based upon the distribution as illustrated in Equation (E.41). Figure S1 shows a plot of Equation (E.42) as a function of N computed using the more complicated form in Equation (E.41) and the normal distribution approximation in Equation (18) with $F = 0.45$ and $x = 2$, and $\phi^+ = 0.49$ as well as $\phi^+ = 0.50$ in the former and latter cases, respectively. The approximation is reasonably good.

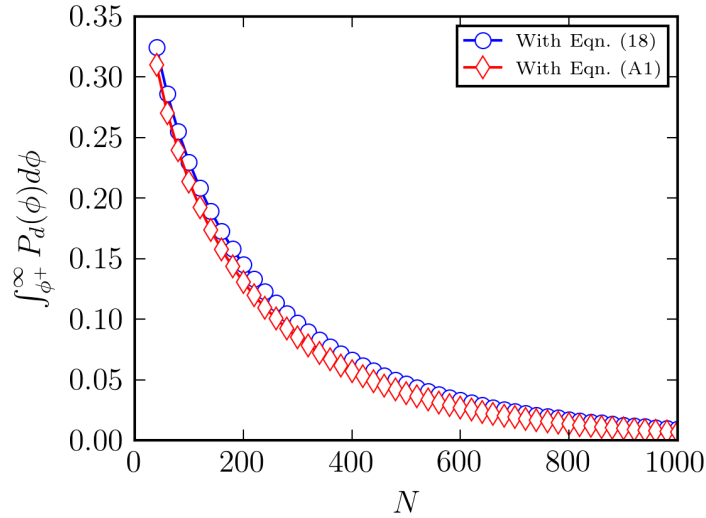


Figure S1: Comparison of $\int_{\phi^+}^{\infty} P_d(\phi) d\phi$ as a function of N evaluated using Equation (E.41) and Equation (18) with $F = 0.45$ and $x = 2$, as well as $\phi^+ = 0.49$ and $\phi^+ = 0.50$ in the former and latter cases, respectively.

E.5 $\hat{\omega}(k)$ of Polyethylene with Different Structures

The total number of $\hat{\omega}_{\alpha,\gamma}(k)$ of a Gaussian polyethylene is always N^2 regardless of their architectures. If this is not clear, one can write a $N \times N$ matrix as shown below:

$$\begin{bmatrix} \hat{\omega}_{1,1} & \hat{\omega}_{1,2} & \hat{\omega}_{1,3} & \hat{\omega}_{1,4} & \hat{\omega}_{1,5} \\ \hat{\omega}_{2,1} & \hat{\omega}_{2,2} & \hat{\omega}_{2,3} & \hat{\omega}_{2,4} & \hat{\omega}_{2,5} \\ \hat{\omega}_{3,1} & \hat{\omega}_{3,2} & \hat{\omega}_{3,3} & \hat{\omega}_{3,4} & \hat{\omega}_{3,5} \\ \hat{\omega}_{4,1} & \hat{\omega}_{4,2} & \hat{\omega}_{4,3} & \hat{\omega}_{4,4} & \hat{\omega}_{4,5} \\ \hat{\omega}_{5,1} & \hat{\omega}_{5,2} & \hat{\omega}_{5,3} & \hat{\omega}_{5,4} & \hat{\omega}_{5,5} \end{bmatrix} \quad (\text{E.43})$$

where we have let $N = 5$ as an example. Note that $\hat{\omega}_{\alpha,\gamma}(k)$ is the Fourier Transform of the probability of finding site γ of the polyethylene with site α as reference site ($\omega_{\alpha,\gamma}(r)$). We assume that such probability is a normal distribution function of r . Consider two beads that are separated by one bond in linear and four-arm symmetrical star polyethylene, then $\omega_{\alpha,\alpha+1}(r)$ is:

$$\omega_{\alpha,\alpha+1}(r) = \left(\frac{b}{\pi}\right)^{1.5} 4\pi e^{-br^2} r^2 \quad (\text{E.44})$$

where $b = \frac{3}{2\langle r^2 \rangle}$. To evaluate the Fourier Transform of $\omega_{\alpha,\alpha+1}(r)$, we have:

$$\frac{1}{k} \left(\frac{b}{\pi}\right)^{1.5} 4\pi \int_0^\infty e^{-br^2} r \left(\frac{e^{ikr} - e^{-ikr}}{2i}\right) dr \quad (\text{E.45})$$

where k is the magnitude of a wavevector and $i = \sqrt{-1}$.

Then, it can be rewritten:

$$\frac{1}{2ik} \left(\frac{b}{\pi}\right)^{1.5} 4\pi \left[e^{-\frac{k^2}{4b}} \int_0^\infty e^{-b(r-\frac{ik}{2b})^2} r dr - e^{-\frac{k^2}{4b}} \int_0^\infty e^{-b(r+\frac{ik}{2b})^2} r dr \right] \quad (\text{E.46})$$

$$= \frac{1}{2ik} \left(\frac{b}{\pi}\right)^{1.5} 4\pi e^{-\frac{k^2}{4b}} \frac{ik}{2b} \sqrt{\frac{\pi}{b}} \quad (\text{E.47})$$

$$= e^{-\frac{k^2}{4b}} \quad (\text{E.48})$$

Given the fact that $b = \frac{3}{2\langle r^2 \rangle}$, we get:

$$\frac{1}{k} \left(\frac{b}{\pi}\right)^{1.5} 4\pi \int_0^\infty e^{-br^2} r \left(\frac{e^{ikr} - e^{-ikr}}{2i}\right) dr = \exp\left(-\frac{k^2 \langle r^2 \rangle}{6}\right) \quad (\text{E.49})$$

And if site α and site γ is separated by n bonds, then we have $\hat{\omega}_{\alpha,\gamma} = \exp(-\frac{nk^2\sigma^2}{6})$. In ring polymer, it is slightly more tricky that [109, 97]:

$$\hat{\omega}_{\alpha,\gamma} = \exp\left[-\frac{k^2\sigma^2 n(N-n)}{6N}\right] \quad (\text{E.50})$$

To see the effect of architecture on the resultant sum $\hat{\omega}(k)$ more clearly, consider again the case when $N = 5$:

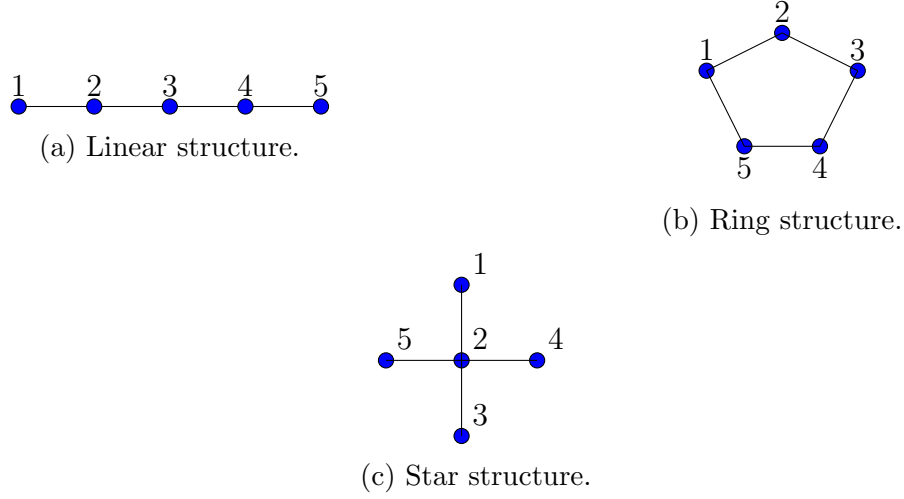


Figure S2: Nomenclature of different bead in polyethylene with different structure.

Let $f = \exp(-\frac{k^2\sigma^2}{6})$, then based on the illustration as shown in Figure S2, the corresponding matrices for these three different structures are as below, for linear structure:

$$\begin{bmatrix} 1 & f & f^2 & f^3 & f^4 \\ f & 1 & f & f^2 & f^3 \\ f^2 & f & 1 & f & f^2 \\ f^3 & f^2 & f & 1 & f \\ f^4 & f^3 & f^2 & f & 1 \end{bmatrix} \quad (\text{E.51})$$

For ring structure:

$$\begin{bmatrix} 1 & f^{4/5} & f^{6/5} & f^{6/5} & f^{4/5} \\ f^{4/5} & 1 & f^{4/5} & f^{6/5} & f^{6/5} \\ f^{6/5} & f^{4/5} & 1 & f^{4/5} & f^{6/5} \\ f^{6/5} & f^{6/5} & f^{4/5} & 1 & f^{4/5} \\ f^{4/5} & f^{6/5} & f^{6/5} & f^{4/5} & 1 \end{bmatrix} \quad (\text{E.52})$$

For four-arm symmetrical star structure:

$$\begin{bmatrix} 1 & f & f^2 & f^2 & f^2 \\ f & 1 & f & f & f \\ f^2 & f & 1 & f^2 & f^2 \\ f^2 & f & f^2 & 1 & f^2 \\ f^2 & f & f^2 & f^2 & 1 \end{bmatrix} \quad (\text{E.53})$$

To reiterate, $\hat{\omega}(k)$ for a particular structure is the summation of all the components in the corresponding matrix.

E.6 Intramolecular Contribution to the Equation of State

To incorporate the intramolecular term in the pressure equation, we firstly have to know the nature of the $g^{(1)}(r)$, which must be normalized as follows:

$$\frac{1}{V} \int_0^\infty 4\pi r^2 g^{(1)}(r) dr = 1 \quad (\text{E.54})$$

For monoatomic particle, $g^{(1)}(r) = 1$ as it does not have any internal structure like polymer. Similarly, for a Gaussian polymer, in which $g^{(1)}(r)$ is the intramolecular radial distribution function per two interacting beads of the same chain. Then, this means that for Gaussian polymer, $g^{(1)}(r)/V$ must be a normalized probability distribution function $P(r)$ describing the intramolecular interaction of two beads that $P(r) = g^{(1)}(r)/V$. Such probability distribution function for two beads connected with one another in a Gaussian chain is well-known:

$$P(r) = \left(\frac{3}{2\pi \langle r^2 \rangle} \right)^{3/2} \exp \left(- \frac{3r^2}{2 \langle r^2 \rangle} \right) \quad (\text{E.55})$$

$\langle r^2 \rangle$ is the mean square statistical step length of the Gaussian chain. Now, we consider the harmonic bond stretching potential u_{bond} .

$$\frac{du_{bond}}{dV} = \frac{du_{bond}}{dr} \frac{dr}{dV} \quad (\text{E.56})$$

r , which is the distance between two beads interacting with one another by $u_{bond}(r)$, can be expressed as follows:

$$r = \sqrt{V^{2/3}(x'^2 + y'^2 + z'^2)} \quad (\text{E.57})$$

Then,

$$\frac{dr}{dV} = \frac{r}{3V} \quad (\text{E.58})$$

Therefore:

$$\frac{du_{bond}}{dV} = \frac{du_{bond}}{dr} \frac{dr}{dV} = \frac{r}{3V} \frac{du_{bond}}{dr} \quad (\text{E.59})$$

The internal energy of one Gaussian chain with only intramolecular interaction is:

$$U_N = \sum_{\alpha=1}^{N-1} u_{bond}(\mathbf{r}_\alpha, \mathbf{r}_{\alpha+1}) \quad (\text{E.60})$$

In statistical mechanics, the pressure of one chain with only intramolecular interaction, P_1 can be expressed as:

$$P_1 \beta = \frac{1}{Z} \left(\frac{\partial Z}{\partial V} \right)_{N,T} \quad (\text{E.61})$$

where $Z = \int_0^\infty e^{-\beta U_N} d\mathbf{r}_1 d\mathbf{r}_2 \dots d\mathbf{r}_N$ if we only consider the intramolecular harmonic bond stretching interaction. Then, we have:

$$\left(\frac{\partial Z}{\partial V}\right)_{N,T} = - \int_0^\infty e^{-\beta U_N} \beta \frac{dU_N}{dV} d\mathbf{r}_1 d\mathbf{r}_2 \dots d\mathbf{r}_N \quad (\text{E.62})$$

It is known that:

$$\frac{dU_N}{dV} = N \frac{d}{dV} u_{bond}(\mathbf{r}_1, \mathbf{r}_2) \quad (\text{E.63})$$

This is because all the bonds are identical, and $u_{bond}(r)$ is a type of two-body interaction. In addition, by definition, for a single chain, we have:

$$g^{(1)}(\mathbf{r}_1, \mathbf{r}_2) = \frac{\rho^{-1} V \int_0^\infty \dots \int_0^\infty e^{-\beta U_N} d\mathbf{r}_3 d\mathbf{r}_4 \dots d\mathbf{r}_N}{Z} \quad (\text{E.64})$$

Therefore, we can rewrite Equation (E.62) in spherical coordinates:

$$\frac{1}{Z} \left(\frac{\partial Z}{\partial V}\right)_{N,T} = -4\pi N \rho \int_0^\infty g^{(1)}(r) \beta r^2 \frac{du_{bond}}{dV} dr = -\frac{4\pi N \rho}{3V} \int_0^\infty g^{(1)}(r) \beta r^3 \frac{du_{bond}}{dr} dr \quad (\text{E.65})$$

Note that $\rho_b = N\rho$. Then we have:

$$P_1 = -\frac{4\pi \rho_b}{3V} \int_0^\infty g^{(1)}(r) r^3 \frac{du_{bond}}{dr} dr \quad (\text{E.66})$$

Honnell *et al.* [73] also demonstrated similar results. We then obtained Equation (30) by the fact that $P(r) = g^{(1)}(r)/V$.